การดัดแปลงโครงสร้างของออกซิเรสเวอราทรอลเพื่อฤทธิ์ปกป้องดีเอ็นเอและฤทธิ์ยับยั้งไวรัสเริมและนิวรามินิเดสของไวรัสไข้หวัดนก

นางสาวนัฏฐ์ภัสสร ชาติสัมปันน์

วิทยานิพนธ์นี้เป็นส่วนหนึ่งของการศึกษาตามหลักสูตรปริญญาวิทยาศาสตรดุษฎีบัณฑิต
สาขาวิชาเภสัชเวท ภาควิชาเภสัชเวทและเภสัชพฤกษศาสตร์
คณะเภสัชศาสตร์ จุฬาลงกรณ์มหาวิทยาลัย
ปีการศึกษา 2557

STRUCTURE MODIFICATION OF OXYRESVERATROL FOR DNA PROTECTIVE PROPERTY AND INHIBITORY ACTIVITIES AGAINST HERPES SIMPLEX VIRUS AND AVIAN INFLUENZA NEURAMINIDASE

Miss Nutputsorn Chatsumpun

A Dissertation Submitted in Partial Fulfillment of the Requirements
for the Degree of Doctor of Philosophy Program in Pharmacognosy
Department of Pharmacognosy and Pharmaceutical Botany
Faculty of Pharmaceutical Sciences
Chulalongkorn University
Academic Year 2014

Thesis Title	STRUCTURE MODIFICATION OF OXYRESVERATROL FOR DNA PROTECTIVE PROPERTY AND INHIBITORY ACTIVITIES AGAINST HERPES SIMPLEX VIRUS AND AVIAN INFLUENZA NEURAMINIDASE
By	Miss Nutputsorn Chatsumpun
Field of Study	Pharmacognosy
Thesis Advisor	Professor Kittisak Likhitwitayawuid, Ph.D.
Thesis Co-Advisor	Poonsakdi Ploypradith, Ph.D.

Accepted by the Faculty of Pharmaceutical Sciences, Chulalongkorn University in Partial Fulfillment of the Requirements for the Doctoral Degree

.....Dean of the Faculty of Pharmaceutical Sciences
(Assistant Professor Rungpetch Sakulbumrungsil, Ph.D.)

THESIS COMMITTEE

.....Chairman
(Associate Professor Nijsiri Ruangrungsi, Ph.D.)

.....Thesis Advisor
(Professor Kittisak Likhitwitayawuid, Ph.D.)

.....Thesis Co-Advisor
(Poonsakdi Ploypradith, Ph.D.)

.....Examiner
(Associate Professor Boonchoo Sritularak, Ph.D.)

.....Examiner
(Associate Professor Vimolmas Lipipun, Ph.D.)

.....Examiner
(Assistant Professor Taksina Chuanasa, Ph.D.)

.....External Examiner
(Chaisak Chansriniyom, Ph.D.)

นัฏฐ์ภัสสร ชาติสัมปันน์ : การดัดแปลงโครงสร้างของออกซิเรสเวอราทรอลเพื่อฤทธิ์ปกป้องดีเอ็นเอและฤทธิ์ยับยั้งไวรัสเริมและนิวรามินิเดสของไวรัสไข้หวัดนก (STRUCTURE MODIFICATION OF OXYRESVERATROL FOR DNA PROTECTIVE PROPERTY AND INHIBITORY ACTIVITIES AGAINST HERPES SIMPLEX VIRUS AND AVIAN INFLUENZA NEURAMINIDASE) อ.ที่ปรึกษาวิทยานิพนธ์หลัก: ศ. ภก. ดร.กิตติศักดิ์ ลิขิตวิทยาวุฒิ, อ.ที่ปรึกษาวิทยานิพนธ์ร่วม: อ. ดร. พูนศักดิ์ พลอยประดิษฐ์, 191 หน้า.

ออกซิเรสเวอราทรอลหรือ 2,3′,4,5′-tetrahydroxystilbene เป็นสาร secondary metabolite ที่พบปริมาณมากในแก่นของ *Artocarpus lakoocha* Roxb. (วงศ์ Moraceae) เนื่องจากออกซิเรสเวอราทรอลมีฤทธิ์ทางชีวภาพที่หลากหลายประกอบกับสามารถสกัดแยกจากพืชได้ง่าย โครงการวิจัยจึงได้เลือกสารนี้เป็นโครงสร้างต้นแบบสำหรับการดัดแปลงโครงสร้างเพื่อให้ได้สารกลุ่มสติลบีนที่มีออกซิเจนหลายหมู่และมีฤทธิ์ทางชีวภาพสูงขึ้นและมีความจำเพาะมากขึ้น ในการศึกษานี้ปฏิกิริยาที่ใช้ได้แก่การเติมหมู่อัลคิล เอซิลที่ออกซิเจนและการเติมหมู่แทนที่ที่วงอะโรมาติกจนเตรียมได้สารอนุพันธ์ 26 ชนิด หลังจากนั้นได้ศึกษาฤทธิ์ทางชีวภาพของสารอนุพันธ์ที่เตรียมได้เปรียบเทียบกับสารต้นแบบ โดยได้ศึกษาฤทธิ์ปกป้องดีเอ็นเอและฤทธิ์ในการยับยั้งไวรัสเริมและเอนไซม์นิวรามินิเดสของไข้หวัดนก นอกจากนี้ยังได้ทำการศึกษาฤทธิ์ยับยั้งเอนไซม์อัลฟากลูโคซิเดสและความเป็นพิษต่อเซลล์มะเร็งอีกด้วย

ในการศึกษานี้ได้พัฒนาวิธีการทดสอบฤทธิ์ปกป้องดีเอ็นเอขึ้นใหม่ และนำวิธีดังกล่าวไปตรวจวัดฤทธิ์ปกป้องดีเอ็นเอของออกซิเรสเวอราทรอลและอนุพันธ์ที่เตรียมได้ จากการทดลองพบว่าออกซิเรสเวอราทรอลแสดงฤทธิ์สูงกว่าโทรลอกซ์และวิตามินซี นอกจากนี้ยังพบว่าอนุพันธ์จำนวน 16 ชนิดแสดงฤทธิ์สูงกว่าสารต้นแบบ สารที่แสดงฤทธิ์สูงที่สุดคือ 2,3′,4-tri-*O*-methyloxyresveratrol ซึ่งมีฤทธิ์เป็น 7 เท่าของสารต้นแบบ นอกจากนี้ยังพบว่าสารนี้และอนุพันธ์อื่นอีกจำนวน 3 ชนิดมีฤทธิ์ยับยั้งไวรัสเริมสูงกว่าออกซิเรสเวอราทรอล โดย 2,3′,4-tri-*O*-methyloxyresveratrol มีฤทธิ์สูงสุดคิดเป็น 4 เท่าของออกซิเรสเวอราทรอล ในการทดสอบฤทธิ์ยับยั้งเอนไซม์นิวรามินิเดสของอนุพันธ์ที่เตรียมได้ พบว่ามีเพียงสาร 5-carboxyoxyresveratrol ที่แสดงฤทธิ์ใกล้เคียงกับสารต้นแบบ ในขณะที่สารอื่นแสดงฤทธิ์ลดลง ส่วนการทดสอบความเป็นพิษต่อเซลล์มะเร็งพบอนุพันธ์จำนวน 16 และ 10 ชนิดที่แสดงความเป็นพิษต่อเซลล์ KB และ MCF-7 ตามลำดับ สารที่แสดงฤทธิ์ความเป็นพิษต่อ KB สูงที่สุดคือ 3′,5′-*O*-diacetyl-2,4-di-*O*-isopropyloxyresveratrol ส่วนสารที่แสดงฤทธิ์ต่อ MCF-7 แรงที่สุดคือ 2,3′,4-tri-*O*-isopropyloxyresveratrol นอกจากนี้เป็นที่น่าสนใจว่า 2,3′,4-tri-*O*-isopropyloxyresveratrol แสดงฤทธิ์ยับยั้งเอนไซม์อัลฟากลูโคซิเดสใกล้เคียงกับออกซิเรสเวอราทรอลอีกด้วย

ภาควิชา	เภสัชเวทและเภสัชพฤกษศาสตร์	ลายมือชื่อนิสิต	.....
สาขาวิชา	เภสัชเวท	ลายมือชื่อ อ.ที่ปรึกษาหลัก	.....
ปีการศึกษา	2557	ลายมือชื่อ อ.ที่ปรึกษาร่วม	.....

5276953233 : MAJOR PHARMACOGNOSY
KEYWORDS: OXYRESVERATROL / STRUCTURE MODIFICATION / DNA PROTECTIVE PROPERTY / ANTIHERPES SIMPLEX VIRUS

NUTPUTSORN CHATSUMPUN: STRUCTURE MODIFICATION OF OXYRESVERATROL FOR DNA PROTECTIVE PROPERTY AND INHIBITORY ACTIVITIES AGAINST HERPES SIMPLEX VIRUS AND AVIAN INFLUENZA NEURAMINIDASE. ADVISOR: PROF. KITTISAK LIKHITWITAYAWUID, Ph.D., CO-ADVISOR: POONSAKDI PLOYPRADITH, Ph.D., 191 pp.

Oxyresveratrol, or 2,3′,4,5′-tetrahydroxystilbene, is a secondary metabolite found in large amounts in the heartwood of *Artocarpus lakoocha* Roxb. (Moraceae). Because of the wide range of potential biological activities, together with the easy extractability from the plant material, oxyresveratrol was chosen as a lead structure for chemical modification in an attempt to prepare polyoxygenated stilbenes with higher potency and selective activity. In this study, several types of reactions were carried out, including *O*-alkylation, *O*-acylation and aromatic substitution. As a result, a total of twenty-six derivatives were prepared. Biological studies of these semi-synthetic products were conducted, in comparison with the parent compound, to investigate their DNA protective activity, and their inhibitory activity against the herpes simplex virus and the enzyme avian influenza neuraminidase. In addition, these compounds were further evaluated for their anti-**α**-glucosidase activity and cytotoxicity against selected cancer cells.

In this study, a new assay for DNA protective activity was developed and then applied on oxyresveratrol and its semisynthetic analogues. Oxyresveratrol was found to possess stronger DNA protective activity than Trolox and ascorbic acid. Sixteen of the prepared analogues showed activity even higher than the parent compound, with an 7-fold increase of the activity observed for the most potent compound, 2,4,3′-tri-*O*-methyloxyresveratrol. This same compound was also the strongest analogue against herpes simplex virus; it was about 4-time as strong as oxyresveratrol. Three other derivatives were also found to possess enhanced anti-HSV activity. Regarding the inhibitory activity on the enzyme neuraminidase, only 5-carboxyoxyresveratrol exhibited activity close to that of the precursor, whereas the others were less active. Concerning the cytotoxicity against cancer cells, sixteen and ten oxyresveratrol derivatives were active against KB and MCF-7 cells, respectively. 3′,5′-*O*-Diacetyl-2,4-di-*O*-isopropoyloxyresveratrol was the most cytotoxic compound against KB cells, while 2,4,3′-tri-*O*-isopropyloxyresveratrol was the most potent against MCF-7 cells. Interestingly, the latter was also found to have anti-**α**-glucosidase activity approximately equal to that of oxyresveratrol.

Department:	Pharmacognosy and Pharmaceutical Botany	Student's Signature	.....
		Advisor's Signature	.....
Field of Study:	Pharmacognosy	Co-Advisor's Signature	.....
Academic Year:	2014		

ACKNOWLEDGEMENTS

I would like to express my gratitude to my thesis advisor, Professor Dr. Kittisak Likhitwitayawuid of the Department of Pharmacognosy and Pharmaceutical Botany, Faculty of Pharmaceutical Sciences, Chulalongkorn University, for his advice and encouragement, and my co-advisor, Dr. Poonsakdi Ploypradith of Chulabhorn Research Institute, for his close guidance and support, as well as for providing me with all the facilities needed to carry out my research smoothly.

I would also like to express my appreciation to:

Professor Dr. Somsak Ruchirawat of Chulabhorn Research Institute for allowing me to work in his Medicinal Chemistry Laboratory throughout this study.

Associate Professor Dr. Vimolmas Lipipun of the Department of Biochemistry and Microbiology, Chulalongkorn University, for her kind assistance in the evaluation of anti-herpes simplex virus activity.

Assistant Professor Dr. Taksina Chuanasa and Associate Professor Dr. Boonchoo Sritularak of the Department of Pharmacognosy and Pharmaceutical Botany, Faculty of Pharmaceutical Sciences, Chulalongkorn University, for providing comments and research facilities regarding the evaluation of DNA protective property.

Associate Professor Dr. Nijsiri Ruangrungsri, and Dr. Chaisak Chansriniyom, the Chairperson and the External Examiner of the Examination Committee, respectively, for their critical and useful comments on the writing of this dissertation.

The Pharmaceutical Research Instrument Center of the Faculty of Pharmaceutical Sciences, Chulalongkorn University, for supporting the instruments and research facilities.

The Thailand Research Fund for a research grant (BRG 5580004), and the Graduate School of Chulalongkorn University for partial financial support.

Finally, I wish to express my infinite gratitude to my family for their love, understanding, help, support and encouragement.

CONTENTS

Page

Page

Page

Page

LIST OF TABLES

LIST OF FIGURES

ABBREVIATIONS

DPPH	1,1-diphenyl-2-picrylhydrazyl
HMBC	^{1}H-detected Heteronuclear Multiple Bond Correlation
DMAP	4-Dimethylaminopyridine
AcCl	Acetyl chloride
α	Alpha
Ar	Argon
β	Beta
BBr_3	Boron tribromide
BCl_3	Boron trichloride
MCF-7	Breast cancer cell line
calcd	Calculated
^{13}C NMR	Carbon-13 Nuclear Magnetic Resonance
δ	Chemical shift
IC_{50}	Concentration showing 50% inhibition
J	Coupling constant
°C	Degree Celsius
Acetone-d_6	Deuterated acetone
$CDCl_3$	Deuterated chloroform

Methanol-d_4	Deuterated methanol
CH_2Cl_2	Dichloromethane
DMF	Dimethylformamide
d	Doublet (for NMR spectra)
dd	Doublet of doublets (for NMR spectra)
EIMS	Electron Impact Mass Spectrometry
EtOH	Ethanol
EtOAc	Ethyl acetate
EDTA	Ethylene diamine tetraacetic acid
$FeSO_4$	Ferrous sulfate
g	Gram
HSV	Herpes simplex virus
Hz	Hertz
HRTOF	High resolution time of flight
h	Hour
IR	Infrared
m/z	Mass to charge ratio
MHz	Mega Hertz
MeOH	Methanol

MeI	Methyl iodide
µg	Microgram
µL	Microliter
µM	Micromolar
mg	Milligram
mL	Milliliter
min	Minute
m	Multiplet (for NMR spectra)
nm	Nanometer
NA	Neuraminidase
NBT	Nitroblue tetrazolium
NMR	Nuclear Magnetic Resonance
OC	Open circular conformation
KB	Oral cavity cancer cell line
ppm	Part per million
$POCl_3$	Phosphoryl chloride
PNP	*p*-Nitrophenol
PNPG	*p*-Nitrophenyl alpha-d-glucoside
K_2CO_3	Potassium carbonate

KOH	Potassium hydroxide
^{1}H-NMR	Proton Nuclear Magnetic Resonance
p-TsOH·H2O	*p*-Toluenesulfonic acid monohydrate
q	Quartet (for NMR spectra)
rt	Room temperature
sept	Septet (for NMR spectra)
s	Singlet (for NMR spectra)
Na_2CO_3	Sodium carbonate
$NaH_2PO_4{\cdot}2H_2O$	Sodium dihydrogen phosphate dihydrate
$NaClO_2$	Sodium chlorite
Na_2SO_4	Sodium sulfate
SC	Supercoil conformation
TLC	Thin layer chromatography
Et_3N	Triethylamine
t	Triplet (for NMR spectra)
UATR	Universal attenuated total reflectance

CHAPTER I

INTRODUCTION

Oxyresveratrol (**1**), or 2,3′,4,5′-tetrahydroxystilbene, is a secondary metabolite found in several plants in the family Moraceae, such as *Morus alba* L. (Lorenz *et al.*, 2003) and *Artocarpus lakoocha* Roxb. (Likhitwitayawuid *et al.*, 2005). The compound has also been reported from other plant families, for instance, *Glycosmis pentaphylla* Retz. (Rutaceae) (Wu *et al.*, 2012) and *Smilax china* L. (Liliaceae) (Wu *et al.*, 2010). Various biological activities have been reported for oxyresveratrol, for example, antioxidant, neuroprotective, antiviral and anti-tyrosinase activities.

With regard to the antioxidant activity, oxyresveratrol showed an inhibitory effect against $FeSO_4$-induced lipid peroxidation in rat microsomes and a scavenging activity against 1,1-diphenyl-2-picrylhydrazly (DPPH) radical with IC_{50} values of 3.6 and 15.1 μM, respectively, and inhibited the expression of nitric oxide synthase and the accumulation of nitrite (Chung *et al.*, 2003). Compared with resveratrol (**2**), oxyresveratrol (**1**) was a better free radical scavenger against DPPH, hydrogen peroxide and nitric oxide (Lorenz *et al.*, 2003); in addition, the two compounds were later found to possess synergistic antioxidant activity in the heme-enhanced TMPD oxidation assay (Aftab *et al.*, 2010). Oxyresveratrol (**1**) was shown to be neuroprotective in mice, and this activity was thought to be due to its antioxidant

activity (Andrabi *et al.*, 2004). In connection to this theory, it is interesting to investigate whether oxyresveratrol and structurally related stilbenes can protect DNA against the damage induced by oxidative stress.

Concerning the antiviral activity, oxyresveratrol (**1**) exhibited inhibitory effects against herpes simplex virus (HSV) types 1 and 2, as well as varicella-zoster virus (VZV) (Likhitwitayawuid *et al.*, 2005; Sasivimolphan *et al.*, 2009). It inhibited the growth of both types of HSV at the early and late phase of viral replication, and in a preliminary study this compound in the form of 30% ointment could significantly delay the development of skin lesions and protected mice from death (Chuanasa *et al.*, 2008). In a recent report, Lipipun and co-workers presented a novel 10% oxyresveratrol cream that was as effective as a 5% acyclovir cream in treating mice with HSV-1 skin infection (Lipipun *et al.*, 2011). In an unrelated, but exciting study, oxyresveratrol (**1**) was reported to possess significant inhibitory activity against avian influenza neuraminidase, an enzyme found on the surface of the bird flu virus that enables the virus to be released from the host cell (Kongkamnerd, 2010). The above findings have posed a question of whether stronger anti-HSV or anti-neuraminidase compounds can be obtained by modifying the structure of oxyresveratrol.

In recent years, oxyresveratrol has received tremendous attention for its ability to inhibit tyrosinase enzyme and suppress skin melanin production. Its inhibitory activity against mushroom tyrosinase was found to be higher than that of

kojic acid, a widely used ingredient in commercial skin-whitening products (Likhitwitayawuid *et al.*, 2006c). Subsequent studies in animals and human volunteers confirmed its effectiveness in reducing dermal hyperpigmentation (Tengamnuay *et al.*, 2006). During an attempt to prepare stronger tyrosinase inhibitors from oxyresveratrol, it was found that the four phenolic groups were essential for the activity, and that *O*-methylation of the OHs led to lessened activity, and simultaneously introduced cytotoxicity (Likhitwitayawuid *et al.*, 2006c).

The wide range of biological activities of oxyresveratrol (**1**) and structurally related compounds suggests that there are still other research areas that are worth further investigation. For example, it is interesting to explore the possibility of using oxyresveratrol as a DNA protective agent. It is also challenging to modify the structure of oxyresveratrol to see whether stronger DNA protective agents or more potent anti-herpetic or anti-neuraminidase analogues can be obtained. Moreover, it is stimulating to try to find answers to the question of whether the diverse biological activities of oxyresveratrol and related compounds are separable.

It is also important to mention that during the initial phase of this research, a thought-provoking report has appeared, describing oxyresveratrol as a strong inhibitor of α-glucosidase, an enzyme which is responsible for the break-down of starch and disaccharides into glucose in the intestine, and thus plays an important role in glycemic control (He & Lu, 2013). This information has inspired the author to extend

the scope of her research to look into the possibility of preparing hypoglycemic compounds from the core structure of oxyresveratrol.

In the present study, the first focus would be on developing a new assay for DNA protective activity, and employing this assay to examine the ability of oxyresveratrol to protect against DNA damage. Then, attention would be placed on the structural modification of oxyresveratrol and the evaluation of the compound and reaction products for some biological activities, including DNA protective property, and inhibitory activities against HSV and avian influenza neuraminidase. In addition, the products would be subjected to assays for cytotoxicity and anti-α-glucosidase activity. Thus, the overall objectives of this research can be summarized as follows:

(1) To develop an assay for DNA protective property and evaluate oxyresveratrol for this activity.

(2) To study the chemical modification of oxyresveratrol using various types of reaction.

(3) To conduct comparative biological evaluation of the reaction products for the following biological activities: antioxidant activity, DNA protective property, cytotoxicity, and inhibitory effects against herpes simplex virus, avian influenza A virus neuraminidase and α-glucosidase.

It is hoped that the results obtained from this study would shed some light on the relationships between the structures of 2,3′,4,5′-tetraoxygenated stilbenes and their broad spectrum biological activities. During the synthetic study, important chemical behaviors of oxyresveratrol and related analogues with regard to their reactivity and selectivity would be examined. It is expected that the results from this investigation should provide chemical and biological data useful for the future development of stilbene-based medicinal agents.

CHAPTER II

LITERATURE REVIEW

This brief review describes some of the biological activities reported for natural and synthetic polyoxygenated *trans*-stilbenes, including antioxidant and antiviral activities, inhibitory effects on the enzymes neuraminidase and α-glucosidase, as well as cytotoxicity against cancer cells.

2.1 Antioxidant activity

Free radicals are molecules that contain an unpaired electron in the outer orbit. They are generally unstable and very reactive. Examples of oxygen free radicals, known as reactive oxygen species, are superoxide ($O_2^{\bullet -}$), hydroxyl ($^{\bullet}OH$), peroxyl ($RO_2^{\bullet}$), alkoxyl ($RO^{\bullet}$), and hydroperoxyl ($HO_2^{\bullet}$) radicals, whereas nitric oxide ($^{\bullet}NO$) and nitrogen dioxide ($^{\bullet}NO_2$) are two nitrogen free radicals (Fang *et al.*, 2002). Reactive oxygen species are like a two-edged sword. Positive roles are involved in energy production, phagocytosis, regulation of cell growth and intercellular signaling, and synthesis of biologically important compounds. On the other hand, they can destroy lipids in cell membranes, proteins in tissues or enzymes, carbohydrates, and DNA by inducing oxidations, which cause membrane damage, protein modification (including enzymes), and DNA damage. These deteriorative events lead to the development of several diseases such as heart disease, cataracts, cognitive

dysfunction, and cancer. For protection of these damages, humans have 2 main antioxidant systems. First is the enzymatic defense, for example, *Se*-glutathione peroxidase, catalase, and superoxide dismutase, and the second is the nonenzymatic defense such as glutathione, histidine-peptides, the iron-binding proteins transferrin and ferritin, dihydrolipoic acid, reduced CoQ10, melatonin, urate, and plasma protein thiols (Pietta, 2000). Under certain conditions, the natural antioxidant defense system is not sufficient to deal with the amount of free radicals, and it is thought that an intake of antioxidants is essential for lowering the risk of disorders (Rajendran *et al.*, 2004).

A number of *trans*-stilbenes have been studied for scavenging activity against several free radicals, as shown in Table 1. It should be noted that these compounds all have hydroxylation in their structures.

Table 1: Examples of *trans*-stilbenes with free radical scavenging activity

Compound	Source	Free radical	IC_{50} (μM)	Reference
Oxyresveratrol (**1**)	*Morus alba*	DPPH	23.4	Oh *et al.*, 2002
		Superoxide	3.81	Chung *et al.*,
		DPPH	15.1	2003
		Lipid peroxidation	3.6	Lorenz *et al.*,
		Nitric oxide	45.31	2003

Table 1: Examples of *trans*-stilbenes with free radical scavenging activity (continued)

Compound	Source	Free radical	IC_{50} (μM)	Reference
Resveratrol (**2**)	*Morus alba*	DPPH	21.7	Chung *et al.*, 2003
		Lipid peroxidation	6.1	Lorenz *et al.*, 2003
		Nitric oxide	22.36	
	Cajanus cajan	Superoxide	48.41	Wu *et al.*, 2011
		Hydroxyl radical	36.92	
Mulberroside A (**3**)	*Morus alba*	DPPH	91.3	Chung *et al.*, 2003
		Lipid peroxidation	78.4	
4-Hydroxystilbene (**4**)	*Morus alba*	DPPH	39.6	Lorenz *et al.*, 2003
Resveratrodehyde A (**5**)	*Alternaria* sp.	DPPH	447.62	Wang *et al.*, 2014
Resveratrodehyde B (**6**)	*Alternaria* sp.	DPPH	>900	Wang *et al.*, 2014
Resveratrodehyde C (**7**)	*Alternaria* sp.	DPPH	572.68	Wang *et al.*, 2014
Cajaninstilbene acid (**8**)	*Cajanus cajan*	Superoxide	19.03	Wu *et al.*, 2011
		Hydroxyl radical	6.36	
		Nitric oxide	39.65	
		Lipid peroxidation	20.58	

Table 1: Examples of *trans*-stilbenes with free radical scavenging activity (continued)

Compound	Source	Free radical	IC_{50} (μM)	Reference
(*E*) 4′-Fluoro-4-methoxy-3,3′,5′ -trihydroxystilbene (**9**)	Synthetic	DPPH	50	Csuk *et al.*, 2013
(*E*) 1-(3,5-Dihydroxy-phenyl)-2-(2′-fluoro-5′-hydroxy-4′-methoxy-phenyl ethane (**10**)	Synthetic	DPPH	>130	Csuk *et al.*, 2013
(*E*) 3-Hydroxy-4-methoxy-3′,4′,5′-trifluorostilbene (**11**)	Synthetic	DPPH	>130	Csuk *et al.*, 2013
(*E*) 3′,5′-Dimethoxy-3,4-dihydroxy-4′-fluorostilbene (**12**)	Synthetic	DPPH	64	Csuk *et al.*, 2013
(*E*) 2′,5′,3,4-Tetra-hydroxystilbene (**13**)	Synthetic	DPPH	11	Csuk *et al.*, 2013

DNA is the genetic material of living organisms, comprising two polynucleotide strands wound around each other. DNA damage, an undesired alteration of the chemical structure of DNA, can occur naturally, and can cause mutagenesis, aging and carcinogenesis as well as other diseases (Lin *et al.*, 2008). The damage to DNA usually involves two major chemical processes. The first process is known as “oxidative stress”, which is usually induced by the products of normal cellular metabolism, such as reactive oxygen species (ROS) and the products of lipid

peroxidation, whereas the second one concerns hydrolysis, which cleaves chemical bonds in DNA. There is currently much research interest in naturally derived products that are capable of protecting DNA against various damage-inducing agents. So far, several methods for the evaluation of DNA protective effects of different substances have been described (Wu *et al.*, 2011; McCarthy *et al.*, 2012), and they can be classified into two categories: chemical-based and cell-based assays.

In chemical-based assays, bacterial plasmid DNA, such as pBR 322 or pUC18, was used (Kumar *et al.*, 2011; Wu *et al.*, 2011) as the substrate, and damage to the DNA could then be induced by different oxidizing or free radical producing agents, such as H_2O_2 and Fenton's reagent, or by ultraviolet radiation (Wu *et al.*, 2011; Marimuthu *et al.*, 2013; George *et al.*, 2015). After incubation, the reaction mixture was analyzed by gel electrophoresis (Wu *et al.*, 2011). The DNA protective potential of the test sample was then determined by measuring the amounts of the damaged DNA (nicked DNA), which has lower electrophoretic mobility than the intact DNA (supercoiled DNA) (Lin *et al.*, 2008). Otherwise, the damaged DNA could be quantified by employing the *in vitro* repair reaction of DNA damage (3D assay), which determines the amounts of the incorporated digoxygenylated dUMP (Saint-Cricq de Gaulejac *et al.*, 1999).

In cell-based assays, U937 lymphocyte cells were treated with H_2O_2 to induce damage to the DNA (McCarthy *et al.*, 2012). The cell lysate was then analyzed by

the comet assay or the single-cell gel electrophoresis (SCGE) method (Maurya *et al.*, 2007). The DNA protective activity of the sample could be calcd from the relative amount of the DNA in tail, tail length, tail moment and Olive tail moment (Maurya *et al.*, 2007).

Cajaninstilbene acid (**8**) (Wu *et al.*, 2011) and pterostilbene (**31**) (Acharya & Ghaskadbi, 2013) are examples of *trans*-stilbenes with DNA protective property.

2.2 Herpes simplex virus

Herpes simplex virus (HSV)-associated diseases are among the most widespread global infections, affecting nearly 60% to 95% of human adults (Fatahzadeh & Schwartz, 2007). They are incurable and persist during the lifetime of the host, often in latent form. Herpes simplex viruses are categorized into 2 types: HSV-1 and HSV-2. HSV-1 is primarily associated with oral, pharyngeal, facial, ocular, and central nervous system infections and is largely transmitted by oral secretions and nongenital contact. HSV-2 is frequently involved with anal and genital infections and is mainly transmitted sexually by genital secretions. Clinical symptoms of HSV infection range from asymptomatic infection to mucocutaneous conditions, such as orolabial, ocular, and genital herpes, herpetic whitlow, herpes gladiatorum, and eczema herpeticum, as well as central nervous complications such as neonatal herpes and herpetic encephalitis and fatal dissemination, a particular threat in the immunosuppressed host. After primary infection, herpes viruses ascend in a

retrograde manner through the periaxonal sheath of sensory nerves to the trigeminal, cervical, lumbosacral, or autonomic ganglia of the host nervous system that can cause the recurrence when the host gets reactivation (Fatahzadeh & Schwartz, 2007). Nucleoside analogues such as acyclovir, penciclovir, valaciclovir, famciclovir and ganciclovir have been used for the treatment of HSV infections, but there have been reports of acyclovir-resistant HSV (Chuanasa *et al.*, 2008). The naturally occurring *trans*-stilbenes oxyresveratrol (**1)** and resveratrol (**2**) are examples of non-nucleoside anti-herpetic agents (Docherty *et al.*, 1999; Likhitwitayawuid *et al.*, 2005; Likhitwitayawuid *et al.*, 2006a). A *trans*-stilbene with sulfonate functionality (4,4′-diisothiocyanatostilbene-2,2′-disulfonic acid (**14**) is an example of a synthetic non-nucleoside with anti-HSV activity (Cardin & Tyms, 1992).

2.3 Neuraminidase

Influenza A virus is classified to the family of Orthomyxoviridae. The subtypes of the virus are based on the variation of two glycoproteins on the surface of virus particle: hemagglutinin (HA) and neuraminidase (NA). HA and NA have been identified into 16 and 9 subtypes, respectively (Cheung & Poon, 2007). Avain influenza A virus (H5N1) is a highly pathogenic virus; it can cause symptoms of fever, cough and shortness of breath, and pneumonia (de Jong & Hien, 2006). Neuraminidase plays an important role in viral replication, hydrolyzing the glycosidic linkage of sialic acid to release new virion from the host cell (De Clercq & Neyts, 2007). This enzyme is used

as the compromised target for anti-influenza drugs. The drug of choice to treat the H5N1 infection is oseltamivir, an antineuraminidase drug, but there has been a report of viral resistance to this compound (De Clercq & Neyts, 2007). Table 2 illustrates some *trans*-stilbenes with anti-neuraminidase activity.

Table 2: Examples of *trans*-stilbenes with inhibitory effect against neuraminidase

Compound	Source	IC_{50} (μM)	Reference
Resveratrol (**2**)	*Gnetum pendulum*	79.22	Liu *et al.*, 2010
Isorhapontigenin (**15**)	*Gnetum pendulum*	35.66	Liu *et al.*, 2010
Gnetupendin B (**16**)	*Gnetum pendulum*	13.16	Liu *et al.*, 2010
Piceid (**17**)	*Vitis amurensis*	110.79	Nguyen *et al.*, 2011
R1 (**18**)	unknown	54.10	Li *et al.*, 2015
R2 (**19**)	unknown	42.12	Li *et al.*, 2015
R8 (**20**)	unknown	34.15	Li *et al.*, 2015
R10 (**21**)	unknown	98.55	Li *et al.*, 2015
R12 (**22**)	unknown	179.11	Li *et al.*, 2015
R13 (**23**)	unknown	103.87	Li *et al.*, 2015
R35 (**24**)	unknown	38.43	Li *et al.*, 2015

2.4 α-Glucosidase

α-Glucosidase, an enzyme located on the surface membrane of intestinal cells, hydrolyzes oligosaccharide to absorbable monosaccharide, such as glucose. The result of inhibition of this enzyme is the reduction of postprandial glucose level,

one of the strategies of diabetes mellitus treatment especially type II (Lordan *et al.*, 2013). Current anti-α-glucosidase drugs include acarbose, miglitol and voglibose. These drugs, however, can cause several side effects, for example diarrhea, flatulence, abdominal pain and liver disorders (Peng *et al.*, 2016). Examples of *trans*-stilbenes with anti-α-glucosidase activity are shown in Table 3.

Table 3: Examples of *trans*-stilbenes with anti-α-glucosidase activity

Compound	Source	IC_{50} (μM)	Reference
Oxyresveratrol (**1**)	*Morus* sp.	32.80	He and Lu, 2013
Resveratrol (**2**)	Unknown	60.75	He and Lu, 2013
	Syagrus romanzoffiana Cham.	23.9	Lam *et al.*, 2008
Piceatannol (**25**)	*Syagrus romanzoffiana* Cham.	23.2	Lam *et al.*, 2008
3,3′,4,5,5′-Pentahydroxy-*trans*-stilbene (**26**)	*Syagrus romanzoffiana* Cham.	19.2	Lam *et al.*, 2008
4′-*O*-Methylpiceid (**27**)	*Rheum palmaturn* L.	693	Kubo *et al.*, 1991
Rhapontin (**28**)	*Rheum palmaturn* L.	1429	Kubo *et al.*, 1991

2.5 Cytotoxicity

Cancer is known as a major global health concern, causing death and affecting approximately 28.8 million people in 2008 (Roleira *et al.*, 2015). It involves cell physiological changes, leading to abnormal cell growth. The invasion of cancer cells to surrounding tissues and distant organs is the cause of morbidity and mortality of most cancer patients (Seyfried & Shelton, 2010). Several currently useful cancer

drugs are derived from plants, for example, vinblastine and vincristine from *Catharanthus roseus* G. Don. (Apocynaceae), paclitaxel from *Taxus brevifolia* Nutt. (Taxaceae), topotecan and irinotecan, developed from camptothecin from *Camptotheca acuminata* Decne. (Nyssaceae) (Cragg & Newman, 2005). Several natural and synthetic *trans*-stilbenes have been reported to possess significant cytotoxicity against cancer cells (Table 4).

Table 4: Examples of *trans*-stilbenes with cytotoxicity against cancer cells.

Compound	Source	Cell line	IC_{50} (μM)	Reference
Oxyresveratrol (**1**)	*Smilax china* L.	MCF-7	18.4	Wu *et al.*, 2010
		MDA-MB-231	22.9	Wu *et al.*, 2010
	Morus alba L.	HT-29	74.4	Li *et al.*, 2010
Resveratrol (**2**)	*Smilax china* L.	MCF-7	9.2	Wu *et al.*, 2010
		MDA-MB-231	12.7	Wu *et al.*, 2010
	Unknown	HT-29	152.1	Li *et al.*, 2010
Resveratrodehyde A (**5**)	*Alternaria* sp.	MDA-MB-435	8.6	Wang *et al.*, 2014
		HepG2	35.3	
		HCT-116	7.8	
Resveratrodehyde B (**6**)	*Alternaria* sp.	MDA-MB-435	7.7	Wang *et al.*, 2014
		HepG2	32.7	
		HCT-116	6.9	
Resveratrodehyde C (**7**)	*Alternaria* sp.	MDA-MB-435	16.5	Wang *et al.*, 2014
		HepG2	41.9	
		HCT-116	18.6	
Piceatannol (**25**)	Synthetic	HT-29	86.5	Li *et al.*, 2010

Table 4: Examples of *trans*-stilbenes with cytotoxicity against cancer cells (continued)

Compound	Source	Cell line	IC_{50} (μM)	Reference
3,3′,4,5,5′-Pentahydroxy-*trans*-stilbene (**26**)	Synthetic	HT-29	44.0	Li *et al.*, 2010
3,4,4′,5-Tetrahydroxy-*trans*-stilbene (**29**)	Synthetic	HT-29	75.5	Li *et al.*, 2010
3,3′,4,4′,5,5′-Hexahydroxy-*trans*-stilbene (**30**)	Synthetic	HT-29	57.6	Li *et al.*, 2010
Pterostilbene (**31**)	Unknown	COLO205	33.4	Cheng *et al.*, 2014
		HCT-116	47.1	
		HT-29	80.6	
3′-Hydroxyptero-stilbene (**32**)	Unknown	COLO205	9.0	Cheng *et al.*, 2014
		HCT-116	40.2	
		HT-29	70.9	
(*E*)-3,5-Difluoro-4′-acetoxystilbene (**33**)	Synthetic	HL-60	54.6	Moran *et al.*, 2009
		HT29	73.7	
		T-47D	79.8	
trans-2,3′-Dimethoxy-4,5′-dihydroxystilbene (**34**)	Synthetic	KB	5.5	Likhitwitayawuid *et al.*, 2006c
		BC	10.8	
		NCI-H187	10.9	
trans-2,3′,4,5′-Tetramethoxystilbene (**35**)	Synthetic	KB	8.6	Likhitwitayawuid *et al.*, 2006c
		BC	5.6	
		NCI-H187	8.0	

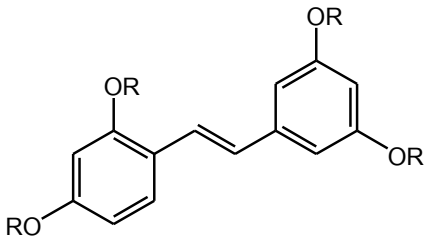

(1) = H

(35) = Me

(36) = COOEt

(37) = $CON(Et)_2$

(38) = $COCH_3$

(39) = 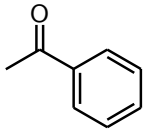

(40) = 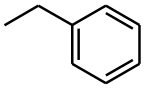

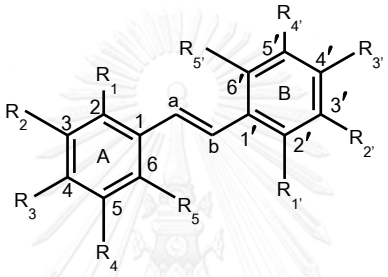

Cpd	R_1	R_2	R_3	R_4	R_5	$R_{1'}$	$R_{2'}$	$R_{3'}$	$R_{4'}$	$R_{5'}$
(2)	H	H	OH	H	H	H	OH	H	OH	H
(3)	OH	H	OGlc	H	H	H	H	H	OGlc	H
(4)	H	H	OH	H	H	H	H	H	H	H
(5)	H	H	OH	CHO	H	H	OH	H	OH	H
(6)	H	H	OH	CHO	H	H	OH	H	OH	CHO
(7)	H	H	OH	H	H	H	OH	H	OH	CHO
(8)	H	H	H	H	H	COOH	OH		OMe	H
(9)	H	OH	OMe	H	H	H	OH	F	OH	H
(10)	H	OH	OMe	H	F	H	OH	H	OH	H
(11)	H	OH	OMe	H	H	H	F	F	F	H
(12)	H	OMe	OMe	H	H	H	OH	F	OH	H
(13)	H	OH	OH	H	H	OH	H	H	OH	H
(14)	SO_3Na	H	S=C=N	H	H	SO_3Na	H	S=C=N	H	H
(15)	H	H	OH	OMe	H	H	OH	H	OH	H
(16)	H	H	OH	OMe	H	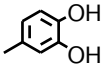	OH	H	OH	H

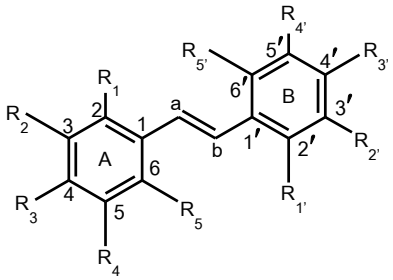

Cpd	R_1	R_2	R_3	R_4	R_5	$R_{1'}$	$R_{2'}$	$R_{3'}$	$R_{4'}$	$R_{5'}$
(17)	H	H	OH	H	H	H	OH	H	OGlc	H
(18)	H	OH	OH	OH	H	H	OH	H	OH	H
(19)	H	OH	OH	H	H	H	H	H	OH	H
(20)	H	H	OH	OH	H	H	OH	H	OH	H
(21)	H	OH	H	OH	H	H	OH	H	OH	H
(22)	H	H	H	OH	H	H	H	H	OH	H
(23)	H	OH	H	H	H	H	OH	H	OH	H
(24)	H	OH	H	H	H	H	OH	H	OH	H
(25)	H	OH	OH	H	H	H	OH	H	OH	H
(26)	H	OH	OH	OH	H	H	OH	H	OH	H
(27)	H	H	OMe	H	H	H	OGlc	H	OH	H
(28)	H	OH	OMe	H	H	H	OGlc	H	OH	H
(29)	H	H	OH	H	H	H	OH	OH	OH	H
(30)	H	OH	OH	OH	H	H	OH	OH	OH	H
(31)	H	H	OH	H	H	H	OMe	H	OMe	H
(32)	H	OH	OH	H	H	H	OMe	H	OMe	H
(33)	H	H	$OCOCH_3$	H	H	H	F	H	F	H
(34)	OMe	H	OH	H	H	H	OMe	H	OH	H

2.6 Chemistry

Recently, methods for the total synthesis of biologically important stilbenes, such as oxyresveratrol and resveratrol, have been described. Sun and co-workers reported the syntheses of the two compounds based on Perkin type reactions. The synthetic route consisted of five steps from the commercially available 3,5-

dihydoxyacetophenone (Sun *et al*., 2010). In a different approach, Galindo and his group presented a four-step preparation of oxyresveratrol, starting from the commercially available 3,5-dimethoxybenzyl bromide (Galindo *et al*., 2011). Both methods, however, required the demethylation and isomerization reactions of the *Z*-tetramethoxystilbene intermediate in the final step. In a more facile synthetic strategy, *trans*-stilbene derivatives with different substitution patterns were prepared using only two chemical reactions, i.e. Wittig reaction and Mizoroki-Heck reaction (Csuk *et al*., 2013). Various suitable substituted benzaldehydes can be used as substrates for Witttig reaction. First, the starting material was allowed to react with methyl triphenylphosphonium iodide and *t*-BuOK in THF to yield a styrene. Then the styrene was subjected to Mizoroki–Heck coupling reaction to give an (*E*)-configurated stilbene (Scheme 1).

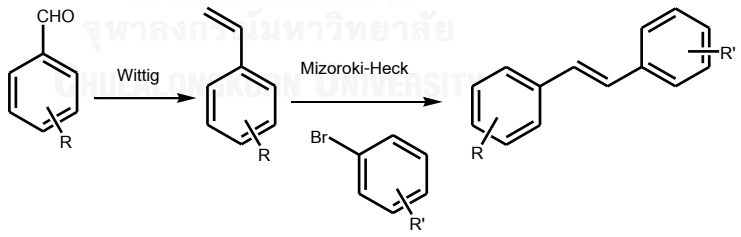

Scheme 1: Synthesis of trans-stilbene

Oxyresveratrol (**1**), with its tetrahydroxy structure, offers an alternative approach for the synthetic study of polyoxygenated stilbenes. In an earlier work, several *O*-alkylated/*O*-acylated derivatives were prepared from **1**, including *trans*-2,3′-dimethoxy-4,5′-dihydroxystilbene (**34**), *trans*-2,3′,4,5′-tetramethoxystilbene (**35**),

oxyresveratrol tetra-ethylcarbonate (**36**), oxyresveratrol tetradiethylcarbamate (**37**), oxyresveratrol tetra-acetate (**38**), oxyresveratrol tetrabenzoate (**39**) and tetra-*O*-phenylmethyl oxyresveratrol (**40**) (Sornsute, 2006). These compounds were then evaluated for tyrosinase inhibitory activity and cytotoxicity. The present investigation is a continuation of that effort, with the intention of obtaining more understanding of the chemistry and biological potential of polyoxygenated stilbenes. In addition to the simple etherification and esterification reactions of **1** using different alkylating/acylating agents, electrophilic aromatic substitution reactions of **1** and its *O*-alkylated/*O*-acylated products with a variety of electrophiles would also be investigated.

CHAPTER III

EXPERIMENTAL

3.1 Source of oxyresveratrol

Oxyresveratrol was isolated and purified from the heartwood of *Artocarpus lakoocha* Roxb. as previously reported (Sritularak *et al.*, 1988).

3.2 General Techniques

Reactions were run in oven-dried round-bottom flasks. The crude reaction mixtures were concentrated under reduced pressure by removing organic solvents on a rotary evaporator. Column chromatography was performed using silica gel 60 (particle size 0.06-0.2 mm; 70-230 mesh). Analytical thin-layer chromatography (TLC) was performed using silica gel 60 F_{254} aluminum sheets. Chemical shifts for ^{1}H nuclear magnetic resonance (NMR) spectra were reported in parts per million (ppm, δ) downfield from tetramethylsilane (TMS). Splittng patterns were described as singlet (s), doublet (d), triplet (t), quartet (q), septet (sept), multiplet (m), doublet of doublets (dd) and broad singlet (br s). Coupling constants were expressed as the *J* value in Herz (Hz). Resonances for infrared (IR) spectra were reported in wavenumber (cm^{-1}). Low resolution mass spectra (LRMS) were obtained using electron ionization (EI), while high resolution (HRMS) mass spectra were obtained using time-of-flight

(TOF) via the atmospheric-pressure chemical ionization (APCI) or electrospray ionization (ESI).

3.2.1 Reagents and Solvents

All organic solvents were of commercial grade and were redistilled prior to use. *N*-Chlorosuccinimide, 2-bromopropane, sodium chlorite and *p*-toluenesulfonic acid were purchased from Fluka. Methyl iodide, ethyl bromoacetate, phosphoryl chloride, hydrogen peroxide and boron tribromide were obtained from Merck. Acetyl chloride and boron trichloride were purchased from Acros. Potassium hydroxide, 2-methyl-2-butene and carbethoxymethylene triphenylphosphorane were purchased from Sigma-Aldrich. Poatassium carbonate was purchased from Qrec. Acetic anhydride was obtained from J.T. Baker. Glacial acetic acid was purchased from RCI Labscan. Sodium dihydrogen phosphate dihydrate was purchased from SIAL.

3.3 Structure modifications of oxyresveratrol

In this study, oxyresveratrol was chemically modified in 2 major directions (Scheme II), with the intention of obtaining analogues with more potent and selective biological activity.

The first line of tasks was involved with the alkylation and/or acylation of all/some of the four phenolic groups. It was anticipated that these reactions should give products with higher stability than the parent compound, which is prone to air-oxidation. The obtained *O*-alklylation/*O*-acylation products were then subjected to

biological evaluation to assess the effects of the phenolic/ether/ester functionalities on the potency and selectivity.

On the second line, efforts were made to place heteroatoms such as halogen and oxygen, as well as alkyl/acyl groups, onto the aromatic rings. The biological activities of the products were also investigated, and analyzed in terms of potency and selectivity.

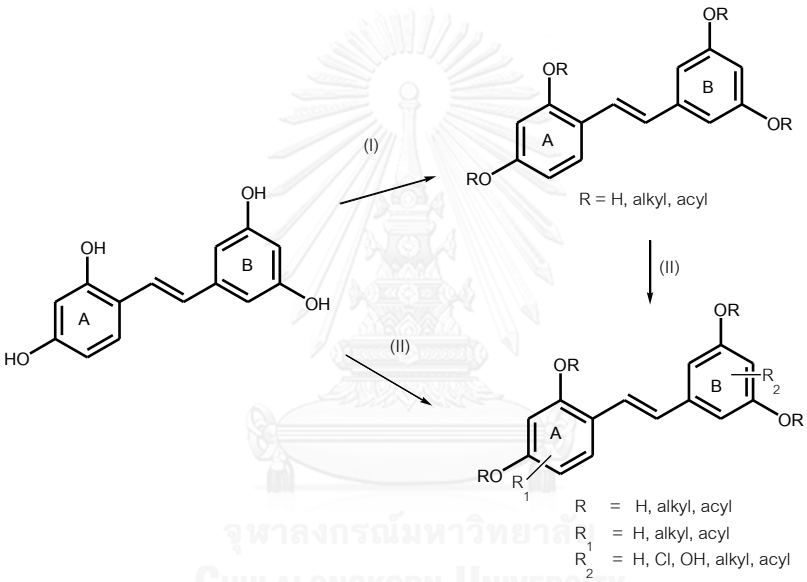

Scheme II

As summarized in scheme II, a total of 26 analogues were prepared from oxyresveratrol. The details of each step of chemical modifications are as follows.

3.3.1 Preparation of 2′-chloro oxyresveratrol (MC-1, 41)

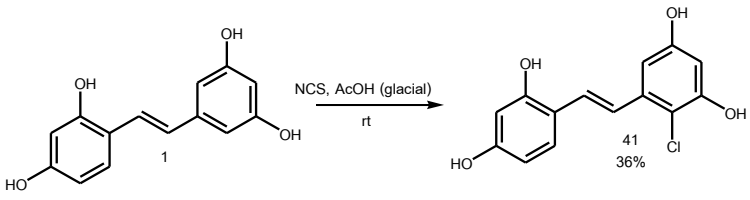

A mixture of oxyresveratrol (**1**) (100 mg, 0.41 mmol) and *N*-chlorosuccinimide (54.8 mg, 0.41 mmol) in glacial acetic acid (4 mL) was stirred at room temperature under argon for 3 h. The reaction was monitored by TLC (silica gel, 15% MeOH in CH_2Cl_2). After completion, solvent was removed under reduced pressure. Purification by column chromatography (Silica gel, 10% MeOH in CH_2Cl_2) gave 42 mg of MC-1 (**41**) (36% yield).

MC-1: IR (UATR) ν_{max} cm^{-1}: 3196, 1599 (Figure 5); EIMS: *m/z* 279 $[M+H]^+$ (Figure 6); HRMS: *m/z* 279.0408 $[M+H]^+$ (found) 279.0419 (calcd for $C_{14}H_{12}ClO_4$) (Figure 7); ^{1}H NMR (300 MHz, acetone-d_6): Table 5 (Figure 8); ^{13}C NMR (75 MHz, acetone-d_6): Table 6 (Figure 9).

3.3.2 Preparation of 2′-chloro-2,3′,4,5′-tetra-*O*-methyloxyresveratrol (MC-2, 42)

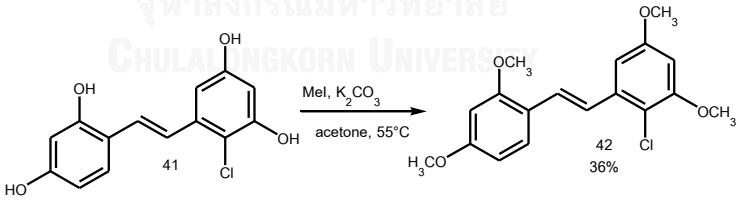

To a well-stirred solution of compound MC-1 (**41**) (88 mg, 0.3 mmol) in acetone (15 mL), potassium carbonate (K_2CO_3) (265 mg, 1.92 mmol) and methyl iodide (MeI) (0.11 mL, 1.8 mmol) were added. The reaction mixture was stirred at 55°C overnight and monitored by TLC. After completion of the reaction, the mixture was diluted with water, and extracted with EtOAc (3x10mL). The organic phase was

washed with brine. The organic extract was dried over anhydrous sodium sulfate (Na_2SO_4), filtered and evaporated *in vacuo*. The residue obtained was purified over silica gel using 20% EtOAc in hexanes resulting in separation of MC-2 (**42**) (40 mg, 36%).

MC-2: EIMS: *m/z* 334 $[M]^+$ (Figure 10); HRMS: *m/z* 335.1035 $[M]^+$ (found) 335.1045 (calcd for $C_{18}H_{20}ClO_4$) (Figure 11); ^{1}H NMR (300 MHz, $CDCl_3$): Table 5 (Figure 12); ^{13}C NMR (75 MHz, $CDCl_3$): Table 6 (Figure 13)

3.3.3 Preparation of 2,3′,4,5′-tetra-*O*-isopropyloxyresveratrol (MC-3, 43), 2,3′,4,-tri-*O*-isopropyloxyresveratrol (MC-4, 44) and 2,4-di-*O*-isopropyloxyresveratrol (MC-5, 45)

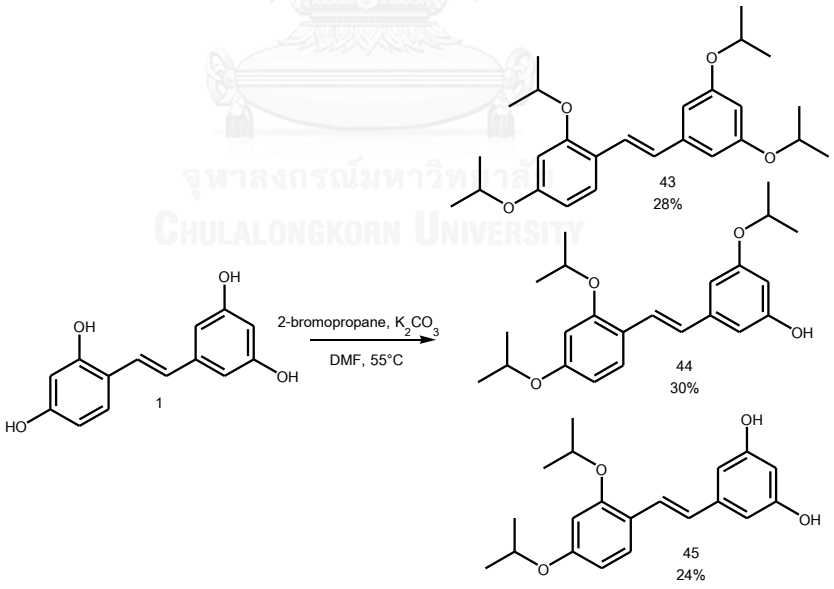

To a mixture of oxyresveratrol (**1**) (100 mg, 0.41 mmol) in dimethylformamide (DMF) (2 mL), K_2CO_3 (283 mg, 2.05 mmol) and 2-bromopropane (2.30 mL, 24.6 mmol) were added. Then 2-bromopropane (1.15 mL, 12.3 mmol) was added every 24 h. The

reaction mixture was stirred at 55°C for 3 days and monitored by TLC. After completion, water (5 mL) was added and the reaction was extracted with EtOAc (3x5mL). The organic phase was washed with water (7x5mL) and brine, dried over anhydrous sodium sulfate (Na_2SO_4), filtered and concentrated. Column chromatographic purification with gradient EtOAc/hexanes gave MC-3 (**43**) (47 mg, 28%), MC-4 (**44**) (46 mg, 30%) and MC-5 (**45**) (32 mg, 24%).

MC-3: IR (UATR) ν_{max} cm^{-1}; 2976, 1585 (Figure 14); EIMS: *m/z* 412 $[M]^+$ (Figure 15); HRMS: *m/z* 413.2679 $[M+H]^+$ (found) 413.2686 (calcd for $C_{26}H_{37}O_4$) (Figure 16); ^1H NMR (300 MHz, $CDCl_3$): Table 5 (Figure 17); ^{13}C NMR (75 MHz, $CDCl_3$): Table 6 (Figure 18)

MC-4: IR (UATR) ν_{max} cm^{-1} ; 3393,2976,1588 (Figure 19); EIMS: *m/z* 370 $[M]^+$ (Figure 20); HRMS: *m/z* 369.2066 $[M-H]^-$ (found) 369.2071 (calcd for $C_{23}H_{29}O_4$) (Figure 21); ^1H NMR (400 MHz, $CDCl_3$): Table 5 (Figure 22); ^{13}C NMR (100 MHz, $CDCl_3$): Table 6 (Figure 23)

MC-5: IR (UATR) ν_{max} cm^{-1}; 3379, 2976, 1598 (Figure 24); EIMS: *m/z* 328 $[M]^+$ (Figure 25); HRMS: *m/z* 327.1594 $[M-H]^-$ (found) 327.1602 (calcd for $C_{20}H_{23}O_4$) (Figure 26); ^1H NMR (400 MHz, $CDCl_3$): Table 5 (Figure 27); ^{13}C NMR (100 MHz, $CDCl_3$): Table 6 (Figure 28)

3.3.4 Preparation of 2,3′,4,5′-tetra-*O*-methyloxyresveratrol (MC-6, 35), 2,3′,4-tri-*O*-methyloxyresveratrol (MC-7, 46), 2,4-di-*O*-methyl oxyresveratrol (MC-8, 47)

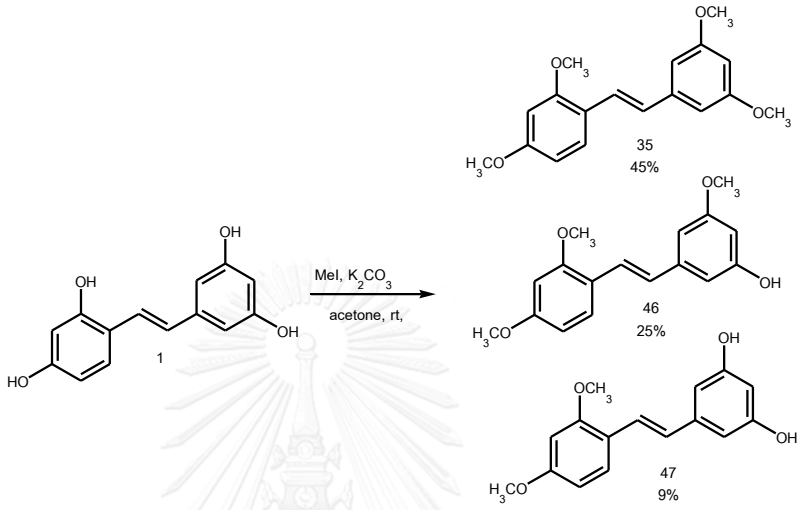

K_2CO_3 (680 mg, 4.92 mmol) and methyl iodide (0.11 mL, 1.8 mmol) were added to the solution of oxyresveratrol (**1**) (200 mg, 0.82 mmol) in acetone (4 mL) at room temperature. The reaction mixture was stirred overnight. Then, the reaction mixture was diluted with water and extracted with EtOAc (3x5mL). The EtOAc layer was washed with brine, dried over anhydrous Na_2SO_4, filtered and concentrated under reduced pressure to give a crude product which, after purification by preparative TLC (50% EtOAc/hexanes), furnished MC-6 (**35**) (112 mg, 45%), MC-7 (**46**) (60 mg, 25%) and MC-8 (**47**) (19 mg, 9%).

MC-6: HRMS: *m/z* 301.1440 $[M+H]^+$ (found) 301.1434 (calcd for $C_{18}H_{21}O_4$) (Figure 31); ^{1}H NMR (300 MHz, $CDCl_3$): Table 5 (Figure 32); ^{13}C NMR (75 MHz, $CDCl_3$): Table 6 (Figure 33)

MC-7: IR (UATR) ν_{max} cm^{-1}; 3408, 2938, 1590 (Figure 34); EIMS: *m/z* 286 $[M]^+$ (Figure 35); HRMS: *m/z* 287.1285 $[M+H]^+$ (found) 287.1278 (calcd for $C_{17}H_{19}O_4$) (Figure 36); ^1H NMR (300 MHz, $CDCl_3$): Table 5 (Figure 37); ^{13}C NMR (75 MHz, $CDCl_3$): Table 6 (Figure 38)

MC-8: IR (UATR) ν_{max} cm^{-1}; 3374, 2931, 1601 (Figure 40); EIMS: *m/z* 272 $[M]^+$ (Figure 41); HRMS: *m/z* 273.1118 $[M+H]^+$ (found) 273.1121 (calcd for $C_{16}H_{17}O_4$) (Figure 42); ^1H NMR (300 MHz, $CDCl_3$): Table 5 (Figure 43); ^{13}C NMR (75 MHz, $CDCl_3$): Table 6 (Figure 44)

3.3.5 Preparation of 2,3′,4,5′-tetra-*O*-acetyloxyresveratrol (MC-9, 38)

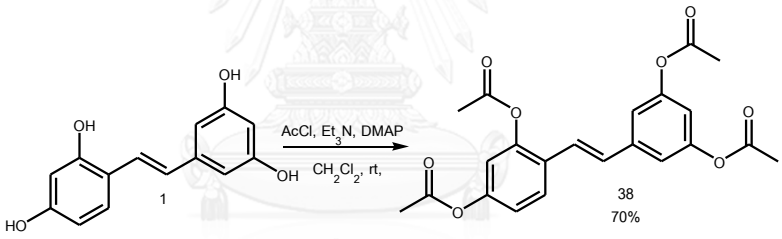

To a well stirred solution of oxyresveratrol (**1**) (50 mg, 0.21 mmol) in CH_2Cl_2 (2 mL), Et_3N (0.17 mL, 1.23 mmol), 4-dimethylaminopyridine (DMAP) (63 mg, 0.51 mmol) and acetyl chloride (0.04 mL, 0.61 mmol) were added at room temperature and the reaction mixture was stirred for 3 h. After completion of the reaction, it was extracted with EtOAc (3x5mL). The EtOAc layer was washed with brine, dried over anhydrous Na_2SO_4, filtered and concentrated under reduced pressure to give a crude product. Purification with column chromatography eluting with 40% EtOAc in hexanes gave MC-9 (**38**) (60 mg, 70%).

MC-9: IR (UATR) ν_{max} cm^{-1}; 1762, 1605 (Figure 46); HRMS: *m/z* 435.1050 $[M+Na]^+$ (found) 435.1050 (calcd for $C_{22}H_{20}NaO_8$) (Figure 47); ^1H NMR (300 MHz, $CDCl_3$): Table 5 (Figure 48); ^{13}C NMR (75 MHz, $CDCl_3$): Table 6 (Figure 49)

3.3.6 Preparation of 3′-*O*-carbethoxymethyl-2,4,5′-tri-*O*-isopropyloxyresveratrol (MC-10, 48)

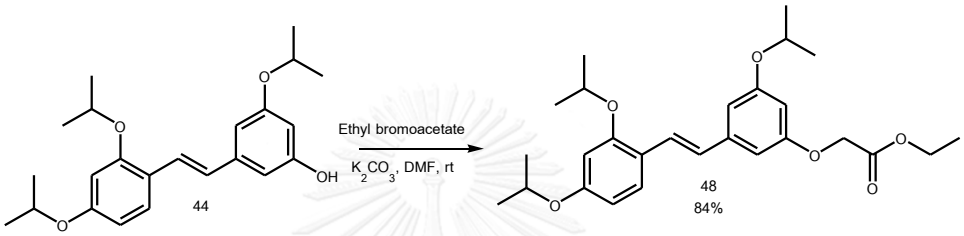

To a mixture of MC-4 (**44**) (100 mg, 0.27 mmol) in DMF (4 mL), K_2CO_3 (56 mg, 0.40 mmol) and ethyl bromoacetate (0.04 mL, 0.4 mmol) were added at room temperature and the reaction was stirred overnight. After completion of the reaction, water (5 mL) was added and the mixture was extracted with EtOAc (3x5mL). The organic layer was washed with water (7x5mL) and brine, dried over anhydrous sodium sulfate (Na_2SO_4), filtered and concentrated under reduced pressure to give a crude product, which was purified by column chromatography on silica (15% EtOAc/hexanes) to furnish MC-10 (**48**) (103 mg, 84%).

MC-10: IR (UATR) ν_{max} cm^{-1}; 2976, 1759, 1587 (Figure 50); EIMS: *m/z* 456 $[M]^+$ (Figure 51); HRMS: *m/z* 479.2388 $[M+Na]^+$ (found) 479.2404 (calcd for $C_{27}H_{36}NaO_6$) (Figure 52); ^1H NMR (300 MHz, $CDCl_3$): Table 5 (Figure 53); ^{13}C NMR (75 MHz, $CDCl_3$): Table 6 (Figure 54)

3.3.7 Preparation of 3′-*O*-carbethoxymethyl oxyresveratrol (MC-11, 49)

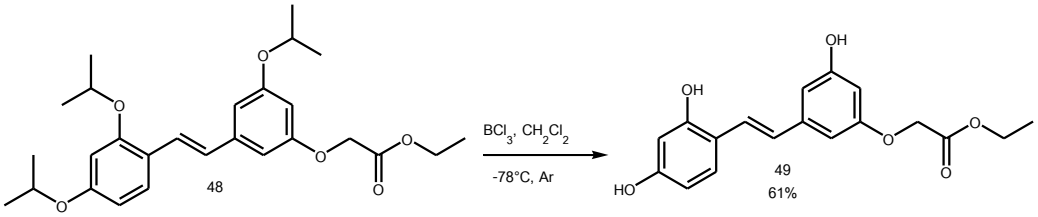

A solution of BCl_3 (3.07 mL, 3. 07 mmol) was added to a solution of MC-10 (**48**) (233 mg, 0.51 mmol) in CH_2Cl_2 (8 mL) at -78°C under argon. Then it was allowed to warm to room temperature and stirred overnight. The reaction mixture was quenched with water (10 mL) and then extracted with EtOAc (3x10mL). The organic phase was washed with brine, dried over anhydrous Na_2SO_4, filtered and concentrated under reduced pressure to give a crude product which was purified by preparative TLC (50% EtOAc/hexanes) to give MC-11 (**49**) (102mg, 61%).

MC-11: IR (UATR) ν_{max} cm^{-1}; 3369, 1731, 1591 (Figure 55); HRMS: *m/z* 353.0989 $[M+Na]^+$ (found) 353.0996 (calcd for $C_{18}H_{18}NaO_6$) (Figure 56); ^1H NMR (300 MHz, acetone-d_6): Table 5 (Figure 57); ^{13}C NMR (75 MHz, acetone-d_6): Table 6 (Figure 58)

3.3.8 Preparation of 3′-*O*-carboxymethyl oxyresveratrol (MC-12, 50)

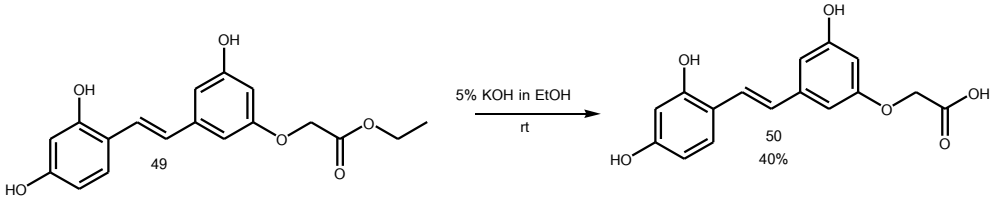

To MC-11 (**49**) (13 mg, 0.03 mmol), 1 mL of 5% potassium hydroxide (KOH) in ethanol (EtOH) was added at room temperature and the reaction mixture was stirred for 10 min. The reaction was acidified with 2 N hydrochloric acid (HCl) to pH 5. The material was extracted with EtOAc (3x5mL), and the combined organic layers were dried over Na_2SO_4, filtered, and concentrated under reduced pressure to provide MC-12 (**50**) (3 mg, 40%).

MC-12: IR (UATR) ν_{max} cm-1 ; 3322, 2921, 2851, 1713 (Figure 59); HRMS: *m/z* 301.0708 $[M-H]^-$ (found) 301.0718 (calcd for $C_{16}H_{13}O_6$) (Figure 60); ^{1}H NMR (300 MHz, methanol-d_4): Table 5 (Figure 61); ^{13}C NMR (75 MHz, methanol-d_4): Table 6 (Figure 62)

3.3.9 Preparation of 3′,5′-di-*O*-acetyl-2,4-di-*O*-isopropyloxyresveratrol (MC-13, 51)

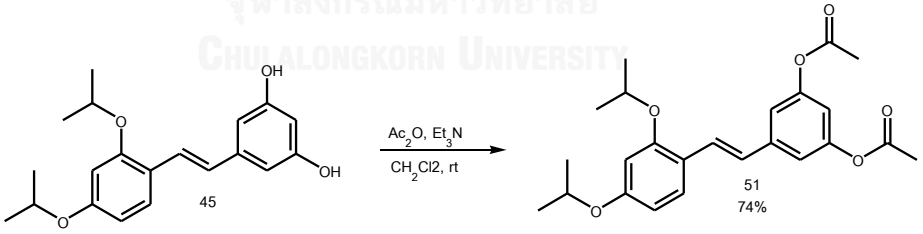

Triethylamine (Et_3N) (0.05 mL, 0.33 mmol) and acetic anhydride (0.03 mL, 0.33 mmol) were added to a solution of MC-5 (**45**) (50 mg, 0.15 mmol) in CH_2Cl_2 (2 mL) at room temperature. The reaction mixture was stirred for 2 h. Water (5 mL) was added, and the reaction mixture was extracted with EtOAc (3x5mL). The organic phase was washed with brine, dried over anhydrous Na_2SO_4, filtered and concentrated under

reduced pressure to give a crude product. Purification with column chromatography eluting with 20% EtOAc in hexanes gave MC-13 (**51**) (46 mg, 74%).

MC-13: IR (UATR) ν_{max} cm^{-1}; 2978, 1768, 1599 (Figure 63); EIMS: *m/z* 412 $[M]^+$ (Figure 64); HRMS: *m/z* 435.1796 $[M+Na]^+$ (found) 435.1778 (calcd for $C_{24}H_{28}NaO_6$) (Figure 65); ^1H NMR (300 MHz, $CDCl_3$): Table 5 (Figure 66); ^{13}C NMR (75 MHz, $CDCl_3$): Table 6 (Figure 67)

3.3.10 Preparation of 2′-formyl-2,3′,4,5′-tetra-*O*-isopropyloxyresveratrol (MC-14, 52)

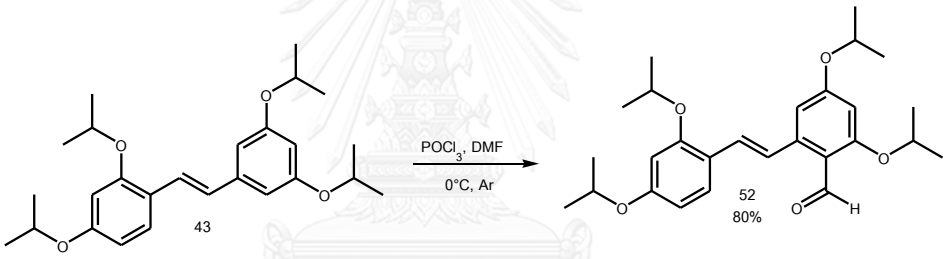

Phosphoryl chloride ($POCl_3$) (0.16 mL, 1.69 mmol) was stirred with dry DMF (4 mL) at room temperature for 2 h under argon. A solution of MC-3 (**43**) (200 mg, 0.48 mmol) in dry DMF (4 mL) was added at 0°C and the reaction mixture was further stirred overnight. After completion of the reaction, cool water (10 mL) was added and extracted with EtOAc (3x10mL). The organic layer was washed with water (7x10mL) and brine, dried over anhydrous sodium sulfate (Na_2SO_4), filtered and concentrated under reduced pressure to give a crude product, which was purified by column chromatography on silica (15% EtOAc/hexanes) to furnish MC-14 (**52**) (171 mg, 80%).

MC-14: IR (UATR) ν_{max} cm^{-1}; 2976, 1671, 1586 (Figure 68); EIMS: *m/z* 440 $[M]^+$ (Figure 69); HRMS: *m/z* 441.2639 $[M+H]^+$ (found) 441.2635 (calcd for $C_{27}H_{37}O_5$) (Figure 70); ^1H NMR (300 MHz, $CDCl_3$): Table 5 (Figure 71); ^{13}C NMR (75 MHz, $CDCl_3$): Table 6 (Figure 72)

3.3.11 Preparation of 2′-carboxy-2,3′,4,5′-tetra-*O*-isopropyloxyresveratrol (MC-15, 53)

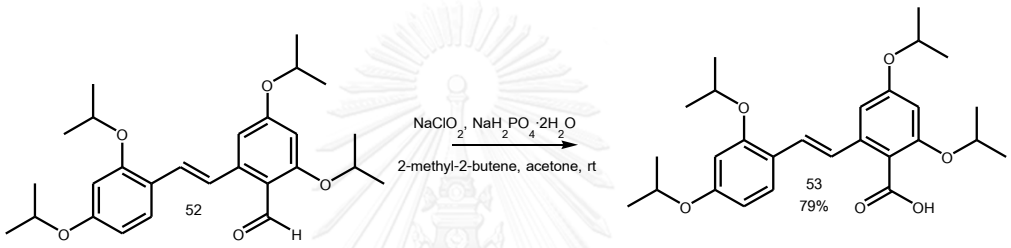

A solution of sodium chlorite ($NaClO_2$) (260 mg, 2.88 mmol) and sodium dihydrogen phosphate dihydrate ($NaH_2PO_4{\cdot}2H_2O$) (447 mg, 2.86 mmol) in water (1.5 mL) was added to the solution of MC-14 (**52**) (157 mg, 0.36 mmol) and 2-methyl-2-butene (0.13 mL, 1.5 mmol) in acetone (1.5 mL) at room temperature. The reaction mixture was stirred for 1 h, and monitored by TLC. After completion, water (5 mL) was added and the reaction mixture was extracted with EtOAc (3x5mL). The EtOAc phase was washed with brine, dried over anhydrous Na_2SO_4, filtered and concentrated under reduced pressure to give crude product, which was purified by column chromatography on silica (40% EtOAc/hexane) to furnish MC-15 (**53**) (129 mg, 79%).

MC-15: IR (UATR) ν_{max} cm^{-1}; 2976, 1730, 1697, 1592 (Figure 73); EIMS: *m/z* 456 $[M]^+$ (Figure 74); HRMS: *m/z* 457.2587 $[M+H]^+$ (found) 441.2635 (calcd for $C_{27}H_{37}O_6$) (Figure 75); ^{1}H NMR (300 MHz, $CDCl_3$): Table 5 (Figure 76); ^{13}C NMR (75 MHz, $CDCl_3$): Table 6 (Figure 77)

3.3.12 Preparation of 3-(2,4-dihydroxyphenyl)-6,8-dihydroxyisochroman-1-one (MC-16, 54)

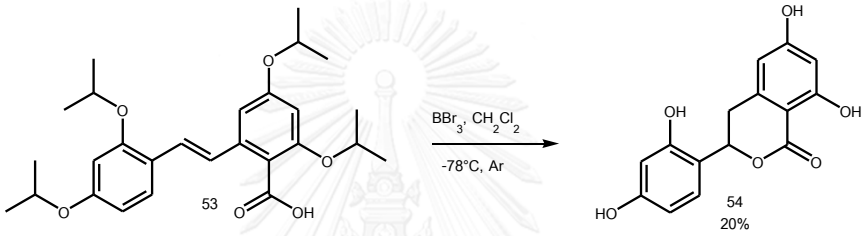

To a solution of MC-15 (**53**) (104 mg, 0.23 mmol) in dry CH_2Cl_2 (2 mL), a solution of boron tribromide (BBr_3) (0.96 mL, 0.96 mmol) in CH_2Cl_2 was added under argon at -78°C, and the mixture was stirred for 20 min. After completion of the reaction, the mixture was extracted with EtOAc (3x5mL). The organic phase was washed with brine, dried over anhydrous Na_2SO_4, filtered and concentrated under reduced pressure to give a crude product. Purification with column chromatography eluting with 5% methanol in CH_2Cl_2 gave MC-16 (**54**) (13 mg, 20%).

MC-16: IR (UATR) ν_{max} cm^{-1}; 3340, 3190, 1611 (Figure 78); EIMS: *m/z* 288 $[M]^+$ (Figure 79); HRMS: *m/z* 311.0529 $[M+Na]^+$ (found) 311.0526 (calcd for $C_{15}H_{12}NaO_6$) (Figure 80); ^{1}H NMR (300 MHz, acetone-d_6): Table 5 (Figure 81); ^{13}C NMR (75 MHz, acetone-d_6): Table 6 (Figure 82)

3.3.13 Preparation of 2′-formyloxyresveratrol (MC-17, 55)

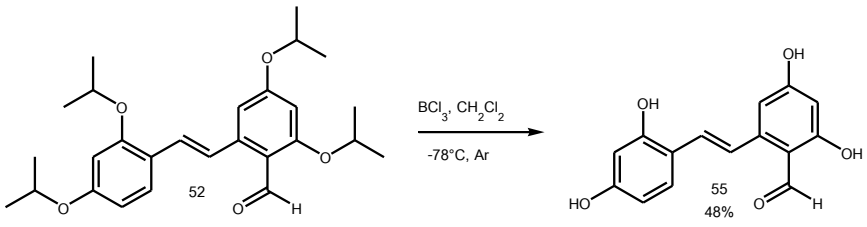

A solution of boron trichloride (BCl_3) (2.17 mL, 2.17 mmol) was added to a solution of MC-14 (**52**) (119 mg, 0.27 mmol) in CH_2Cl_2 (4 mL) at -78°C under argon. The reaction was allowed to warm up to room temperature and stirred overnight. Then, water (5mL) was added, and the reaction was extracted with EtOAc (3x5mL). The EtOAc phase was washed with brine, dried over anhydrous Na_2SO_4, filtered and concentrated under reduced pressure to give a crude product which was purified by using preparative TLC (40% EtOAc/hexanes) to give MC-17 (**55**) (35 mg, 48%).

MC-17: IR (UATR) ν_{max} cm^{-1}; 3337, 1602 (Figure 84); EIMS: *m/z* 149 (Figure 85); HRMS: *m/z* 271.0607 $[M-H]^-$ (found) 271.0612 (calcd for $C_{15}H_{11}O_5$) (Figure 86); ^{1}H NMR (300 MHz, methanol-d_4): Table 5 (Figure 87); ^{13}C NMR (75 MHz, methanol-d_4): Table 6 (Figure 88)

3.3.14 Preparation of 2′-hydroxy-2,3′,4,5′-tetra-*O*-isopropyloxyresveratrol (MC-18, 56)

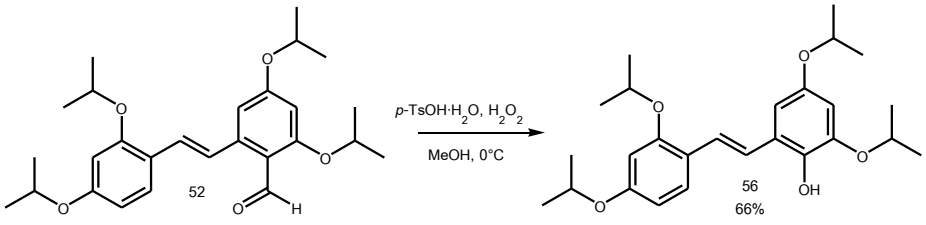

Compound MC-14 (**52**) (121 mg, 0.27 mmol) and *p*-toluenesulfonic acid monohydrate (*p*-TsOH·H_2O) (15 mg, 0.09 mmol) were dissolved in methanol (1 mL). Then 30% hydrogen peroxide (0.07 mL, 0.54 mmol) was added at 0°C, and the reaction was then warmed to room temperature and stirred for 1 h. Half-saturated sodium sulfite solution was added and the mixture was extracted with CH_2Cl_2 (3x5mL). The organic phase was washed with brine, dried over anhydrous Na_2SO_4, filtered and concentrated under reduced pressure to give a crude product. Purification with preparative TLC (10% EtOAc/hexanes) gave MC-18 (**56**) (78 mg, 66% yield).

MC-18: IR (UATR) ν_{max} cm^{-1}; 3536, 2975, 1600 (Figure 89); EIMS: *m/z* 428 $[M]^+$ (Figure 90); HRMS: *m/z* 429.2643 $[M+H]^+$ (found) 429.2635 (calcd for $C_{26}H_{37}O_5$) (Figure 91); ^{1}H NMR (300 MHz, $CDCl_3$): Table 5 (Figure 92); ^{13}C NMR (75 MHz, $CDCl_3$): Table 6 (Figure 93)

3.3.15 Preparation of 2′-(*E*)-carbethoxyethenyl-2,3′,4,5′-tetra-*O*-isopropyloxyresveratrol (MC-19, 57)

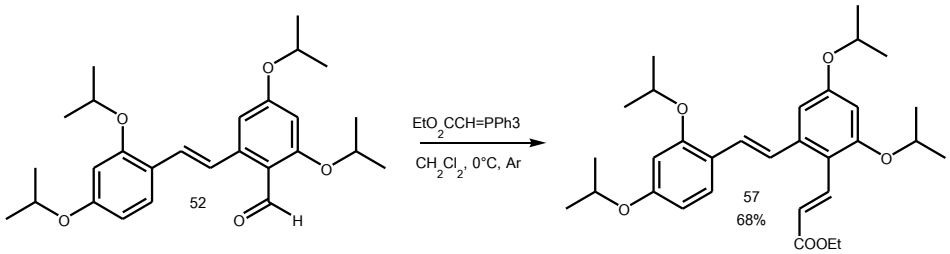

A solution of MC-14 (**52**) in dry CH_2Cl_2 (4 mL) was added to ethoxycarbonylmethylenetriphenylphosphorane ($EtO_2CCH=PPh_3$) (176 mg, 0.51

mmol) at 0°C under argon. Then the reaction mixture was allowed to warm to room temperature and stirred overnight. After completion of the reaction, water (5 mL) was added and the mixture was extracted with EtOAc (3x5mL). The organic layer was washed with brine, dried over anhydrous Na_2SO_4, filtered and concentrated under reduced pressure to give a crude product. Purification with column chromatography eluting with 50% CH_2Cl_2 in hexanes gave MC-19 (**57**) (134 mg, 68%).

MC-19: IR (UATR) ν_{max} cm^{-1}; 2977, 2932, 1706, 1589 (Figure 94); HRMS: *m/z* 511.3077 $[M+H]^+$ (found) 511.3054 (calcd for $C_{31}H_{43}O_6$) (Figure 95); ^1H NMR (300 MHz, $CDCl_3$): Table 5 (Figure 96); ^{13}C NMR (75 MHz, $CDCl_3$): Table 6 (Figure 97)

3.3.16 Preparation of 3′,5′-di-*O*-acetyl-5-formyl-2,4-di-*O*-isopropyloxyresveratrol (MC-20, 58)

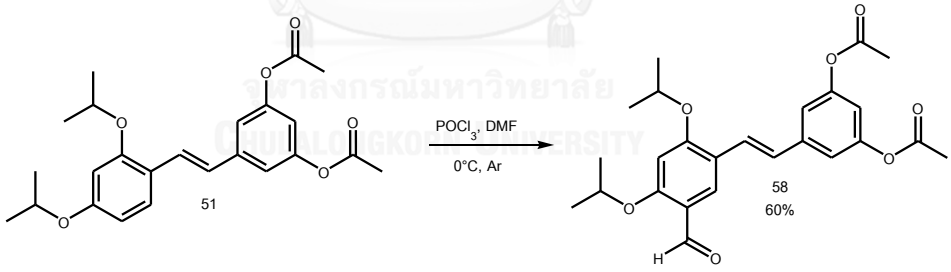

Phosphoryl chloride ($POCl_3$) (0.16 mL, 1.77 mmol) was stirred with dry DMF (1 mL) at room temperature for 2 h under argon. The solution of MC-13 (**51**) (73 mg, 0.18 mmol) in dry DMF (1 mL) was added at 0°C. Then the reaction mixture was allowed to warm to room temperature and stirred overnight. After completion of the reaction, cool water (5 mL) was added and the reaction mixture was extracted with EtOAc (3x5mL). The organic layer was washed with water (7x5mL) and brine, dried

over anhydrous sodium sulfate (Na_2SO_4), filtered and concentrated under reduced pressure to give a crude product, which was purified by preparative TLC (20% EtOAc/hexanes) to furnish MC-20 (**58**) (46 mg, 60%).

MC-20: IR (UATR) ν_{max} cm^{-1}; 2979, 1768, 1671, 1593 (Figure 98); EIMS: *m/z* 440 $[M]^+$ (Figure 99); HRMS: *m/z* 463.1743 $[M+Na]^+$ (found) 463.1727 (calcd for $C_{25}H_{28}NaO_7$) (Figure 100); ^1H NMR (300 MHz, $CDCl_3$): Table 5 (Figure 101); ^{13}C NMR (75 MHz, $CDCl_3$): Table 6 (Figure 102)

3.3.17 Preparation of 3′,5′-di-*O*-acetyl-5-carboxy-2,4-di-*O*-isopropyloxyresveratrol (MC-21, 59)

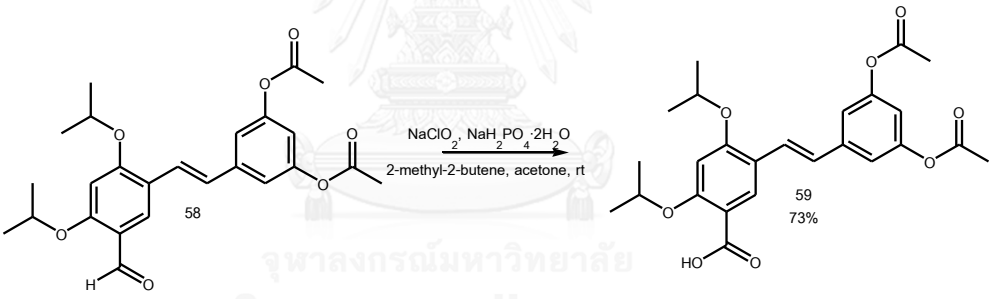

A solution of $NaClO_2$ (85 mg, 0.93 mmol) and $NaH_2PO_4{\cdot}2H_2O$ (145 mg, 0.93 mmol) in water (0.5 mL) was added to a solution of MC-20 (**58**) (51 mg, 0.12 mmol) and 2-methyl-2-butene (0.04 mL, 0.49 mmol) in acetone (0.5 mL) at room temperature. The reaction mixture was stirred for 1 h, and monitored by TLC. After completion, water (5 mL) was added and the reaction mixture was extracted with EtOAc (3x5mL). The organic layer was washed with brine, dried over anhydrous Na_2SO_4, filtered and concentrated under reduced pressure to give a crude product,

which was purified by column chromatography on silica (40% EtOAc/hexanes) to furnish MC-21 (**59**) (39 mg, 73%).

MC-21: IR (UATR) ν_{max} cm^{-1}; 3267, 2980, 1769, 1732, 1601 (Figure 103); EIMS: *m/z* 456 $[M]^+$ (Figure 104); HRMS: *m/z* 479.1695 $[M+Na]^+$ (found) 479.1676 (calcd for $C_{25}H_{28}NaO_8$) (Figure 105); ^1H NMR (300 MHz, $CDCl_3$): Table 5 (Figure 106); ^{13}C NMR (75 MHz, $CDCl_3$): Table 6 (Figure 107)

3.3.18 Preparation of 5-formyloxyresveratrol (MC-22, 60)

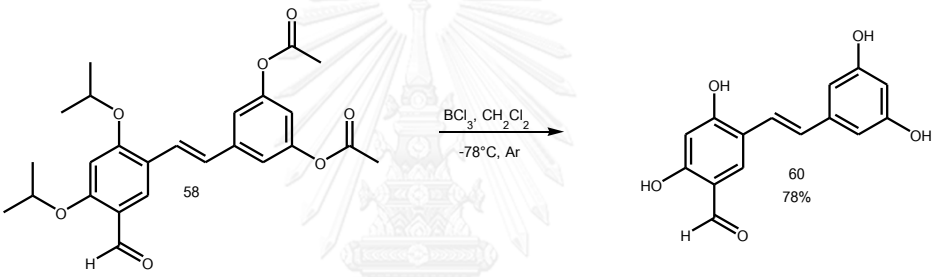

A solution of BCl_3 (0.42 mL, 0.42 mmol) was added to a solution of MC-20 (**58**) (30 mg, 0.07 mmol) in CH_2Cl_2 (2 mL) at -78°C under argon. Then it was allowed to warm to room temperature and stirred overnight. Water (5 mL) was then added and the reaction mixture was extracted with EtOAc (3x5mL). The EtOAc was washed with brine, dried over anhydrous Na_2SO_4, filtered and concentrated under reduced pressure to give a crude product which was purified by preparative TLC (40% EtOAc/hexanes) to give MC-22 (**60**) (15 mg, 78%).

MC-22: IR (UATR) ν_{max} cm^{-1}; 3208, 1626 (Figure 108); EIMS: *m/z* 272 $[M]^+$ (Figure 109); HRMS: *m/z* 271.0603 $[M-H]^-$ (found) 271.0612 (calcd for $C_{15}H_{11}O_5$) (Figure 110);

^{1}H NMR (300 MHz, methanol-d_4): Table 5 (Figure 111); ^{13}C NMR (75 MHz, methanol-d_4): Table 6 (Figure 112)

3.3.19 Preparation of 5-carboxyoxyresveratrol (MC-23, 61)

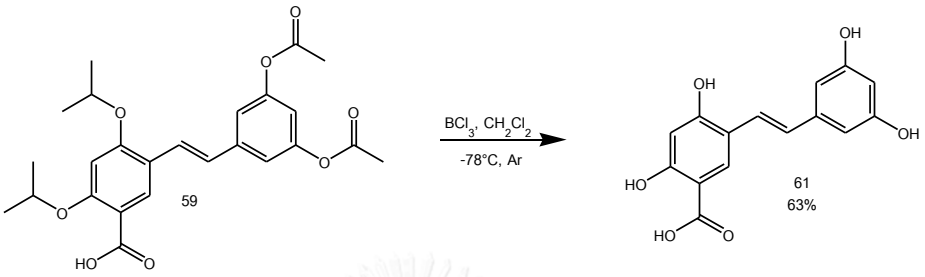

A solution of BCl_3 (0.88 mL, 0.88 mmol) was added to a solution of MC-21 (**59**) (68 mg, 0.15 mmol) in CH_2Cl_2 (2 mL) at -78°C under argon. Then the reaction was allowed to warm to room temperature and stirred overnight. Water (5 mL) was added and the mixture was extracted with EtOAc (3x5mL). The organic layer was washed with brine, dried over anhydrous Na_2SO_4, filtered and concentrated under reduced pressure to give a crude product which was purified by Sephadex LH20 (methanol) to give MC-23 (**61**) (27 mg, 63%).

MC-23: IR (UATR) ν_{max} cm^{-1}; 3337, 1616 (Figure 113); EIMS: *m/z* 288 $[M]^+$ (Figure 114); HRMS: *m/z* 287.0549 $[M-H]^-$ (found) 287.0561 (calcd for $C_{15}H_{11}O_6$) (Figure 115); ^{1}H NMR (300 MHz, methanol-d_4): Table 5 (Figure 116); ^{13}C NMR (75 MHz, methanol-d_4): Table 6 (Figure 117)

3.3.20 Preparation of 5-formyl-2,4-di-*O*-isopropyloxyresveratrol (MC-24, 62)

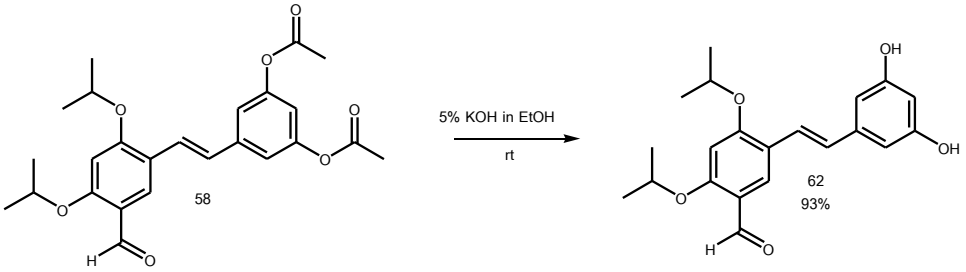

To MC-20 (**58**) (59 mg, 0.12 mmol), 5% potassium hydroxide (KOH) in ethanol (EtOH) was added at room temperature and the reaction mixture was stirred for 10 min. After completion of the reaction, the reaction was extracted with EtOAc (3x5mL). The EtOAc phase was washed with brine, dried over anhydrous Na_2SO_4, filtered and concentrated under reduced pressure to give a crude product. Purification with column chromatography eluting with 50% EtOAc in hexanes gave MC-24 (**62**) (41 mg, 93% yield).

MC-24: IR (UATR) ν_{max} cm^{-1}; 3525, 2976, 1766 (Figure 118); EIMS: *m/z* 356 $[M]^+$ (Figure 119); HRMS: *m/z* 357.1712 $[M+H]^+$ (found) 357.1696 (calcd for $C_{21}H_{25}O_5$) (Figure 120); ^{1}H NMR (300 MHz, acetone-d_6): Table 5 (Figure 121); ^{13}C NMR (75 MHz, acetone-d_6): Table 6 (Figure 122)

3.3.21 Preparation of 5-carboxy-2,4-di-*O*-isopropyloxyresveratrol (MC-25, 63)

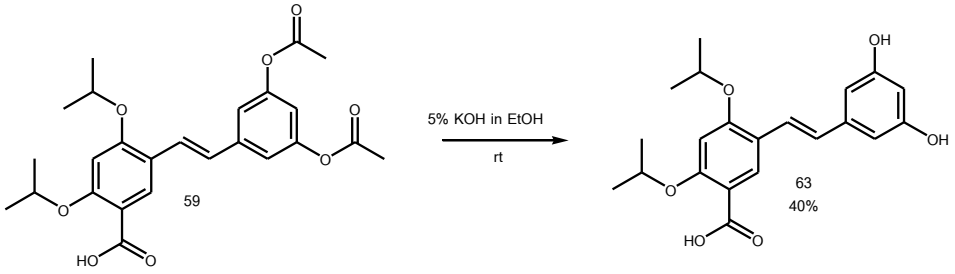

To MC-21 (**59**) (30 mg, 0.07 mmol), 5% potassium hydroxide (KOH) in ethanol (EtOH) was added at room temperature and the reaction mixture was stirred for 10 min. The reaction was acidified with 2 N HCl to pH 5. The material was extracted with EtOAc (3x5mL), and the combined organic layers were dried over Na_2SO_4, filtered, and concentrated under reduced pressure to provide MC-25 (**63**) (10 mg, 40%).

MC-25: HRMS: *m/z* 357.1712 $[M+H]^+$ (found) 357.1696 (calcd for $C_{21}H_{25}O_5$) (Figure 123);

^{1}H NMR (300 MHz, acetone-d_6): Table 5 (Figure 124); ^{13}C NMR (75 MHz, acetone-d_6): Table 6 (Figure 125)

3.3.22 Preparation of 3′,5′-di-*O*-acetyl-5-hydroxy-2,4-di-*O*-isopropyloxyresveratrol (MC-26, 64)

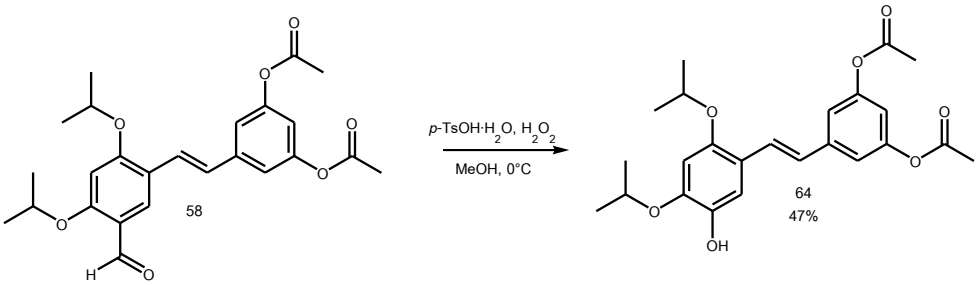

A solution of 30% hydrogen peroxide (0.03 mL, 0.192 mmol) was added to a methanolic mixture of MC-14 (**58**) (44 mg, 0.10 mmol) and *p*-TsOH·H_2O (5 mg, 0.03 mmol) at 0°C. The reaction mixture was allowed to warm to room temperature and stirred for 1 h. Half-saturated sodium sulfite solution (1 mL) was added and the mixture was extracted with CH_2Cl_2 (3x5mL). The CH_2Cl_2 layer was washed with brine, dried over anhydrous Na_2SO_4, filtered and concentrated under reduced pressure to give a crude product. Purification with preparative TLC (30% EtOAc/hexanes) gave MC-21 (**64**) (19 mg, 47% yield).

MC-26: IR (UATR) ν_{max} cm^{-1}; 3355, 1978, 1588 (Figure 126); HRMS: *m/z* 451.1723 $[M+Na]^+$ (found) 451.1727 (calcd for $C_{24}H_{28}NaO_7$) (Figure 127); ^1H NMR (300 MHz, $CDCl_3$): Table 5 (Figure 128); ^{13}C NMR (75 MHz, $CDCl_3$): Table 6 (Figure 129)

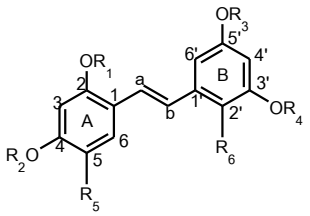

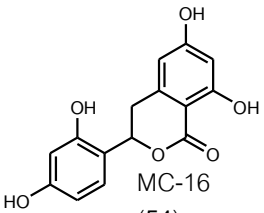

MC-16
(54)

Cpd	R_1	R_2	R_3	R_4	R_5	R_6
MC-1 (41)	H	H	H	H	H	Cl
MC-2 (42)	Me	Me	Me	Me	H	Cl
MC-3 (43)	Isp	Isp	Isp	Isp	H	H
MC-4 (44)	Isp	Isp	Isp	H	H	H
MC-5 (45)	Isp	Isp	H	H	H	H
MC-6 (35)	Me	Me	Me	Me	H	H
MC-7 (46)	Me	Me	Me	H	H	H
MC-8 (47)	Me	Me	H	H	H	H
MC-9 (38)	Ac	Ac	Ac	Ac	H	H
MC-10 (48)	Isp	Isp	Isp	CH_2COOEt	H	H
MC-11 (49)	H	H	H	CH_2COOEt	H	H
MC-12 (50)	H	H	H	CH_2COOH	H	H
MC-13 (51)	Isp	Isp	Ac	Ac_2	H	H
MC-14 (52)	Isp	Isp	Isp	Isp	H	CHO
MC-15 (53)	Isp	Isp	Isp	Isp	H	COOH
MC-17 (55)	H	H	H	H	H	CHO
MC-18 (56)	Isp	Isp	Isp	Isp	H	OH
MC-19 (57)	Isp	Isp	Isp	Isp	H	CH=CHCOOEt
MC-20 (58)	Isp	Isp	Ac	Ac	CHO	H
MC-21 (59)	Isp	Isp	Ac	Ac	COOH	H
MC-22 (60)	H	H	H	H	CHO	H
MC-23 (61)	H	H	H	H	COOH	H
MC-24 (62)	Isp	Isp	H	H	CHO	H
MC-25 (63)	Isp	Isp	H	H	COOH	H
MC-26 (64)	Isp	Isp	Ac	Ac	OH	H

Table 5: ^{1}H-NMR data

A: ^{1}H-NMR data for stilbene skeleton of synthesized compounds

Position	**δ (ppm) (multiplicity, *J* in Hz) ($CDCl_3$)**												
H	**MC-1***	**MC-2**	**MC-3**	**MC-4**	**MC-5**	**MC-6**	**MC-7**	**MC-8**	**MC-9**	**MC-10**	**MC-11***	**MC-12#**	**MC-13**
3	6.45 (d,2.4)	6.46 (d,2.1)	6.45 (d,3.9)	6.46 (d,2.3)	6.45 (d,2.2)	6.42 (d,2.4)	6.45 (d,2.4)	6.44 (d,2.1)	6.95 (d,2.1)	6.45 (d,2.1)	6.49 (d,2.1)	6.30 (s)	6.45 (br s)
5	6.41 (dd,8.4, 2.4)	6.52 (dd,8.7, 2.1)	6.49 (dd,8.5, 2.3)	6.49 (dd,8.5, 2.3)	6.48 (dd,8.5, 2.3)	6.47 (dd,8.4, 2.4)	6.49 (dd,8.4, 2.4)	6.48 (dd,8.7, 2.1)	7.03 (dd,8.4, 2.4)	6.48 (dd,8.7, 2.4)	6.43 (dd,8.4, 2.1)	6.31 (dd,5.9, 2.3)	6.46 (dd,8.1,2 .4)
6	7.44 (d,8.4)	7.56 (d,8.4)	7.46 (d,8.4)	7.45 (d,8.5)	7.43 (d,8.4)	7.46 (d,8.4)	7.46 (d,8.4)	7.43 (d,8.4)	7.61 (d,8.7)	7.45 (d,8.4)	7.43 (d,8.4)	7.33 (d,8.9)	7.41 (d,8.4)
2′	-	-	6.62 (d,2.2)	6.61 (t,1.5)	6.56 (d,2.1)	6.66 (d,2.4)	6.62 (d,1.8)	6.55 (d,2.1)	7.08 (d,2.1)	6.68 (d,1.5)	6.63 (br s)	6.58 (d,1.6)	7.08 (d,2.1)
4′	6.43 (d,2.7)	6.42 (t,2.7)	6.34 (t,2.1)	6.28 (t,2.1)	6.25 (br s)	6.34 (t,2.1)	6.30 (t,2.1)	6.24 (t,2.1)	6.85 (t,2.1)	6.36 (t,2.2)	6.34 (t,2.1)	6.25 (t,2.1)	6.78 (t,2.1)
6′	6.78 (d,2.7)	6.83 (d,2.7)	6.62 (d,2.2)	6.56 (t,1.6)	6.56 (d,2.1)	6.66 (d,2.4)	6.60 (d,1.8)	6.55 (d,2.1)	7.08 (d,2.1)	6.62 (d,1.8)	6.49 (br s)	6.56 (d,1.8)	7.08 (d,2.1)
α	7.38 (d,16.4)	7.44 (d,16.5)	7.33 (d,16.4)	7.32 (d,16.4)	7.31 (d,16.4)	7.36 (d,16.5)	7.33 (d,16.5)	7.30 (d,16.5)	7.05 (d,15.9)	7.33 (d,16.5)	7.36 (d,16.5)	7.30 (d,16.4)	7.34 (d,16.5)
β	7.32 (d,16.4)	7.33 (d,16.5)	6.91 (d,16.4)	6.88 (d,16.4)	6.84 (d,16.4)	6.92 (d,16.5)	6.88 (d,16.5)	6.82 (d,16.5)	6.97 (d,15.9)	6.90 (d,16.5)	6.97 (d,16.5)	6.86 (d,16.4)	6.94 (d,16.5)

* acetone-d_6 # methanol-d_4

A: ^{1}H-NMR data for stilbene skeleton of synthesized compounds (continued)

Position	δ (ppm) (multiplicity, *J* in Hz) ($CDCl_3$)												
H	MC-14	MC-15	MC-16*	MC-17#	MC-18	MC-19	MC-20	MC-21	MC-22#	MC-23#	MC-24*	MC-25*	MC-26
3	6.44 (d,2.4)	6.44 (d,2.1)	6.48 (d,2.1)	6.32 (br s)	6.46 (br s)	6.48 (br s)	6.44 (s)	6.50 (s)	6.25 (s)	6.36 (s)	6.80 (s)	6.88 (s)	6.50 (s)
5	6.50 (dd,8.6, 2.3)	6.42 (dd,8.4, 2.1)	6.43 (dd,8.4, 2.4)	6.33 (dd,8.6, 2.3)	6.48 (dd,10.8, 2.4)	6.49 (dd,8.4 ,2.4)	-	-	-	-	-	-	-
6	7.60 (d,8.6)	7.58 (d,8.4)	7.28 (d,8.4)	7.38 (d,9)	7.53 (d,8.4)	7.45 (d,8.4)	8.03 (s)	8.35 (s)	7.76 (s)	8.01 (s)	8.23 (s)	8.23 (s)	7.13 (s)
2′	-	-	-	-	-	-	7.08 (d,1.8)	7.09 (d,2.1)	6.47 (d,2.4)	6.49 (d,2.1)	6.59 (d,2)	6.59 (d,2)	7.07 (d,2.1)
4′	6.35 (d,2.1)	6.44 (d,2.1)	6.30 (d,2.1)	6.14 (d,2)	6.40 (d,2.4)	6.39 (d,2.1)	6.81 (t,2.1)	6.82 (t,2.1)	6.16 (t,2.1)	6.19 (t,2.1)	6.29 (t,2)	6.30 (t,2)	6.79 (t,1.8)
6′	6.75 (d,2.1)	6.85 (d,2.1)	6.35 (br s)	6.56 (d,2)	6.74 (d,2.7)	6.7 (d,2.1)	7.08 (d,1.8)	7.09 (d,2.1)	6.47 (d,2.4)	6.49 (d,2.1)	6.59 (d,2)	6.59 (d,2)	7.07 (d,2.1)
α	8.08 (d,16.4)	7.85 (d,16.2)	5.83 (dd,12,3)	7.55 (d,15.9)	7.38 (d,16.5)	8.03 (d,16.2)	7.27 (d,16.5)	7.26 (d,16.5)	7.27 (d,16.5)	7.24 (d,16.5)	7.30 (d,16.5)	7.31 (d,16)	7.34 (d,16.2)
β	7.30 (d,16.4)	7.19 (d,16.2)	3.29 (dd,16.5, 12.3) 3.04 (dd,16.5, 3.3)	7.23 (d,15.9)	7.32 (d,16.5)	7.37 (d,16.2)	7.03 (d,16.5)	7.08 (d,16.5)	6.95 (d,16.5)	6.92 (d,16.5)	7.05 (d,16.5)	7.07 (d,16)	6.87 (d,16.2)

* acetone-d_6 # methanol-d_4

B: ^{1}H-NMR data for substituents on stilbene skeleton of synthesized compounds

Position	**δ (ppm) (multiplicity, *J* in Hz) ($CDCl_3$)**												
H	MC-1*	MC-2	MC-3	MC-4	MC-5	MC-6	MC-7	MC-8	MC-9	MC-10	MC-11*	MC-12#	MC-13
R_1	-	OCH_3 3.87, 3.86, 3.85, 3.83	CH 4.55 (m) CH_3 1.37 (d,6)	CH 4.527 (m) CH_3 1.37 (d,6)	CH 4.52 (m) CH_3 1.35 (d,6)	OCH_3 3.81 (s)	OCH_3 3.83 (s)	OCH_3 3.82 (s)	$COCH_3$ 2.36 (s) 2.29 (s)	CH 4.54 (m) CH_3 1.38 (d,6), 1.344 (d,6), 1.339 (d,6)	-	-	CH 4.51 (m) CH_3 1.36 (d,6), 1.31 (d,6),
R_2	-		CH 4.55 (m) CH_3 1.34 (d,6),	CH 4.534 (m) CH_3 1.336 (d,6)	CH 4.52 (m) CH_3 1.33 (d,6)	OCH_3 3.77 (s)	OCH_3 3.78 (s)	OCH_3 3.80 (s)			-	-	
R_3	-			CH 4.534 (m) CH_3 1.343 (d,6)	-		OCH_3 3.81 (s)	-			-	-	
R_4	-		CH 4.55 (m) CH_3 1.35 (d,6),	-	-	OCH_3 3.79 (s)	-	-	$COCH_3$ 2.31 (s)	OCH_2 4.62(s) $^{\times}CH_2CH_3$ 4.62 (q,7.1) $CH_2{}^{\times}CH_3$ 1.30 (t,6.8)	OCH_2 4.70(s) $^{\times}CH_2CH_3$ 4.21 (q,6.9) $CH_2{}^{\times}CH_3$ 1.25 (t,6.9)	OCH_2 4.63(s)	$COCH_3$ 2.25 (s)

* acetone-d_6 # methanol-d_4

B: ^{1}H-NMR data for substituents on stilbene skeleton of synthesized compounds (continued)

Position	**δ (ppm) (multiplicity, *J* in Hz) ($CDCl_3$)**												
H	MC-14	MC-15	MC-16*	MC-17#	MC-18	MC-19	MC-20	MC-21	MC-22#	MC-23#	MC-24*	MC-25*	MC-26
R_1	CH 4.69 (sept,6), 4.48-4.63 (m) CH_3 1.33-1.41 (m)	CH 4.68 (m), 4.54 (m) CH_3 1.44 (d,6.3), 1.40 (d,6.3), 1.37 (d,6.3), 1.34 (d,6)	-	-	CH 4.49 (m) CH_3 unresol-ved signals 1.31-1.40	CH 4.58 (m) CH_3 unresol-ved signals 1.28-1.40	CH 4.66 (m) CH_3 1.43 (d,6) 1.40 (d,6)	CH 4.65 (sept,6) CH_3 1.51 (d,6)	-	-	CH 4.91 (m) CH_3 1.43 (d,6.3), 1.41 (d,6.4)	CH 4.89 (sept,6) CH_3 1.46 (d,6.3)	CH 4.33 (sept,6) CH_3 1.36 (d,6.3)
R_2			-	-				CH 4.83 (sept,6) CH_3 1.45 (d,6)	-	-		CH 5.04 (sept,6) CH_3 1.43 (d,6)	CH 4.54 (sept,6) CH_3 1.34 (d,6.3)
R_3			-	-			$COCH_3$ 2.95 (s)	$COCH_3$ 2.31 (s)	-	-	-	-	$COCH_3$ 2.29 (s)
R_4			-	-					-	-	-	-	

* acetone-d_6 # methanol-d_4

B: ^{1}H-NMR data for substituents on stilbene skeleton of synthesized compounds (continued)

Position	**δ (ppm) (multiplicity, *J* in Hz) ($CDCl_3$)**												
H	MC-14	MC-15	MC-16*	MC-17#	MC-18	MC-19	MC-20	MC-21	MC-22#	MC-23#	MC-24*	MC-25*	MC-26
R_5	-	-	-	-	-	-	CHO 10.32 (s)	-	CHO 9.69 (s)	-	CHO 10.32 (s)	-	-
R_6	CHO 10.53 (s)	-	-	CHO 10.17 (s)	-	CH=CH 7.15 (d,16.2), 6.50 (d,16.2), CH_2 6.24 (q,7.1) CH_3 unresol-ved signals 1.28-1.40	-	-	-	-	-	-	-

* acetone-d_6 # methanol-d_4

Table 6: ^{13}C-NMR data

A: ^{13}C-NMR data for stilbene skeleton of synthesized compounds

Position	δ (ppm)($CDCl_3$)												
C	MC-1*	MC-2	MC-3	MC-4	MC-5	MC-6	MC-7	MC-8	MC-9	MC-10	MC-11*	MC-12#	MC-13
1	116.2	119.2	120.4	120.2	120.3	119.1	119.3	119.2	127.1	120.1	117.1	117.7	119.4
2	156.3	155.9	156.6	156.5	156.5	158.0	158.0	158.1	148.5	156.5	156.9	157.4	156.6
3	102.3	98.4	103.0	103.0	103.2	98.3	98.5	98.5	114.8	102.8	103.5	103.6	106.9
4	158.6	158.6	158.6	158.6	158.6	160.5	160.5	160.6	150.5	158.7	159.4	159.7	158.8
5	107.6	105.0	107.3	107.4	107.5	104.9	105.8	105.1	119.5	104.6	104.4	104.8	113.3
6	127.9	127.7	127.4	127.4	127.4	127.2	127.3	127.3	129.5	127.4	128.4	128.5	127.6
1′	137.9	137.7	140.5	140.8	141.0	140.3	140.6	141.0	139.4	140.7	141.7	142.4	140.7
2′	110.4	113.8	106.4	107.0	105.8	104.2	104.6	105.9	117.0	107.6	108.4	108.4	116.4
3′	153.9	160.9	159.1	159.2	157.0	160.8	156.9	156.9	151.3	159.0	160.4	160.8	151.0
4′	102.7	98.6	102.5	101.8	101.7	99.2	100.4	101.7	116.4	101.4	101.6	101.7	102.5
5′	156.5	158.2	159.1	156.7	157.0	160.8	160.9	156.9	151.3	159.0	159.1	159.4	151.0
6′	103.8	101.9	106.4	105.4	105.8	104.2	105.0	105.9	117.0	107.2	107.1	107.3	116.4
α	126.3	126.0	124.2	124.4	124.3	123.7	123.9	124.1	123.5	124.5	124.9	125.4	124.6
β	121.3	123.2	126.7	126.2	126.1	126.8	126.8	126.2	127.2	126.3	126.0	126.2	125.8

* acetone-d_6 # methanol-d_4

A: ^{13}C-NMR data for stilbene skeleton of synthesized compounds (continued)

Position	δ (ppm)($CDCl_3$)												
C	MC-14	MC-15	MC-16*	MC-17#	MC-18	MC-19	MC-20	MC-21	MC-22#	MC-23#	MC-24*	MC-25*	MC-26
1	120.4	120.4	117.2	117.2	121.1	120.0	119.6	121.4	121.0	118.9	120.1	122.0	120.9
2	156.7	156.6	156.3	158.0	156.5	156.6	161.4	157.2	164.8	162.8	162.3	158.5	145.0
3	102.9	103.0	103.4	103.6	103.3	102.6	113.8	110.9	103.7	103.3	102.9	103.0	111.3
4	158.9	158.0	159.5	160.1	158.4	158.7	161.8	160.2	167.8	164.2	162.7	160.8	149.4
5	107.4	107.4	107.9	108.5	107.5	107.0	118.8	114.2	115.5	106.3	121.1	112.7	141.4
6	128.1	128.1	128.9	131.8	127.4	128.3	126.6	132.1	133.2	130.0	129.2	131.5	113.7
1′	143.9	145.6	143.8	148.0	124.6	145.0	140.1	140.8	141.6	141.6	140.9	140.8	140.6
2′	116.8	107.4	101.88	112.8	138.8	138.9	116.4	116.8	105.9	105.8	105.8	108.0	116.5
3′	163.6	160.9	165.07	167.3	150.7	159.3	151.0	151.2	159.6	159.6	159.6	159.6	151.1
4′	100.1	101.5	101.95	102.0	102.6	100.7	98.1	99.0	102.7	102.7	100.0	101.1	103.7
5′	162.7	158.8	165.13	167.2	145.0	158.6	151.0	151.2	159.6	159.6	159.6	159.6	151.1
6′	105.0	107.4	107.3	107.4	104.9	115.7	116.4	116.8	105.9	105.8	105.8	108.0	116.5
α	125.4	126.5	76.5	120.4	120.8	125.5	124.2	123.9	123.8	123.4	122.9	122.9	125.2
β	127.3	126.6	34.4	129.6	124.1	127.4	126.3	127.5	128.4	128.5	126.6	129.6	125.3

* acetone-d_6 # methanol-d_4

B: ^{13}C-NMR data for substituents on stilbene skeleton of synthesized compounds

Position	δ (ppm)($CDCl_3$)												
C	MC-1*	MC-2	MC-3	MC-4	MC-5	MC-6	MC-7	MC-8	MC-9	MC-10	MC-11*	MC-12#	MC-13
R_1	-		CH 71.0 CH_3 22.2	CH 71.0 CH_3 22.2	CH 71.2 CH_3 22.1		CH_3 55.5		CO 168.89 168.77 $COCH_3$ 21.09, 20.99		-	-	CH 70.6, 69.7 CH_3 21.9, 21.8
R_2	-		CH 69.9 CH_3 22.1	CH 70.0 CH_3 22.0	CH 70.1 CH_3 22.0	CH_3 55.3, 55.2	CH_3 55.3	CH_3 55.5, 55.4		CH 70.8, 69.9 CH_3 22.1, 22.0	-	-	
R_3	-	CH_3 56.2, 55.6, 55.5, 55.4	CH 69.8 CH_3 22.1	CH 69.9 CH_3 22.0	-		CH_3 55.4	-			-	-	CO 168.7 $COCH_3$ 28.8
R_4	-		CH 69.8 CH_3 22.1	-	-	CH_3 55.1	-	-	CO 168.93 $COCH_3$ 21.10	OCH_2 61.8 CO 168.9 $^{\times}CH_2CH_3$ 61.3 $CH_2{}^{\times}CH_3$ 14.1	OCH_2 65.8 CO 169.4 $^{\times}CH_2CH_3$ 61.3 $CH_2{}^{\times}CH_3$ 14.4	OCH_2 65.9 CO 172.9	

* acetone-d_6 # methanol-d_4

B: ^{13}C-NMR data for substituents on stilbene skeleton of synthesized compounds (continued)

Position	δ (ppm)($CDCl_3$)												
C	MC-14	MC-15	MC-16*	MC-17#	MC-18	MC-19	MC-20	MC-21	MC-22#	MC-23#	MC-24*	MC-25*	MC-26
R_1	CH 71.4 CH_3 22.2	CH 74.1, 71.0, 70.2, 70.0 CH_3 22.2,	-	-	CH 71.8, 71.1, 71.0, 69.9 CH_3 22.2, 22.14, 22.13, 22.1	CH 70.8, 70.6, 69.7, 69.6 CH_3 21.94, 21.89, 21.86	CH 71.2 CH_3 21.67	CH 74.2 CH_3 21.92	-	-	CH 72.1, CH_3 22.2,	CH 74.4 CH_3 22.2	CH 73.3 CH_3 22.2
R_2	CH 70.9 CH_3 22.04		-	-			CH 70.9 CH_3 21.66	CH 71.4 CH_3 21.88	-	-	CH 71.8 CH_3 22.1	CH 73.3 CH_3 22.1	CH 71.8 CH_3 22.0
R_3	CH 70.1, 69.9	22.1, 22.0,	-	-			CO 168.7 $COCH_3$	CO 168.9 $COCH_3$	-	-	-	-	CO 169.0 $COCH_3$
R_4	CH_3 21.98	21.9	-	-			20.8	21.0	-	-	-	-	21.0
R_5	-	-	-	-	-	-	CHO 188.1	COOH 165.3	CHO 194.9	COOH 173.5	CHO 188.0	COOH 165.7	-
R_6	CHO 191.1	COOH 166.0	CO 171.1	CHO 194.3	-	CH=CH 120.2, 105.5 CO 168.0 CH_2 59.7 CH_3 14.2	-	-	-	-	-	-	-

* acetone-d_6 # methanol-d_4

3.4. Biological activities

3.4.1 DPPH radical assay

The experiment was performed according to an established method (Likhitwitayawuid et al., 2006b). In each reaction, 20 µL of the methanolic sample solution was mixed with 180 µL of 50 mM 1,1-diphenyl-2-picrylhydrazyl (DPPH) in methanol at room temperature for 30 min. The reduction of the DPPH, a purple-colored stable free radical, was measured by reading the absorbance at 510 nm (Victor^3 multilabel counter, Perkin Elmer). DPPH was reduced to the yellow-colored diphenylpicrylhydrazine when antioxidants are present. Methanol was used as a negative control and Trolox was used as a positive control. The percent inhibition was calculated by the equation:

% Inhibition = [A-(B-C)] x 100 / A

A = the absorbance of the negative control reaction

B = the absorbance of the sample reaction

C = the absorbance of the sample control reaction (without DPPH solution)

3.4.2 Superoxide radical assay

The assay was based on the capacity of the sample to inhibit the reduction of nitroblue tetrazolium (NBT) in the riboflavin-light-NBT system (Dasgupta & De, 2004). Riboflavin absorbs visible light to become excited to its triplet state, initiates redox reactions and then becomes fully reduced. In the presence of oxygen, reduced

riboflavin is reoxidized spontaneously univalently to a flavin radical, with attendant formation of $O_2^{\bullet-}$. The overall reaction is as follows (Korycka-Dahl & Richardson, 1977):

$$Fl_{reduced}H_2 + 2O_2 \rightarrow Fl_{oxidized} + 2O_2^{\bullet-} + 2H^+$$

The experiment was done in a 96-well plate. The reaction mixture (200 µL) in each well contained 20 µL of 50 mM potassium phosphate buffer, 100 µL of 266 µM riboflavin, 20 µL of 1 mM EDTA, 20 µL of 750 µM NBT and 40 µL of sample solution. The production of blue formazan was monitored by measuring the increase in absorbance at 570 nm after a 10-min illumination with a fluorescent lamp. The entire reaction proceeded in a closed box lined with aluminum foil. A similar reaction mixture was kept in the dark and served as the blank. Trolox was used as positive control and 30% methanol in potassium phosphate buffer was used as negative control. The percent inhibition was calculated by the equation:

% Inhibition = [(A-B)-(C-D)] x 100 / (A-B)

A = the absorbance of the negative control reaction in light condition

B = the absorbance of the negative control reaction in dark condition

C = the absorbance of the sample reaction in light condition

D = the absorbance of the sample reaction in dark condition

3.4.3 Inhibitory effect on supercoiled DNA breakage

This assay measured the ability of the test sample to protect DNA against damage induced by the photochemical reaction of riboflavin. First double-strand pBR 322 plasmid DNA was allowed to interact with the reactive chemical species (including superoxide radicals and others) which were produced from photo-sensitized riboflavin. Before the reaction, the DNA was in compact supercoiled conformation (SC) and had a relatively high electrophoretic mobility. After the reaction with the free radicals, the DNA was nicked, meaning that the double-strand was broken. The DNA was now in an open-circle conformation (OC) and had a reduced electrophoretic mobility (Dasgupta & De, 2004; Lin *et al.*, 2008). Based on this principle, the nicked DNA and the intact DNA could be differentiated by agarose gel electrophoresis.

Each reaction mixture (10 µL) contained 2 µL of sample solution in 30% methanol in potassium phosphate buffer, mixed with 50 mM potassium phosphate buffer (1 µL), 266 µM riboflavin (5 µL), 1 mM EDTA (1 µL) and pBR322 plasmid DNA (1 µL). The mixture was then irradiated with a fluorescent lamp in a box lined with aluminum foil. An identical reaction mixture was kept in the dark as a blank. After 30 min, the incubated mixture was treated with 2 µL of loading dye (0.25% bromophenol blue, 0.25% xylene cyanol and 40% sucrose in water), and 12 µL of the reaction mixture was then loaded onto a 0.7% agarose gel. Gel electrophoresis

was performed at 100 V in a Tris-acetic-EDTA buffer. After electrophoresis, the gel was stained with ethidium bromide (0.5 μg/mL ethidium bromide in deionized water) and visualized under ultraviolet light. Images were taken with MiniBIS Gel Documentation and analyzed with Gel Quant Analysis (DNR BioImaging Systems, Jerusalem Israel). The supercoiled DNA (SC) and the nicked or opened circular form (OC) were identified from their mobilities on the gel. All experiments were run in triplicate. Trolox was used as positive control. The inhibitory effect was calculated by the following equation:

$$\% \text{ Inhibition} = [A-(B-C)] \times 100 / A$$

A = the intensity of the SC fraction of the control in dark condition

B = the intensity of the SC fraction of the sample in dark condition

C = the intensity of the SC fraction of the sample in light condition

3.4.4 Determination of anti-herpes simplex virus activity

This assay was performed by Associate Professor Dr. Vimolmas Lipipun's laboratory, Faculty of Pharmaceutical Sciences, Chulalongkorn University.

Viruses and cells

The HSV strain used in this study was HSV-1 (KOS). Vero cells (ATCC CCL81) were grown and maintained in Eagle's minimum medium supplemented with 10% fetal bovine serum.

Plaque reduction assay

Anti-HSV activity of the compound was determined by the plaque reduction assay modified from the previously reported method (Lipipun *et al.*, 2003). Briefly, in the post-treatment assay, Vero cells, in a 96-well tissue culture plate, were infected with 30 plaque forming units of HSV-1 (KOS). After 1 h incubation at room temperature for virus adsorption, the cells were added with overlay media containing various concentrations of the compound. The infected cultures were incubated at 37°C for 2 days. The infected cells were fixed and stained, and then the number of plaques was counted. The 50% inhibitory concentration (IC_{50}) was determined from the curve relating the plaque number to the concentration of the compound. Acyclovir was used as a positive control.

3.4.5 Neuraminidase (NA) inhibition assay

The test samples were evaluated for inhibitory activity against neuraminidase by the Bioassay Laboratory, the National Center for Genetic Engineering and Biotechnology (BIOTEC) of the National Science and Technology Development Agency (NSTDA). This assay was performed using the method described by Potier and co-workers (Potier *et al.*, 1979). The assay was carried out by adding 5 µL of neuraminidase (~0.2 unit) to each well of a 384-well black plate, which contained 5 µL of test compound. The mixture was incubated at 37°C for 30 min. Subsequently, 10 µL of 4-(methylumbelliferyl)-*N*-acetylneuraminic acid (MUNANA), a substrate, at

1500 µM was added into the mixture and the reaction was then incubated at 37°C for an additional 60 min. The enzymatic reaction was terminated by the addition of 30 µL of stop solution (100 µM glycine, pH 10.7 in 25% ethanol). The fluorescence of the released product was measured using SpectraMax M5 multi-detection microplate reader (Molecular Devices, USA) with excitation and emission wave lengths of 365 and 450nm respectively. Percent inhibition of NA activity was calculated using the following formula:

$$\%\text{inhibition} = [1-[(FU_T-FU_B)/(FU_F-FU_B)]] \times 100$$

Where FU_T, FU_F, and FU_B are the average fluorescent signal units of tested well; control well containing NA alone; and the blank control, respectively.

3.4.6 Determination of α-Glucosidase Inhibitory Activity

The assay was performed in a 96-well plate. The assay was based on the capacity of the sample to inhibit the hydrolysis of *p*-nitrophenyl-α-D-glucoside (PNPG) by α-glucosidase to release *p*-nitrophenol (PNP), a yellow color agent that can be monitored at 405 nm (He & Lu, 2013). Briefly, 10 µL of sample solution and 40 µL of 0.1 unit/mL α-glucosidase were incubated at 37°C for 10 min. Then 50 µL of 2 mM PNPG was added, and the mixture was further incubated at 37°C for 20 min. 100 µL of 1 mM Na_2CO_3 was added, and the progress of the enzyme inhibition was monitored by measuring the absorbance at 405 nm with a microplate reader (Victor^3

multilabel counter, Perkin Elmer). Acarbose was used as a positive control. The percent inhibition was calculated by the equation:

% Inhibition = [A-(B-C)] x 100 / A

A = the absorbance of the negative control reaction

B = the absorbance of the sample reaction

C = the absorbance of the sample control reaction (without enzyme solution)

3.4.7 Determination of cytotoxic activity

The assay was performed by the Bioassay Laboratory, the National Center for Genetic Engineering and Biotechnology (BIOTEC) of the National Science and Technology Development Agency (NSTDA).

Resazurin microplate assay (REMA)

Two human cancer cell lines were used in this study, including oral cavity (KB) and breast (MCF-7). This assay was performed using the method described by O'Brien and co-workers (O'Brien *et al*., 2000). In brief, cells at a logarithmic growth phase were harvested and diluted to $7x10^4$ cells/mL for KB and $9x10^4$ cells/mL for MCF-7, in fresh medium. Successively, 5 µL of test sample diluted in 5% DMSO, and 45 µL of cell suspension were added to 384-well plates, and the mixture was incubated at 37°C in 5% CO_2 incubator. After the incubation period (3 days for KB and MCF-7), 12.5 µL of 62.5 µg/mL resazurin solution was added to each well, and

the plates were then incubated at 37°C for 4 h. Fluorescence signals were measured using SpectraMax M5 multi-detection microplate reader (Molecular Devices, USA) at the excitation and emission wavelengths of 530 nm and 590 nm. Percent inhibition of cell growth was calculated by the following equation.

% inhibition = $[1-(FU_T/FU_C)] \times 100$

FU_T = The mean fluorescence unit from treated conditions

FU_C = The fluorescence unit from untreated conditions

The dose response curves were plotted from 6 conditions of 2-fold serially diluted test compounds, and the sample concentrations that inhibit cell growth by 50% (IC_{50}) can be derived using the SOFTMax Pro software (Mollecular Devices, USA). Ellipticine, doxorubicin and tamoxifen were used as positive controls, and 0.5% DMSO was used as a negative control.

CHAPTER IV

RESULTS AND DISCUSSION

4.1 Chemistry

In a previous report (Sornsute, 2006), the structure modification of oxyresveratrol (**1**) was focused on the etherification and esterification of the four OHs with ethylcarbonyl, diethylcarbamyl, acetyl, benzoyl, phenylmethyl and methyl groups, in addition to chlorination and hydrogenation reactions. In the present investigation, *O*-alkylation reactions of oxyresveratrol were further studied with different reagents, such as isopropyl bromide and ethyl bromoacetate. In addition, attempts to introduce different types of functional groups to the aromatic rings of oxyresveratrol, including Cl, Br, I, OH, CHO, COOH and CH=CHOOEt, were made. The overall reactions in this project are summarized in the following schemes.

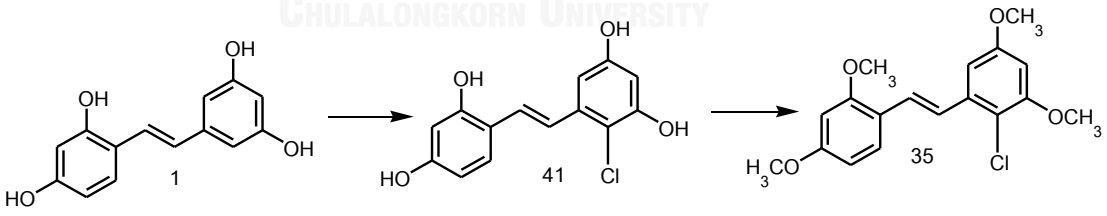

Scheme III: Halogenation

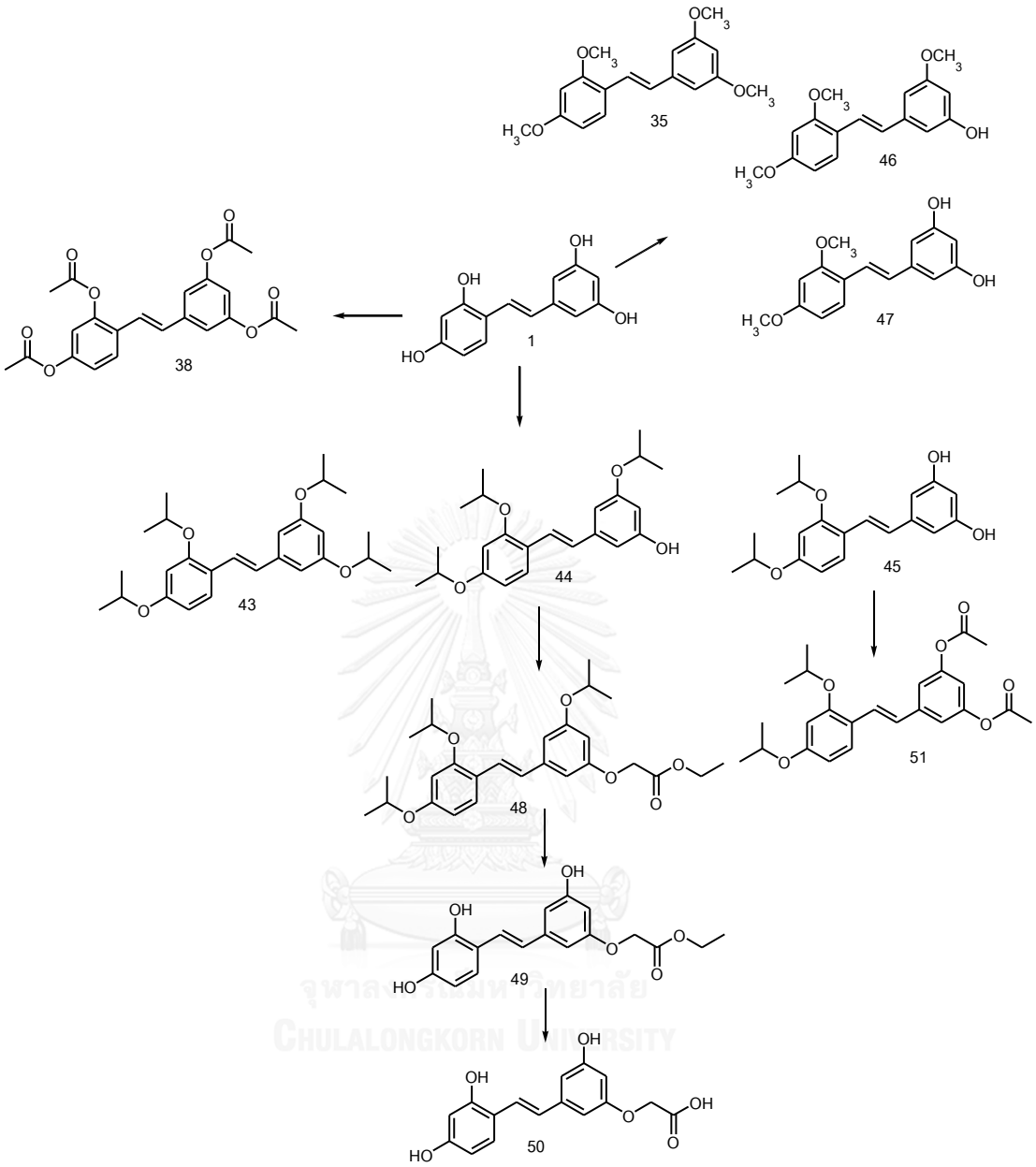

Scheme IV: *O*-alkylation and *O*-acylation

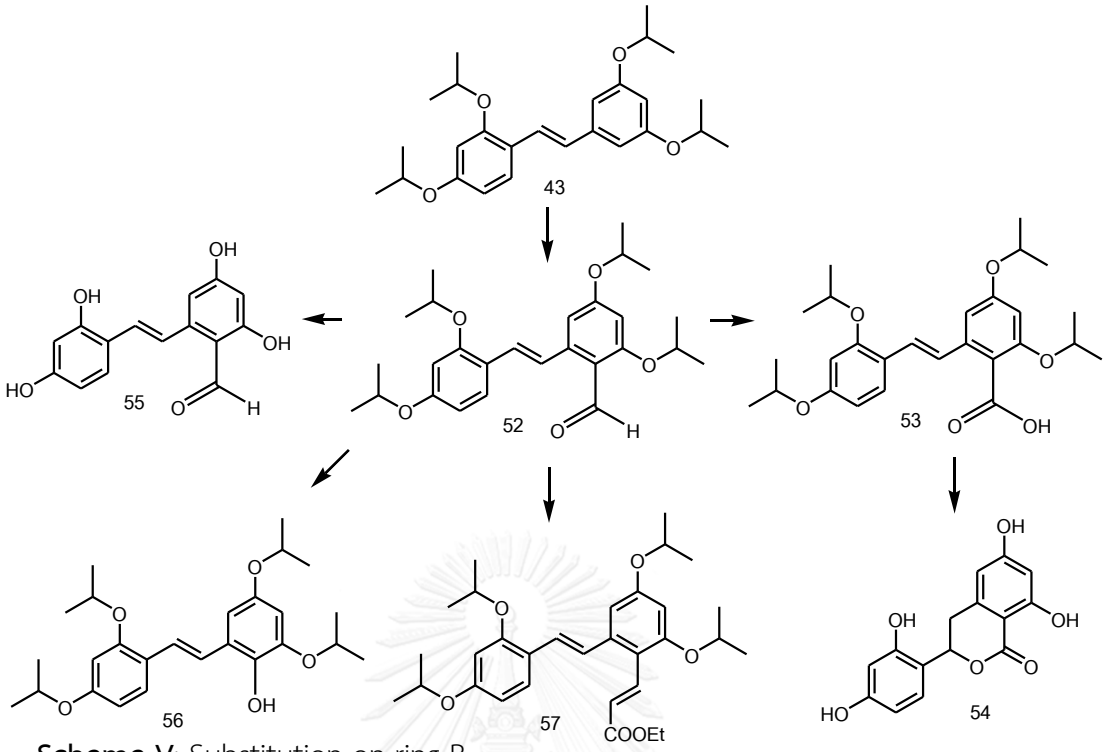

Scheme V: Substitution on ring B

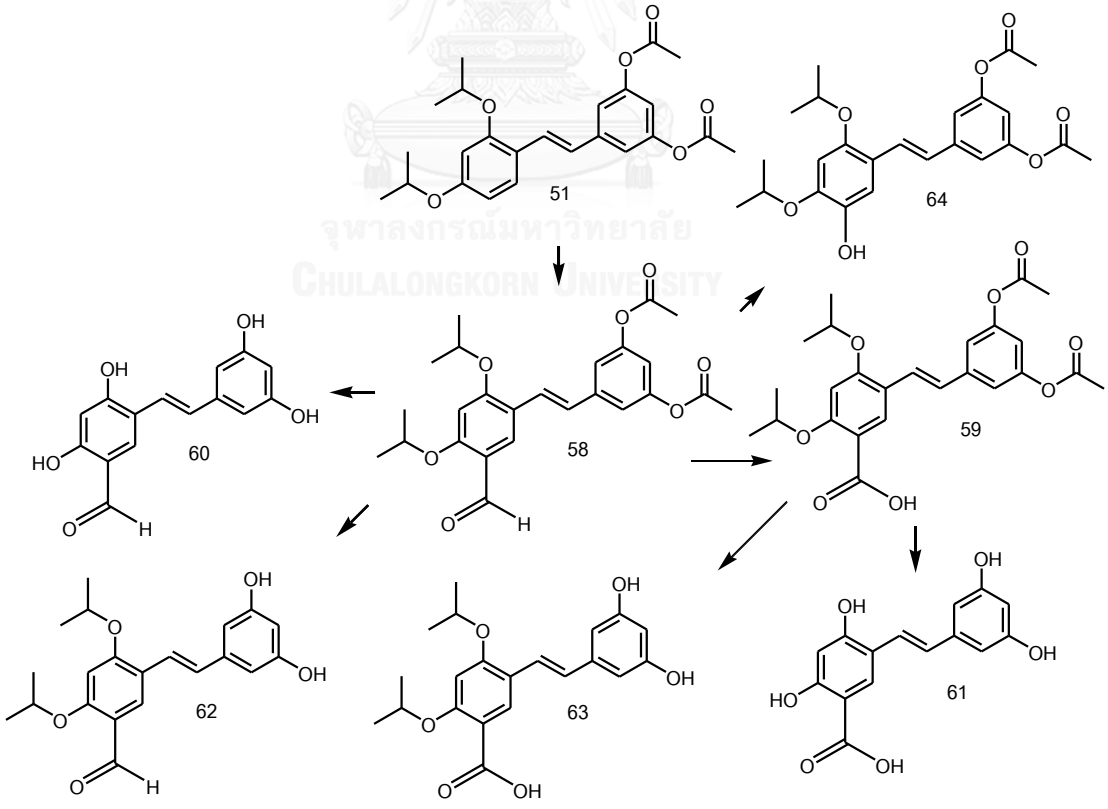

Scheme VI: Substitution on ring A

Several efforts to perform halogenation on the B aromatic ring of oxyresveratrol (**1**) were made (Table 7). It was expected that aromatic halogenation on **1** would be facile due to the high electron density which is contributed by the hydroxyl groups. Because the hydroxyl groups on ring A are conjugated with the olefin, the B ring should be more nucleophilic, particularly at the position 2′/6′, and this difference should give rise to regioselective electrophilic aromatic halogenation under appropriate and mild conditions. Using *N*-chlorosuccinimide (NCS) and glacial acetic acid, the corresponding 2′-mono-chlorinated product **41** was obtained in 36% yield (Scheme III). Chlorination was also attempted on the other analogues of **1**, including **43** and **51**; however, no desired chlorinated product was obtained. Compound **41** smoothly underwent full methylation to give the tetramethylether **42** in 36% yield. In addition, several attempts to carry out aromatic bromination on **1** or **35** under various conditions failed to give the brominated product; only a mixture of unidentified decomposed products was obtained. Iodination of **1** with NIS was not also successful.

Table 7: Halogenation

Starting	Halogen source	Conditions	Results
1	NCS	AcOH (glacial), Ar, rt, 3 h	**41** (36%)
43	NCS	CH_2Cl_2, Ar, rt, 4 h	Mixed product
51	NCS	CH_2Cl_2, Ar, rt, O/N	No reaction
51	NCS	AcOH (glacial), Ar, rt, 3 h	decomposed

NCS = *N*-chlorosuccinimide; NBS = *N*-bromosuccinimide; NIS = *N*-iodosuccinimide

Table 7: Halogenation (continued)

Starting	Halogen source	Conditions	Results
1	NBS	CH_2Cl_2, Ar, rt, 3 h	decomposed
1	NBS	AcOH (glacial), Ar, rt, 3 h	decomposed
35	NBS	CH_2Cl_2, Ar, rt, 3 h	decomposed
35	Pyridine hydrobromide perbromide	CH_2Cl_2, Ar, rt, 3 h	decomposed
35		CH_2Cl_2, Ar, -40°C, O/N	decomposed
35	polymer-bound	CH_2Cl_2, Ar, -20°C, 20 min	decomposed
35	Pyridinium tribromide	CH_2Cl_2, Ar, rt, 20 min	decomposed
1	NIS	CH_2Cl_2, Ar, rt, O/N	No reaction

NCS = *N*-chlorosuccinimide; NBS = *N*-bromosuccinimide; NIS = *N*-iodosuccinimide

Rings A and B of oxyresveratrol (**1**) could be further differentiated in terms of reactivity by manipulating the type and the number of protecting groups on the four phenol functionalities. After some experimentation, the isopropyl group gave the best result, providing the corresponding di-*O*-isopropyl, tri-*O*-isopropyl, and tetra-*O*-isopropyl compounds **43**-**45** in 24%, 30%, and 28% yields, respectively. It should be noted that it was difficult to avoid the formation of **43**, perhaps due to the greater solubility of the more alkylated ethers in DMF under the reaction conditions. The same pattern can be seen in the *O*-methylation reaction of **1**; di-*O*-methyl, tri-*O*-methyl, and tetra-*O*-methyl compounds **35**, **46**, **47** were obtained in 9%, 25%, and

45% yields, respectively. The di-*O*-substitution occurred on the two hydroxyl groups of ring A and tri-*O*-substitution occupied both hydroxyl groups of ring A and one hydroxyl group of ring B for both reactions. These results suggested the phenolic groups on ring A were more reactive than their counterparts on ring B. The higher reactivity of the OH groups on ring A may be due to the conjugation with olefin, which is not possible for the OHs on ring B.

When the tetra-*O*-isopropyl compound **43** reacted under the Vilsmeier-Haack formylation condition**,** the corresponding ring B-formylated product **52** was obtained in good yield (80%). The aldehyde functional group could be further oxidized to the corresponding carboxylic acid in 79% yield. The attempts to cleave all the *O*-isopropyl groups are shown in Table 8. The deisopropylation of **53** with BBr_3 gave the isochromanone **54** in 20% yield as a result of the Lewis acid-mediated removal of the *O*-isopropyl groups followed by C-O bond formation on the olefinic carbon of the stilbene system. The aldehyde **52** smoothly underwent BCl_3-mediated deprotection of the isopropyl groups to provide the 2′-formyloxyresveratrol **55** in moderate 48% yield. In addition, the aldehyde **52** could also undergo the acid-mediated Baeyer-Villiger-type, Dakin reaction conversion to the corresponding formate which was cleaved *in situ* under the reaction condition to provide 2′-hydroxy-tetra-*O*-isopropyl oxyresveratrol **56** in good yield of 66%. Unfortunately, any

attempt to deprotect the isopropyl groups failed; only a mixture of decomposed products was obtained.

Table 8: Deisopropylation conditions

Starting	Reagent	Conditions	Results
48	$AlCl_3$	CH_2Cl_2, Ar, 0°C, 1 h	decomposed
43	PTS-Si	toluene, 80°C, 1 d	decomposed
43	PTS-Si	toluene, rt, 1 d	decomposed
43	TFA	TFA, rt, 1 d	No reaction
53	BBr_3	CH_2Cl_2, Ar, -78°C, 20 min	**54** (20%)
58	BCl_3	CH_2Cl_2, Ar, -78°C, 2 h	No reaction
58	BCl_3	CH_2Cl_2, Ar, -78°C ⟶ rt, O/N	**60** (78%)
52	BCl_3	CH_2Cl_2, Ar, -78°C ⟶ rt, O/N	**55** (48%)
56	BCl_3	CH_2Cl_2, Ar, -78°C ⟶ rt, O/N	decomposed

PTS-Si = *p*-toluene sulfonic acid immobilized on silica; TFA = trifluoroacetic acid

Alkylation of the tri-*O*-isopropyl compound **44** with ethyl bromoacetate under basic conditions went smoothly, in 84% yield, to furnish the ethyl ester **48** which underwent BCl_3-mediated deprotection of the isopropyl groups to give the tri-hydroxyl compound **49** in 61% yield. Subsequent saponification of the ethyl ester using 5% KOH in ethanol provided the corresponding acid in moderate 40% yield.

In order to affect the reactions on ring A of oxyresveratrol, the di-*O*-isopropyl compound **45** was acetylated under standard conditions to provide ring A-di-*O*-

isopropyl ring B-di-*O*-acetyl compound **51** in 74% yield. After some experimentation (Table 9), ring A could be formylated on the 5-position to give **58** exclusively, in 60% yield under the best Vilsmeier-Haack condition: 10 eq of $POCl_3$ at 0°C ⟶ rt overnight under argon. Subsequent oxidation of the aldehyde to the corresponding acid **59** gave the acid in 73% yield. BCl_3-mediated cleavage of all the *O*-isopropyl groups as well as the *O*-acetyl groups finally gave the desired 5-formyl- and 5-carboxy-oxyresveratrol **60** and **61** in 78% and 63% yields, respectively. Saponification of **58** and **59** using 5% KOH in ethanol gave 5-formyl- and 5-carboxy-di-*O*-isopropyl oxyresveratrol **62** and **63** in 93% and 40% yields, respectively. The aldehyde **58** was subjected to the Dakin reaction to give 5-hydroxy-di-*O*-acetyl-di-*O*-isopropyl oxyresveratrol **64** in 47% yield.

Table 9: Vilsmeier-Haack condition of **51**

Starting	Reagent	Conditions	Results
51	$POCl_3$ (3.5eq)	CH_2Cl_2, Ar, 0°C, O/N	No reaction
51	$POCl_3$ (3.5eq)	CH_2Cl_2, Ar, 70°C, 2 h	decomposed
51	$POCl_3$ (3.5eq)	CH_2Cl_2, Ar, 0°C ⟶ rt, O/N	**58** (11%)
51	$POCl_3$ (5eq)	CH_2Cl_2, Ar, 0°C ⟶ rt, O/N	**58** (30%)
51	$POCl_3$ (10eq)	CH_2Cl_2, Ar, 0°C ⟶ rt, O/N	**58** (60%)
51	$POCl_3$ (20eq)	CH_2Cl_2, Ar, 0°C ⟶ rt, O/N	**58** (62%)

From the results obtained in this study, it should be pointed out that the difference of the protecting groups could be used to manipulate the selectivity of the reaction. In the Vilsmeier-Haack reaction of the tetra-*O*-isopropyl compound **43**, all the protecting groups were electron donating groups, which effected the 2′ and 6′ position of ring B to be the most reactive position. But in the Vilsmeier-Haack reaction of the di-*O*-acetyl-di-*O*-isopropyl compound **51**, the acetyl groups were electron withdrawing groups, and thus reduced the electron density of ring B. This resulted in the deactivation of ring B, virtually equivalent to forcing the formylation to occur on ring A. This synthetic strategy could be applicable to the synthesis of other aromatic structures, particularly when selective electrophilic attack on similarly substituted rings is desired.

4.2 Biological activities

4.2.1 Free radical scavenging activities

All of the oxyresveratrol derivatives were initially tested for DPPH and superoxide scavenging activity at a concentration of 100 μg/mL. Compounds that showed more than 65% inhibition were further evaluated for IC_{50} values. Oxyresveratrol and Trolox were used as positive controls. The results are summarized in the Tables 10 and 11.

4.2.1.1 DPPH scavenging activity

Ten compounds were found to possess more than 65% inhibition against DPPH radicals. Compound **64** was the most potent analogue, with activity significantly higher than that of oxyresveratrol.

4.2.1.1.1 *O*-alkylation/acylation

The results indicated that *O*-alkylation/acylation of oxyresveratrol led to the loss or decrease of DPPH scavenging activity. As can be seen from Table 10, total loss of activity was observed for analogues with full *O*-alkylation/acylation (**35**, **38,** **43**, **48** and **51**) or tri-*O*-alkylation/acylation (**44** and **46**), whereas partial reduction of activity was found in derivatives with mono- or di-*O*-alkylation/acylation (**45**, **47**, and **50**). However, it is interesting to note that the DPPH scavenging activity was slightly enhanced when the OH at position 3′ was replaced with an *O*-carbethoxymethyl ($OCH_2COOCH_2CH_3$), as seen in **49**. The reason for this, at this stage, is still not clear. Nevertheless, the weak or lessened activity of the *O*-alkylation/acylation products could be completely reversed by introducing an OH onto C-5 or C-2′ of ring A or B (see below).

It should be emphasized here that, apart from the free OHs, the olefinic linkage was also indispensable, as indicated from the entire loss of activity observed for **54**.

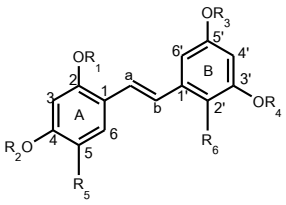

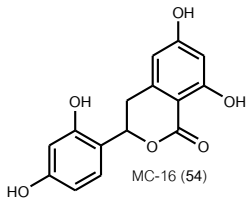

Table 10: Free radicals scavenging activity of synthesized compounds against DPPH

Cpd	Substitution						DPPH	
	R_1	R_2	R_3	R_4	R_5	R_6	% inhibition (100 μg/mL)	IC_{50} (μM)
1	H	H	H	H	H	H	96.19 ± 0.59	11.67 ± 1.94
41	H	H	H	H	H	Cl	96.16 ± 0.32	14.65 ± 3.85
42	Me	Me	Me	Me	H	Cl	13.04 ± 1.92	nd
43	Isp	Isp	Isp	Isp	H	H	12.80 ± 0.41	nd
44	Isp	Isp	Isp	H	H	H	54.72 ± 2.16	nd
45	Isp	Isp	H	H	H	H	75.61 ±2.52	147.71 ± 9.78*
35	Me	Me	Me	Me	H	H	12.24 ± 1.00	nd
46	Me	Me	Me	H	H	H	61.12 ± 0.88	nd
47	Me	Me	H	H	H	H	95.87 ± 1.66	77.04 ± 6.43*
38	Ac	Ac	Ac	Ac	H	H	14.37 ± 4.82	nd
48	Isp	Isp	Isp	CH_2COOEt	H	H	14.32 ± 0.96	nd
49	H	H	H	CH_2COOEt	H	H	96.41 ± 0.67	9.67 ± 0.15
50	H	H	H	CH_2COOH	H	H	95.80 ± 0.29	19.44 ± 3.07
51	Isp	Isp	Ac	Ac	H	H	12.37 ± 1.02	nd
52	Isp	Isp	Isp	Isp	H	CHO	11.76 ± 0.13	nd
53	Isp	Isp	Isp	Isp	H	COOH	40.68 ± 2.35	nd
54	-	-	-	-	-	CO	35.41 ± 1.90	nd
55	H	H	H	H	H	CHO	96.40 ± 1.19	16.37 ± 5.14
56	Isp	Isp	Isp	Isp	H	OH	96.22 ± 0.45	11.74 ± 0.26
57	Isp	Isp	Isp	Isp	H	CH=CH COOEt	14.66 ± 1.45	nd
58	Isp	Isp	Ac	Ac	CHO	H	12.82 ± 0.50	nd
59	Isp	Isp	Ac	Ac	COOH	H	13.84 ± 1.05	nd
60	H	H	H	H	CHO	H	72.74 ± 1.70	170.06 ± 11.78
61	H	H	H	H	COOH	H	81.40 ± 2.96	48.33 ± 5.84*
62	Isp	Isp	H	H	CHO	H	46.75 ± 1.71	nd
63	Isp	Isp	H	H	COOH	H	48.89 ± 1.30	nd
64	Isp	Isp	Ac	Ac	OH	H	95.80 ± 0.50	6.98 ± 0.20*
Trolox	-						96.82 ± 0.87	8.72 ± 1.08

nd = not determined due to < 65% inhibition; * P < 0.05 relative to **1**, one way ANOVA.

4.2.1.1.2 Substitution on ring B

Chlorination at C-2′ had no influence on the activity, as seen from the roughly equal activity obtained for following pairs: oxyresveratrol (**1**) *vs* **41**; **42** *vs* **35**. Neither did the formyl (CHO) nor the carboxyl (COOH) group at this position significantly affect the activity. This was deduced by comparing the activities of the following pairs of structures: oxyresveratrol *vs* **55**; **43** *vs* **52** or **53**. A similar observation was also found for the carbethoxyethenyl ($CH=CHCOOCH_2CH_3$) substituent, as seen in **57** in comparison with **43**.

4.2.1.1.3 Substitution on ring A

The presence of CHO or COOH group at C-5 of the A ring decreased the activity, as evident from the lessened activity of **60** and **61** when compared with that of oxyresveratrol, and the weaker activity of **62** and **63**, as compared with that of **45**.

The reason behind the diminished activity of analogues with CHO, COOH or $CH=CHCOOCH_2CH_3$ group on ring A or B was likely to be the electron-withdrawing nature of these substituents. As previously pointed out, the DPPH scavenging activity of these polyoxygenated stilbenes required the presence of free OHs and an olefinic bridge connecting the two aromatic rings. This implied that the electrons of the OHs were involved, probably through the generation of short-lived oxygen radical structures, and that electron delocalization within the structure was vital to the

activity. The above-mentioned electron-withdrawing groups may interrupt the movement of the electrons and accordingly decreased the activity.

4.2.1.1.4 Introduction of OH to ring A or B

From the data obtained in this study, the introduction of an OH group to either of the aromatic rings appeared to be able to restore the activity of fully *O*-alkylated/acylated analogues. For example placing an OH onto C-2′ of ring B of **43**, a fully *O*-alkylated structure, gave **56** which was as strong as oxyresveratrol. The activity of **51**, a di-*O*-alkylated di-*O*-acylated derivative of oxyresveratrol, was recovered when the compound was hydroxylated at C-5 of the A ring, as seen in **64**. It is interesting to note that the introduction of only one phenolic group onto the C-2′ or C-5 position could completely recover the loss of activity caused by *O*-alkylation/*O*-acylation.

Thus, **56** and **64** can be viewed as *O*-alkyl/acyl analogues of oxyresveratrol with stronger or equal DPPH free radical scavenging activity. Because of the relatively less polarity of the substituents, these two structures, **56** and **64**, should have greater lipophilicity, in addition to higher stability, than oxyresveratrol. From the two improved chemical properties, **56** and **64** might provide better anti-free radical activity in the areas where hydrophobicity, such as the brain, are required.

4.2.1.2 Superoxide scavenging activity

Twelve compounds were found to possess more than 65% inhibition for superoxide scavenging and were more significantly potent than oxyresvertrol (Table 11). The most potent compound was **59**, followed by **61** and **55**.

4.2.1.2.1 *O*-alkylation/acylation

The data obtained for *O*-alkylation/acylation products regarding their inhibitory activity against superoxide radicals were not parallel to their effects against DPPH (Table 10), suggesting different structural requirements or mechanisms for the two radical scavenging activities. Of equal importance is that the olefinic functionality was not necessary for superoxide scavenging activity since **54** showed stronger activity than oxyresveratrol. As summarized in Table 11, superoxide scavenging activity was weakened or lost in some of the alkylated/acylated products of oxyresveatrol (**35**, **38**, **43**-**45** and **51**), but was enhanced in the others (**46**-**50**). However, for **49** and **50**, the importance of the *O*-carbethoxymethyl ($OCH_2COOCH_2CH_3$) or *O*-carboxymethyl (OCH_2COOH) group at position 3′ should be noted. A similar phenomenon was earlier found for **49** in the activity against DPPH (see above), although a logical explanation is still needed.

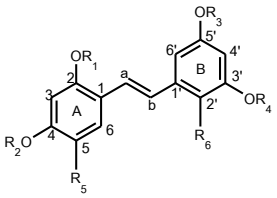

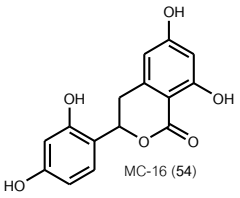

MC-16 (**54**)

Table 11: Free radicals scavenging activity of synthesized compounds against superoxide anion

Cpd	Substitution						Superoxide anion	
	R_1	R_2	R_3	R_4	R_5	R_6	% inhibition (100 µg/mL)	IC_{50} (µM)
1	H	H	H	H	H	H	76.07 ± 3.39	303.09 ± 7.94
41	H	H	H	H	H	Cl	87.27 ± 5.29	98.36 ± 6.97*
42	Me	Me	Me	Me	H	Cl	27.69 ± 2.22	nd
43	Isp	Isp	Isp	Isp	H	H	43.49 ± 5.85	nd
44	Isp	Isp	Isp	H	H	H	43.48 ± 3.56	nd
45	Isp	Isp	H	H	H	H	40.83 ± 6.03	nd
35	Me	Me	Me	Me	H	H	61.06 ± 8.21	nd
46	Me	Me	Me	H	H	H	89.15 ± 4.85	120.08 ± 14.92*
47	Me	Me	H	H	H	H	67.36 ± 8.99	163.27 ± 9.77*
38	Ac	Ac	Ac	Ac	H	H	47.98 ± 4.84	nd
48	Isp	Isp	Isp	CH_2COOEt	H	H	68.21 ± 4.40	75.31 ± 12.53*
49	H	H	H	CH_2COOEt	H	H	97.69 ± 1.83	154.85 ± 14.74*
50	H	H	H	CH_2COOH	H	H	87.90 ± 4.25	81.91 ± 12.28*
51	Isp	Isp	Ac	Ac	H	H	59.01 ± 2.18	nd
52	Isp	Isp	Isp	Isp	H	CHO	25.29 ± 2.16	nd
53	Isp	Isp	Isp	Isp	H	COOH	35.63 ± 8.58	nd
54	-	-	-	-	-	CO	97.18 ± 2.44	107.31 ± 8.74*
55	H	H	H	H	H	CHO	91.02 ± 6.39	43.37 ± 4.38*
56	Isp	Isp	Isp	Isp	H	OH	59.83 ± 1.93	nd
57	Isp	Isp	Isp	Isp	H	CH=CH COOEt	50.97 ± 0.58	nd
58	Isp	Isp	Ac	Ac	CHO	H	68.61 ± 5.75	157.09 ± 10.87*
59	Isp	Isp	Ac	Ac	COOH	H	95.25 ± 1.65	17.73 ± 3.50*
60	H	H	H	H	CHO	H	94.22 ± 3.48	88.34 ± 9.69*
61	H	H	H	H	COOH	H	95.97 ± 3.56	38.63 ± 1.41*
62	Isp	Isp	H	H	CHO	H	17.61 ± 5.14	nd
63	Isp	Isp	H	H	COOH	H	45.39 ± 4.58	nd
64	Isp	Isp	Ac	Ac	OH	H	52.85 ± 5.89	Nd
Trolox				-			61.45 ± 3.59	293.47 ± 19.27

nd = not determined due to < 65% inhibition; * P < 0.05 relative to **1**, one way ANOVA.

4.2.1.2.2 Substitution on ring B

The effect of Cl at C-2′ on the activity was still inconclusive because oxyresveratrol was weaker than its chloro-product **41**; on the other hand **35** was stronger than its chloro-derivative **42**. Introduction of a CHO group to this position brought in stronger activity (**55**), but reversed results were obtained when **43** was formylated (CHO) or carboxylated (COOH) to give **52** or **53**. The carbethoxyethenyl ($CH=CHCOOCH_2CH_3$) substituent introduced to C-2′ also reduced the activity (**57**).

4.2.1.2.3 Substitution on ring A

It is exciting to see that the presence of CHO or COOH group at C-5 of the A ring tends to increase the activity, as evident from the enhanced activity of following pairs: **58** or **59** *vs* **51**; **60** or **61** *vs* oxyresveratrol. In particular, **59** was the most active compound among the series of stilbenes evaluated in this study, with 17- and 16-fold stronger activity than oxyresveratrol and Trolox, respectively. However, unclear results were observed for **45** when the compound was transformed into **62** or **63**.

It should be mentioned that analogues with a COOH group on either aromatic ring were slightly stronger than those with a CHO group, as can be seen in the following pairs: **53** *vs* **52**; **59** *vs* **58**; **61** *vs* **60**.

4.2.1.2.4 Introduction of OH to ring A or B

No significant effects of OH at C-2′ or C-5 on the activity were recognized, as deduced from the comparison of the activities of the following pairs of structures: **43** *vs* **56**, and **51** *vs* **64**.

4.2.2 DNA protective activity

An assay for DNA protective property was newly developed in this study. It was based on the DNA damage induced by the photochemical reaction of riboflavin. First the reactive chemical species (RCS) were produced by photosensitized riboflavin, and then they were allowed to interact with double-strand pBR322 plasmid DNA. It is known that DNA is prone to oxidation by reactive oxygen species (ROS) (Lin *et al.*, 2008). In the intact state, the double-strand pBR322 plasmid DNA has a compact supercoiled conformation (SC) with a relatively high electrophoretic mobility. When the DNA is nicked, the double-strand is broken, and this results in an open-circle conformation (OC), which has a reduced electrophoretic mobility (Dasgupta & De, 2004; Lin *et al.*, 2008). On this basis, the nicked DNA (OC) could be separated from the SC form by agarose gel electrophoresis.

A preliminary study was conducted on Trolox to examine the validity of the experiment. The electrophoresis results, as shown in Figure 1(a), display the inhibitory effect of Trolox on DNA strand scission. Lane 1 is untreated DNA while DNAs treated with riboflavin in dark and in light condition are in lanes 2 and 3, respectively. Lanes 4 -7 are DNA products from riboflavin-photo reaction in the presence of Trolox at different concentrations. In each lane, the lower band was due to supercoiled DNA

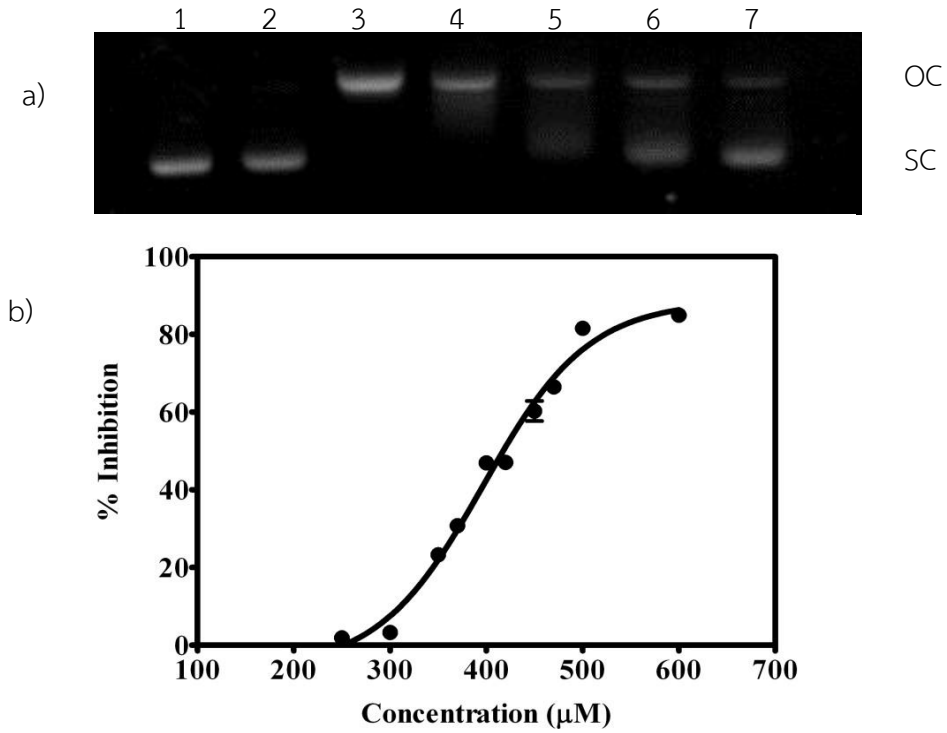

Figure 1: (a) Effect of Trolox in preventing DNA nicking. Lane 1 = pBR322 DNA without treatment; Lane 2 = pBR322 DNA with riboflavin in dark condition; Lane 3 = pBR322 DNA with riboflavin in light condition; Lane 4-7 = pBR322 DNA with riboflavin in light condition in the presence of Trolox 300, 370, 450 and 600 μM, respectively. OC = open circular form or nicked DNA, SC = close circular form or supercoiled DNA; **(b)** Trolox showed concentration-dependent inhibition of DNA damage induced by photosensitized riboflavin.

Table 12: Inhibitory effect of Trolox on DNA breakage

Concentration (μM)	% Inhibition
250	3.15 ± 1.23
300	3.17 ± 1.59
350	23.25 ± 1.37
370	30.74 ± 1.50
400	46.94 ± 1.33
420	47.07 ± 1.75
450	60.27 ± 4.46
470	66.50 ± 1.48
500	81.57 ± 1.19
600	84.93 ± 1.29

(SC), and the upper to nicked or open-circular DNA (OC). It can be seen that in lanes 1 and 2, DNAs were undamaged, but in lane 3 DNA was completely nicked. The increased amount of SC form in lanes 5 to 7 indicated that Trolox could reduce photoriboflavin mediated DNA strand cleavage. The data in Figure 1(b) and Table 12 show the ability of Trolox (at varying concentrations) to inhibit DNA strand scission. It can be seen that the DNA protective effect of Trolox was concentration-dependent, with an EC_{50} value of 421.68 μM.

For comparison, ascorbic acid, another well-known antioxidant, was evaluated for DNA protective activity in a similar fashion as seen in (Figure 2(a). Figure 2(b) and Table 13 show concentration-activity relationships for ascorbic acid. In this test system, ascorbic acid had low capability of DNA protection, showing an EC_{50} value of 2.27 mM.

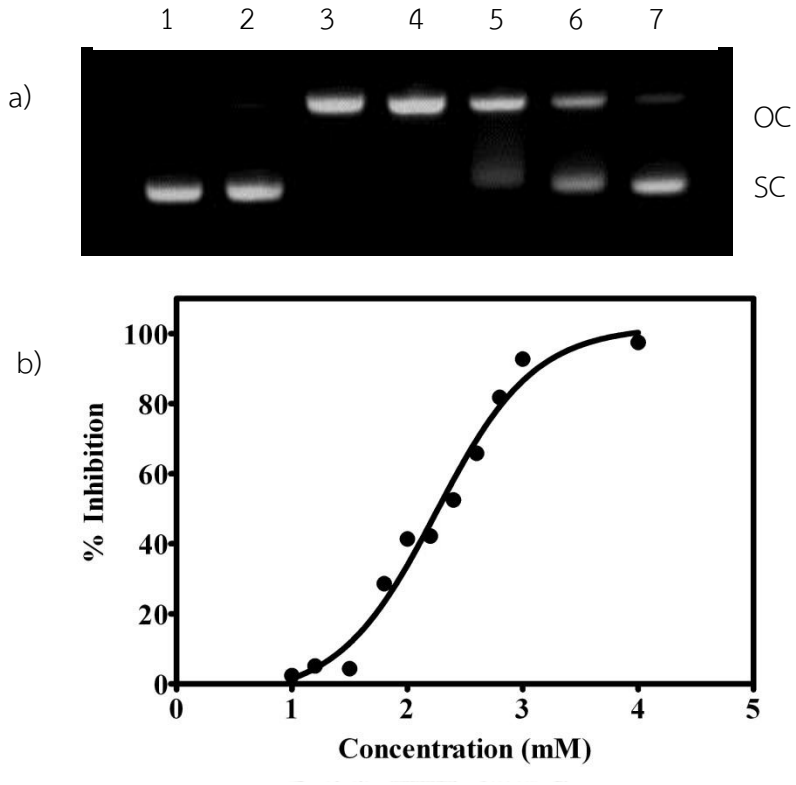

Figure 2: **(a)** Effect of ascorbic acid in preventing DNA nicking. Lane 1 = pBR322 DNA without treatment; Lane 2 = pBR322 DNA with riboflavin in dark condition; Lane 3 = pBR322 DNA with riboflavin in light condition; Lane 4-7 = pBR322 DNA with riboflavin in light condition in the presence of ascorbic acid 1, 2.2, 2.6 and 4 mM, respectively. OC = open circular form or nicked DNA, SC = close circular form or supercoiled DNA; **(b)** Ascorbic acid showed concentration-dependent inhibition of DNA damage induced by photosensitized riboflavin.

Table 13: Inhibitory effect of ascorbic acid on DNA breakage

Concentration (mM)	% Inhibition
1.0	2.38 ± 1.93
1.2	5.14 ± 3.41
1.5	4.33 ± 3.17
1.8	28.63 ± 1.04
2.0	41.38 ± 2.23
2.2	42.21 ± 0.28
2.4	52.53 ± 0.48
2.6	65.83 ± 2.95
2.8	81.79 ± 2.80
3.0	92.73 ± 2.56
4.0	97.47 ± 0.35

This newly developed DNA damage assay was then employed to determine the DNA protective potential of oxyresveratrol. Figure 3(a) is the image of agarose gel electrophoretic patterns of the DNA exposed to the RCS produced by photosensitized riboflavin in the presence of oxyresveratrol at varying concentrations. The DNA protective activity of oxyresveratrol was found to be concentration-dependent, showing an EC_{50} value of 83.01 μM, as seen in Figure 3(b) and Table 14.

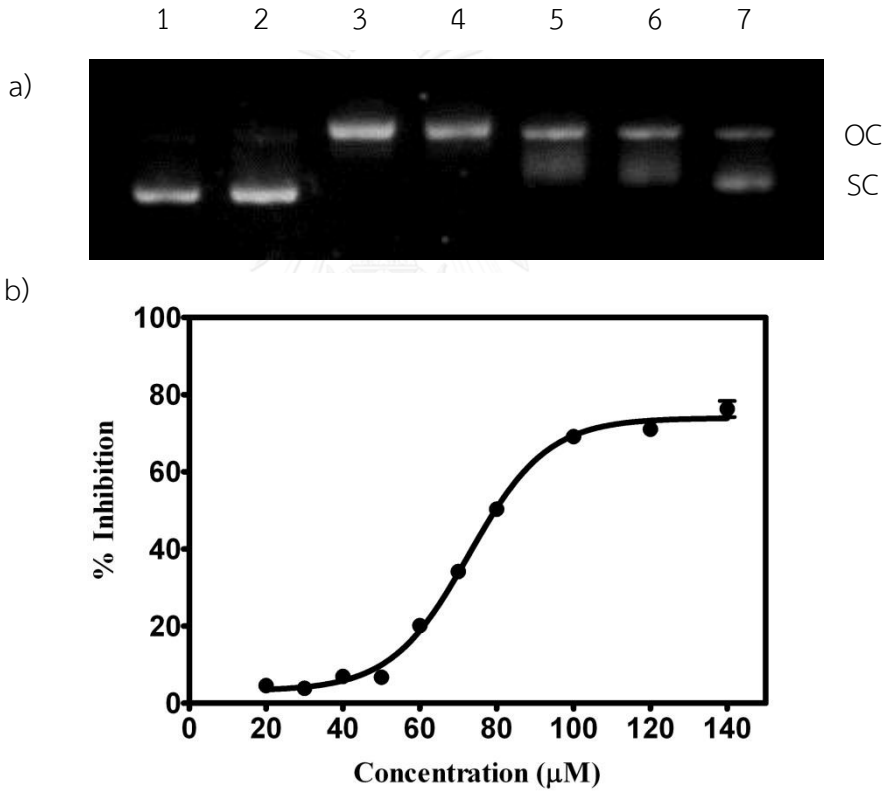

Figure 3: (a) Effect of oxyresveratrol in preventing DNA nicking. Lane 1= pBR322 DNA without treatment; Lane 2 = pBR322 DNA with riboflavin in dark condition; Lane 3 = pBR322 DNA with riboflavin in light condition; Lane 4-7 = pBR322 DNA with riboflavin in light condition in the presence of oxyresveratrol 50, 80, 100 and 140 μM, respectively. OC = open circular form or nicked DNA, SC = close circular form or supercoiled DNA; **(b)** Oxyresveratrol showed concentration-dependent inhibition of DNA damage induced by photosensitized riboflavin.

Table 14: Inhibitory effect of oxyresveratrol on DNA breakage

Concentration (μM)	% Inhibition
20	4.50 ± 0.77
30	2.94 ± 0.83
40	4.60 ± 2.61
50	5.16 ± 2.65
60	20.12 ± 0.73
70	34.14 ± 0.83
80	50.32 ± 0.83
100	69.15 ± 0.88
120	71.0 ± 0.76
140	76.30 ± 2.11

The ROS produced from the photochemical reaction of riboflavin include superoxide anion ($O_2^{\bullet-}$) and singlet oxygen ($^1O_2$) as the major and minor chemical entities, respectively (Cardoso *et al.*, 2007). To investigate the involvement of $O_2^{\bullet-}$ in the supercoiled DNA breakage, the riboflavin-nitrobluetetrazolium (NBT)-light assay was employed. Superoxide anion can reduce nitrobluetetrazolium (NBT) to form blue formazan. Low intensity of the blue color is observed if a scavenger of $O_2^{\bullet-}$ is present.

In this test system, oxyresveratrol showed strong $O_2^{\bullet-}$ scavenging activity, consistent with the result previously obtained by the superoxide dismutase method (Oh *et al.*, 2002). From Figure 4, it is clear that ascorbic acid was a poor $O_2^{\bullet-}$

scavenger, with maximum inhibition of 26% at 2.0 mM. Oxyresveratrol demonstrated lower superoxide quenching activity than Trolox.

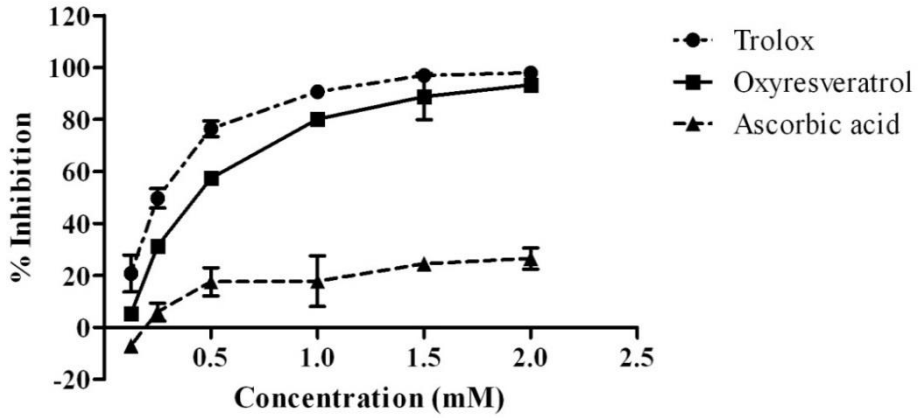

Figure 4 : Inhibitory effects of oxyresveratrol, Trolox and ascorbic acid on formazan formation induced by photodegradation of riboflavin.

In fact, its $O_2^{\bullet-}$ scavenging activity was only about three-fifths of that of Trolox (EC_{50} 0.45 *vs* 0.27 mM.). This was opposite to their comparative DNA protective activities (see above). These results suggested that in addition to superoxide anion, other RCS such as singlet oxygen and triplet-excited riboflavin might also play important roles in the DNA scission. Oxyresveratrol could possibly interfere with these RCS better than Trolox and ascorbic acid, and therefore was a much stronger DNA protective agent.

Among the twenty-six derivatives of **1**, only fourteen showed more than 80% inhibition at a concentration of 100 µg/mL, and were further evaluated for IC_{50} values. The results, as summarized in the Table 15, show that **46** was the most potent with an IC_{50} value of 5.97 µM.

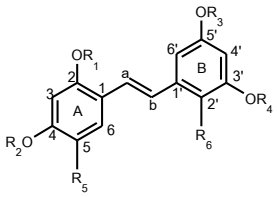

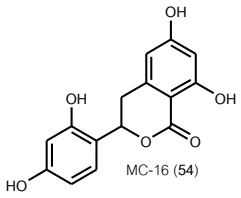

Table 15: Inhibitory effect of synthesized compounds on DNA breakage

Cpd	Substitution						DNA breakage	
	R_1	R_2	R_3	R_4	R_5	R_6	% inhibition (100 µg/mL)	IC_{50} (µM)
1	H	H	H	H	H	H	96.65 ± 3.99	43.31 ± 6.73
41	H	H	H	H	H	Cl	93.75 ± 0.90	31.96 ± 1.42
42	Me	Me	Me	Me	H	Cl	20.18 ± 7.85	nd
43	Isp	Isp	Isp	Isp	H	H	20.97 ± 2.47	nd
44	Isp	Isp	Isp	H	H	H	63.52 ± 4.53	nd
45	Isp	Isp	H	H	H	H	97.04 ± 1.81	59.11 ± 9.85
35	Me	Me	Me	Me	H	H	72.13 ± 2.80	nd
46	Me	Me	Me	H	H	H	94.25 ± 0.80	5.97 ± 1.27*
47	Me	Me	H	H	H	H	91.94 ± 3.87	39.42 ± 1.22
38	Ac	Ac	Ac	Ac	H	H	57.91 ± 4.09	nd
48	Isp	Isp	Isp	CH_2COOEt	H	H	11.22 ± 3.61	nd
49	H	H	H	CH_2COOEt	H	H	96.25 ± 5.34	19.85 ± 2.76*
50	H	H	H	CH_2COOH	H	H	90.47 ± 4.21	28.58 ± 3.76
51	Isp	Isp	Ac	Ac	H	H	71.26 ± 4.81	nd
52	Isp	Isp	Isp	Isp	H	CHO	18.51 ± 2.28	nd
53	Isp	Isp	Isp	Isp	H	COOH	9.39 ± 1.96	nd
54	-	-	-	-	-	CO	95.80 ± 3.32	28.32 ± 4.34
55	H	H	H	H	H	CHO	96.33 ± 0.85	32.22 ± 4.84
56	Isp	Isp	Isp	Isp	H	OH	16.83 ± 3.87	nd
57	Isp	Isp	Isp	Isp	H	CH=CH COOEt	11.39 ± 3.18	nd
58	Isp	Isp	Ac	Ac	CHO	H	39.46 ± 2.69	nd
59	Isp	Isp	Ac	Ac	COOH	H	92.24 ± 5.99	81.43 ± 4.17*
60	H	H	H	H	CHO	H	98.25 ± 1.06	54.70 ± 8.25
61	H	H	H	H	COOH	H	92.44 ± 5.70	79.40 ± 14.94*
62	Isp	Isp	H	H	CHO	H	92.55 ± 3.34	111.77 ± 7.26*
63	Isp	Isp	H	H	COOH	H	94.92 ± 2.89	104.72 ± 8.46*
64	Isp	Isp	Ac	Ac	OH	H	97.12 ± 1.27	18.55 ± 7.12*
Trolox				-			92.12 ± 2.18	113.11 ± 4.60*

nd = not determined due to < 80% inhibition; * P < 0.05 relative to **1**, one way ANOVA.

4.2.2.1 *O*-alkylation/acylation

O-alkylation/acylation of oxyresveratrol resulted in the loss or decrease of DNA protective activity in some derivatives, such as **35, 43**-**45**, **48** and **51**. However, **46** demonstrated pronounced enhanced activity, being significantly 7-fold and 19-fold stronger than oxyresveratrol and Trolox, respectively, while **47** exhibited marginally increased activity (Table 15). The disappearance of the olefinic bond slightly improved the activity, as seen in **54**.

It should be highlighted that, once more, replacing the OH at C-3′ of oxyresveratrol with a *O*-carbethoxymethyl ($OCH_2COOCH_2CH_3$) or *O*-carboxymethyl (OCH_2COOH) group provided more potent analogues, **49** and **50**, resembling the outcomes in the study on anti-DPPH and anti-superoxide activity (see above). However, after statistical analysis, only **49** was found to be significantly stronger than oxyresveratrol.

4.2.2.2 Substitution on ring B

The effect of Cl at C-2′ on the activity could not be concluded since oxyresveratrol gave a chloro-product (**41**) with a little stronger activity, but **35** was stronger than its chloro-derivative **42**. The CHO and COOH group appeared to have no significant effect on the activity because no recognizable alteration of the activity was observed when **43** was transformed into the 2′-formyl (**52**) or 2′-carboxyl derivative (**53**). Only a little improvement of activity was seen in **55**, a 2′-formyl

product of oxyresveratrol. A small decrease of activity was observed when a carbethoxyethenyl ($CH=CHCOOCH_2CH_3$) substituent was placed at C-2′, as seen in **57** in comparison with **43**.

4.2.2.3 Substitution on ring A

Only insignificant change in the magnitude of the activity was observed when the CHO or COOH was introduced to the A ring. For example, placing a CHO group at C-5 of the A ring could slightly decrease the activity of **51**, as seen in **58**, whereas the COOH appeared to somewhat enhance the activity (**59**). The activity of the 5-formyl (**60**) or 5-carboxyoxyresveratrol (**61**) was more or less in the same range as oxyresveratrol. Compound **45** had a slightly reduced activity when converted to **62** or **63**.

4.2.2.4 Introduction of OH to ring A or B

On ring B, the introduction of an OH group at C-2′ had no effect on the activity, as can be seen from the approximately equal activity of **43** and **56**. On the contrary, the hydroxylation at C-5 of ring A of **51** transformed the compound into a stronger compound, **64**.

4.2.3 Anti-herpes simplex virus activity

Eleven compounds were considered to have recognizable anti-HSV activity (Table 16). Compound **46** was the most potent with an IC_{50} value of 32.8 μM. This compound was also the analogue with strongest DNA protective activity.

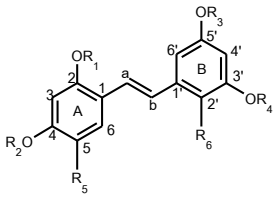

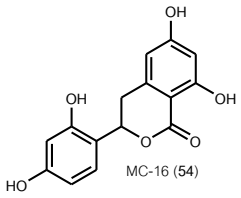

Table 16: Anti-herpes simplex virus activity of synthesized compounds

Cpd	Substitution						Herpes simplex I	
	R_1	R_2	R_3	R_4	R_5	R_6	IC_{50} (μg/mL (μM))	CC_{50} (μg/mL (μM))
1	H	H	H	H	H	H	35.9±4.1 (147.13)	150 (614.75)
41	H	H	H	H	H	Cl	Inactive*	nd
42	Me	Me	Me	Me	H	Cl	Inactive*	nd
43	Isp	Isp	Isp	Isp	H	H	Inactive*	nd
44	Isp	Isp	Isp	H	H	H	39.6±4.1 (107.03)	100 (270.27)
45	Isp	Isp	H	H	H	H	Inactive***	nd
35	Me	Me	Me	Me	H	H	Inactive*	nd
46	Me	Me	Me	H	H	H	9.38±4.2 (32.8)[#]	> 18.7 (>65.38)
47	Me	Me	H	H	H	H	10.94±2.21 (40.22)[#]	> 37.59 (> 137.87)
38	Ac	Ac	Ac	Ac	H	H	Inactive*	nd
48	Isp	Isp	Isp	CH_2COOEt	H	H	Inactive***	nd
49	H	H	H	CH_2COOEt	H	H	60.15±9.54 (189.15)	>150 (>454.54)
50	H	H	H	CH_2COOH	H	H	Inactive*	nd
51	Isp	Isp	Ac	Ac	H	H	Inactive**	nd
52	Isp	Isp	Isp	Isp	H	CHO	57.3±6.5 (130.23)	100 (227.27)
53	Isp	Isp	Isp	Isp	H	COOH	56.3±8.8 (123.46)	100 (219.30)
54	-	-	-	-	-	CO	83.3±11.8 (289.24)[#]	150 (520.83)
55	H	H	H	H	H	CHO	Inactive***	nd
56	Isp	Isp	Isp	Isp	H	OH	Inactive*	nd
57	Isp	Isp	Isp	Isp	H	CH=CH COOEt	Inactive*	nd
58	Isp	Isp	Ac	Ac	CHO	H	82.8±11.0 (188.18)	150 (340.91)
59	Isp	Isp	Ac	Ac	COOH	H	94.55±7.71 (260.29)	>100 (>219.30)
60	H	H	H	H	CHO	H	93.8±8.8 (344.85)[#]	150 (367.62)
61	H	H	H	H	COOH	H	Inactive*	nd
62	Isp	Isp	H	H	CHO	H	Inactive*	nd
63	Isp	Isp	H	H	COOH	H	84.36±13.3 (226.77)[#]	>100 (>268.82)
64	Isp	Isp	Ac	Ac	OH	H	Inactive*	nd
ACV	-						0.37±0.01 (1.64)[#]	nd

ACV = acyclovir; nd = not determined; *inactive at conc 100 μg/mL; **inactive at conc 50 μg/mL

***inactive at conc 25 μg/mL; [#] $P < 0.05$ relative to **1**, one way ANOVA.

Although it is difficult to make a generalization regarding the relationships between the *O*-alkyl/acyl groups and the anti-HSV activity, a preliminary discussion can be made. Some of the modified structures (**35**, **38, 43**, **45**, **48-51)** revealed lost or lessened anti-HSV activity, but the others displayed enhanced activity. The *O*-alkyl/acyl analogues that possessed increased anti-HSV activity in comparison with oxyresveratrol had a free OH at C-3′, with three isopropoxyl (as in **44**) or two or three methoxyl groups (as in **46** and **47**). The smaller alkoxyl groups (i.e. methoxyl in **46** and **47**) seemed more favorable than the larger ones (i.e. isopropoxyl in **44**). In terms of comparative IC_{50} (μM) values, compounds **46** and **47** were 4.5- and 3.7-fold, respectively, more potent than oxyresveratrol. Their respective selectivity indices were found to be 2 and 3.4, which were close to that of oxyresveratrol (4.2).

Chlorination at C-2′ of ring B seemed to destroy the activity as seen in **41**. The introduction of CHO onto C-2′ of oxyresveratrol in the preparation of **55** led to the loss of activity. However, in contrast, placing CHO or COOH at this position of **43** could partially recover the lost activity, as observed in **52** or **53**. For ring A, placing a CHO or COOH functionality at C-5 of oxyresveratrol also resulted in the loss or reduction of activity, as seen in **60** and **61**. Nevertheless, the disappeared activity of **51** can be partly restored when a group of CHO or COOH was placed at C-5, as seen in **58** and **59**. A similar recovery of activity was also found when **45** was provided a COOH at C-5 (as in **63**), but not a CHO (as in **62**).

4.2.4 Neuraminidase inhibitory activity

Oxyresveratrol showed only weak inhibitory activity against the enzyme neuraminidase, as compared with oseltamivir, the positive control. Among the oxyresveratrol analogues prepared in the study, only **61** showed activity in the same range as oxyresveratrol while the others were considered as totally inactive (Table 17).

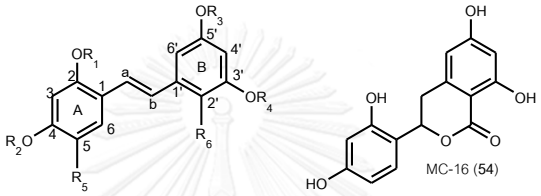

Table 17: Anti-neuraminidase activity of synthesized compounds

Cpd	Substitution						Neuraminidase	
	R_1	R_2	R_3	R_4	R_5	R_6	% inhibition (100 µg/mL)	IC_{50} (µg/mL (µM))
1	H	H	H	H	H	H	71.15	78.11 (319.81)
41	H	H	H	H	H	Cl	48.91	nd
42	Me	Me	Me	Me	H	Cl	ne	ne
43	Isp	Isp	Isp	Isp	H	H	20.69	nd
44	Isp	Isp	Isp	H	H	H	27.20	nd
45	Isp	Isp	H	H	H	H	30.53	nd
35	Me	Me	Me	Me	H	H	35.29	nd
46	Me	Me	Me	H	H	H	ne	ne
47	Me	Me	H	H	H	H	ne	ne
38	Ac	Ac	Ac	Ac	H	H	27.16	nd
48	Isp	Isp	Isp	CH_2COOEt	H	H	25.88	nd
Osel				-				0.5 nM

Osel = oseltamivir; nd = not determined due to < 50% inhibition; ne = not evaluated due to insufficient amount.

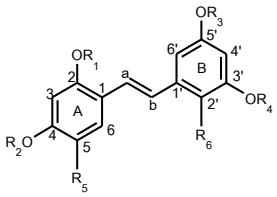

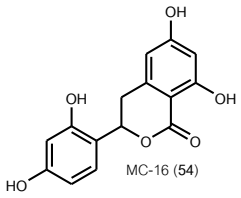

Table 17: Anti-neuraminidase activity of synthesized compounds (continued)

Cpd	Substitution						Neuraminidase	
	R_1	R_2	R_3	R_4	R_5	R_6	% inhibition (100 µg/mL)	IC_{50} (µg/mL (µM))
49	H	H	H	CH_2COOEt	H	H	ne	ne
50	H	H	H	CH_2COOH	H	H	ne	ne
51	Isp	Isp	Ac	Ac	H	H	29.98	nd
52	Isp	Isp	Isp	Isp	H	CHO	17.79	nd
53	Isp	Isp	Isp	Isp	H	COOH	12.80	nd
54	-	-	-	-	-	CO	35.11	nd
55	H	H	H	H	H	CHO	49.16	nd
56	Isp	Isp	Isp	Isp	H	OH	ne	ne
57	Isp	Isp	Isp	Isp	H	CH=CH COOEt	ne	ne
58	Isp	Isp	Ac	Ac	CHO	H	23.03	nd
59	Isp	Isp	Ac	Ac	COOH	H	ne	ne
60	H	H	H	H	CHO	H	39.71	nd
61	H	H	H	H	COOH	H	74.60	74.33 (258.29)
62	Isp	Isp	H	H	CHO	H	ne	ne
63	Isp	Isp	H	H	COOH	H	ne	ne
64	Isp	Isp	Ac	Ac	OH	H	ne	ne
Osel				-				0.5 nM

Osel = oseltamivir; nd = not determined due to < 50% inhibition; ne = not evaluated due to insufficient amount.

4.2.5 Cytotoxicity against cancer cells

Sixteen of the twenty-six oxyresveratrol derivatives were found to be active against for KB cells (IC_{50} < 50 μg/mL), and ten compounds were active for MCF-7 cells (Table 18).

Regarding the compounds that were active against KB cells, almost all, except for **49**, showed greater activity than oxyresveratrol. They included **35, 38, 41**, **42**, **44**-**47, 51**, **53, 55**, **58**, **60**, **62** and **64**. Compound **51** was the most potent compound with activity 7.9-fold stronger than that of the parent compound. Six compounds were selectively active against KB cells, including **35**, **42**, **49**, **53**, **55** and **60**. In this study, analogues with a CHO group on ring A or B (i.e. **55**, **58**, **60** and **62**) were active whereas their counterparts with a COOH group (i.e. **59**, **61** and **63**) were inactive. The reverse was found only between **52** and **53**.

With regard to the ten compounds that showed cytotoxicity against MCF-7 cells, all of them also exhibited activity against KB cells and were more potent than oxyresveratrol. The strongest compound was **44**, showing 4.8- fold higher activity than the parent compound. The effects of the CHO and COOH functionality on the activity against MCF-7 cells were not obvious. The disappearance of the olefinic structure led to the loss of cytotoxicity against both types of cancer cells.

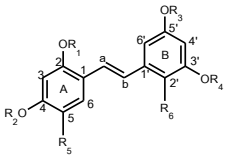

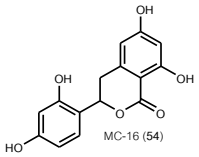

Table 18: IC_{50} values for cytotoxic activity of synthesized compounds

Cpd	Substitution						Cytotoxicity IC_{50} (μg/mL (μM))	
	R_1	R_2	R_3	R_4	R_5	R_6	KB	MCF-7
1	H	H	H	H	H	H	23.30 (95.49)	23.69 (97.09)
41	H	H	H	H	H	Cl	13.32 (47.91)	19.93 (71.69)
42	Me	Me	Me	Me	H	Cl	23.57 (70.57)	inactive
43	Isp	Isp	Isp	Isp	H	H	inactive	inactive
44	Isp	Isp	Isp	H	H	H	8.54 (23.08)	7.44 (20.11)
45	Isp	Isp	H	H	H	H	8.42 (25.67)	11.21 (34.18)
35	Me	Me	Me	Me	H	H	17.71 (57.0)	inactive
46	Me	Me	Me	H	H	H	14.04 (49.09)	20.77 (72.62)
47	Me	Me	H	H	H	H	20.19 (74.23)	20.99 (77.17)
38	Ac	Ac	Ac	Ac	H	H	25.80 (62.62)	19.88 (48.25)
48	Isp	Isp	Isp	CH_2COOEt	H	H	inactive	inactive
49	H	H	H	CH_2COOEt	H	H	41.78(126.61)	inactive
50	H	H	H	CH_2COOH	H	H	inactive	inactive
51	Isp	Isp	Ac	Ac	H	H	4.95 (12.01)	24.67 (59.88)
52	Isp	Isp	Isp	Isp	H	CHO	inactive	inactive
53	Isp	Isp	Isp	Isp	H	COOH	18.74 (41.10)	inactive
54	-	-	-	-	-	CO	inactive	inactive
55	H	H	H	H	H	CHO	14.13 (51.95)	inactive
56	Isp	Isp	Isp	Isp	H	OH	inactive	inactive
57	Isp	Isp	Isp	Isp	H	CH=CH COOEt	inactive	inactive
58	Isp	Isp	Ac	Ac	CHO	H	16.29 (30.02)	24.37 (55.39)
59	Isp	Isp	Ac	Ac	COOH	H	inactive	inactive
60	H	H	H	H	CHO	H	20.79 (76.43)	inactive
61	H	H	H	H	COOH	H	inactive	inactive
62	Isp	Isp	H	H	CHO	H	13.50 (37.92)	18.55 (52.11)
63	Isp	Isp	H	H	COOH	H	inactive	inactive
64	Isp	Isp	Ac	Ac	OH	H	23.38 (54.63)	20.97 (49.00)
Elli				-			1.40 (4.22)	nd
Doxo				-			6.95 (12.79)	0.096 (0.177)
Tam				-			nd	8.31 (22.37)

Elli = Ellipticine; Doxo = Doxorubicin; Tam = Tamoxifen; Inactive at concentration 50 μg/mL; nd = not determined.

4.2.6 Inhibitory activity on α-glucosidase

In this study, ten compounds showed more than 90 % inhibition of the enzyme α-glucosidase and were further evaluated for IC_{50} values (Table 19). Compounds **41**, **44**, **54**, **55**, **60** and **62** displayed activity in the same range as that of oxyresveratrol ($p > 0.05$). Among these compounds, **44** appears to be the most attractive target for further investigation in animals, as predicted from its expected increased resistance to the degradation in the digestive system.

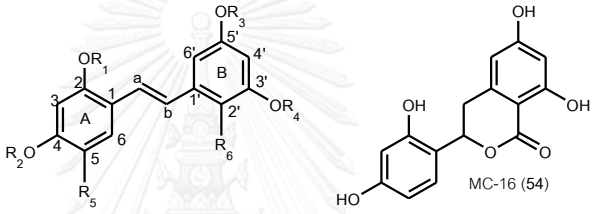

Table 19: Anti α-glucosidase activity of synthesized compounds

Cpd	Substitution						α-glucosidase	
	R_1	R_2	R_3	R_4	R_5	R_6	% inhibition (100 μg/mL)	IC_{50} (μg/mL(μM))
1	H	H	H	H	H	H	95.05±1.35	4.76±0.41 (19.53)
41	H	H	H	H	H	Cl	93.27±1.29	6.31±1.00 (22.70)*
42	Me	Me	Me	Me	H	Cl	34.35±12.2	nd
43	Isp	Isp	Isp	Isp	H	H	57.40±16.2	nd
44	Isp	Isp	Isp	H	H	H	95.12±5.04	7.23±1.32 (19.55)*
45	Isp	Isp	H	H	H	H	101.25±1.46	20.15±1.22 (61.45)
35	Me	Me	Me	Me	H	H	75.11±8.81	nd
Acarbose	-						-	481.54±57.1 (745.88)

nd = not determined due to < 90% inhibition; * P > 0.05 relative to **1**, one way ANOVA.

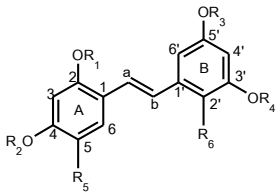

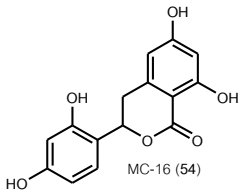

Table 19: Anti α-glucosidase activity of synthesized compounds (continued)

Cpd	Substitution						α-glucosidase	
	R_1	R_2	R_3	R_4	R_5	R_6	% inhibition (100 μg/mL)	IC_{50} (μg/mL(μM))
46	Me	Me	Me	H	H	H	99.82±0.19	115.24
47	Me	Me	H	H	H	H	73.68±18.1	nd
38	Ac	Ac	Ac	Ac	H	H	-6.85±6.86	nd
48	Isp	Isp	Isp	CH_2COOEt	H	H	17.57±14.8	nd
49	H	H	H	CH_2COOEt	H	H	72.47±13.7	nd
50	H	H	H	CH_2COOH	H	H	99.97±0.19	20.81±2.46 (68.90)
51	Isp	Isp	Ac	Ac	H	H	2.65±0.85	nd
52	Isp	Isp	Isp	Isp	H	CHO	46.36±11.24	nd
53	Isp	Isp	Isp	Isp	H	COOH	4.54±4.44	nd
54	-	-	-	-	-	CO	94.84±2.11	7.12±0.43 (24.72)*
55	H	H	H	H	H	CHO	101.37±11.3	8.07±1.61 (29.65)*
56	Isp	Isp	Isp	Isp	H	OH	108.38±8.5	69.20±3.00 (161.69)
57	Isp	Isp	Isp	Isp	H	CH=CHCOOEt	72.82±12.7	nd
58	Isp	Isp	Ac	Ac	CHO	H	2.71±12.2	nd
59	Isp	Isp	Ac	Ac	COOH	H	6.80±4.92	nd
60	H	H	H	H	CHO	H	97.13±1.60	8.10±0.90 (29.78)*
61	H	H	H	H	COOH	H	50.91±10.8	nd
62	Isp	Isp	H	H	CHO	H	98.94±1.88	13.63±1.25 (38.27)*
63	Isp	Isp	H	H	COOH	H	51.38±14.14	nd
64	Isp	Isp	Ac	Ac	OH	H	87.27±8.29	nd
Acarbose	-						-	481.54±57.1 (745.88)

nd = not determined due to < 90% inhibition; * P > 0.05 relative to **1**, one way ANOVA.

CHAPTER V

CONCLUSION

In this study, twenty-six derivatives (**35, 38**, **4**1-**64**) were prepared from oxyresveratrol (**1**) through several types of reactions, including *O*-alkylation/acylation, aromatic electrophilic substitution and oxidation.

Several attempts to carry out halogenation of **1** with Cl, Br or I were made, but only chlorination under a certain condition was successful, giving the expected product 2′-chloro-oxyresveratrol (**41**). *O*-alkylation/acylation reactions of **1** also occurred readily. It was found that the OHs at C-2 and C-4 on ring A were more reactive to etherification than those on ring B, and selective di-*O*-alkylation to obtain a product such as **45** was possible.

The B ring of oxyresveratrol was generally more receptive to electrophilic attack than ring A, particularly at positions 2′/6′. However, the relative reactivity of these two aromatic rings could be reversed by manipulating the type and the number of protecting groups on the four phenol functionalities. A di-*O*-alkyl-di-*O*-acyl structure such as **51** could be easily prepared from **45**. This is equivalent to the deactivation of ring B, and as a result, an electrophile would prefer to attack ring A of **51**. In this manner, substitution with electron-withdrawing groups, such as the CHO, COOH and OH, could be selectively directed to ring A or B. This finding has provided

a new and useful strategy for the future chemical modification of polyoxygenated stilbenes.

Comparative biological studies on oxyresveratrol and analogues were conducted to investigate their ability to protect DNA, and their inhibitory activity against the herpes simplex virus, some cancer cells, and the enzymes neuraminidase and α-glucosidase.

Regarding the DNA protective activity, a new assay was developed. In this assay, oxyresveratrol showed more potent activity than the known antioxidants Trolox and ascorbic acid. Eight of the twenty-six of oxyresveratrol analogues were found to have higher activity than the parent compound. The strongest compound was **46,** followed by **64** and **49.** The DNA protective property of **46** seemed to go in parallel with its scavenging activity against superoxide ion, but not with DPPH. On the contrary, **64** showed strong activity only in the DNA and DPPH assays, but exhibited no activity against the superoxide anion. The results taken from the three assays appear to suggest that **49** might be a better DNA protective agent than **46** or **64**, since the compound exhibited greater activity than **1** in all of the three types of assessment.

Concerning the anti-HSV activity, **46** and **47** were two interesting compounds because they had IC_{50} values significantly lower than that of **1**, but with cytotoxicity similar to that of **1**. The two stilbenes also showed potent DNA protective activity.

From this point of view, **46** and **47** may be considered as lead structures for further investigation if dual biological activities are desired.

As for the anti-neuraminidase activity, only **61** showed slightly better activity than oxyresveratrol, but the activities of both compounds were still considered very weak, as compared with that of oseltamivir. Regarding the inhibitory activity against α-glucosidase, six compounds**,** including **44**, showed activity comparable to that of **1**. The apparently lessened polarity of **44** could be considered as a favorable property since this may render resistance to metabolism in our body, but its cytotoxicity must also be taken into consideration (see below).

Regarding the cytotoxicity against KB and MCF-7 cells, **51** was the most potent, followed by **44** with 7.9- and 4.8-fold higher activity than that of **1**. Some analogues of **1** showed activity against only KB cells for unclear reasons. A preliminary *in vivo* study should be pursued to see whether significant antitumor effects of these compounds can be observed.

It is hoped that the novel chemical and biological data of the polyoxygenated stilbenes obtained in this investigation would provide information useful for the future development of medicinally useful agents.

REFERENCES

Acharya, J., & Ghaskadbi, S. (2013). Protective effect of pterostilbene against free radical mediated oxidative damage. *BMC Complementary and Alternative Medicine, 13*(1), 238.

Aftab, N., Likhitwitayawuid, K., & Vieira, A. (2010). Comparative antioxidant activities and synergism of resveratrol and oxyresveratrol. *Natural Product Research, 24*(18), 1726-1733.

Andrabi, S. A., Spina, M. G., Lorenz, P., Ebmeyer, U., Wolf, G., & Horn, T. F. W. (2004). Oxyresveratrol (*trans*-2,3′,4,5′-tetrahydroxystilbene) is neuroprotective and inhibits the apoptotic cell death in transient cerebral ischemia. *Brain Research, 1017*(1–2), 98-107.

Cardin, A. D., & Tyms, S. A. (1992). Sulfonic stilbene derivatives in the treatment of viral diseases: U.S. Patents.

Cardoso, D. R., Olsen, K., & Skibsted, L. H. (2007). Mechanism of deactivation of triplet-excited riboflavin by ascorbate, carotenoids, and tocopherols in homogeneous and heterogeneous aqueous food model systems. *Journal of Agricultural and Food Chemistry, 55*(15), 6285-6291.

Cheng, T.-C., Lai, C.-S., Chung, M.-C., Kalyanam, N., Majeed, M., Ho, C.-T., Ho, Y.-S., & Pan, M.-H. (2014). Potent anti-cancer effect of 3′-hydroxypterostilbene in human colon xenograft tumors. *PLoS One, 9*(11), e111814.

Cheung, T. K. W., & Poon, L. L. M. (2007). Biology of influenza A virus. *Annals of the New York Academy of Sciences, 1102*(1), 1-25.

Chuanasa, T., Phromjai, J., Lipipun, V., Likhitwitayawuid, K., Suzuki, M., Pramyothin, P., Hattori, M., & Shiraki, K. (2008). Anti-herpes simplex virus (HSV-1) activity of oxyresveratrol derived from Thai medicinal plant: Mechanism of action and therapeutic efficacy on cutaneous HSV-1 infection in mice. *Antiviral Research, 80*(1), 62-70.

Chung, K. O., Kim, B. Y., Lee, M. H., Kim, Y. R., Chung, H. Y., Park, J. H., & Moon, J. O. (2003). *In-vitro* and *in-vivo* anti-inflammatory effect of oxyresveratrol from *Morus alba* L. *Journal of pharmacy and pharmacology, 55*(12), 1695-1700.

Cragg, G. M., & Newman, D. J. (2005). Plants as a source of anti-cancer agents. *Journal of Ethnopharmacology, 100*(1–2), 72-79.

Csuk, R., Albert, S., & Siewert, B. (2013). Synthesis and radical scavenging activities of resveratrol analogs. *Archiv der Pharmazie, 346*(7), 504-510.

Dasgupta, N., & De, B. (2004). Antioxidant activity of *Piper betle* L. leaf extract *in vitro*. *Food Chemistry, 88*(2), 219-224.

De Clercq, E., & Neyts, J. (2007). Avian influenza A (H5N1) infection: Targets and strategies for chemotherapeutic intervention. *Trends in Pharmacological Sciences, 28*(6), 280-285.

de Jong, M. D., & Hien, T. T. (2006). Avian influenza A (H5N1). *Journal of Clinical Virology, 35*(1), 2-13.

Docherty, J. J., Fu, M. M. H., Stiffler, B. S., Limperos, R. J., Pokabla, C. M., & DeLucia, A. L. (1999). Resveratrol inhibition of herpes simplex virus replication. *Antiviral Research, 43*(3), 145-155.

Fang, Y.-Z., Yang, S., & Wu, G. (2002). Free radicals, antioxidants, and nutrition. *Nutrition, 18*(10), 872-879.

Fatahzadeh, M., & Schwartz, R. A. (2007). Human herpes simplex virus infections: Epidemiology, pathogenesis, symptomatology, diagnosis, and management. *Journal of the American Academy of Dermatology, 57*(5), 737-763.

Galindo, I., Hernáez, B., Berná, J., Fenoll, J., Cenis, J. L., Escribano, J. M., & Alonso, C. (2011). Comparative inhibitory activity of the stilbenes resveratrol and oxyresveratrol on African swine fever virus replication. *Antiviral Research, 91*(1), 57-63.

George, V. C., Kumar, D. R. N., Suresh, P. K., & Kumar, R. A. (2015). Antioxidant, DNA protective efficacy and HPLC analysis of *Annona muricata* (soursop) extracts. *Journal of Food Science and Technology, 52*(4), 2328-2335.

He, H., & Lu, Y.-H. (2013). Comparison of inhibitory activities and mechanisms of five mulberry plant bioactive components against α-glucosidase. *Journal of Agricultural and Food Chemistry, 61*(34), 8110-8119.

Kongkamnerd, J. (2010). *Development of non-cell based assays for screening of inhibitiors against avian influenza neuraminidase.* Doctoral dissertation,

Department of Pharmacognosy and Pharmaceutical Botany, Faculty of Pharmaceutical Sciences, Chulalongkorn University.

Korycka-Dahl, M., & Richardson, T. (1977). Photogeneration of superoxide anion in serum of bovine milk and in model systems containing riboflavin and amino acids. *Journal of Dairy Science, 61*(4), 400-407.

Kubo, I., Murai, Y., Soediro, I., Soetarno, S., & Sastrodihardjo, S. (1991). Efficient isolation of glycosidase inhibitory stilbene glycosides from *Rheum palmatum*. *Journal of Natural Products, 54*(4), 1115-1118.

Kumar, M., Kumar, S., & Kaur, S. (2011). Investigations on DNA protective and antioxidant potential of chloroform and ethyl acetate fractions of *Koelreuteria paniculata* Laxm. *African Journal of Pharmacy and Pharmacology, 5*(3), 421-427.

Lam, S.-H., Chen, J.-M., Kang, C.-J., Chen, C.-H., & Lee, S.-S. (2008). α-Glucosidase inhibitors from the seeds of *Syagrus romanzoffiana*. *Phytochemistry, 69*(5), 1173-1178.

Li, C., Fang, J. S., Lian, W. W., Pang, X. C., Liu, A. L., & Du, G. H. (2015). *In vitro* antiviral effects and 3D QSAR study of resveratrol derivatives as potent inhibitors of influenza H1N1 neuraminidase. *Chemical Biology and Drug Design, 85*(4), 427-438.

Li, H., Wu, W. K. K., Zheng, Z., Che, C. T., Li, Z. J., Xu, D. D., Wong, C. C. M., Ye, C. G., Sung, J. J. Y., Cho, C. H., & Wang, M. (2010). 3,3′,4,5,5′-Pentahydroxy-*trans*-

stilbene, a resveratrol derivative, induces apoptosis in colorectal carcinoma cells via oxidative stress. *European Journal of Pharmacology, 637*(1–3), 55-61.

Likhitwitayawuid, K., Chaiwiriya, S., Sritularak, B., & Lipipun, V. (2006a). Antiherpetic flavones from the heartwood of *Artocarpus gomezianus*. *Chemistry and Biodiversity, 3*(10), 1138-1143.

Likhitwitayawuid, K., Klongsiriwet, C., Jongbunprasert, V., Sritularak, B., & Wongseripipatana, S. (2006b). Flavones with free radical scavenging activity from *Goniothalamus tenuifolius*. *Archives of Pharmacal Research, 29*(3), 199-202.

Likhitwitayawuid, K., Sornsute, A., Sritularak, B., & Ploypradith, P. (2006c). Chemical transformations of oxyresveratrol (*trans*-2,4,3′,5′-tetrahydroxystilbene) into a potent tyrosinase inhibitor and a strong cytotoxic agent. *Bioorganic & Medicinal Chemistry Letters, 16*(21), 5650-5653.

Likhitwitayawuid, K., Sritularak, B., Benchanak, K., Lipipun, V., Mathew, J., & Schinazi, R. F. (2005). Phenolics with antiviral activity from *Millettia erythrocalyx* and *Artocarpus lakoocha*. *Natural Product Research, 19*(2), 177-182.

Lin, C.-N., Chen, H.-L., & Yen, M.-H. (2008). Flavonoids with DNA strand-scission activity from *Rhus javanica* var. *Roxburghiana*. *Fitoterapia, 79*(1), 32-36.

Lipipun, V., Kurokawa, M., Suttisri, R., Taweechotipatr, P., Pramyothin, P., Hattori, M., & Shiraki, K. (2003). Efficacy of Thai medicinal plant extracts against herpes

simplex virus type 1 infection *in vitro* and *in vivo*. *Antiviral Research, 60*(3), 175-180.

Lipipun, V., Sasivimolphan, P., Yoshida, Y., Daikoku, T., Sritularak, B., Ritthidej, G., Likhitwitayawuid, K., Pramyothin, P., Hattori, M., & Shiraki, K. (2011). Topical cream-based oxyresveratrol in the treatment of cutaneous HSV-1 infection in mice. *Antiviral Research, 91*(2), 154-160.

Liu, A. L., Yang, F., Zhu, M., Zhou, D., Lin, M., Lee, S. M. Y., Wang, Y. T., & Du, G. H. (2010). *In vitro* anti-influenza viral activities of stilbenoids from the lianas of *Gnetum pendulum*. *Planta Medica, 76*(16), 1874-1876.

Lordan, S., Smyth, T. J., Soler-Vila, A., Stanton, C., & Ross, R. P. (2013). The α-amylase and α-glucosidase inhibitory effects of irish seaweed extracts. *Food Chemistry, 141*(3), 2170-2176.

Lorenz, P., Roychowdhury, S., Engelmann, M., Wolf, G., & Horn, T. F. W. (2003). Oxyresveratrol and resveratrol are potent antioxidants and free radical scavengers: Effect on nitrosative and oxidative stress derived from microglial cells. *Nitric Oxide, 9*(2), 64-76.

Marimuthu, S., Balakrishnan, P., & Nair, S. (2013). Phytochemical investigation and radical scavenging activities of *Melia azedarach* and its DNA protective effect in cultured lymphocytes. *Pharmaceutical Biology, 51*(10), 1331-1340.

Maurya, D. K., Adhikari, S., Nair, C. K. K., & Devasagayam, T. P. A. (2007). DNA protective properties of vanillin against γ-radiation under different conditions:

Possible mechanisms. *Mutation Research/Genetic Toxicology and Environmental Mutagenesis, 634*(1–2), 69-80.

McCarthy, A. L., O'Callaghan, Y. C., Connolly, A., Piggott, C. O., FitzGerald, R. J., & O'Brien, N. M. (2012). Phenolic extracts of brewers' spent grain (BSG) as functional ingredients – assessment of their DNA protective effect against oxidant-induced DNA single strand breaks in U937 cells. *Food Chemistry, 134*(2), 641-646.

Moran, B. W., Anderson, F. P., Devery, A., Cloonan, S., Butler, W. E., Varughese, S., Draper, S. M., & Kenny, P. T. M. (2009). Synthesis, structural characterisation and biological evaluation of fluorinated analogues of resveratrol. *Bioorganic & Medicinal Chemistry, 17*(13), 4510-4522.

Nguyen, T. N. A., Dao, T. T., Tung, B. T., Choi, H., Kim, E., Park, J., Lim, S.-I. L., & Oh, W. K. (2011). Influenza A (H1N1) neuraminidase inhibitors from *Vitis amurensis*. *Food Chemistry, 124*(2), 437-443.

O'Brien, J., Wilson, I., Orton, T., & Pognan, F. (2000). Investigation of the Alamar Blue (resazurin) fluorescent dye for the assessment of mammalian cell cytotoxicity. *European Journal of Biochemistry, 267*(17), 5421-5426.

Oh, H., Ko, E. K., Jun, J. Y., Oh, M. H., Park, S. U., Kang, K. H., Lee, H. S., & Kim, Y. C. (2002). Hepatoprotective and free radical scavenging activities of prenylflavonoids, coumarin, and stilbene from *Morus alba*. *Planta Medica, 68*(10), 932-934.

Peng, X., Zhang, G., Liao, Y., & Gong, D. (2016). Inhibitory kinetics and mechanism of kaempferol on α-glucosidase. *Food Chemistry, 190*(0), 207-215.

Pietta, P.-G. (2000). Flavonoids as antioxidants. *Journal of Natural Products, 63*(7), 1035-1042.

Potier, M., Mameli, L., Bélisle, M., Dallaire, L., & Melançon, S. B. (1979). Fluorometric assay of neuraminidase with a sodium (4-methylumbelliferyl-α-d-*N*-acetylneuraminate) substrate. *Analytical Biochemistry, 94*(2), 287-296.

Rajendran, M., Manisankar, P., Gandhidasan, R., & Murugesan, R. (2004). Free radicals scavenging efficiency of a few naturally occurring flavonoids: A comparative study. *Journal of Agricultural and Food Chemistry, 52*(24), 7389-7394.

Roleira, F. M. F., Tavares-da-Silva, E. J., Varela, C. L., Costa, S. C., Silva, T., Garrido, J., & Borges, F. (2015). Plant derived and dietary phenolic antioxidants: Anticancer properties. *Food Chemistry, 183*(0), 235-258.

Saint-Cricq de Gaulejac, N., Provost, C., & Vivas, N. (1999). Comparative study of polyphenol scavenging activities assessed by different methods. *Journal of Agricultural and Food Chemistry, 47*(2), 425-431.

Sasivimolphan, P., Lipipun, V., Likhitwitayawuid, K., Takemoto, M., Pramyothin, P., Hattori, M., & Shiraki, K. (2009). Inhibitory activity of oxyresveratrol on wild-type and drug-resistant varicella-zoster virus replication *in vitro*. *Antiviral Research, 84*(1), 95-97.

Seyfried, T., & Shelton, L. (2010). Cancer as a metabolic disease. *Nutrition & Metabolism, 7*(1), 7.

Sornsute, A. (2006). *Isolation and structure modification of oxyresveratrol from Artocarpus lakoocha for tyrosinase activity.* Master's Thesis, Department of Pharmacognosy, Faculty of Pharmaceutical Sciences,Chulalongkorn University.

Sritularak, B., De-Eknamkul, W., & Likhitwitayawuid, K. (1988). Tyrosinase inhibitors from *Artocarpus lakoocha*. *Thai Journal of Pharmaceutical Sciences, 22*, 149-155.

Sun, H., Xiao, C., Wei, W., Chen, Y., Lü, Z., & Zou, Y. (2010). Synthesis of oxyresveratrol. *Chinese Journal of Organic Chemistry, 30*(10), 1574-1579.

Tengamnuay, P., Pengrungruangwong, K., Pheansri, I., & Likhitwitayawuid, K. (2006). *Artocarpus lakoocha* heartwood extract as a novel cosmetic ingredient: Evaluation of the *in vitro* anti-tyrosinase and *in vivo* skin whitening activities. *International Journal of Cosmetic Science, 28*(4), 269-276.

Wang, J., Cox, D., Ding, W., Huang, G., Lin, Y., & Li, C. (2014). Three new resveratrol derivatives from the mangrove endophytic fungus *Alternaria* sp. *Marine Drugs, 12*(5), 2840.

Wu, L.-S., Wang, X.-J., Wang, H., Yang, H.-W., Jia, A.-Q., & Ding, Q. (2010). Cytotoxic polyphenols against breast tumor cell in *Smilax china* L. *Journal of Ethnopharmacology, 130*(3), 460-464.

Wu, N., Kong, Y., Fu, Y., Zu, Y., Yang, Z., Yang, M., Peng, X., & Efferth, T. (2011). *In vitro* antioxidant properties, DNA damage protective activity, and xanthine oxidase inhibitory effect of cajaninstilbene acid, a stilbene compound derived from pigeon pea [*Cajanus cajan* (L.) Millsp.] leaves. *Journal of Agricultural and Food Chemistry, 59*(1), 437-443.

Wu, Y., Hu, X., Yang, G.-Z., Mei, Z.-N., & Chen, Y. (2012). Two new flavanols from *Glycosmis pentaphylla*. *Journal of Asian Natural Products Research, 14*(8), 738-742.

APPENDIX

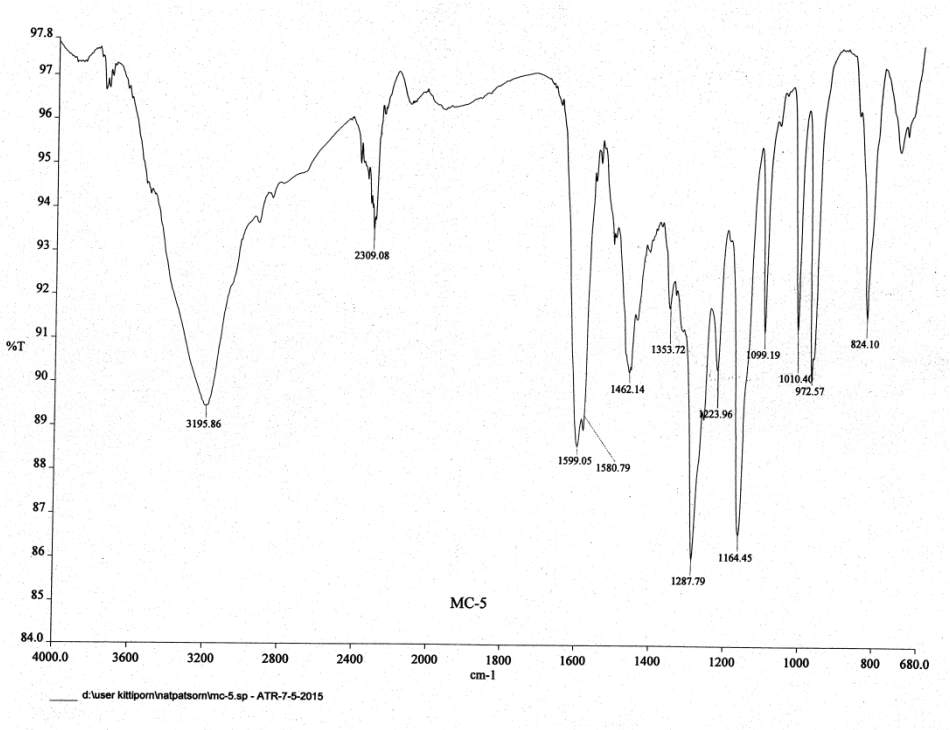

Figure 5 IR Spectrum of compound MC-1 (**41**)

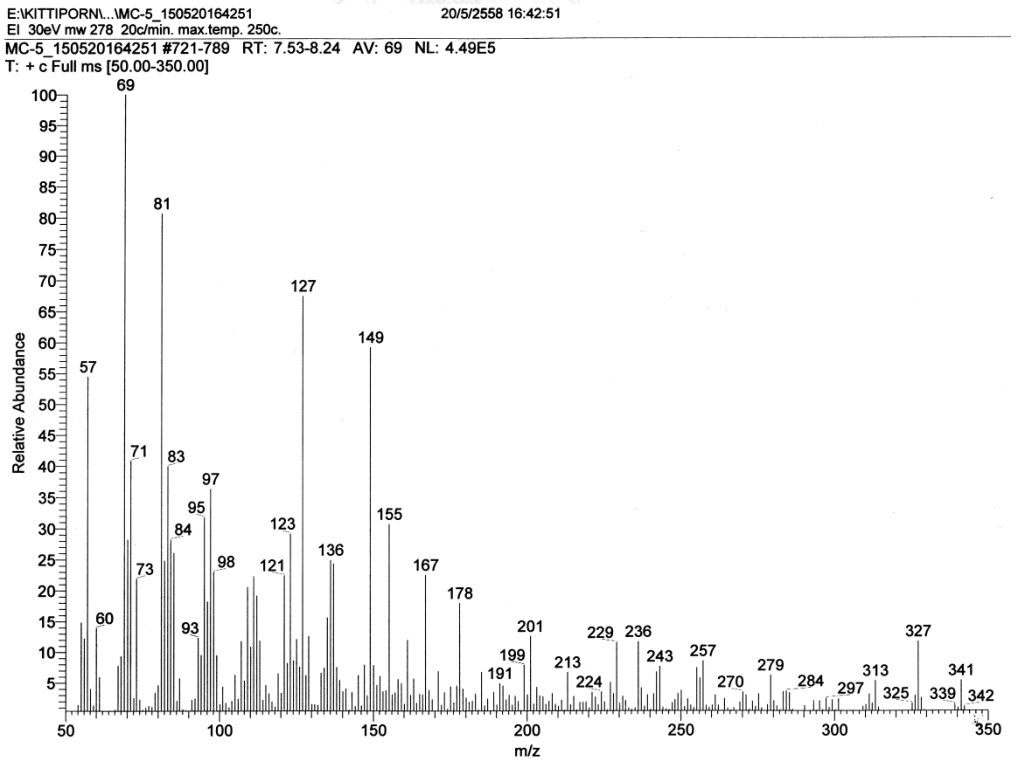

Figure 6 EI Mass spectrum of compound MC-1 (**41**)

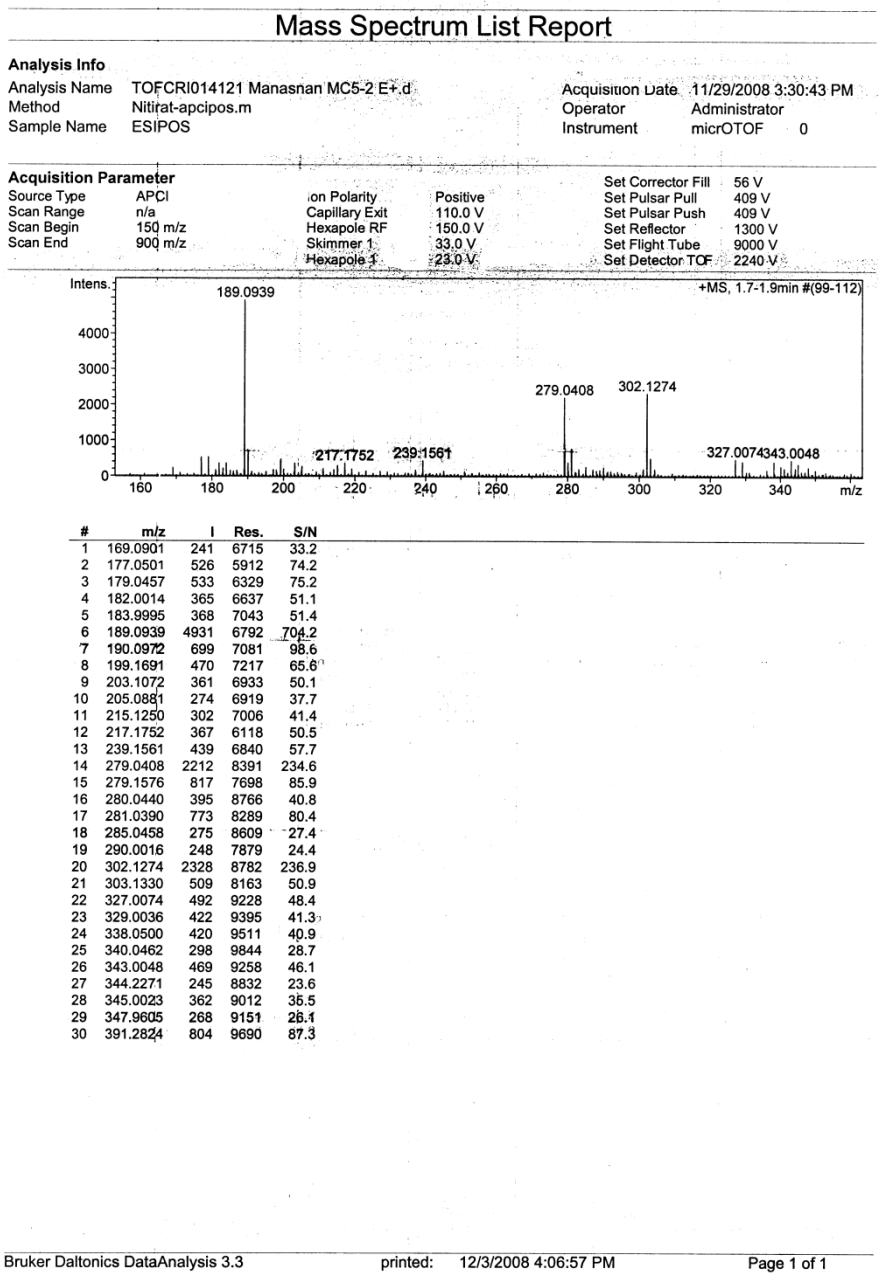

Mass Spectrum List Report

Analysis Info

Analysis Name	TOFCRI014121 Manasnan MC5-2 E+.d	Acquisition Date	11/29/2008 3:30:43 PM
Method	Nitirat-apcipos.m	Operator	Administrator
Sample Name	ESIPOS	Instrument	micrOTOF 0

Acquisition Parameter

Source Type	APCI	Ion Polarity	Positive	Set Corrector Fill	56 V
Scan Range	n/a	Capillary Exit	110.0 V	Set Pulsar Pull	409 V
Scan Begin	150 m/z	Hexapole RF	150.0 V	Set Pulsar Push	409 V
Scan End	900 m/z	Skimmer 1	33.0 V	Set Reflector	1300 V
		Hexapole 1	23.0 V	Set Flight Tube	9000 V
				Set Detector TOF	2240 V

#	m/z	I	Res.	S/N
1	169.0901	241	6715	33.2
2	177.0501	526	5912	74.2
3	179.0457	533	6329	75.2
4	182.0014	365	6637	51.1
5	183.9995	368	7043	51.4
6	189.0939	4931	6792	704.2
7	190.0972	699	7081	98.6
8	199.1691	470	7217	65.6
9	203.1072	361	6933	50.1
10	205.0881	274	6919	37.7
11	215.1250	302	7006	41.4
12	217.1752	367	6118	50.5
13	239.1561	439	6840	57.7
14	279.0408	2212	8391	234.6
15	279.1576	817	7698	85.9
16	280.0440	395	8766	40.8
17	281.0390	773	8289	80.4
18	285.0458	275	8609	27.4
19	290.0016	248	7879	24.4
20	302.1274	2328	8782	236.9
21	303.1330	509	8163	50.9
22	327.0074	492	9228	48.4
23	329.0036	422	9395	41.3
24	338.0500	420	9511	40.9
25	340.0462	298	9844	28.7
26	343.0048	469	9258	46.1
27	344.2271	245	8832	23.6
28	345.0023	362	9012	35.5
29	347.9605	268	9151	26.1
30	391.2824	804	9690	87.3

Bruker Daltonics DataAnalysis 3.3 printed: 12/3/2008 4:06:57 PM Page 1 of 1

Figure 7 HRTOF Mass spectrum of compound MC-1 (**41**)

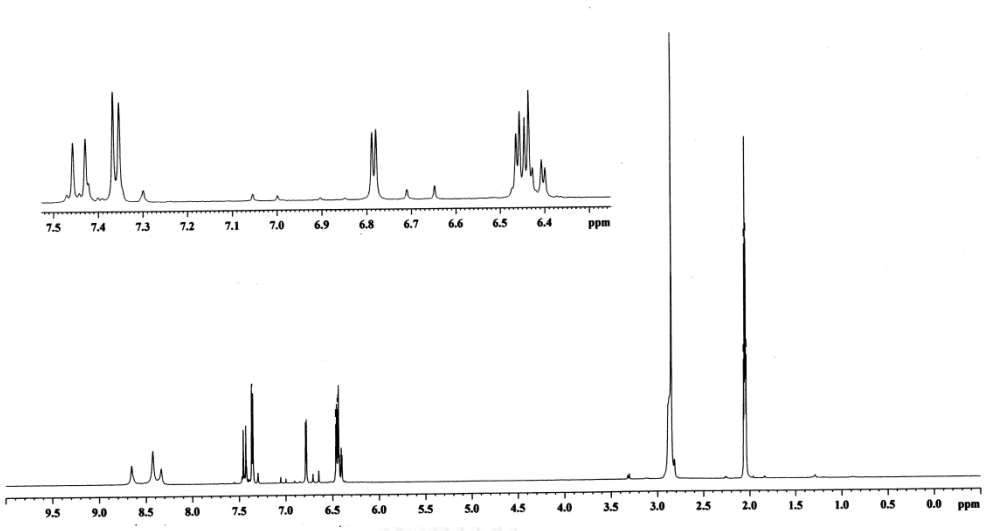

Figure 8 ^{1}H-NMR Spectrum of compound MC-1 (**41**)

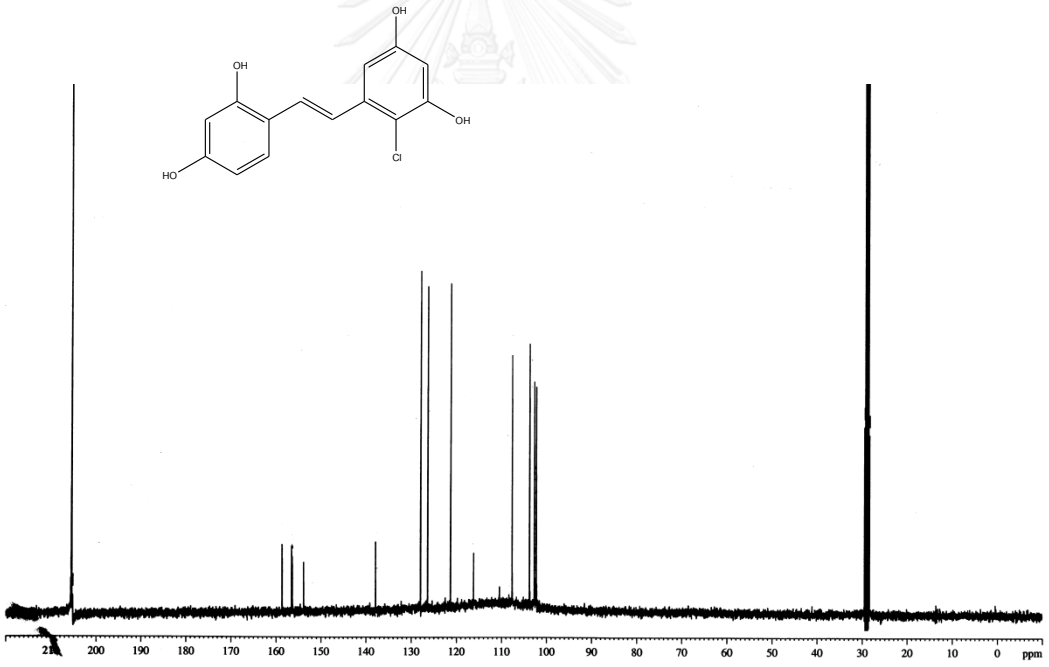

Figure 9 ^{13}C-NMR Spectrum of compound MC-1 (**41**)

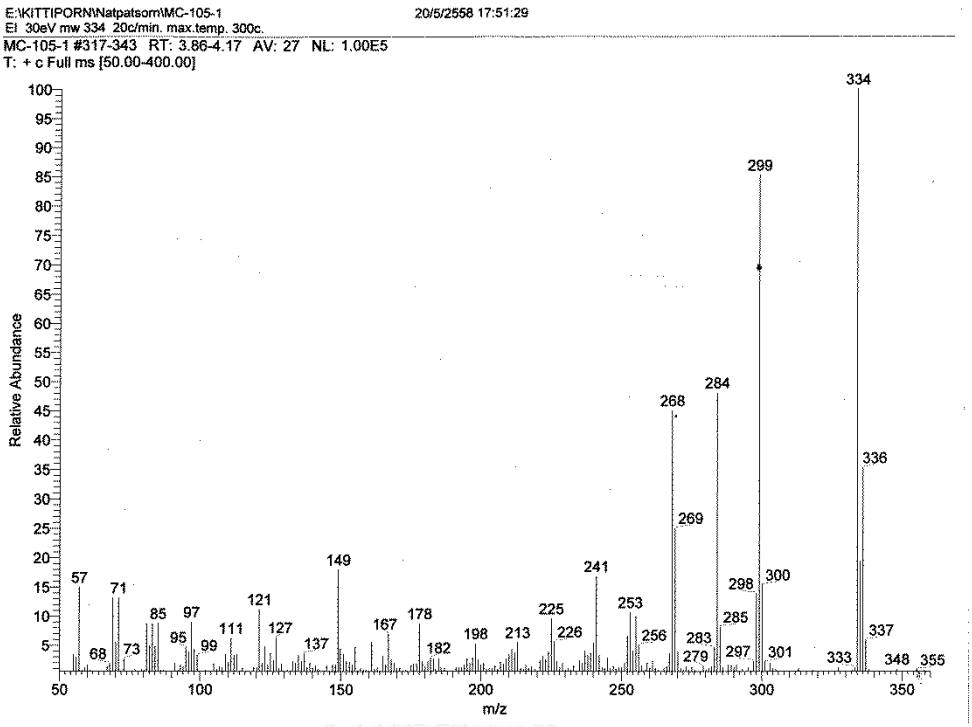

Figure 10 EI Mass spectrum of compound MC-2 (**42**)

Mass Spectrum List Report

Analysis Info

Analysis Name	TOFCRI019701 Natpassorn MC-105 E+.d	Acquisition Date	5/1/2008 5:30:58 PM
Method	Nitirat ESI pos 2014-1.m	Operator	Administrator
Sample Name	ESIpos	Instrument	micrOTOF 74

Acquisition Parameter

Source Type	ESI	Ion Polarity	Positive	Set Corrector Fill	64 V
Scan Range	n/a	Capillary Exit	90.0 V	Set Pulsar Pull	405 V
Scan Begin	120 m/z	Hexapole RF	90.0 V	Set Pulsar Push	405 V
Scan End	600 m/z	Skimmer 1	30.0 V	Set Reflector	1300 V
		Hexapole 1	22.9 V	Set Flight Tube	9000 V
				Set Detector TOF	1870 V

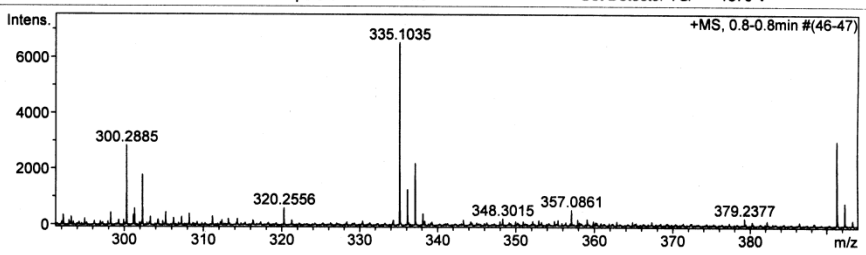

#	m/z	I	Res.
1	122.1054	911	6252
2	157.0899	903	6805
3	228.1508	1113	8139
4	246.2421	3513	8370
5	252.1235	3300	8243
6	257.0780	855	8984
7	260.2575	3614	8652
8	272.2565	2835	9087
9	274.2730	12287	8940
10	275.2767	2093	8113
11	279.2237	1459	8906
12	288.2869	2565	8733
13	291.1953	1284	8311
14	300.2885	2842	9429
15	302.3034	1783	8781
16	335.1035	6537	9305
17	336.1069	1269	9428
18	337.1017	2201	9240
19	391.2836	3032	9546
20	392.2872	814	8931
21	408.3096	1897	9981
22	413.2659	792	10023
23	419.3139	875	9623
24	428.4248	3427	10227
25	429.4277	1250	10849
26	436.3405	832	10300
27	494.5656	839	10944
28	522.5981	2302	10411
29	523.6030	913	10494
30	550.6305	1635	10774

Bruker Daltonics DataAnalysis 3.3 printed: 5/6/2008 4:33:01 PM Page 1 of 1

Figure 11 HRTOF Mass spectrum of compound MC-2 (**42**)

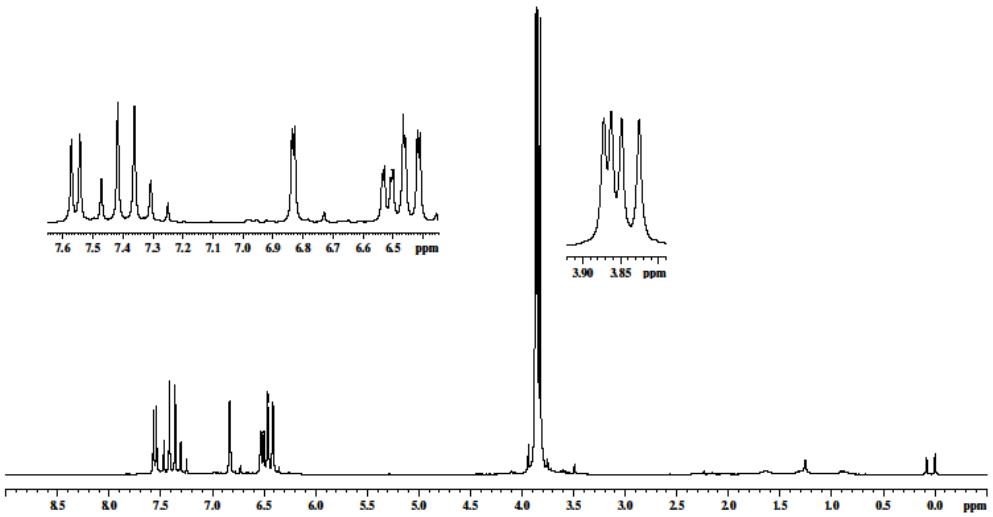

Figure 12 ^{1}H-NMR Spectrum of compound MC-2 (**42**)

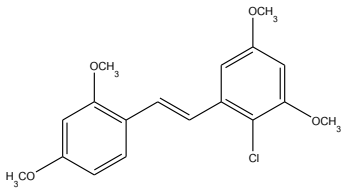

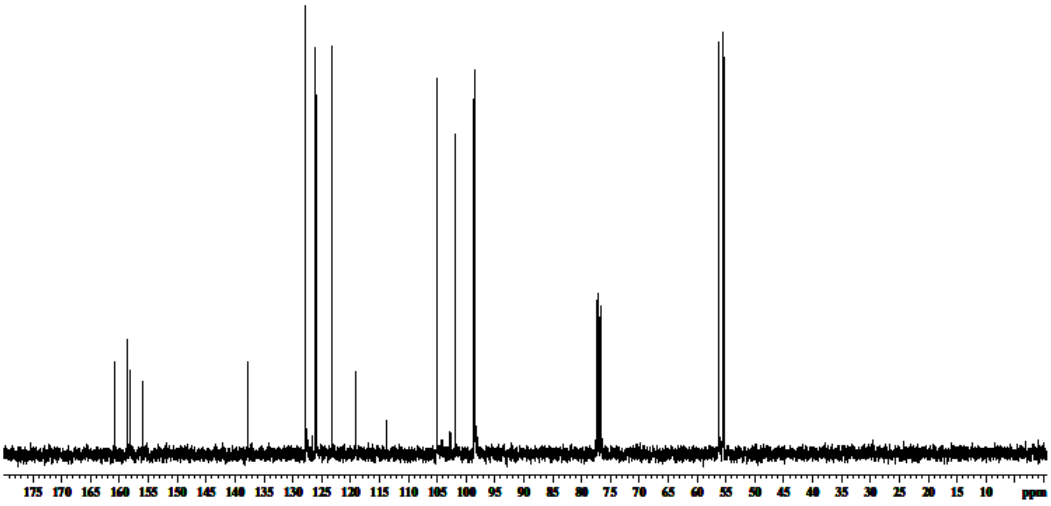

Figure 13 ^{13}C-NMR Spectrum of compound MC-2 (**42**)

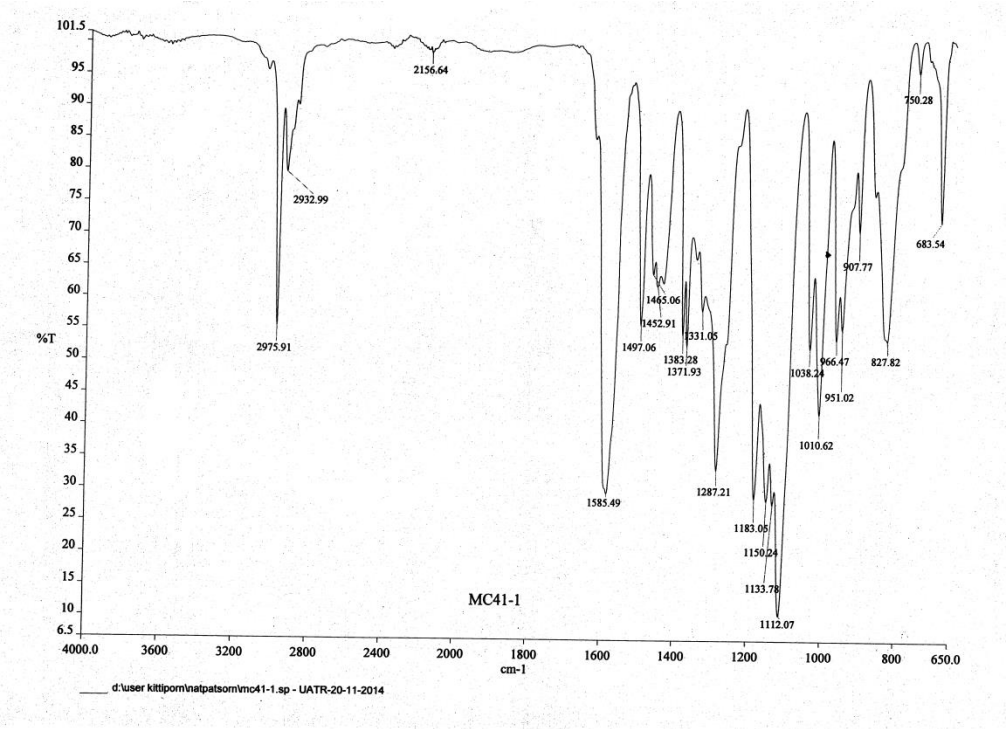

Figure 14 IR Spectrum of compound MC-3 (**43**)

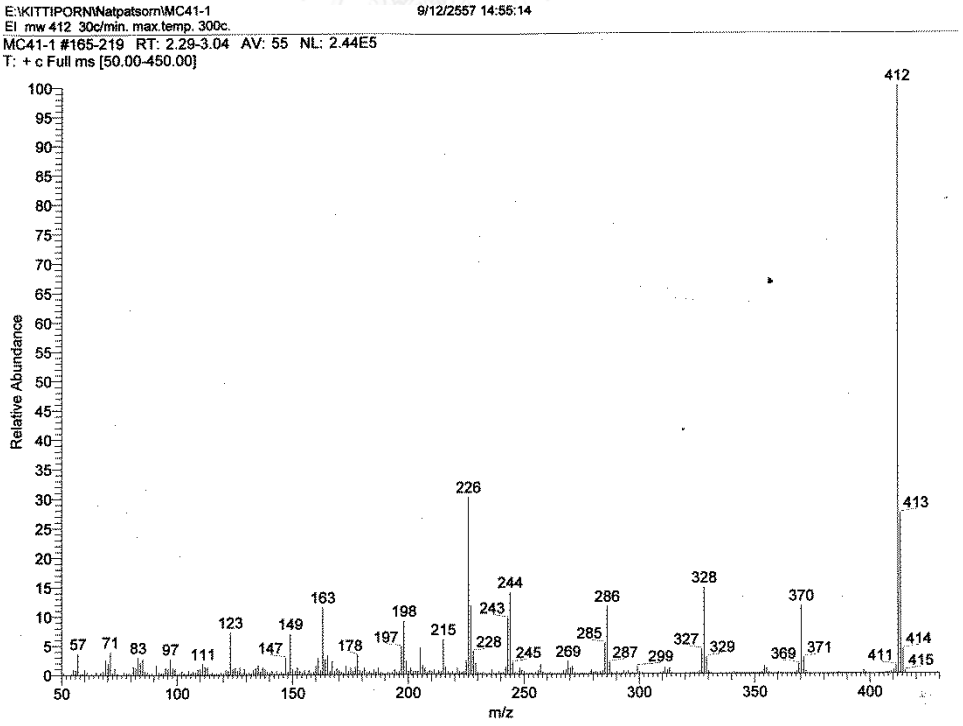

Figure 15 EI Mass spectrum of compound MC-3 (**43**)

Mass Spectrum List Report

Analysis Info

Analysis Name	H:\TOFCRI014724 Manasnun MC28-1 E+.d	Acquisition Date	1/18/2009 3:06:04 PM
Method	Nitirat-apcipos 2012.m	Operator	Administrator
Sample Name	ESIpos	Instrument / Ser#	micrOTOF 0
Comment			

Acquisition Parameter

Source Type	APCI	Ion Polarity	Positive	Set Nebulizer	1.5 Bar
Focus	Not active			Set Dry Heater	85 °C
Scan Begin	150 m/z	Set Capillary	3500 V	Set Dry Gas	7.0 l/min
Scan End	800 m/z	Set End Plate Offset	-500 V	Set Divert Valve	Source

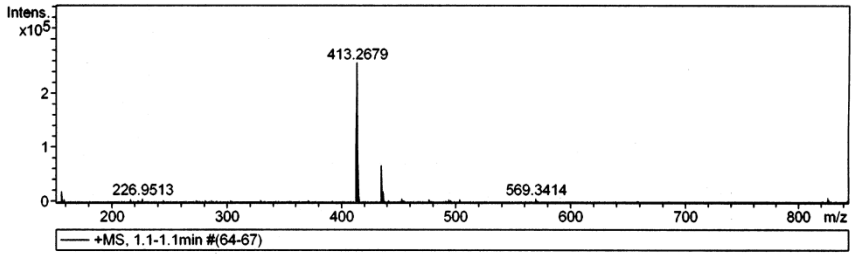

#	m/z	I
1	157.0878	19324
2	158.9683	4022
3	216.9234	4063
4	223.1340	3424
5	226.9513	6683
6	245.0967	2944
7	273.1668	2606
8	281.1745	2093
9	287.1275	2080
10	303.1706	3354
11	329.1747	2145
12	371.2189	2850
13	413.2679	256441
14	414.2705	69132
15	415.2737	11534
16	435.2487	67428
17	436.2520	19513
18	437.2542	3460
19	441.2708	2674
20	453.2603	6681
21	454.2642	2049
22	476.2749	4459
23	493.1951	1956
24	494.2826	3822
25	495.2854	2437
26	503.2364	3763
27	569.3414	6280
28	570.3439	2315
29	825.5304	7930
30	826.5332	4766

Figure 16 HRTOF Mass spectrum of compound MC-3 (**43**)

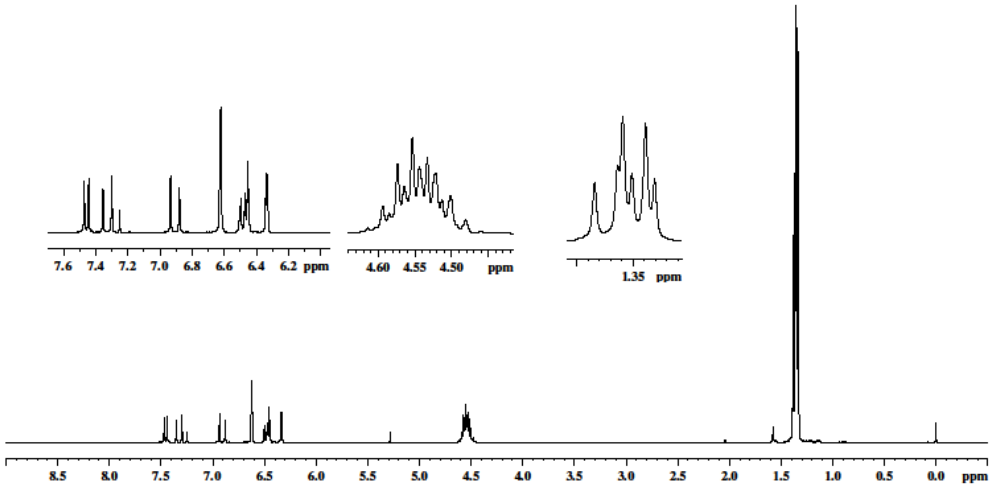

Figure 17 ^{1}H-NMR Spectrum of compound MC-3(**43**)

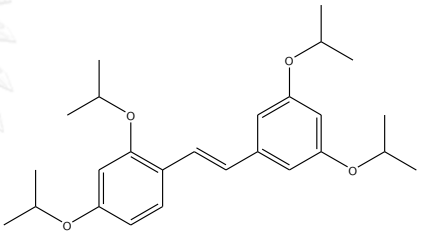

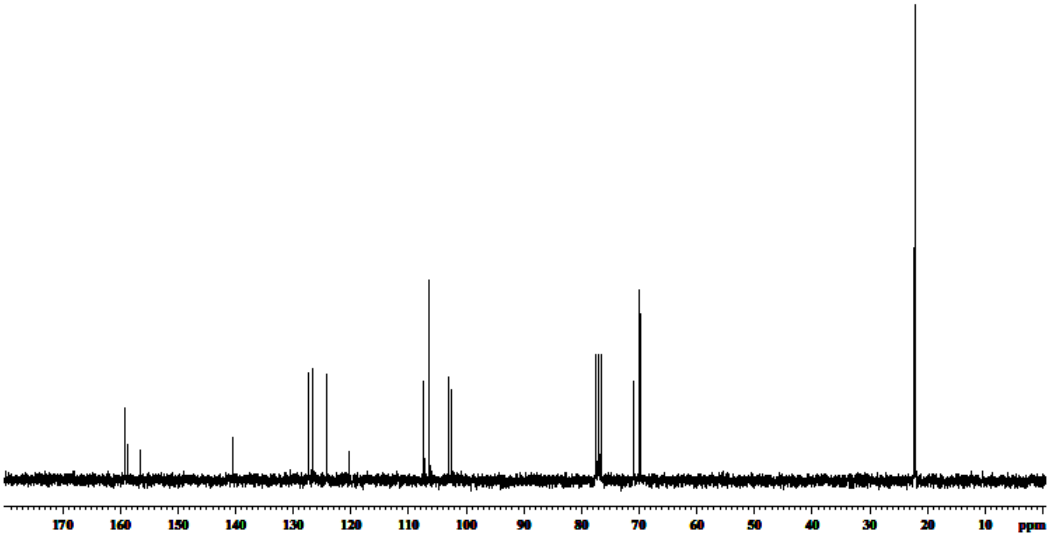

Figure 18 ^{13}C-NMR Spectrum of compound MC-3 (**43**)

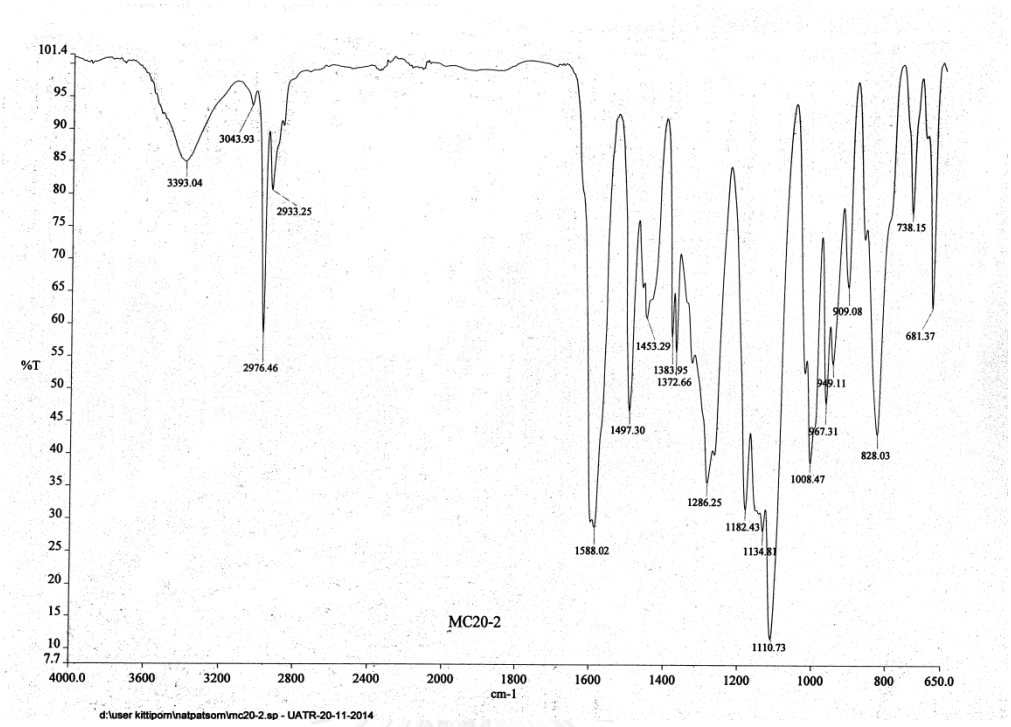

Figure 19 IR Spectrum of compound MC-4 (**44**)

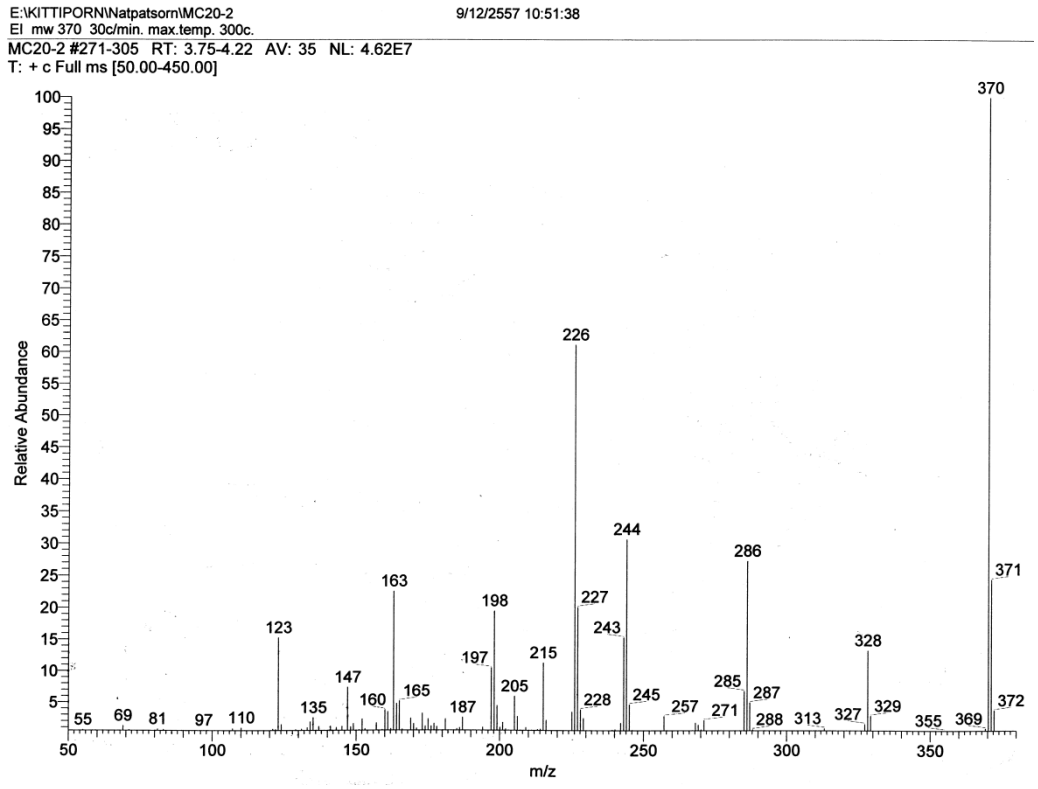

Figure 20 EI Mass spectrum of compound MC-4 (**44**)

Mass Spectrum List Report

Analysis Info

Analysis Name	H:\TOFCRI014720 Manasnun M20A22 E-.d	Acquisition Date	1/18/2009 2:57:43 PM
Method	Nitirat_neg.m	Operator	Administrator
Sample Name	ESIneg	Instrument / Ser#	micrOTOF 0
Comment			

Acquisition Parameter

Source Type	APCI	Ion Polarity	Negative	Set Nebulizer	1.5 Bar
Focus	Not active			Set Dry Heater	85 °C
Scan Begin	150 m/z	Set Capillary	3000 V	Set Dry Gas	7.0 l/min
Scan End	800 m/z	Set End Plate Offset	-500 V	Set Divert Valve	Source

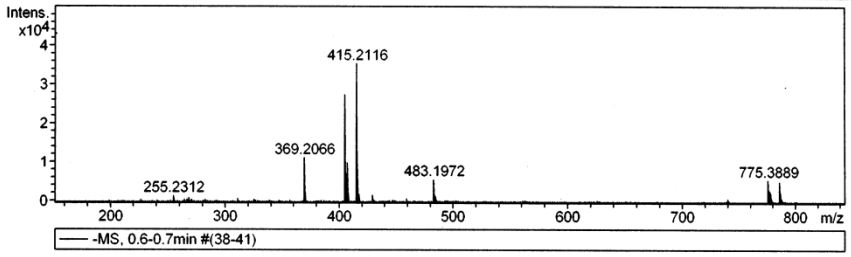

#	m/z	I
1	227.2008	705
2	255.2312	1417
3	265.1458	663
4	266.8035	633
5	268.7990	1073
6	270.7996	586
7	311.1647	883
8	369.2066	11242
9	370.2086	2689
10	405.1826	27397
11	406.1868	7245
12	407.1803	9922
13	408.1838	2420
14	415.2116	35470
15	416.2140	9795
16	417.2158	1930
17	429.2248	1750
18	430.2313	526
19	459.2368	781
20	483.1972	5739
21	484.2006	1576
22	485.0883	615
23	739.4154	752
24	775.3889	5557
25	776.3919	2891
26	777.3894	2345
27	778.3908	1043
28	785.4191	5176
29	786.4222	2615
30	787.4250	812

Figure 21 HRTOF Mass spectrum of compound MC-4 (**44**)

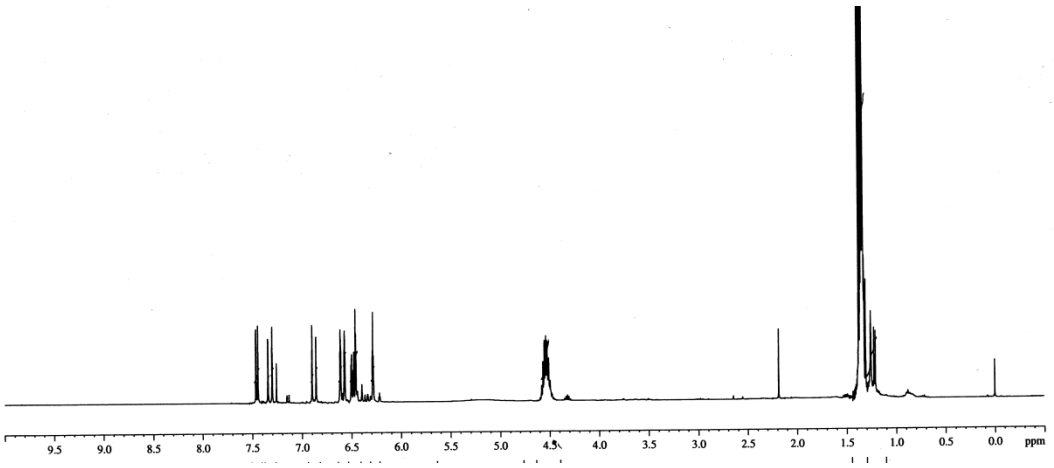

Figure 22 ^{1}H-NMR Spectrum of compound MC-4 (**44**)

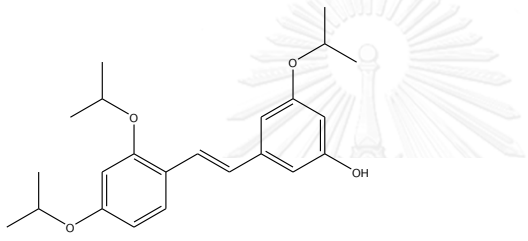

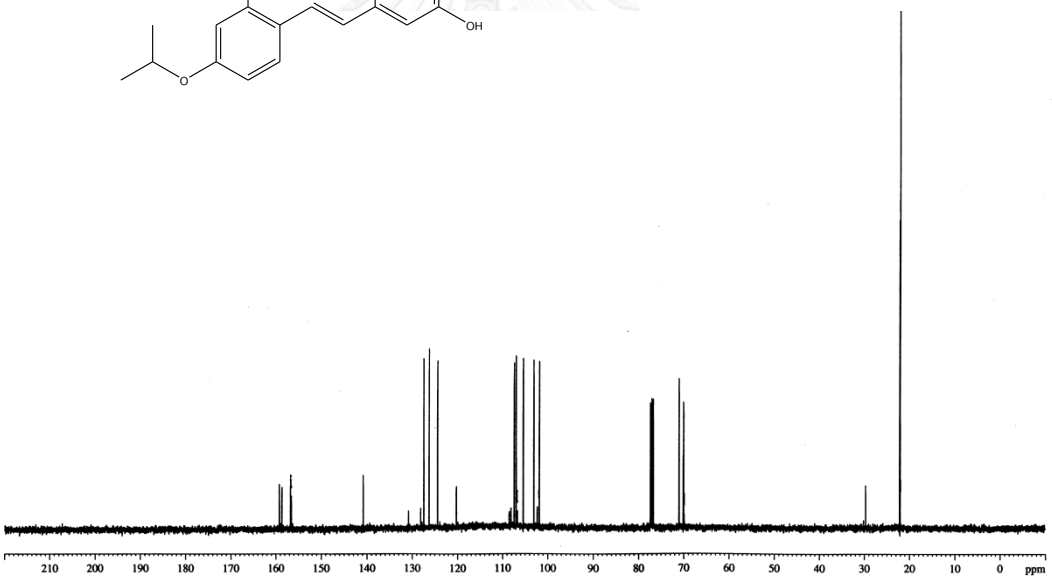

Figure 23 ^{13}C-NMR Spectrum of compound MC-4 (**44**)

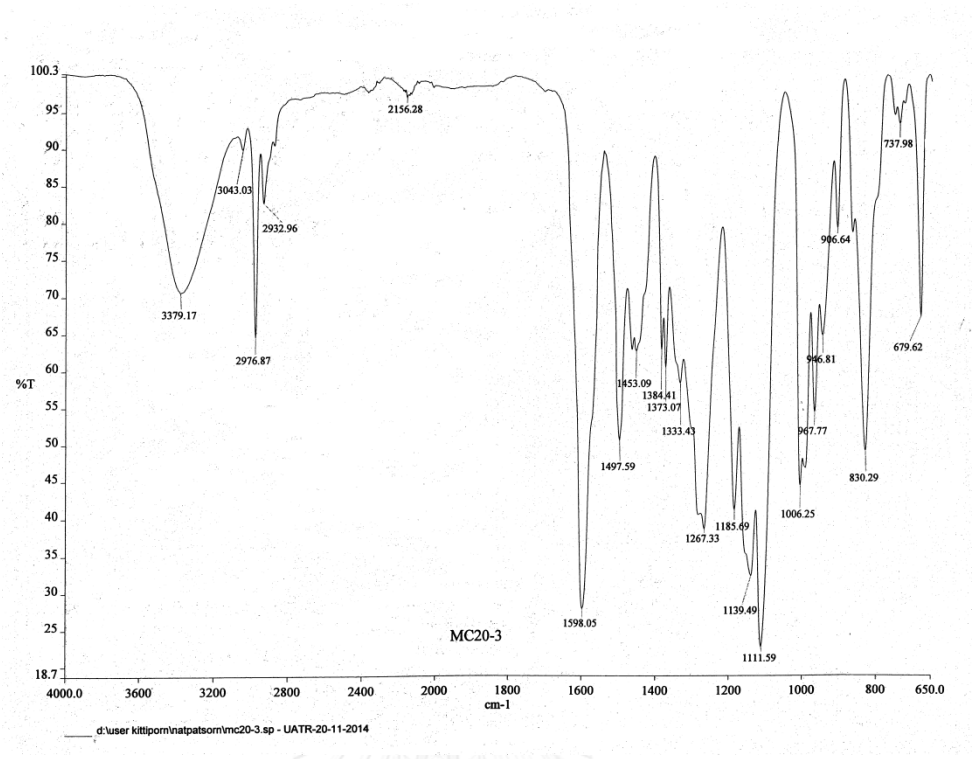

Figure 24 IR Spectrum of compound MC-5 (**45**)

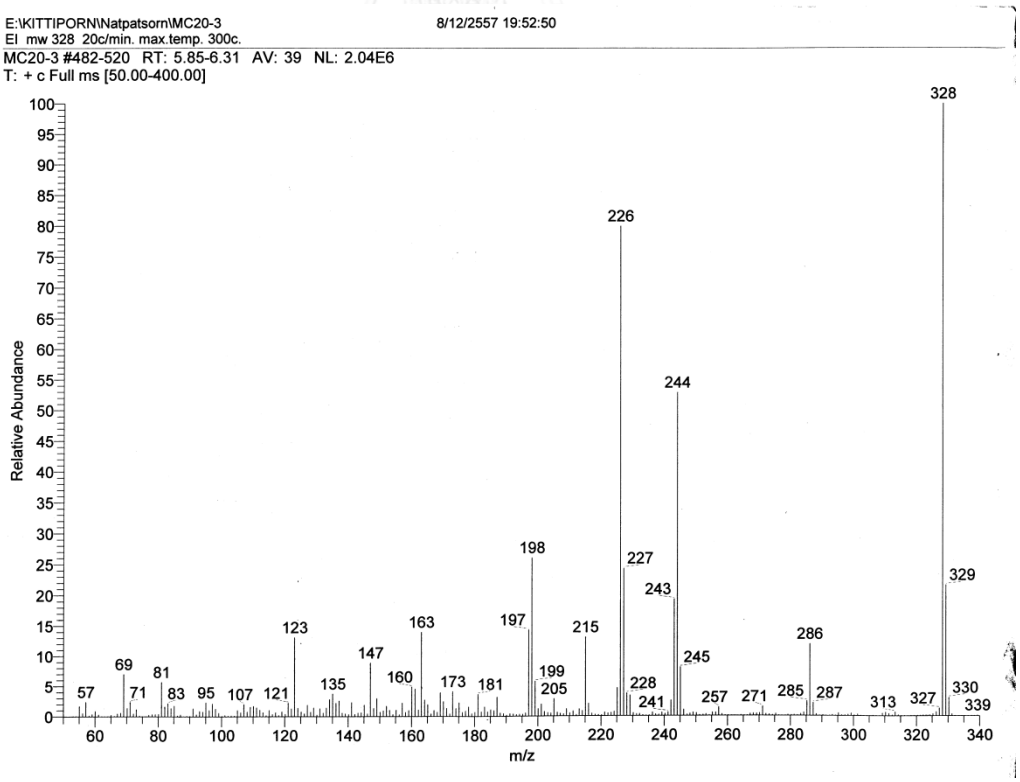

Figure 25 EI Mass spectrum of compound MC-5 (**45**)

Mass Spectrum List Report

Analysis Info

Analysis Name	H:\TOFCRI014721 Manasnun M20A452 E-.d	Acquisition Date	1/18/2009 2:59:17 PM
Method	Nitirat_neg.m	Operator	Administrator
Sample Name	ESIneg	Instrument / Ser#	micrOTOF 0
Comment			

Acquisition Parameter

Source Type	APCI	Ion Polarity	Negative	Set Nebulizer	1.5 Bar
Focus	Not active			Set Dry Heater	85 °C
Scan Begin	150 m/z	Set Capillary	3000 V	Set Dry Gas	7.0 l/min
Scan End	800 m/z	Set End Plate Offset	-500 V	Set Divert Valve	Source

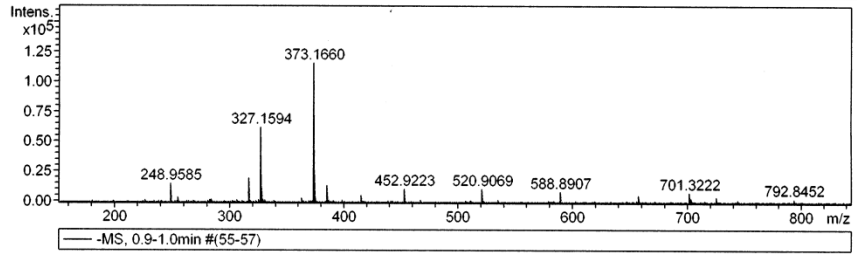

#	m/z	I
1	227.1990	1808
2	248.9585	15364
3	255.2298	3929
4	283.0964	1898
5	284.1035	1990
6	306.9173	2298
7	316.9471	19691
8	325.1838	2162
9	327.1594	62265
10	328.1621	13536
11	329.1653	2066
12	330.9626	2238
13	363.1383	3660
14	373.1660	115591
15	374.1688	26413
16	375.1718	4621
17	384.9354	13660
18	398.9502	1884
19	415.2116	6078
20	452.9223	10770
21	466.9361	1651
22	520.9069	10681
23	534.9207	1866
24	588.8907	8444
25	656.8754	5356
26	701.3222	7615
27	702.3233	3490
28	724.8623	4116
29	743.3655	1888
30	792.8452	2778

Figure 26 HRTOF Mass spectrum of compound MC-5 (**45**)

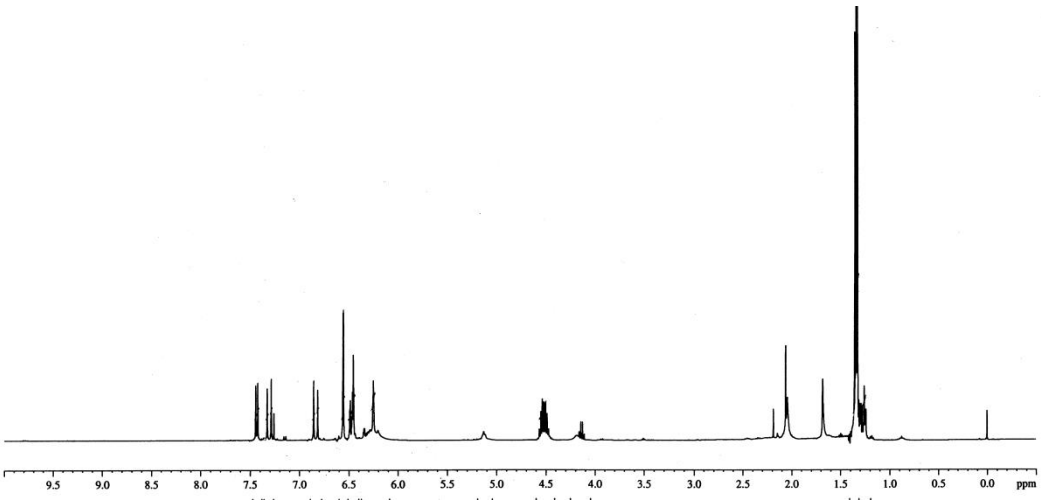

Figure 27 ^{1}H-NMR Spectrum of compound MC-5 (**45**)

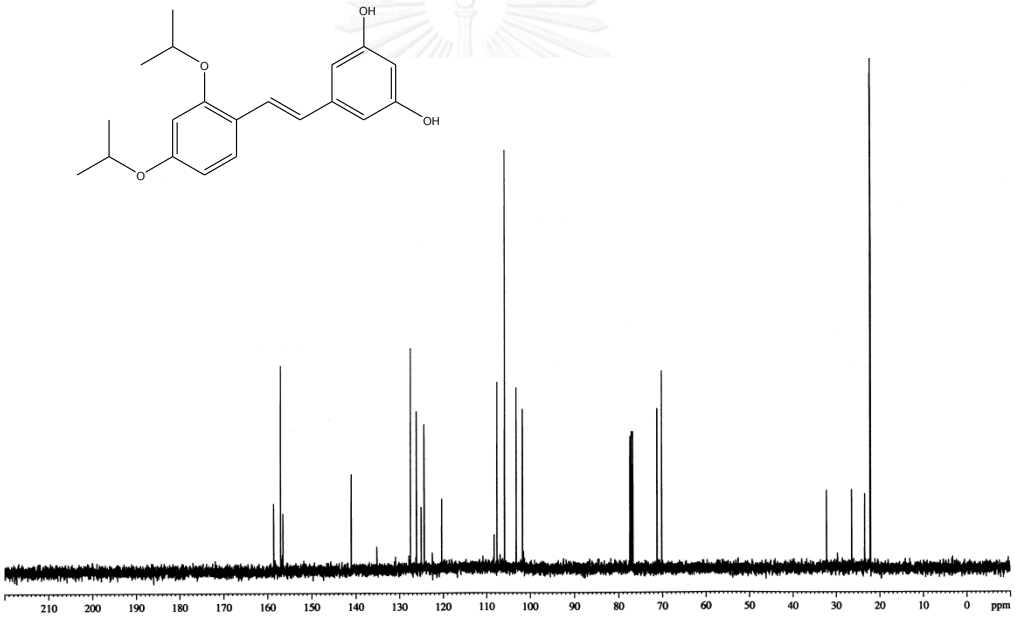

Figure 28 ^{13}C-NMR Spectrum of compound MC-5 (**45**)

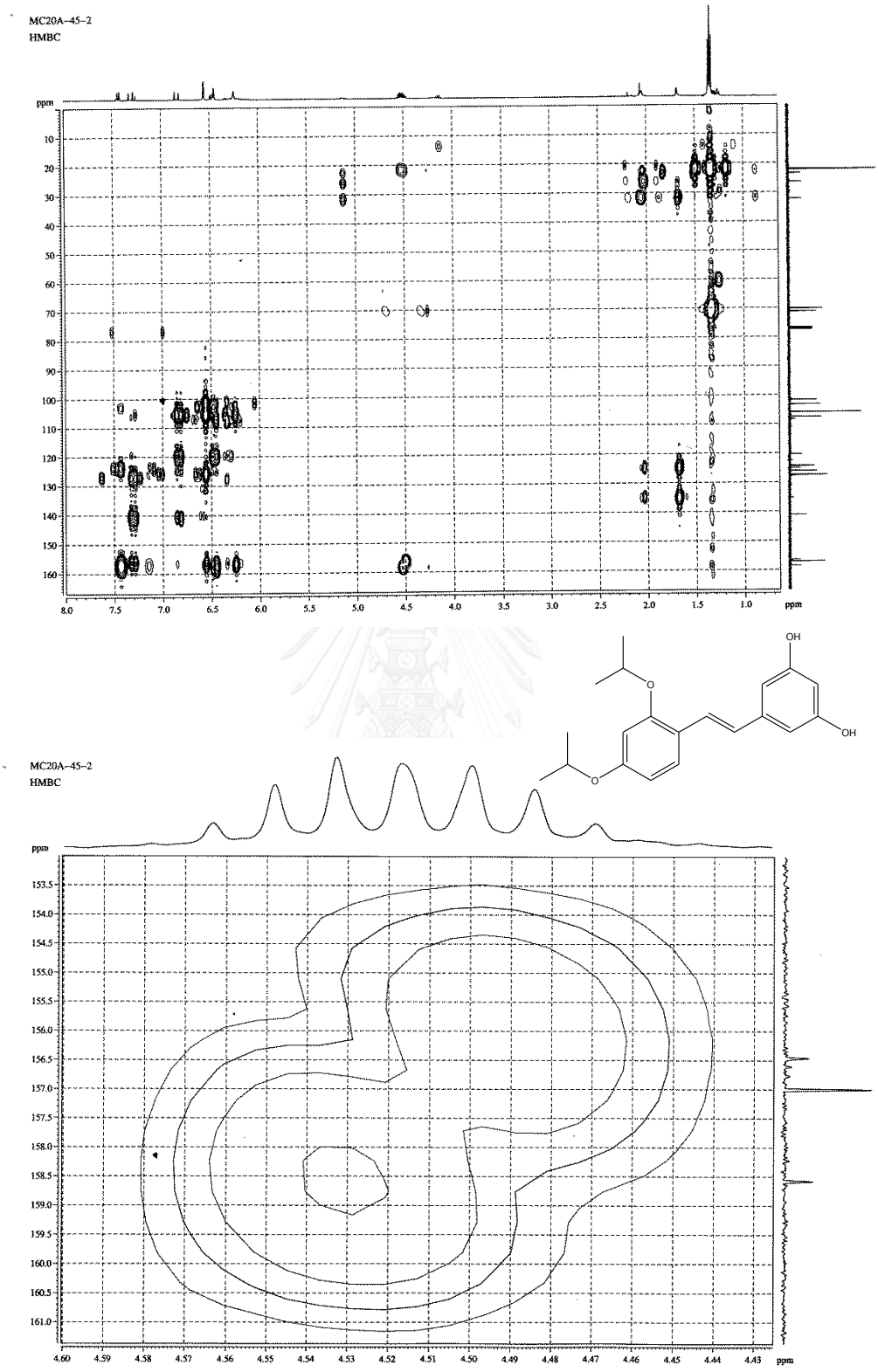

Figure 29 HMBC Spectrum of compound MC-5 (**45**)

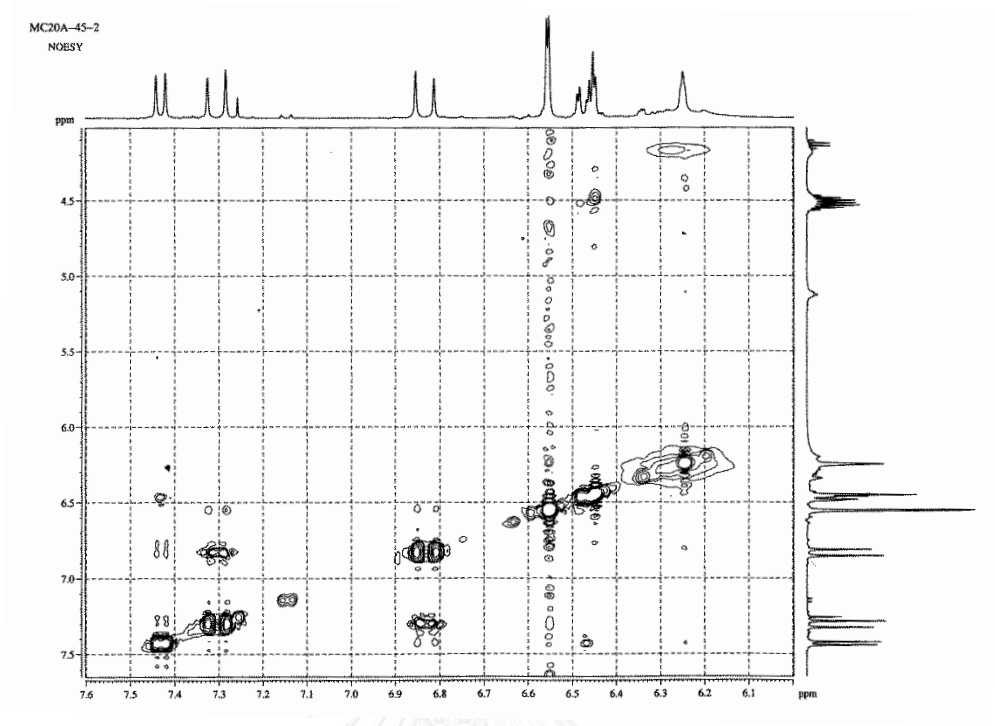

Figure 30 NOESY Spectrum of compound MC-5 (**45**)

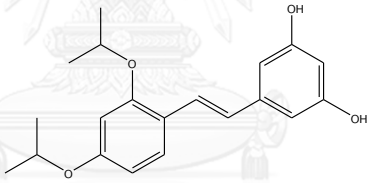

Mass Spectrum List Report

Analysis Info

Analysis Name	TOFCRI019940 Nutpassorn MCB16-1 E+.d	Acquisition Date	6/16/2015 5:54:24 PM
Method	Nitirat ESI pos 2014-1.m	Operator	Administrator
Sample Name	ESIpos	Instrument	micrOTOF 74

Acquisition Parameter

Source Type	ESI	Ion Polarity	Positive	Set Corrector Fill	64 V
Scan Range	n/a	Capillary Exit	90.0 V	Set Pulsar Pull	405 V
Scan Begin	120 m/z	Hexapole RF	120.0 V	Set Pulsar Push	405 V
Scan End	700 m/z	Skimmer 1	30.0 V	Set Reflector	1300 V
		Hexapole 1	22.9 V	Set Flight Tube	9000 V
				Set Detector TOF	1885 V

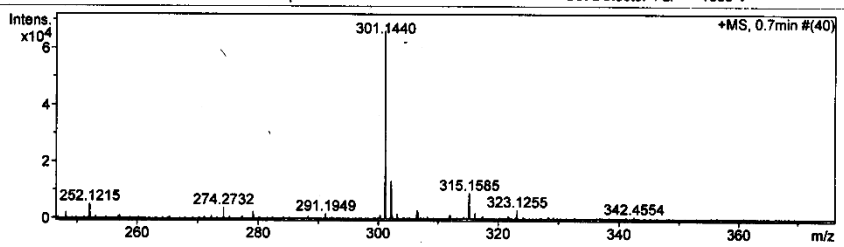

#	m/z	I	Res.
1	157.0871	1187	6493
2	196.8661	1043	7446
3	248.2006	2051	7918
4	252.1215	5043	7669
5	257.0795	1118	7113
6	274.2732	3795	8020
7	279.1604	2451	8426
8	291.1949	1701	8524
9	300.2892	1343	8716
10	301.1440	66184	8196
11	302.1472	13257	8677
12	302.3040	1149	8278
13	303.1520	1715	7882
14	306.4935	2908	9369
15	306.6017	1373	15958
16	311.8847	1132	18997
17	312.0089	1338	25771
18	315.1585	9013	8732
19	316.1626	1937	8857
20	321.6656	1019	19442
21	323.1255	3146	8741
22	391.2842	6363	9229
23	392.2860	1894	9959
24	408.3105	1924	9303
25	413.2636	1734	9227
26	419.3172	1733	8077
27	428.4228	978	9076
28	623.2588	1671	11365
29	680.4756	2150	11062
30	681.4794	1053	10166

Figure 31 HRTOF Mass spectrum of compound MC-6 (**35**)

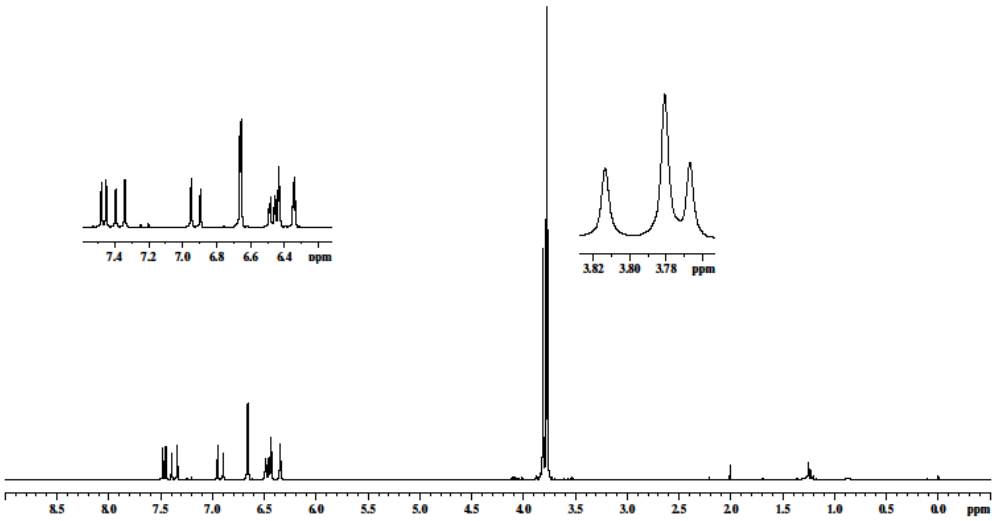

Figure 32 ^{1}H-NMR Spectrum of compound MC-6 (**35**)

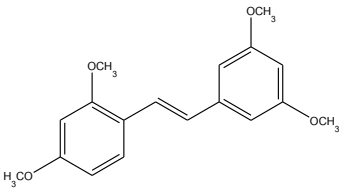

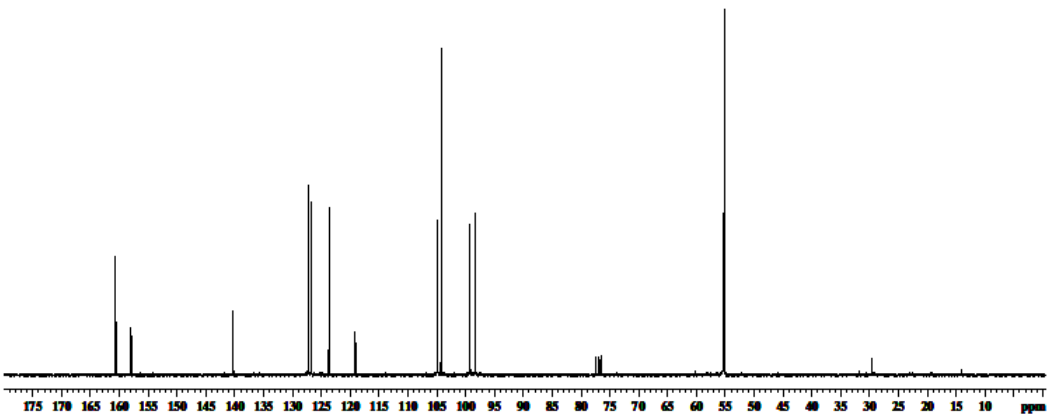

Figure 33 ^{13}C-NMR Spectrum of compound MC-6 (**35**)

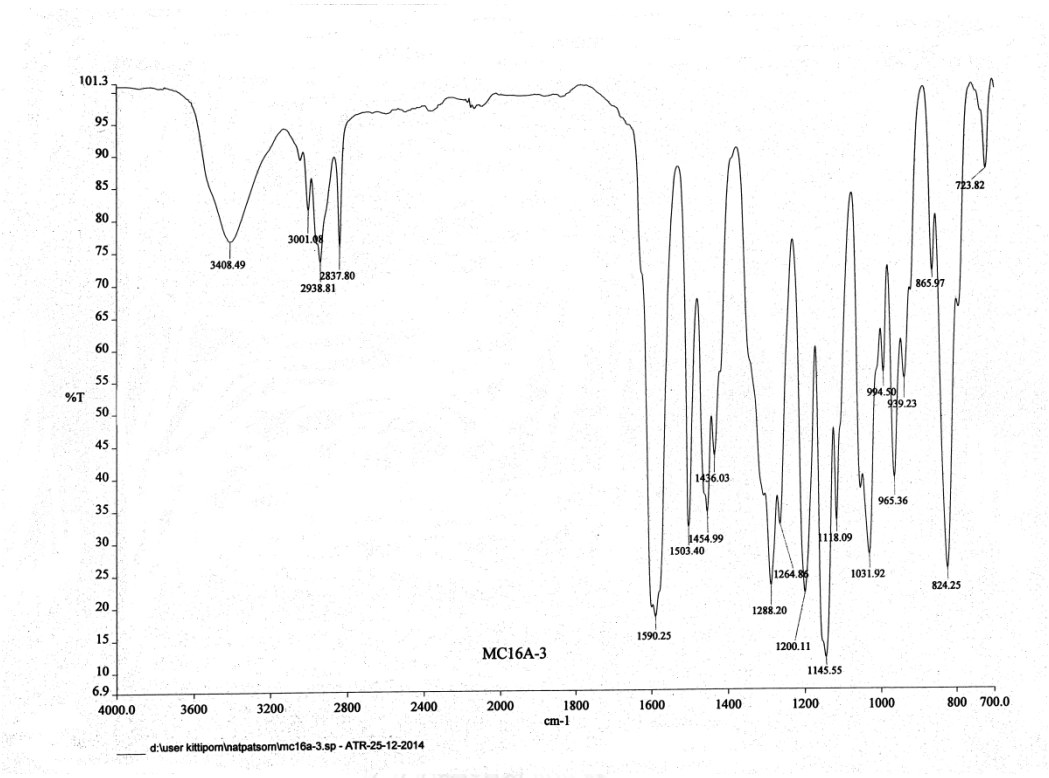

Figure 34 IR Spectrum of compound MC-7 (**46**)

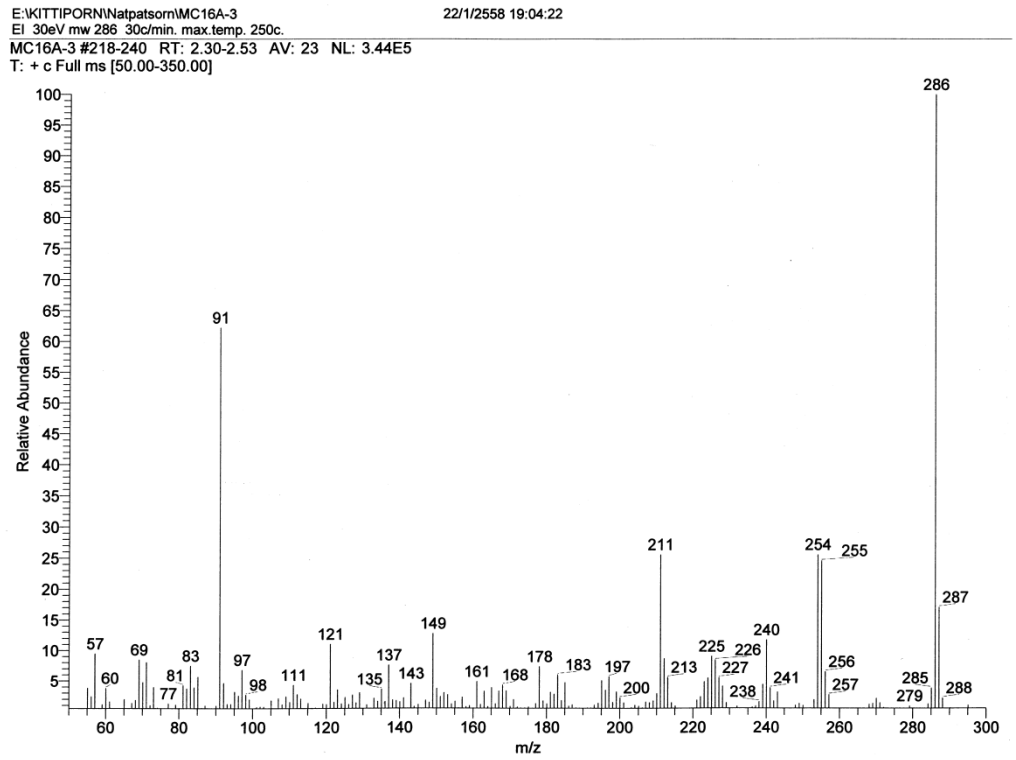

Figure 35 EI Mass spectrum of compound MC-7 (**46**)

Mass Spectrum List Report

Analysis Info

Analysis Name	TOFCRI019096 Natpassorn MC16A-3 E+.d	Acquisition Date	12/26/2014 3:57:25 PM
Method	Nitirat ESI pos 2014-1.m	Operator	Administrator
Sample Name	ESIpos	Instrument	micrOTOF 74

Acquisition Parameter

Source Type	ESI	Ion Polarity	Positive	Set Corrector Fill	64 V
Scan Range	n/a	Capillary Exit	110.0 V	Set Pulsar Pull	405 V
Scan Begin	120 m/z	Hexapole RF	120.0 V	Set Pulsar Push	405 V
Scan End	900 m/z	Skimmer 1	35.0 V	Set Reflector	1300 V
		Hexapole 1	22.9 V	Set Flight Tube	9000 V
				Set Detector TOF	1865 V

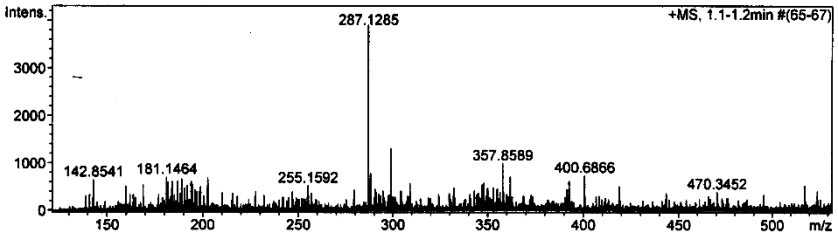

#	m/z	I	Res.
1	142.8541	647	16902
2	159.8796	515	18467
3	168.9255	539	17626
4	181.1464	700	18049
5	182.0030	597	7017
6	183.9985	610	6942
7	186.9584	624	7267
8	188.9542	660	7202
9	191.9124	535	7537
10	193.9097	622	8456
11	194.5385	542	16051
12	198.8634	497	9424
13	202.5840	688	20948
14	255.1592	520	20939
15	287.1285	3896	8417
16	288.1311	779	8757
17	298.8736	1307	24063
18	309.1104	576	9069
19	332.1464	481	23038
20	347.1649	544	25800
21	347.9603	577	9890
22	352.9107	484	9032
23	357.8589	992	15326
24	400.6866	734	28846
25	418.8214	505	28814
26	517.4018	536	29080
27	574.4947	669	35313
28	695.4903	782	36806
29	741.3500	490	35157
30	743.5673	817	40041

Figure 36 HRTOF Mass spectrum of compound MC-7 (**46**)

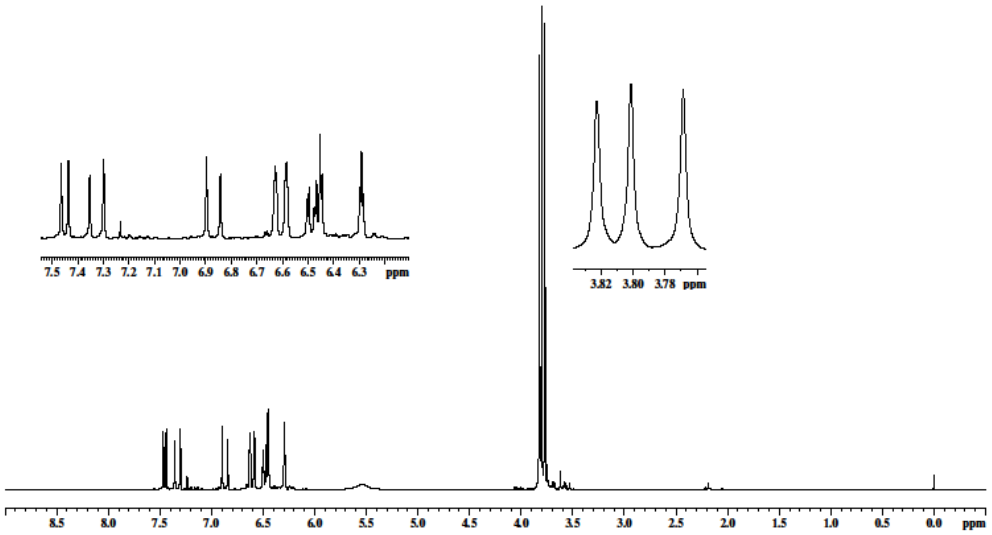

Figure 37 ^{1}H-NMR Spectrum of compound MC-7 (**46**)

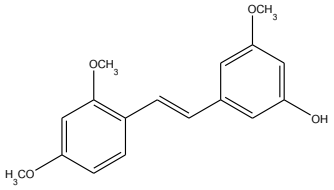

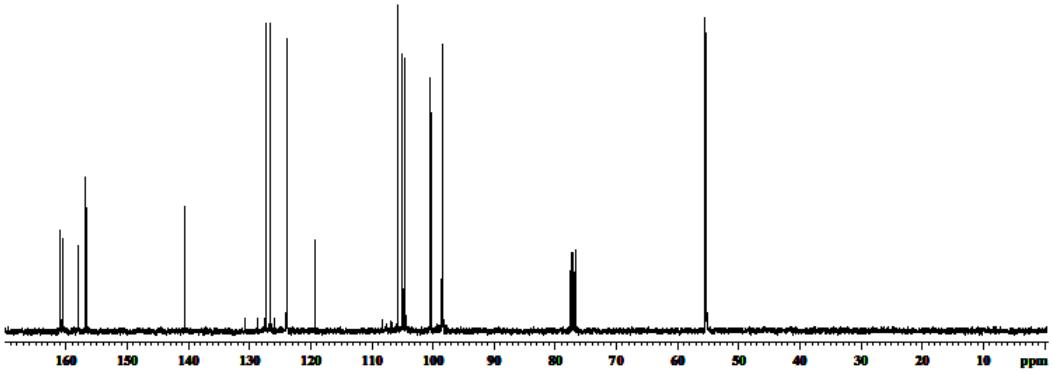

Figure 38 ^{13}C-NMR Spectrum of compound MC-7 (**46**)

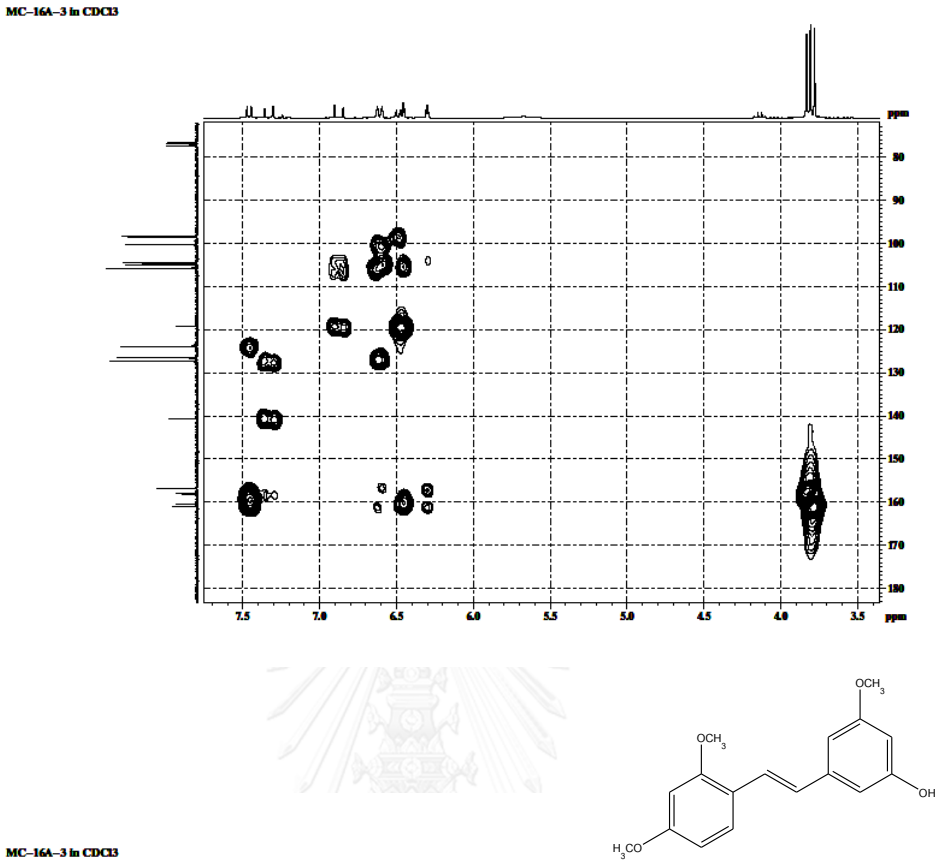

Figure 39 HMBC Spectrum of compound MC-7 (**46**)

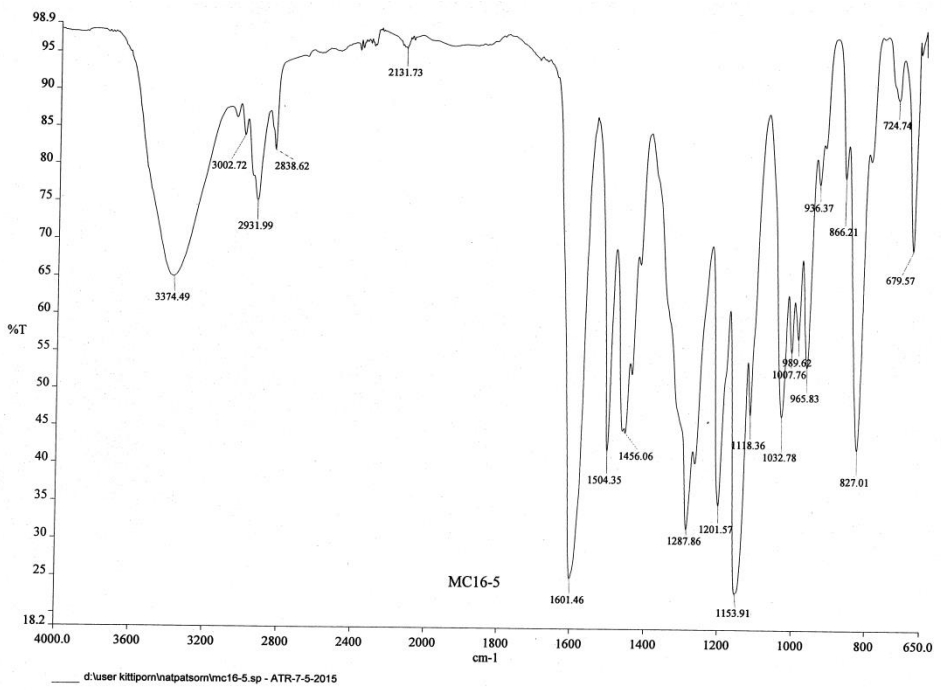

Figure 40 IR Spectrum of compound MC-8 (**47**)

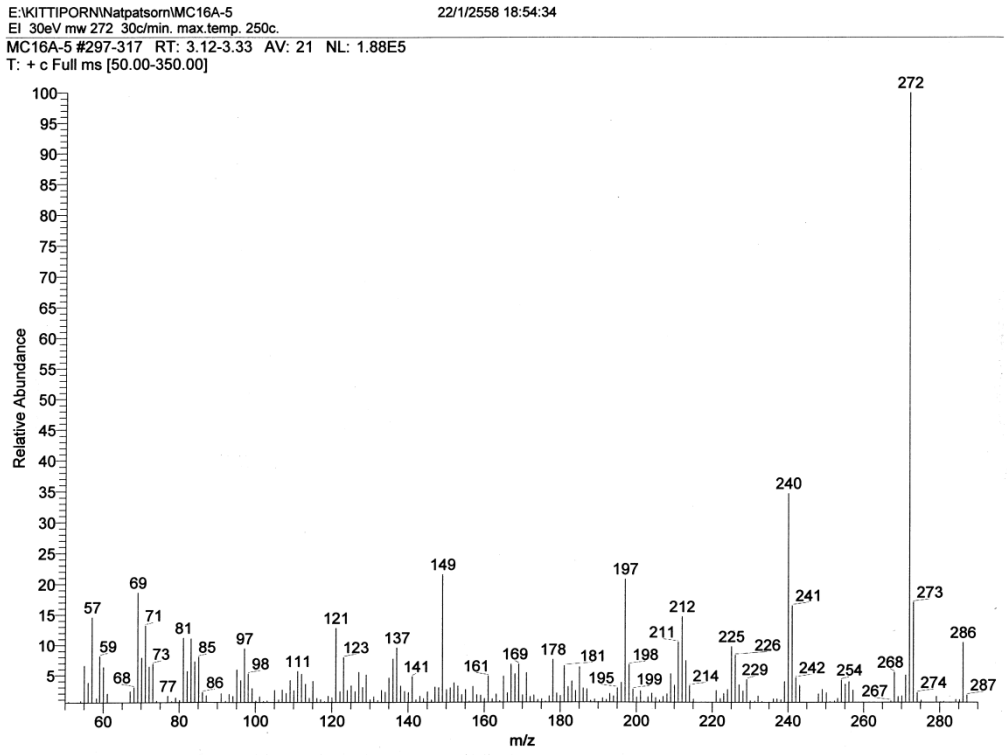

Figure 41 EI Mass spectrum of compound MC-8 (**47**)

Mass Spectrum List Report

Analysis Info

Analysis Name	TOFCRI019097 Natpassorn MC16A-5 E+.d	Acquisition Date	12/26/2014 4:00:00 PM
Method	Nitirat ESI pos 2014-1.m	Operator	Administrator
Sample Name	ESIpos	Instrument	micrOTOF 74

Acquisition Parameter

Source Type	ESI	Ion Polarity	Positive	Set Corrector Fill	64 V
Scan Range	n/a	Capillary Exit	110.0 V	Set Pulsar Pull	405 V
Scan Begin	120 m/z	Hexapole RF	120.0 V	Set Pulsar Push	405 V
Scan End	900 m/z	Skimmer 1	35.0 V	Set Reflector	1300 V
		Hexapole 1	22.9 V	Set Flight Tube	9000 V
				Set Detector TOF	1865 V

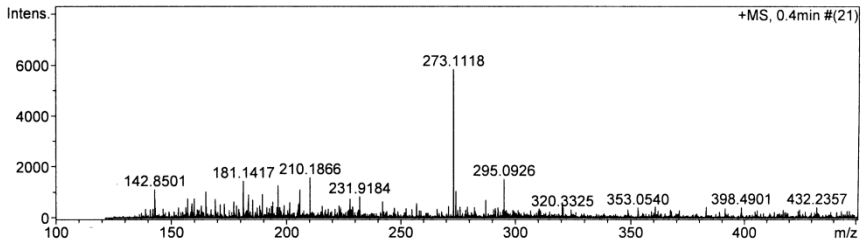

#	m/z	I	Res.
1	142.8501	1112	15302
2	157.0896	754	6647
3	158.9718	566	7133
4	159.8767	757	18545
5	164.9298	996	5947
6	168.9216	737	18024
7	176.9676	639	15554
8	176.9947	624	17387
9	181.1212	1193	12767
10	181.1417	1440	16489
11	183.2452	682	6143
12	183.3446	915	19166
13	185.1808	702	15640
14	189.3578	933	14962
15	193.9061	630	15512
16	196.1714	1275	7090
17	201.3148	610	16152
18	205.7824	1107	18993
19	210.1866	1577	8145
20	227.6543	744	21660
21	231.9184	834	21112
22	241.9679	639	19659
23	256.8216	569	8226
24	273.1118	5840	7988
25	274.1139	1051	8004
26	287.1291	691	8917
27	295.0926	1521	9074
28	566.7077	651	31933
29	697.6442	572	35379
30	738.0946	551	42272

Figure 42 HRTOF Mass spectrum of compound MC-8 (**47**)

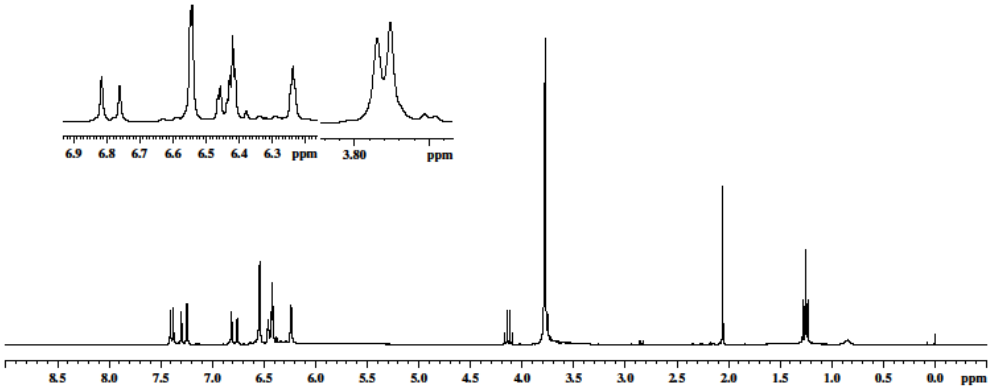

Figure 43 ^{1}H-NMR Spectrum of compound MC-8 (**47**)

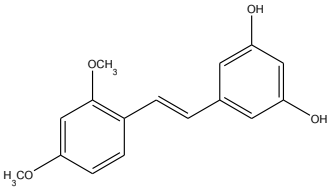

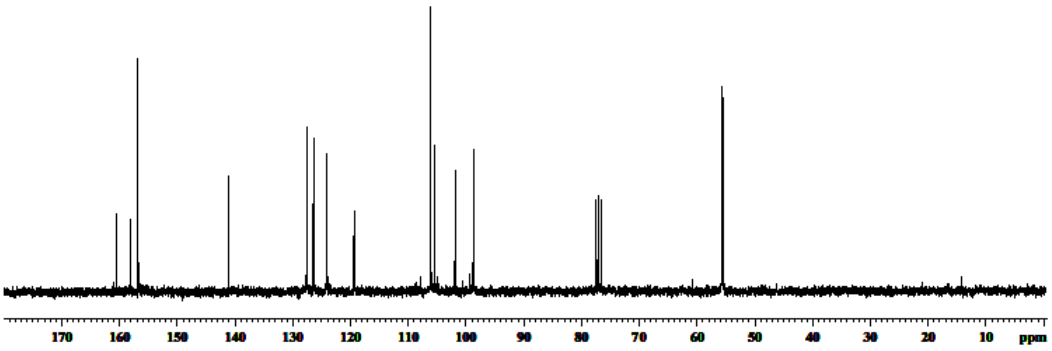

Figure 44 ^{13}C-NMR Spectrum of compound MC-8 (**47**)

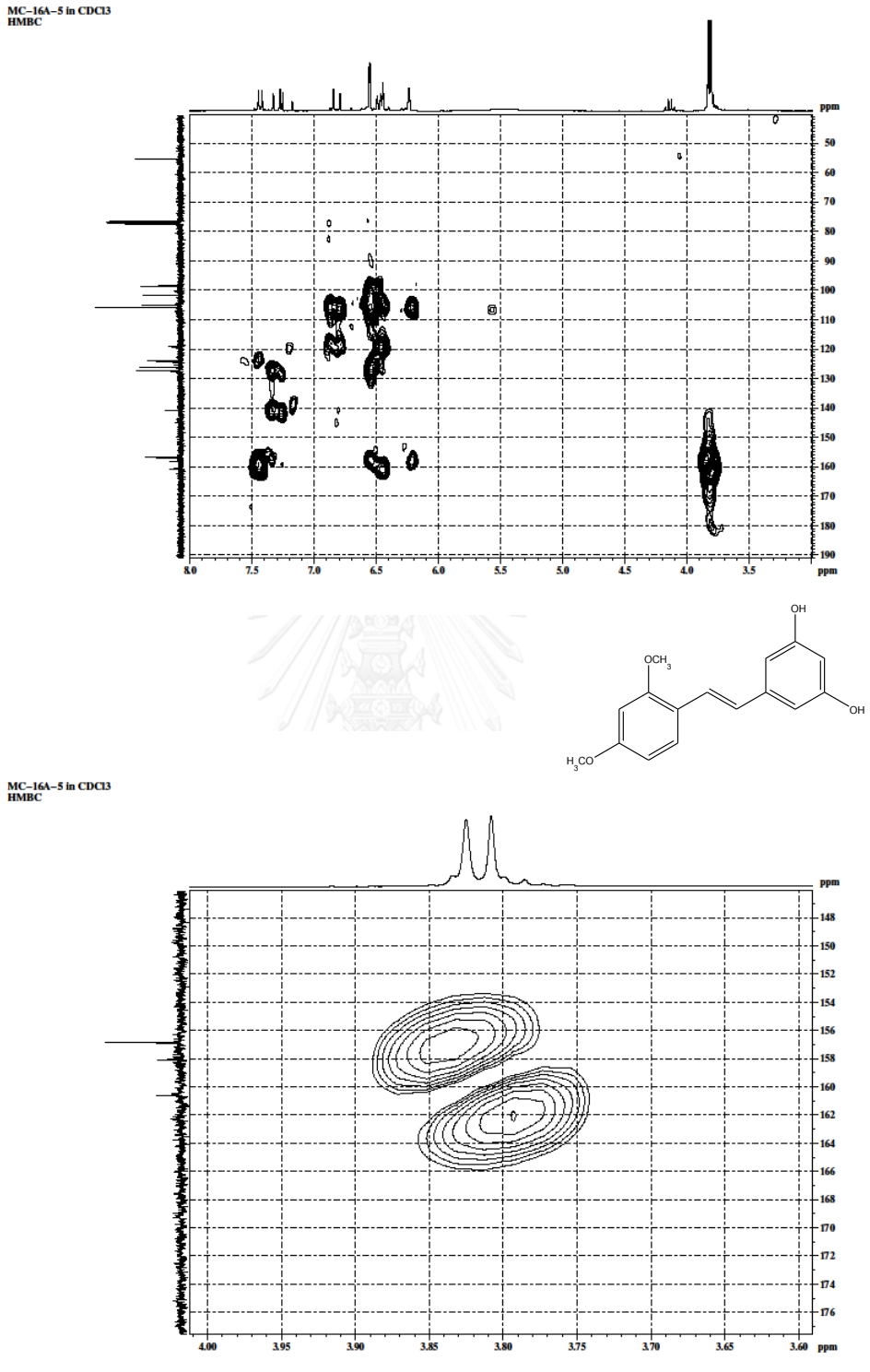

Figure 45 HMBC Spectrum of compound MC-8 (**47**)

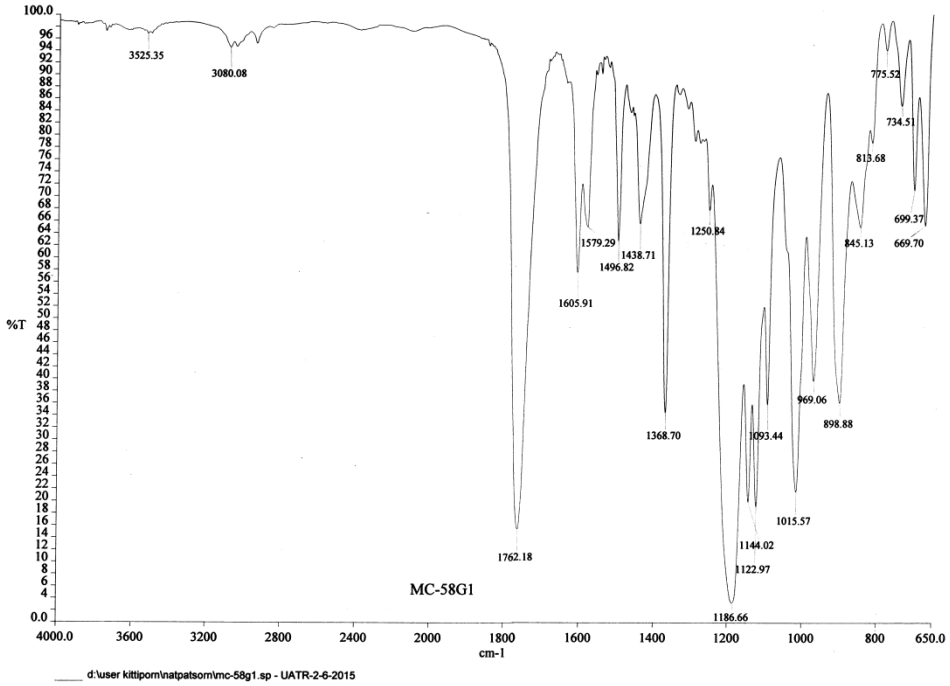

Figure 46 IR Spectrum of compound MC-9 (**38**)

Mass Spectrum List Report

Analysis Info

Analysis Name	H:\TOFCRI014508 Manasnun MC-24-1 E+.d	Acquisition Date	12/28/2008 3:45:52 PM
Method	Nitirat-apcipos 2012.m	Operator	Administrator
Sample Name	ESIpos Na	Instrument / Ser#	micrOTOF 0
Comment			

Acquisition Parameter

Source Type	APCI	Ion Polarity	Positive	Set Nebulizer	1.0 Bar
Focus	Not active			Set Dry Heater	80 °C
Scan Begin	90 m/z	Set Capillary	3500 V	Set Dry Gas	7.0 l/min
Scan End	800 m/z	Set End Plate Offset	-500 V	Set Divert Valve	Source

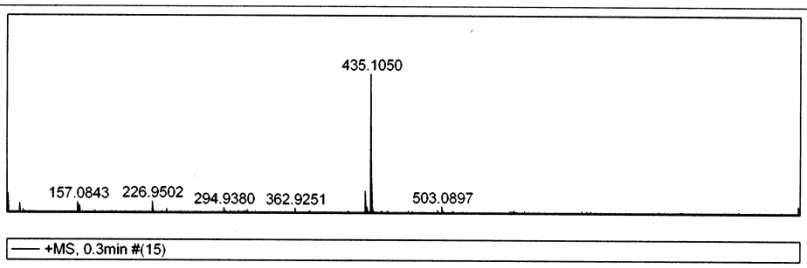

#	m/z	I
1	90.9752	18651
2	102.1273	9168
3	104.9919	2851
4	157.0843	9740
5	158.9651	7121
6	172.9806	1725
7	226.9502	10753
8	240.9648	3658
9	294.9380	4256
10	308.9531	1642
11	315.0827	1375
12	317.0631	2006
13	362.9251	3791
14	376.9384	1766
15	413.2656	1861
16	430.1498	20884
17	430.9128	3369
18	431.1512	5669
19	435.1050	139629
20	436.1076	34456
21	437.1107	6044
22	444.9292	1585
23	451.0786	1670
24	471.1740	1742
25	498.9003	2010
26	503.0897	5658
27	566.8851	1546
28	569.1982	1777
29	571.0757	1857
30	842.2584	6561

Figure 47 HRTOF Mass spectrum of compound MC-9 (**38**)

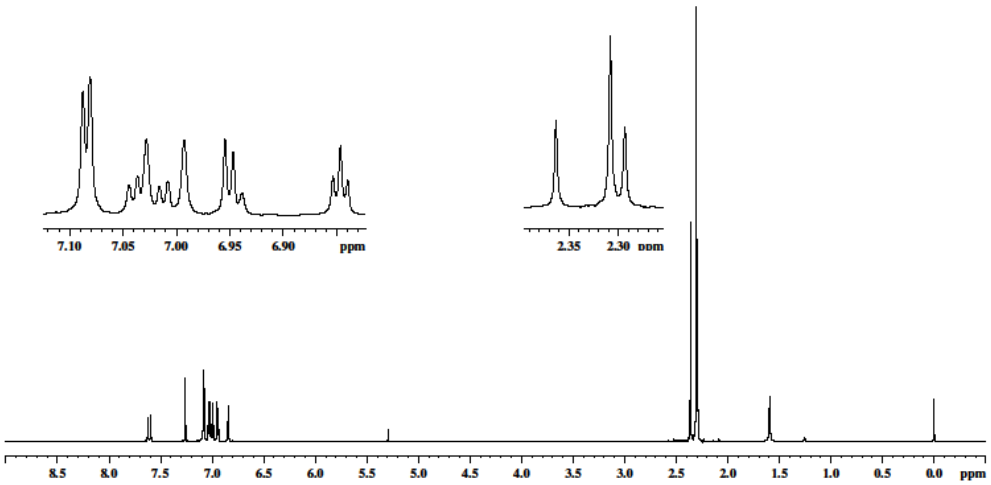

Figure 48 ^{1}H-NMR Spectrum of compound MC-9 (**38**)

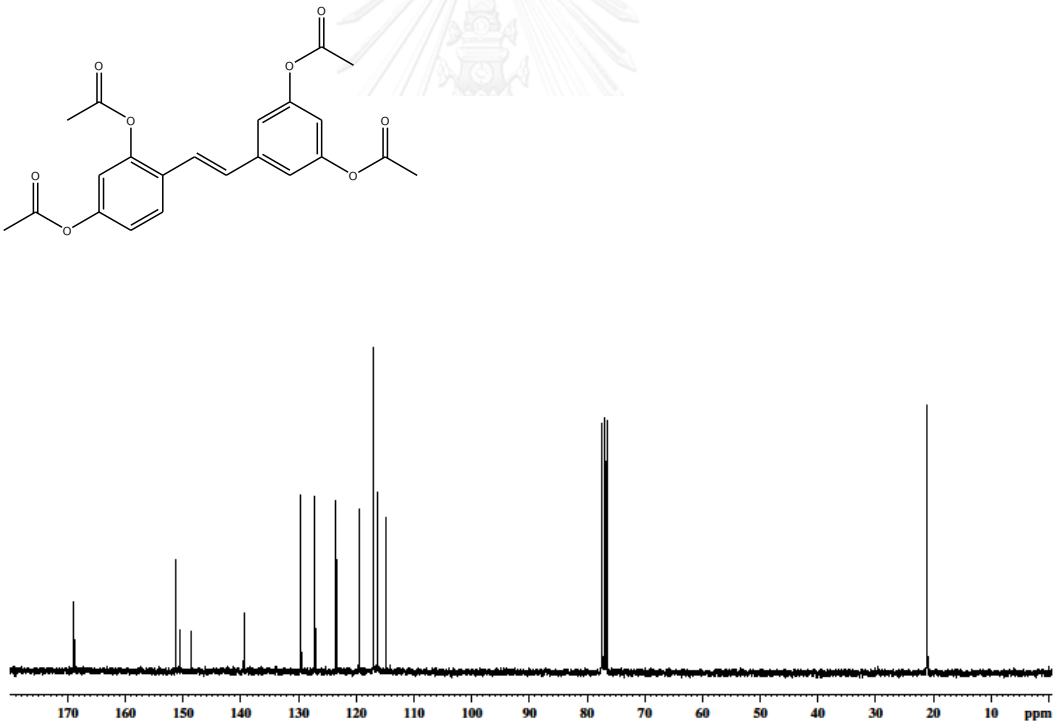

Figure 49 ^{13}C-NMR Spectrum of compound MC-9 (**38**)

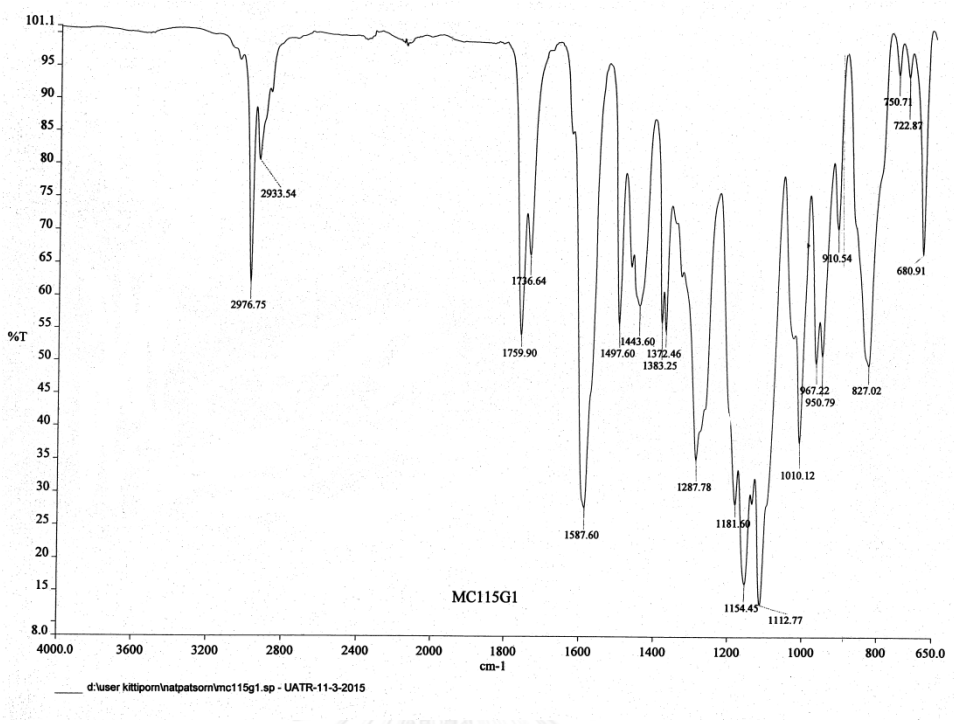

Figure 50 IR Spectrum of compound MC-10 (**48**)

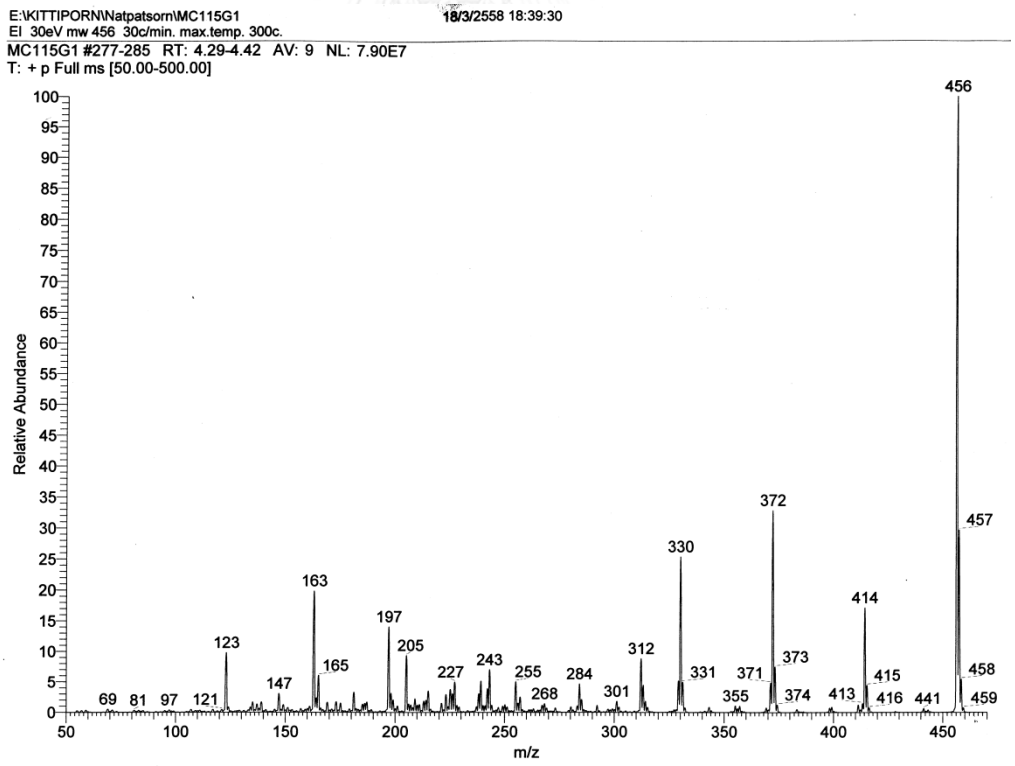

Figure 51 EI Mass spectrum of compound MC-10 (**48**)

Mass Spectrum List Report

Analysis Info

Analysis Name	H:\TOFCRI14856 Manasnun MC-29-2 E+.d	Acquisition Date	2/5/2009 12:21:58 PM
Method	Nitirat-apcipos 2012.m	Operator	Administrator
Sample Name	ESIpos	Instrument / Ser#	micrOTOF 0
Comment			

Acquisition Parameter

Source Type	APCI	Ion Polarity	Positive	Set Nebulizer	1.5 Bar
Focus	Not active			Set Dry Heater	85 °C
Scan Begin	150 m/z	Set Capillary	3500 V	Set Dry Gas	7.0 l/min
Scan End	1000 m/z	Set End Plate Offset	-500 V	Set Divert Valve	Source

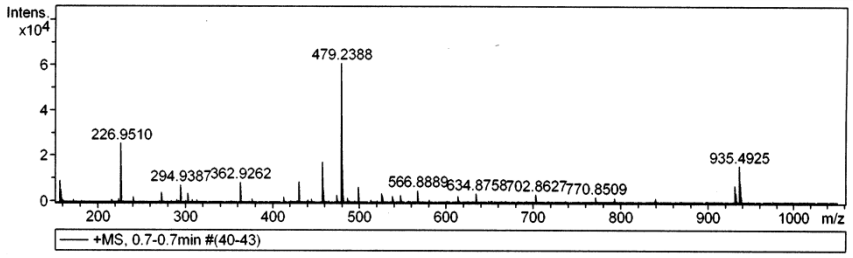

#	m/z	I
1	157.0867	9178
2	158.9671	5213
3	226.9510	25586
4	240.9670	2201
5	273.1672	3992
6	294.9387	7377
7	303.1782	3644
8	362.9262	8681
9	413.2643	2239
10	430.9143	9003
11	457.2572	17449
12	458.2608	5341
13	474.2820	3067
14	479.2388	60961
15	480.2417	16423
16	481.2447	3061
17	498.9005	6563
18	538.2756	2612
19	547.2258	3001
20	566.8889	5050
21	613.3337	2508
22	634.8758	3726
23	702.8627	3277
24	770.8509	2164
25	792.6888	1895
26	930.5372	7370
27	931.5398	4074
28	935.4925	15736
29	936.4960	8475
30	937.4982	2821

Figure 52 HRTOF Mass spectrum of compound MC-10 (**48**)

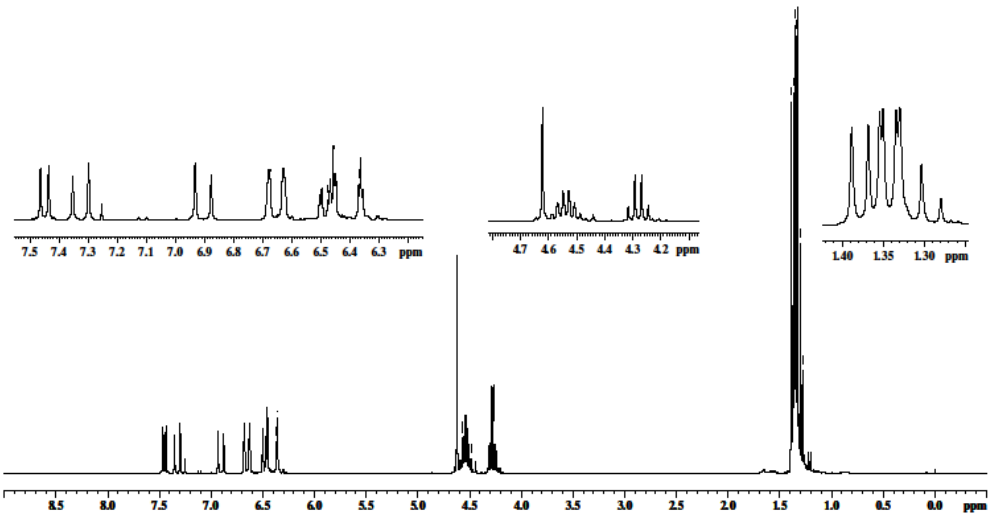

Figure 53 ^{1}H-NMR Spectrum of compound MC-10 (**48**)

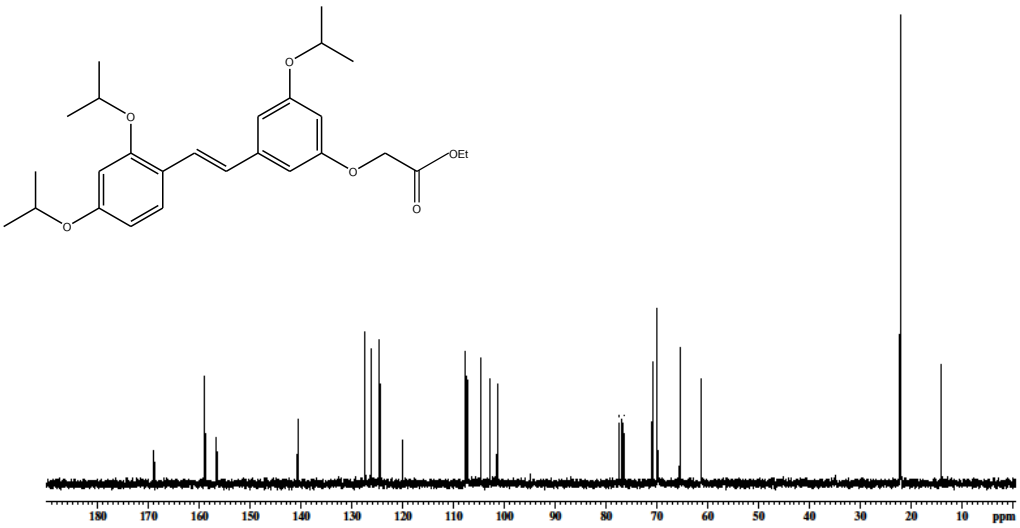

Figure 54 ^{13}C-NMR Spectrum of compound MC-10 (**48**)

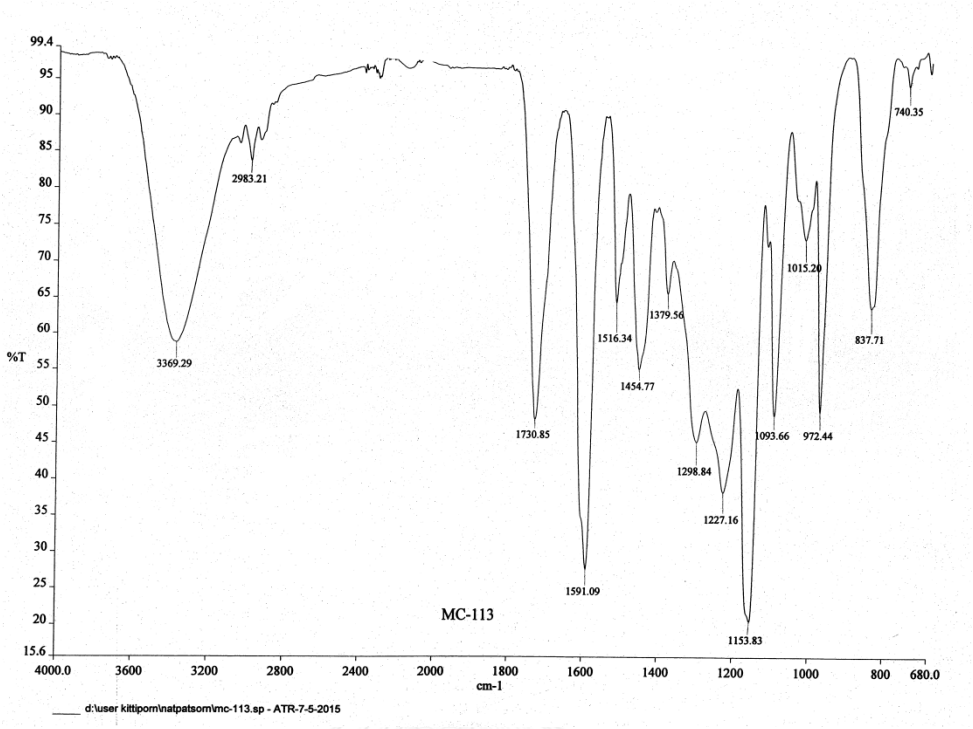

Figure 55 IR Spectrum of compound MC-11 (**49**)

Mass Spectrum List Report

Analysis Info

Analysis Name	TOFCRI015575 Manasnun MC47F2 E+.d	Acquisition Date	5/8/2008 1:12:49 PM
Method	Nitirat ESI pos 2013-2.m	Operator	Administrator
Sample Name	ESIpos	Instrument	micrOTOF 74

Acquisition Parameter

Source Type	ESI	Ion Polarity	Positive	Set Corrector Fill	55 V
Scan Range	n/a	Capillary Exit	120.0 V	Set Pulsar Pull	429 V
Scan Begin	150 m/z	Hexapole RF	150.0 V	Set Pulsar Push	429 V
Scan End	900 m/z	Skimmer 1	40.0 V	Set Reflector	1300 V
		Hexapole 1	23.0 V	Set Flight Tube	9000 V
				Set Detector TOF	2180 V

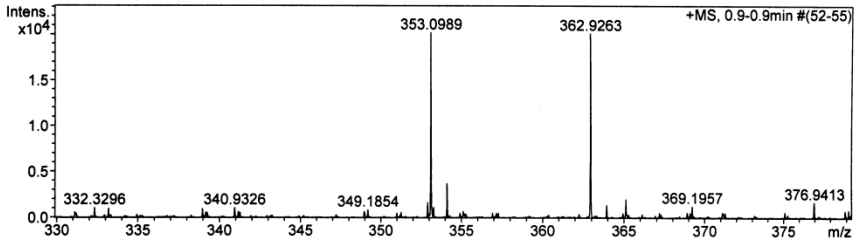

#	m/z	I	Res.
1	212.9678	3318	7320
2	213.2114	3263	6806
3	226.9478	56605	6968
4	240.9636	3338	8029
5	242.2808	35688	7088
6	243.2830	6649	7816
7	270.9748	6482	7524
8	273.1651	8689	7751
9	279.2262	5231	8194
10	294.9364	7140	8576
11	301.1457	4348	7732
12	303.1767	9297	8241
13	304.2960	6089	8338
14	353.0989	20190	8506
15	354.1010	3741	8368
16	362.9263	20107	8462
17	385.2919	21541	8381
18	386.2941	4625	8628
19	413.2823	11392	4161
20	414.2820	3381	7241
21	430.9127	25161	9435
22	441.2983	6695	8829
23	498.9012	15307	8873
24	566.8879	14138	9727
25	634.8766	11346	9804
26	683.2067	3540	10132
27	701.4915	3285	10215
28	702.8633	10228	10308
29	770.8487	6290	10021
30	838.8379	5680	10998

Figure 56 HRTOF Mass spectrum of compound MC-11 (**49**)

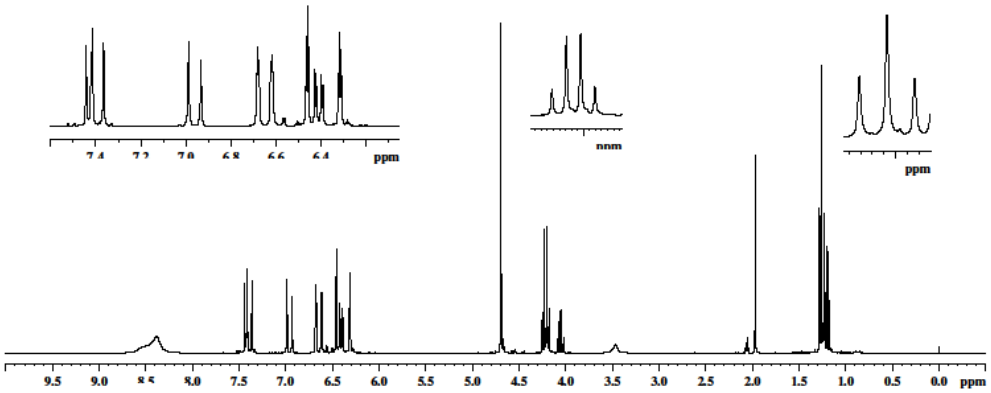

Figure 57 ^{1}H-NMR Spectrum of compound MC-11 (**49**)

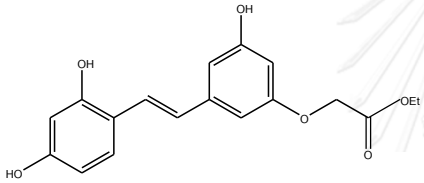

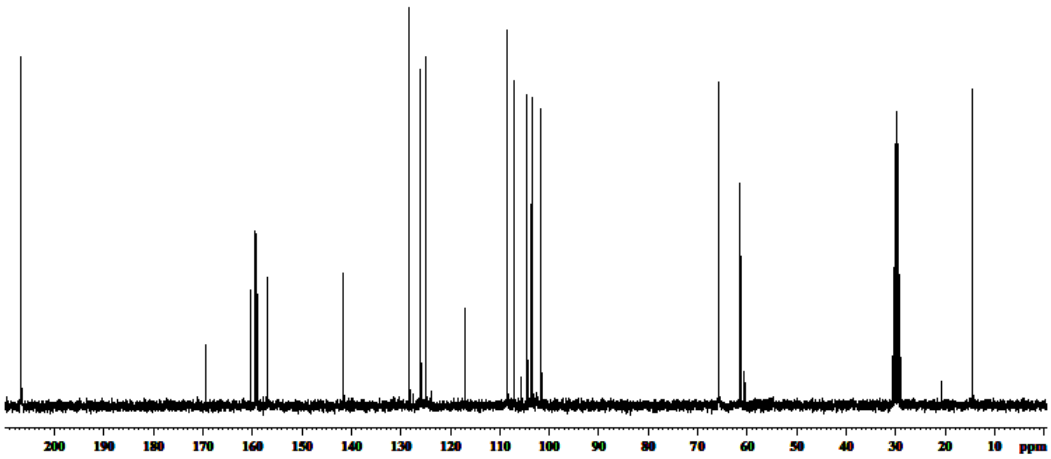

Figure 58 ^{13}C-NMR Spectrum of compound MC-11 (**49**)

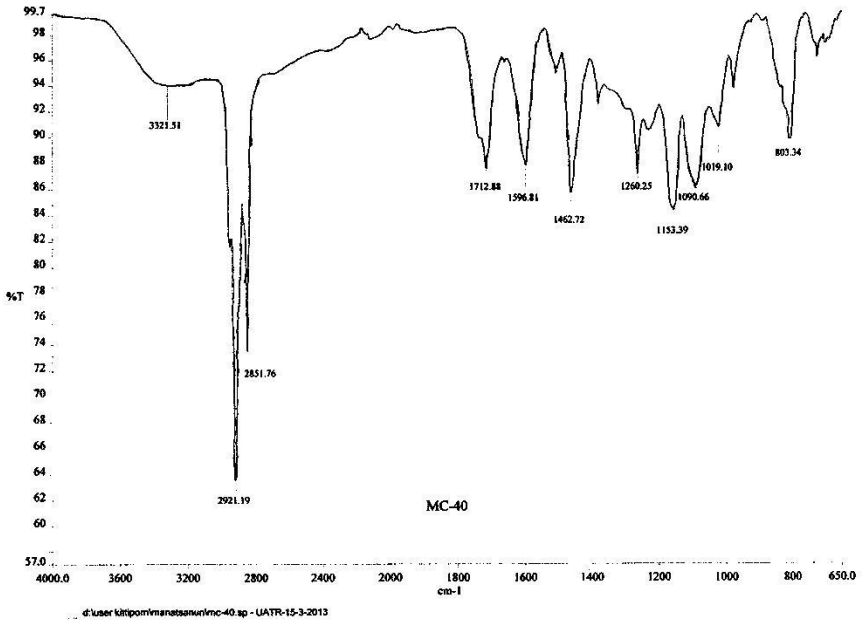

Figure 59 IR Spectrum of compound MC-12 (**50**)

Mass Spectrum List Report

Analysis Info

Analysis Name	TOFCRI016400 Mananan MC63A5 E-.d	Acquisition Date	9/5/2008 4:17:07 PM
Method	Nitirat_ESI neg 2013-2.m	Operator	Administrator
Sample Name	ESIneg	Instrument	micrOTOF 74

Acquisition Parameter

Source Type	ESI	Ion Polarity	Negative	Set Corrector Fill	56 V
Scan Range	n/a	Capillary Exit	-110.0 V	Set Pulsar Pull	409 V
Scan Begin	100 m/z	Hexapole RF	160.0 V	Set Pulsar Push	409 V
Scan End	1000 m/z	Skimmer 1	-35.0 V	Set Reflector	1300 V
		Hexapole 1	-24.0 V	Set Flight Tube	9000 V
				Set Detector TOF	1825 V

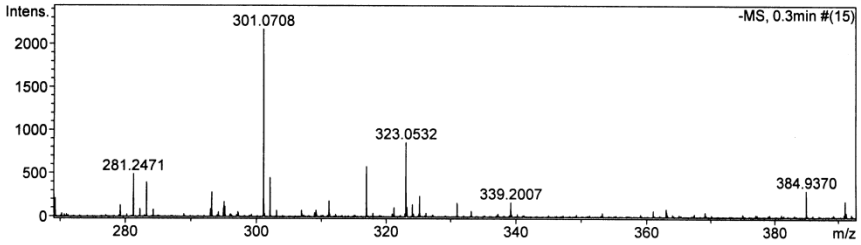

#	m/z	I	Res.
1	227.2005	396	8736
2	236.0469	172	8652
3	241.2153	383	8603
4	243.0635	337	8377
5	248.9599	602	8742
6	251.0695	863	8325
7	252.0750	160	8739
8	253.2154	548	8612
9	254.2183	150	10127
10	255.2308	1246	8954
11	256.2333	278	8732
12	265.1453	1028	8806
13	266.1494	152	9917
14	269.2464	213	8269
15	281.2471	489	9021
16	283.2610	397	9665
17	293.1798	282	9589
18	295.0591	173	9694
19	301.0708	2168	9155
20	302.0741	449	9666
21	311.1702	181	8950
22	316.9487	576	9580
23	323.0532	859	10280
24	324.0573	144	10189
25	325.1834	240	10364
26	330.9638	158	9254
27	339.2007	166	9602
28	384.9370	306	10269
29	391.0430	188	11106
30	452.9287	176	10649

Figure 60 HRTOF Mass spectrum of compound MC-12 (**50**)

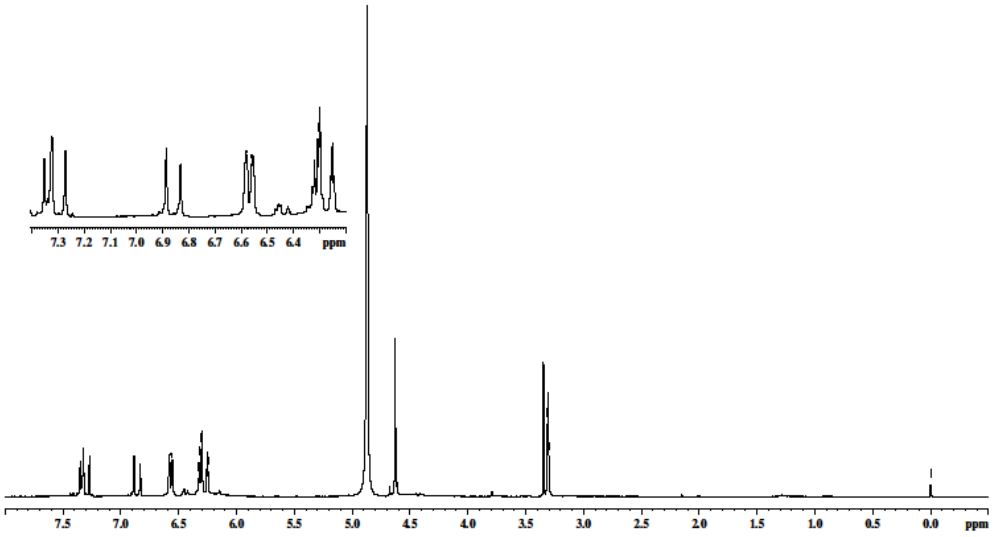

Figure 61 ^{1}H-NMR Spectrum of compound MC-12 (**50**)

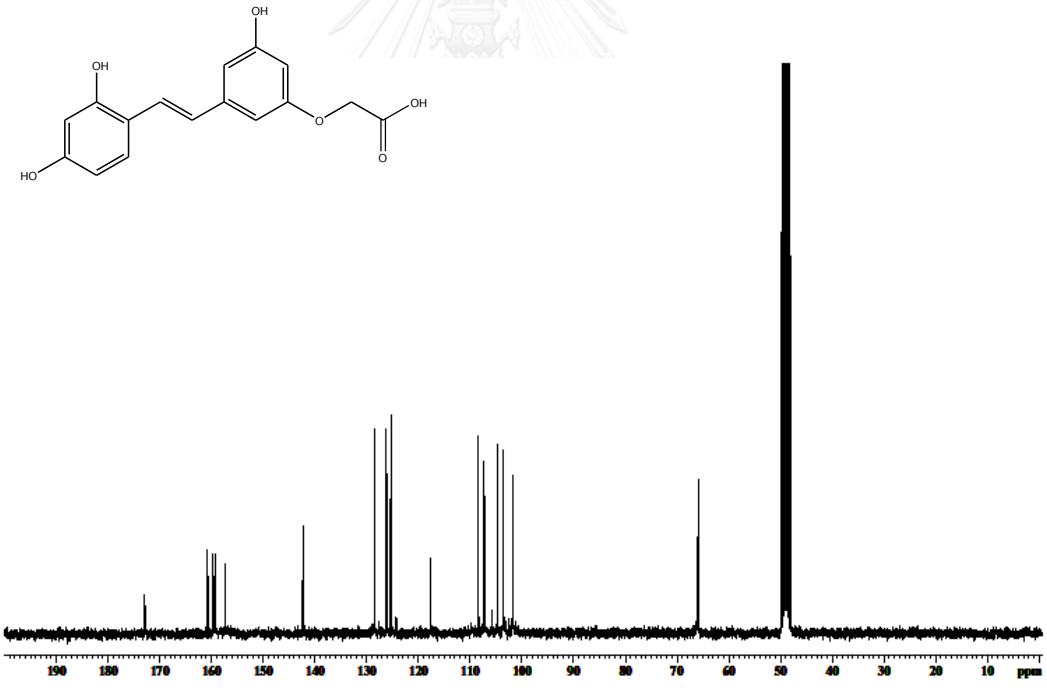

Figure 62 ^{13}C-NMR Spectrum of compound MC-12 (**50**)

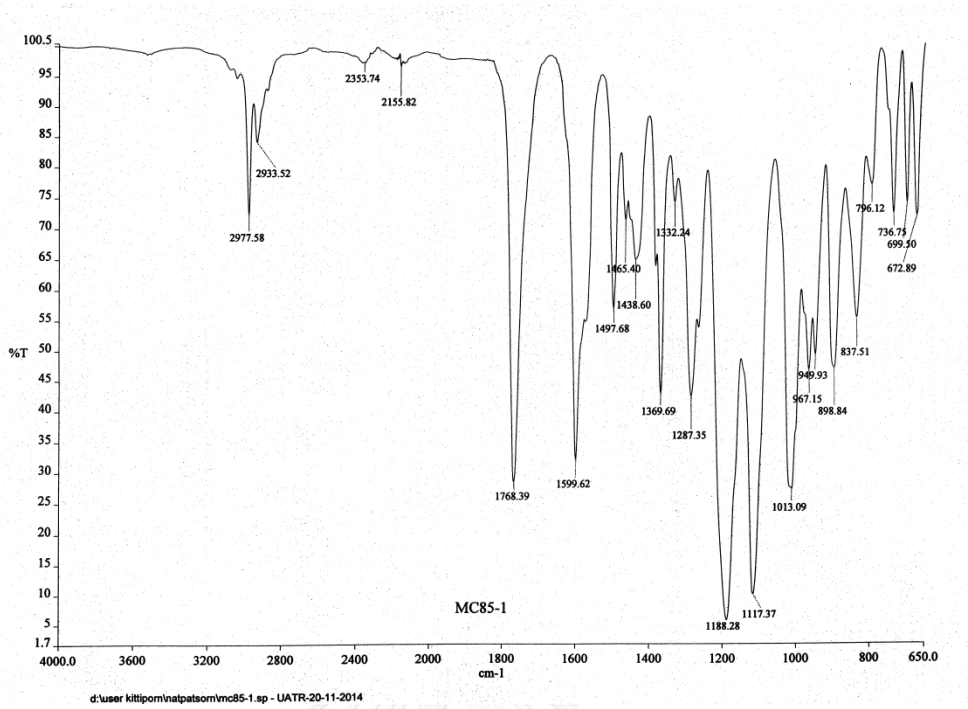

Figure 63 IR Spectrum of compound MC-13 (**51**)

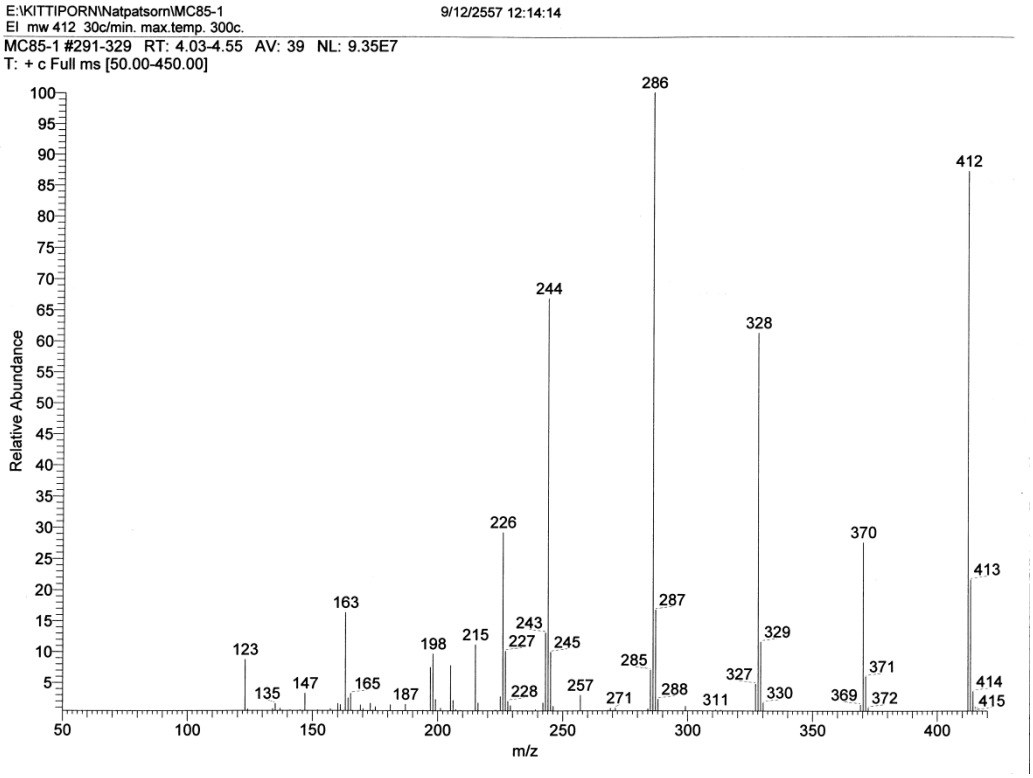

Figure 64 EI Mass spectrum of compound MC-13 (**51**)

Mass Spectrum List Report

Analysis Info

Analysis Name	TOFCRI017449 Natpassorn MC85-2 E+.d	Acquisition Date	2/20/2014 1:59:36 PM
Method	Nitirat ESI pos 2013-4.m	Operator	Administrator
Sample Name	ESIpos	Instrument	micrOTOF 74

Acquisition Parameter

Source Type	ESI	Ion Polarity	Positive	Set Corrector Fill	86 V
Scan Range	n/a	Capillary Exit	120.0 V	Set Pulsar Pull	406 V
Scan Begin	150 m/z	Hexapole RF	120.0 V	Set Pulsar Push	406 V
Scan End	700 m/z	Skimmer 1	40.0 V	Set Reflector	1300 V
		Hexapole 1	23.0 V	Set Flight Tube	9000 V
				Set Detector TOF	1840 V

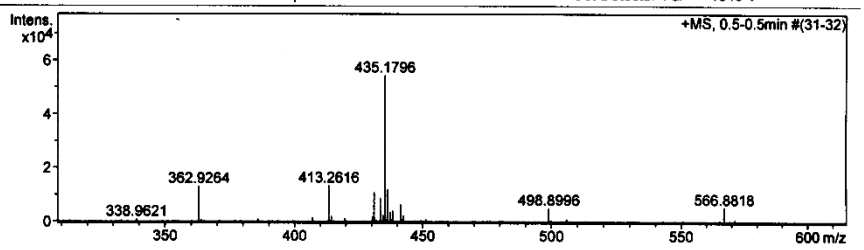

#	m/z	I	Res.
1	157.0881	13620	7465
2	158.9684	28643	7486
3	210.0925	18140	8171
4	211.0960	2377	8372
5	223.1646	3232	8511
6	226.9515	5451	8858
7	251.1972	5921	9251
8	265.2121	4476	9182
9	273.1658	3537	8606
10	277.2111	2963	8966
11	279.2287	9446	8831
12	294.9388	15262	8646
13	301.1474	2568	6993
14	303.1795	4330	8664
15	362.9264	13050	9051
16	413.2616	13306	10791
17	430.9137	11020	9645
18	433.3764	8705	10943
19	434.3800	2371	10914
20	435.1796	54308	8570
21	436.1820	11979	9168
22	437.1822	3593	11281
23	437.3409	3214	30378
24	438.1840	3980	29121
25	441.2999	6395	8532
26	442.3039	2229	9343
27	498.8996	5072	9251
28	566.8818	5301	10461
29	634.8740	4521	11694
30	702.8609	2365	9576

Bruker Daltonics DataAnalysis 3.3 printed: 2/20/2014 5:53:39 PM Page 1 of 1

Figure 65 HRTOF Mass spectrum of compound MC-13 (**51**)

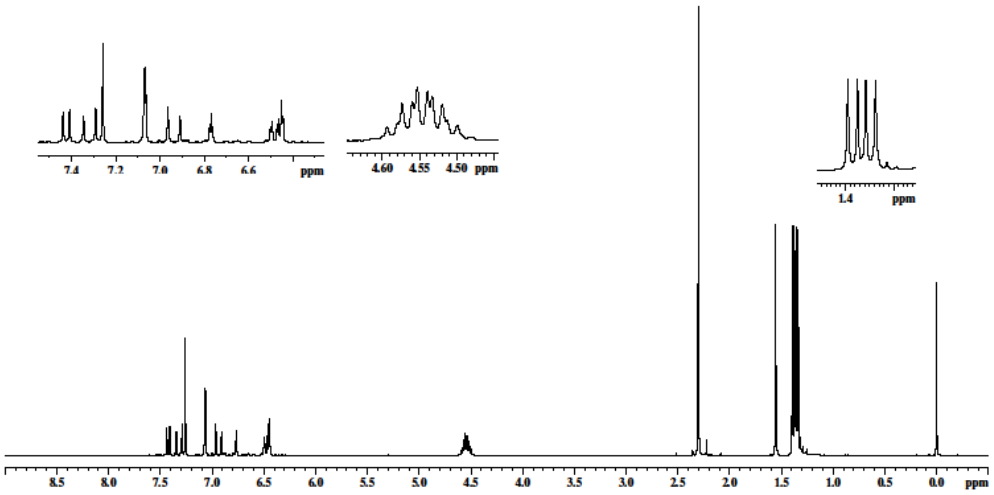

Figure 66 ^{1}H-NMR Spectrum of compound MC-13 (**51**)

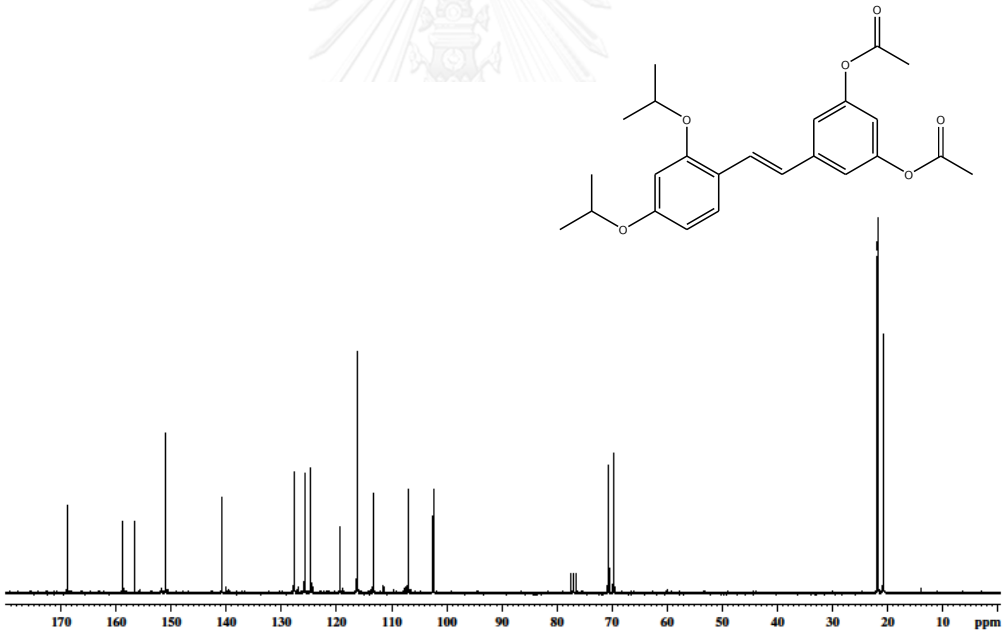

Figure 67 ^{13}C-NMR Spectrum of compound MC-13 (**51**)

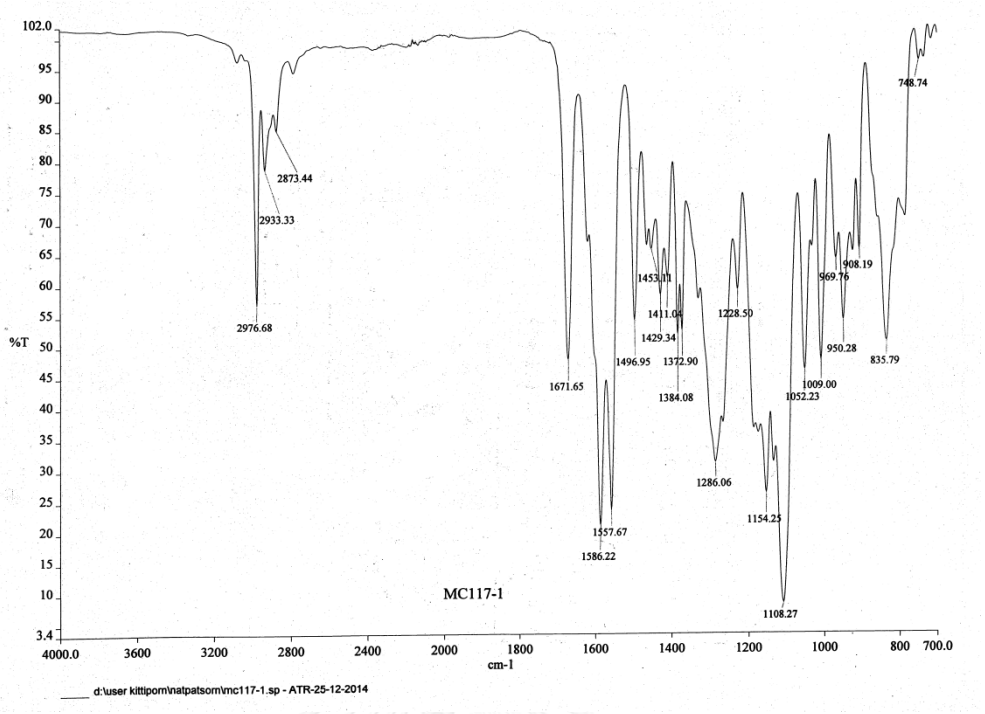

Figure 68 IR Spectrum of compound MC-14 (**52**)

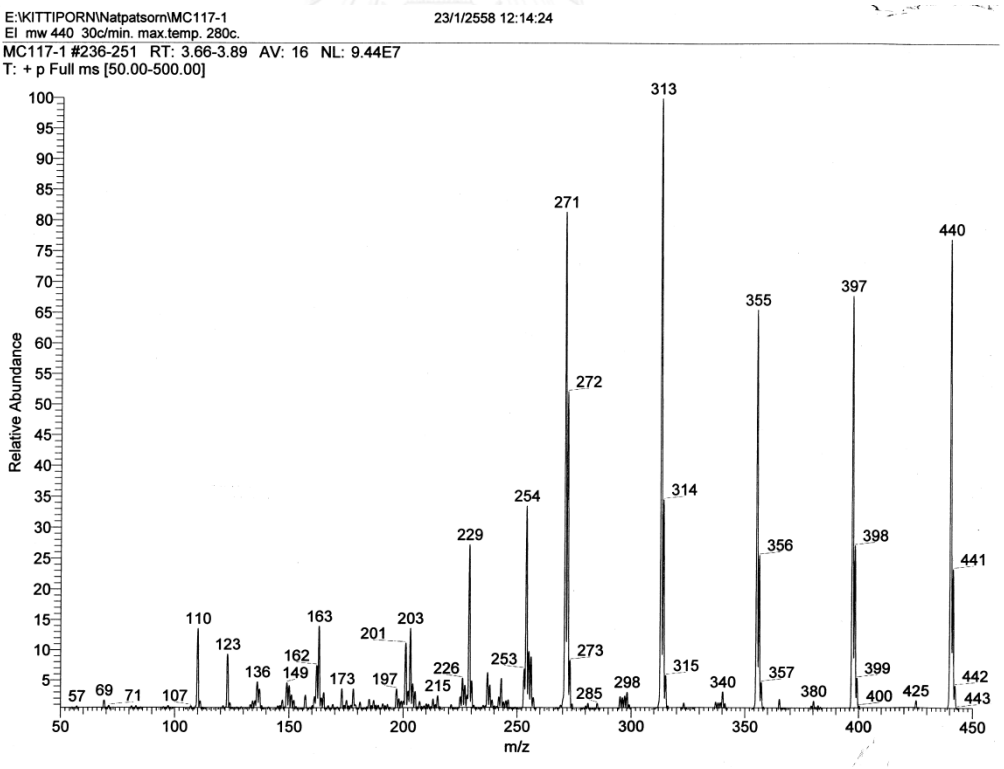

Figure 69 EI Mass spectrum of compound MC-14 (**52**)

Mass Spectrum List Report

Analysis Info

Analysis Name	TOFCRI019095 Natpassorn MC117-1 E+.d	Acquisition Date	12/26/2014 3:56:34 PM
Method	Nitirat ESI pos 2014-1.m	Operator	Administrator
Sample Name	ESIpos	Instrument	micrOTOF 74

Acquisition Parameter

Source Type	ESI	Ion Polarity	Positive	Set Corrector Fill	64 V
Scan Range	n/a	Capillary Exit	110.0 V	Set Pulsar Pull	405 V
Scan Begin	120 m/z	Hexapole RF	120.0 V	Set Pulsar Push	405 V
Scan End	900 m/z	Skimmer 1	35.0 V	Set Reflector	1300 V
		Hexapole 1	22.9 V	Set Flight Tube	9000 V
				Set Detector TOF	1865 V

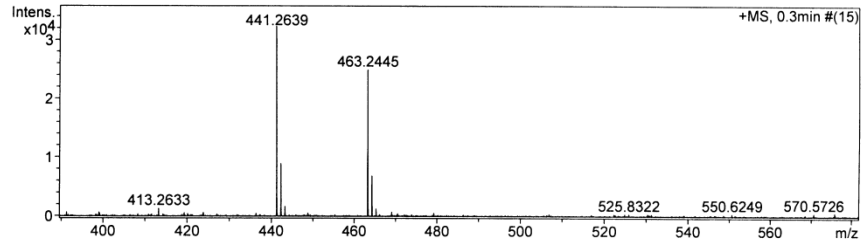

#	m/z	I	Res.
1	157.0787	2778	6732
2	158.9596	3605	7062
3	162.8808	1316	13564
4	162.9734	1588	18609
5	166.8060	1440	17997
6	210.1805	1073	8079
7	216.9187	1839	8097
8	226.9472	1442	7717
9	413.2633	1309	9833
10	441.2639	32266	9364
11	442.2678	8891	9411
12	443.2696	1689	9972
13	463.2445	24905	9642
14	464.2471	6823	9719
15	465.2499	1262	10766
16	793.1975	1567	40124
17	863.3062	919	37228
18	863.5142	1041	37070
19	881.4899	1307	9705
20	898.5003	7216	10705
21	899.5056	4008	10412
22	900.5069	1252	11221
23	903.4542	8989	11253
24	904.4572	5064	11656
25	905.4646	1501	11169
26	908.5684	1437	12800
27	908.7345	1308	41010
28	908.9758	1182	38639
29	913.1850	982	22402
30	913.9001	1351	38260

Figure 70 HRTOF Mass spectrum of compound MC-14 (**52**)

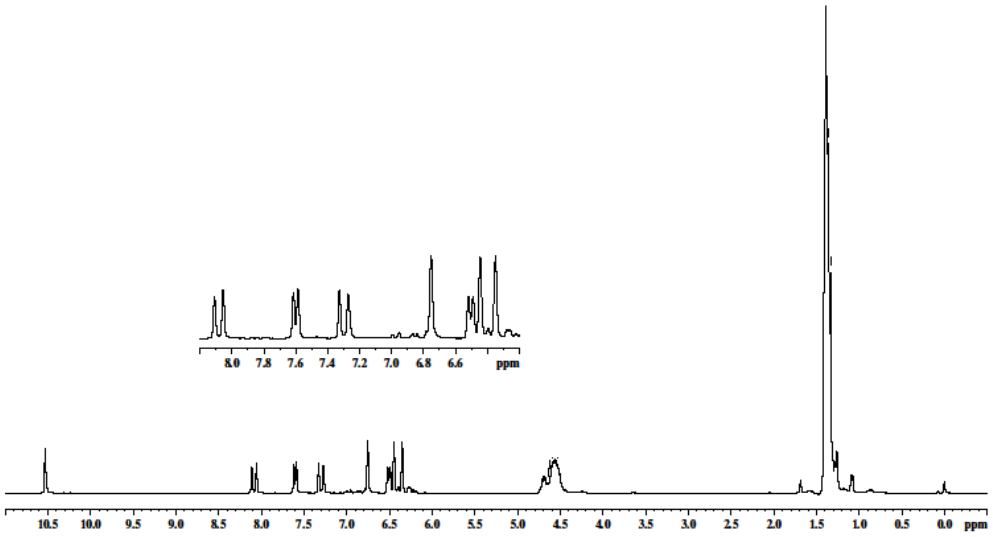

Figure 71 ^{1}H-NMR Spectrum of compound MC-14 (**52**)

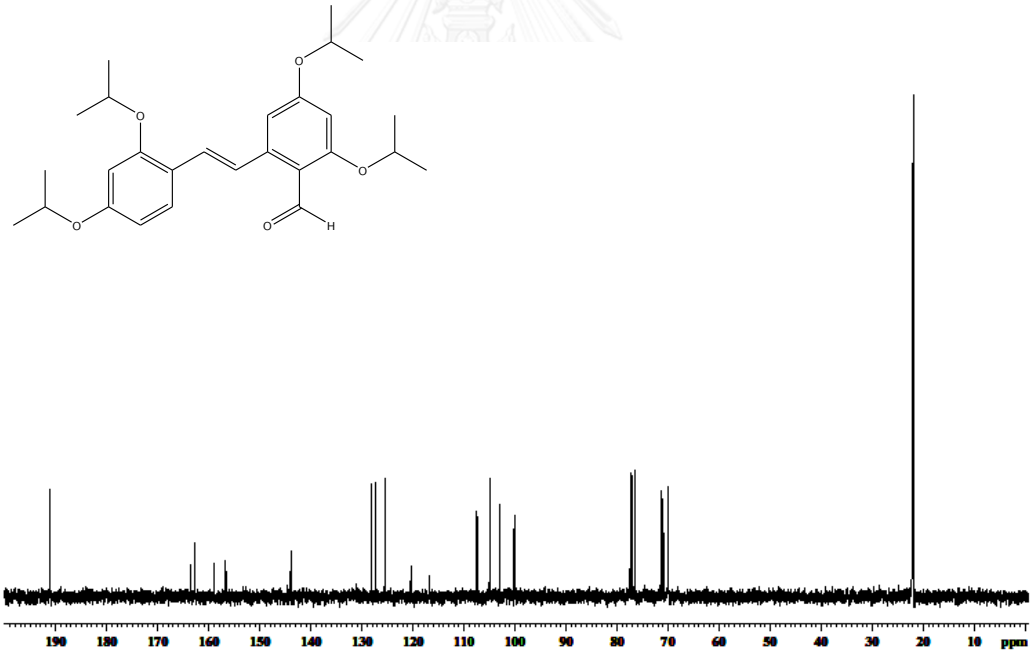

Figure 72 ^{13}C-NMR Spectrum of compound MC-14 (**52**)

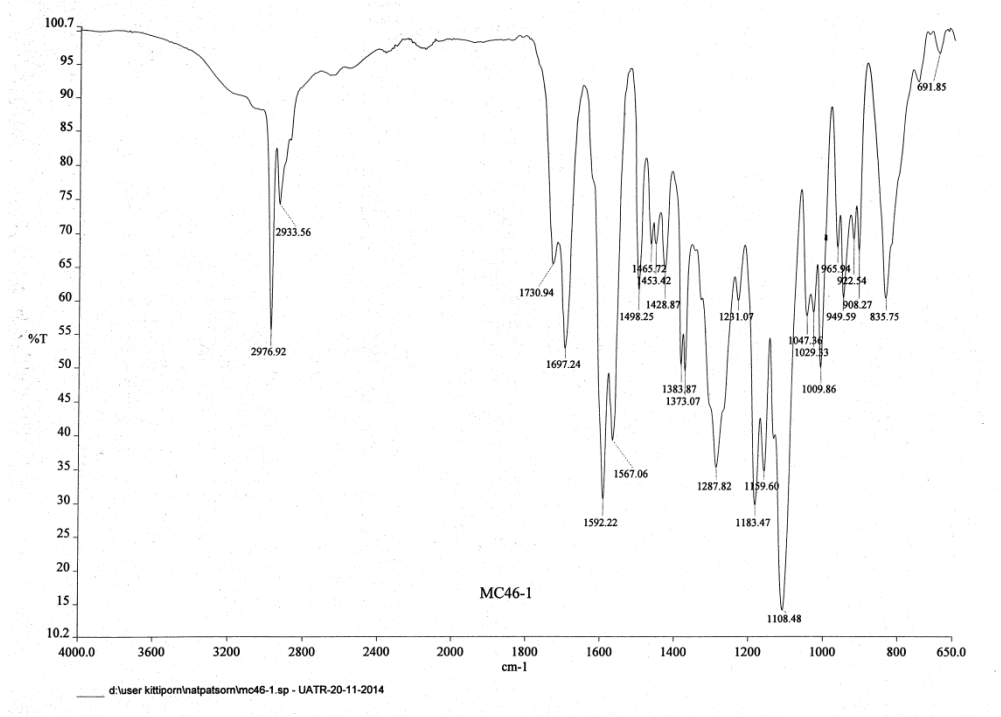

Figure 73 IR Spectrum of compound MC-15 (**53**)

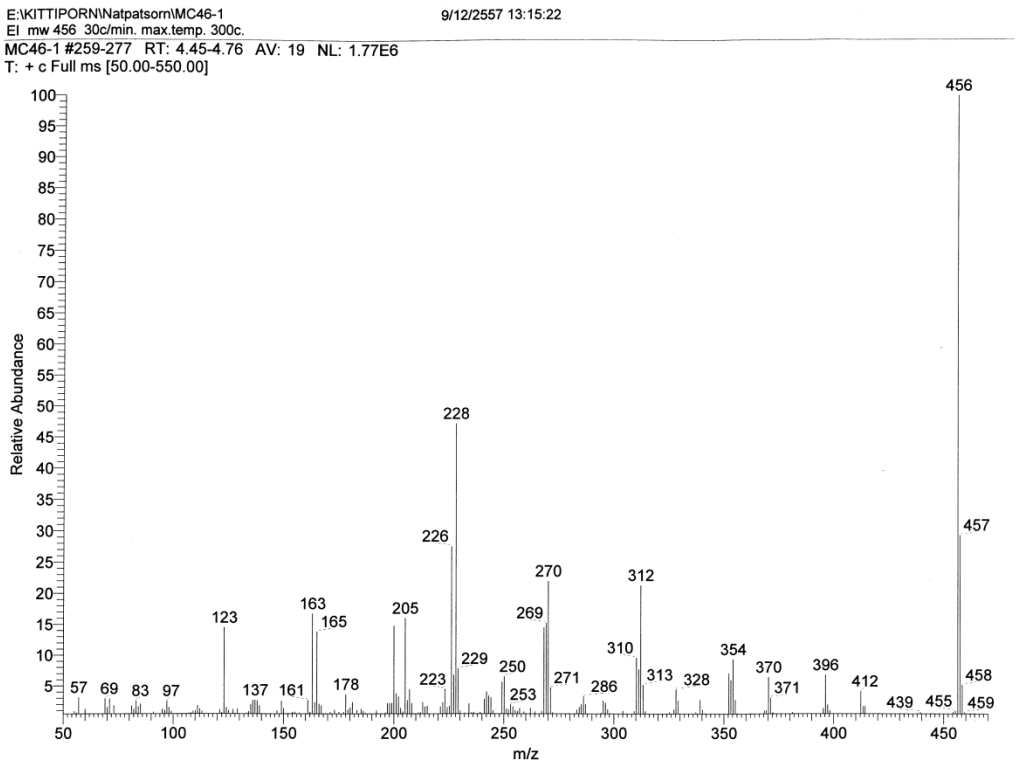

Figure 74 EI Mass spectrum of compound MC-15 (**53**)

Mass Spectrum List Report

Analysis Info

Analysis Name	TOFCRI015078 Manasnun MC36-3 E+.d	Acquisition Date	2/27/2009 3:58:40 PM
Method	Nitirat-apcipos 2012.m	Operator	Administrator
Sample Name	ESIpos	Instrument	micrOTOF 0

Acquisition Parameter

Source Type	APCI	Ion Polarity	Positive	Set Corrector Fill	56 V
Scan Range	n/a	Capillary Exit	110.0 V	Set Pulsar Pull	409 V
Scan Begin	220 m/z	Hexapole RF	120.0 V	Set Pulsar Push	409 V
Scan End	800 m/z	Skimmer 1	33.0 V	Set Reflector	1300 V
		Hexapole 1	23.0 V	Set Flight Tube	9000 V
				Set Detector TOF	2200 V

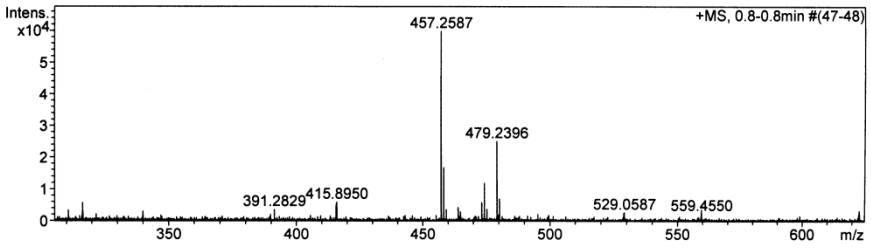

#	m/z	I	Res.
1	239.1277	4182	7480
2	293.5944	3583	24552
3	304.3005	4863	8800
4	310.7748	3375	27571
5	316.2245	2716	28043
6	316.3665	5797	27169
7	339.9775	3148	25960
8	391.2829	3605	9731
9	415.4905	4617	21336
10	415.6542	5034	30752
11	415.8950	5975	29466
12	457.2587	59763	10222
13	458.2617	16776	10180
14	459.2638	3612	10321
15	464.0064	3680	12702
16	464.8413	2933	33943
17	473.2537	5810	10573
18	474.2829	11881	9391
19	475.2870	3693	9714
20	479.2396	25012	10654
21	480.2436	7015	10244
22	622.8501	3320	33898
23	655.2793	5766	19883
24	655.4775	4649	37734
25	655.5404	5455	34557
26	655.6006	5874	32795
27	655.6736	3339	37372
28	655.7834	10424	38023
29	796.1335	4451	40056
30	833.3458	4106	37179

Figure 75 HRTOF Mass spectrum of compound MC-15 (**53**)

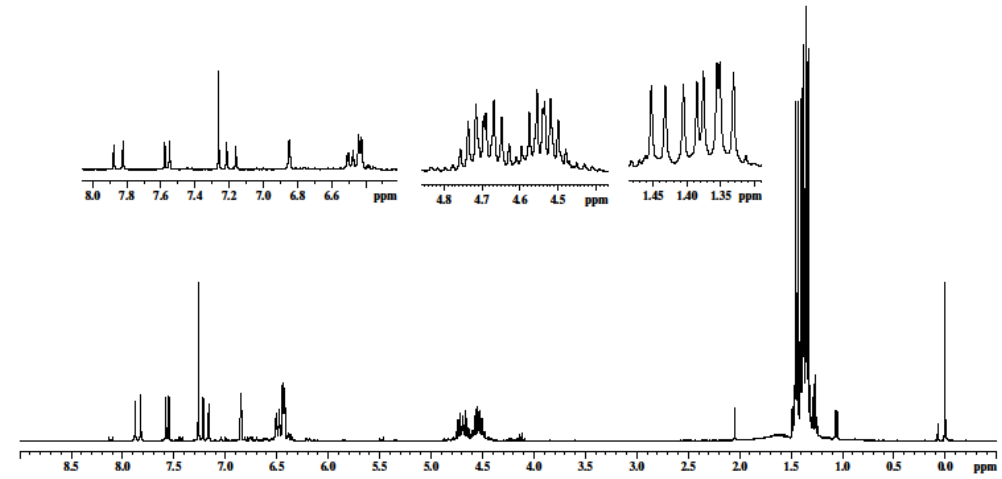

Figure 76 ^{1}H-NMR Spectrum of compound MC-15 (**53**)

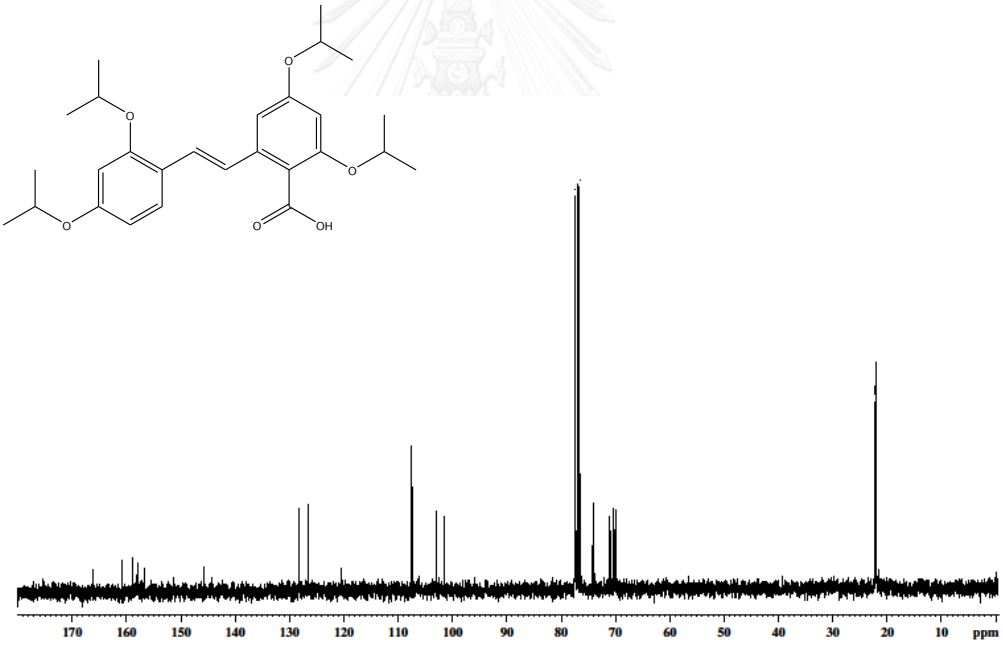

Figure 77 ^{13}C-NMR Spectrum of compound MC-15 (**53**)

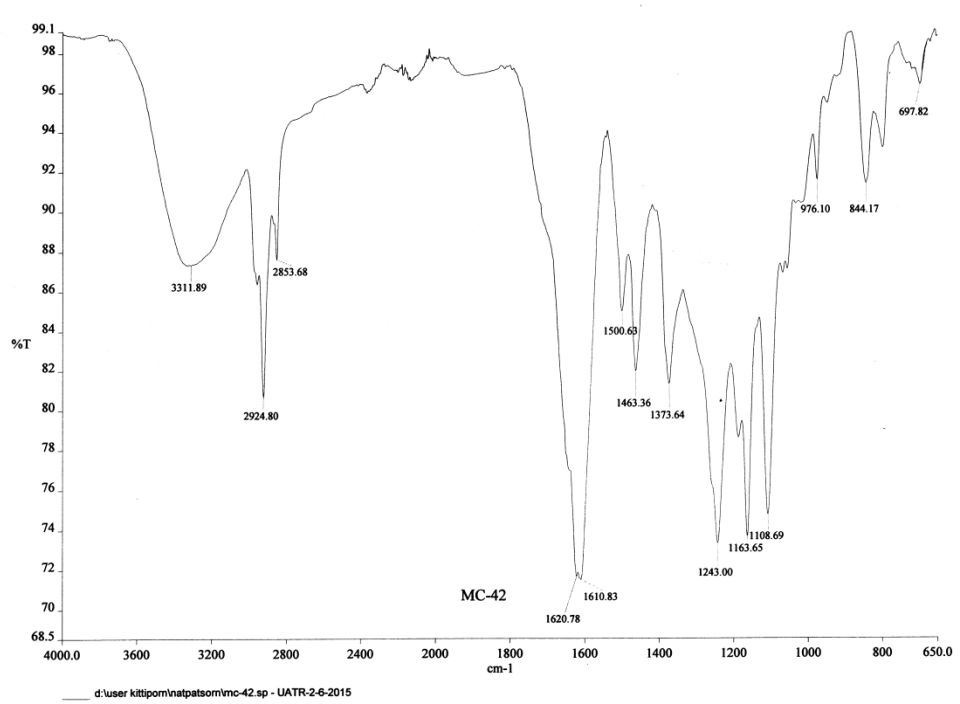

Figure 78 IR Spectrum of compound MC-16 (**54**)

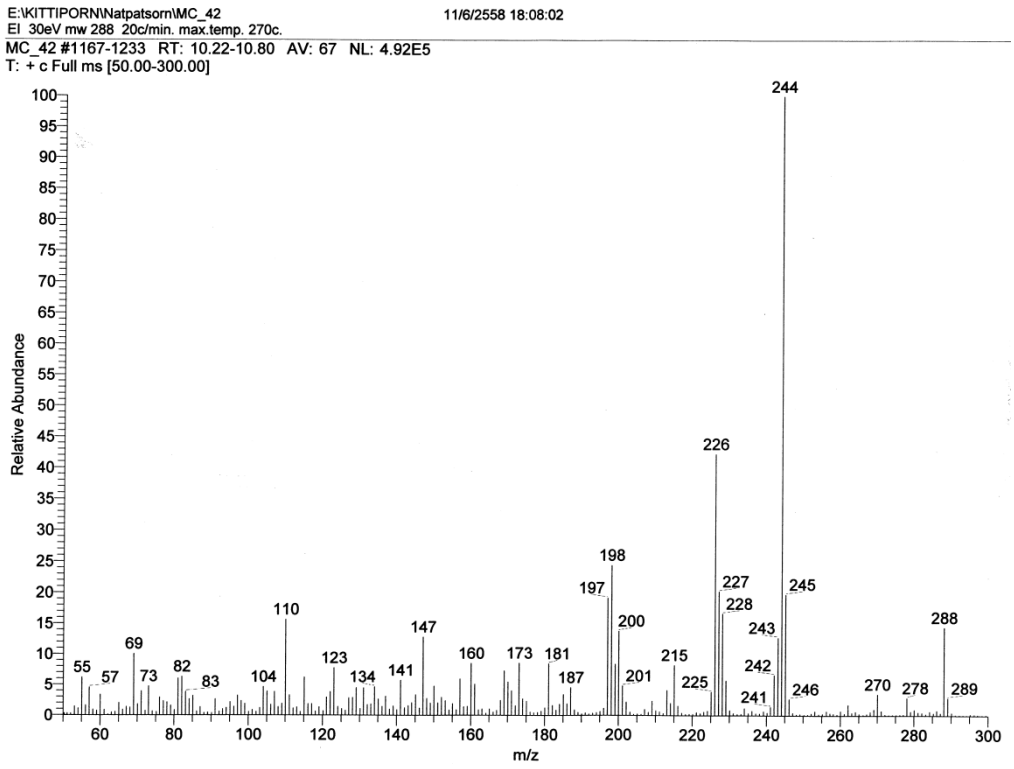

Figure 79 EI Mass spectrum of compound MC-16 (**54**)

Mass Spectrum List Report

Analysis Info

Analysis Name	TOFCRI0152688 Manusnan MC42-32 E+.d	Acquisition Date	3/29/2008 5:25:37 PM
Method	Nitirat ESI pos 2013-2.m	Operator	Administrator
Sample Name	ESIpos	Instrument	micrOTOF 74

Acquisition Parameter

Source Type	ESI	Ion Polarity	Positive	Set Corrector Fill	55 V
Scan Range	n/a	Capillary Exit	120.0 V	Set Pulsar Pull	429 V
Scan Begin	110 m/z	Hexapole RF	120.0 V	Set Pulsar Push	429 V
Scan End	800 m/z	Skimmer 1	40.0 V	Set Reflector	1300 V
		Hexapole 1	23.0 V	Set Flight Tube	9000 V
				Set Detector TOF	2160 V

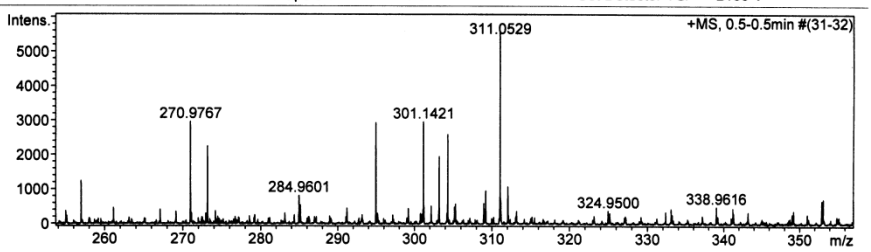

#	m/z	I	Res.
1	157.0869	9894	5949
2	158.9677	4240	6635
3	189.0739	2230	6773
4	211.0939	1239	7283
5	212.9720	1584	7470
6	226.9515	17696	7379
7	237.1091	1323	7274
8	240.9663	2692	7999
9	256.9602	1246	7503
10	270.9767	2962	8449
11	273.1673	2246	7985
12	294.9386	2935	8223
13	301.1421	2962	8221
14	303.1760	1955	8517
15	304.2961	2594	8990
16	311.0529	5588	8140
17	312.0554	1087	8928
18	362.9263	5583	9555
19	365.1106	1120	6712
20	376.9414	1073	9669
21	413.2651	4302	9898
22	414.2668	1065	9863
23	430.9129	5738	9977
24	441.2940	1683	10235
25	444.9290	1062	9629
26	498.9012	3930	10121
27	566.8865	3398	10631
28	634.8760	2609	10978
29	702.8613	1997	11079
30	770.8533	1100	10407

Figure 80 HRTOF Mass spectrum of compound MC-16 (**54**)

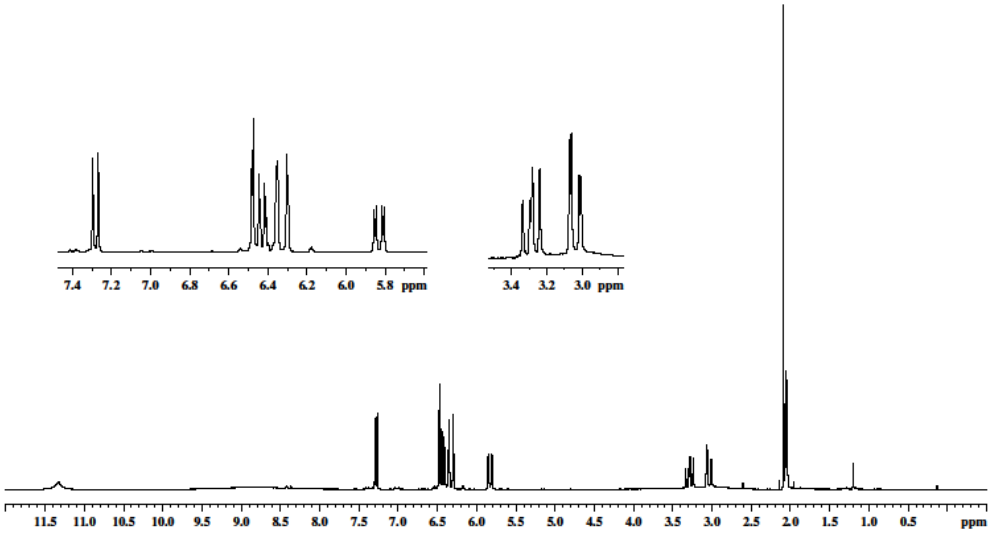

Figure 81 ^{1}H-NMR Spectrum of compound MC-16 (**54**)

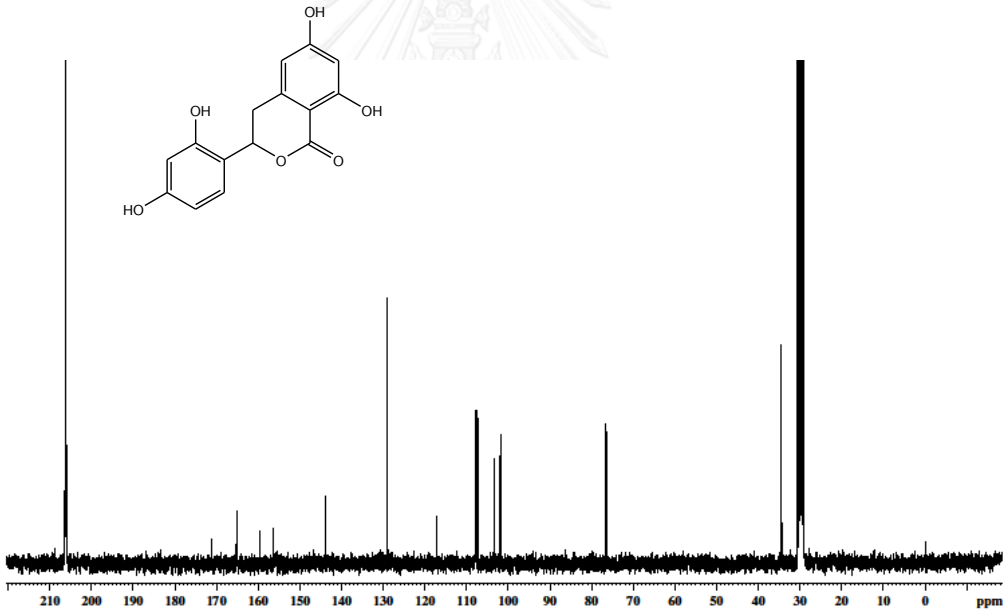

Figure 82 ^{13}C-NMR Spectrum of compound MC-16 (**54**)

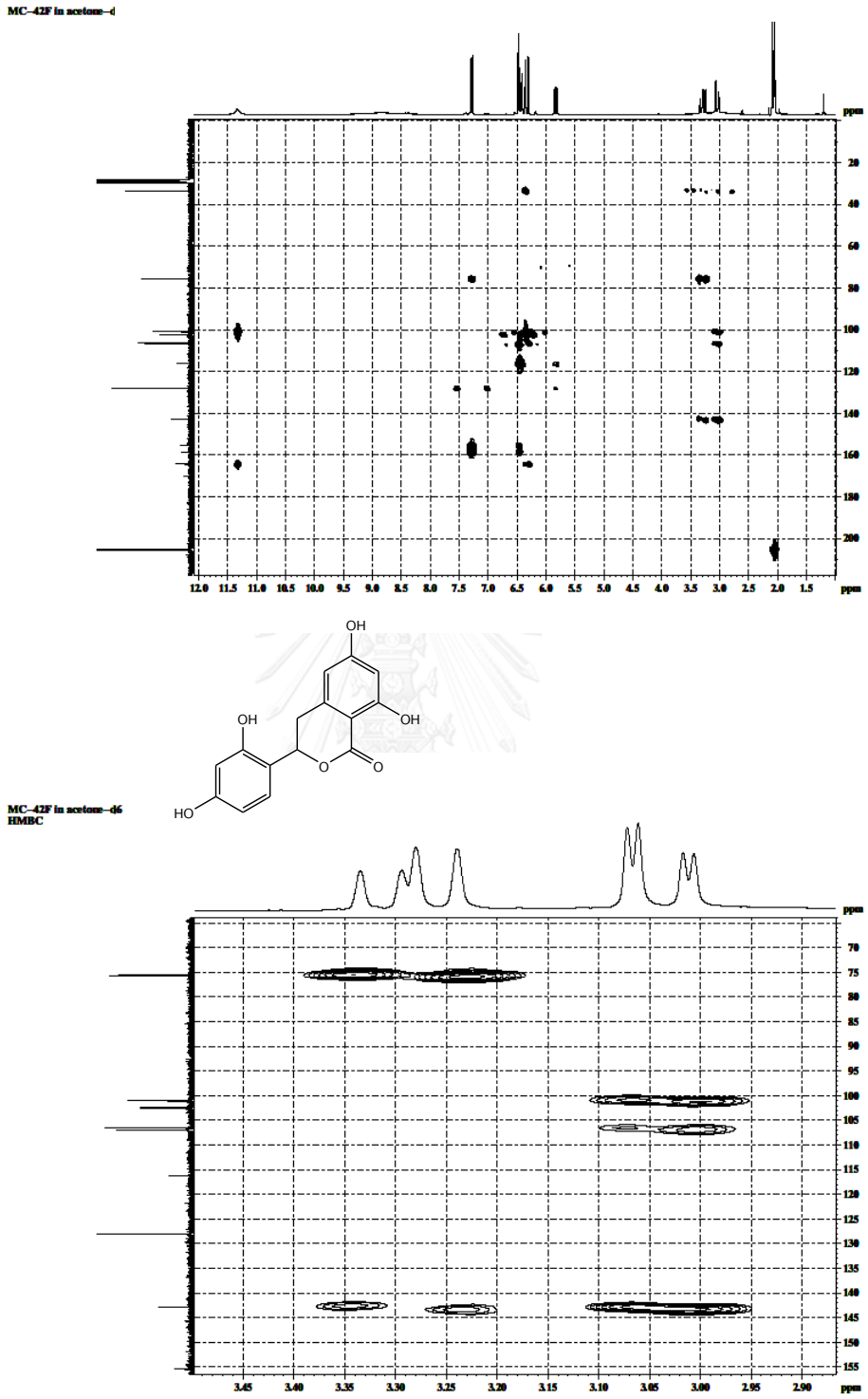

Figure 83 HMBC Spectrum of compound MC-16 (**54**)

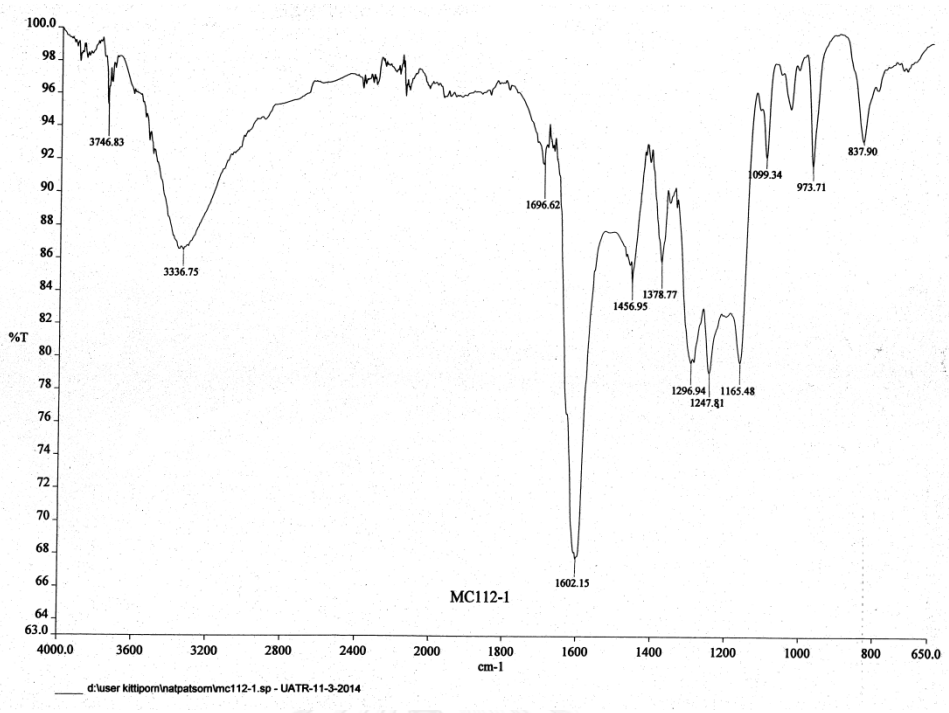

Figure 84 IR Spectrum of compound MC-17 (**55**)

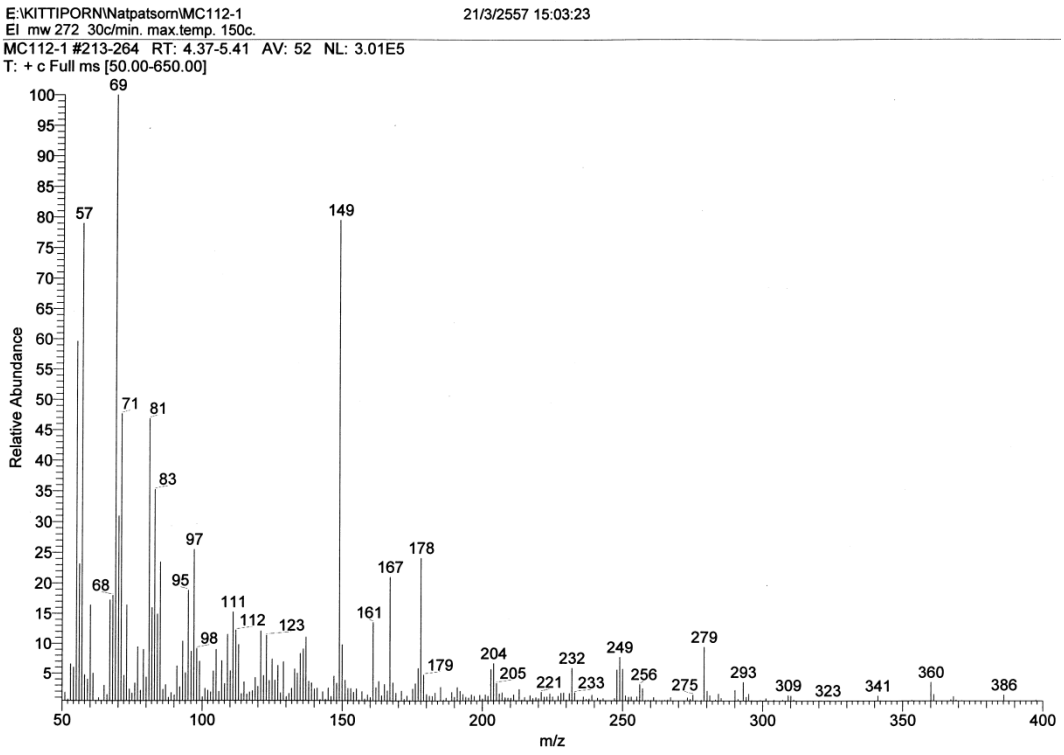

Figure 85 EI Mass spectrum of compound MC-17 (**55**)

Mass Spectrum List Report

Analysis Info

Analysis Name	TOFCRI017458 Nutpassom MC-112-1 E-.d	Acquisition Date	2/20/2014 2:18:43 PM
Method	Nitirat_ESI neg 2013-2.m	Operator	Administrator
Sample Name	ESIneg	Instrument	micrOTOF 74

Acquisition Parameter

Source Type	ESI	Ion Polarity	Negative	Set Corrector Fill	56 V
Scan Range	n/a	Capillary Exit	-110.0 V	Set Pulsar Pull	409 V
Scan Begin	100 m/z	Hexapole RF	150.0 V	Set Pulsar Push	409 V
Scan End	1000 m/z	Skimmer 1	-35.0 V	Set Reflector	1300 V
		Hexapole 1	-24.0 V	Set Flight Tube	9000 V
				Set Detector TOF	1845 V

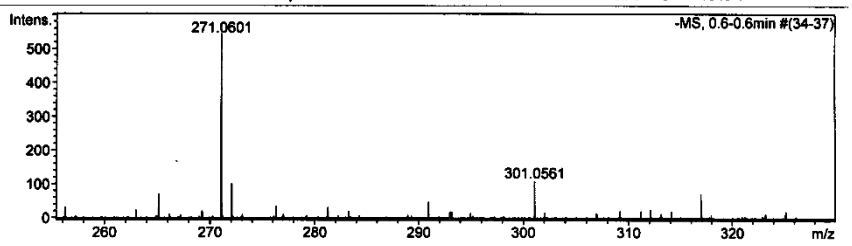

#	m/z	I	Res.
1	248.9594	1461	9311
2	255.2293	171	10554
3	271.0601	544	9994
4	272.0641	102	11075
5	301.0561	109	9889
6	384.9353	333	12443
7	415.0500	141	12216
8	520.9077	211	13193
9	577.1287	237	11684
10	609.0848	202	12502

Bruker Daltonics DataAnalysis 3.3 printed: 2/20/2014 5:48:44 PM Page 1 of 1

Figure 86 HRTOF Mass spectrum of compound MC-17 (**55**)

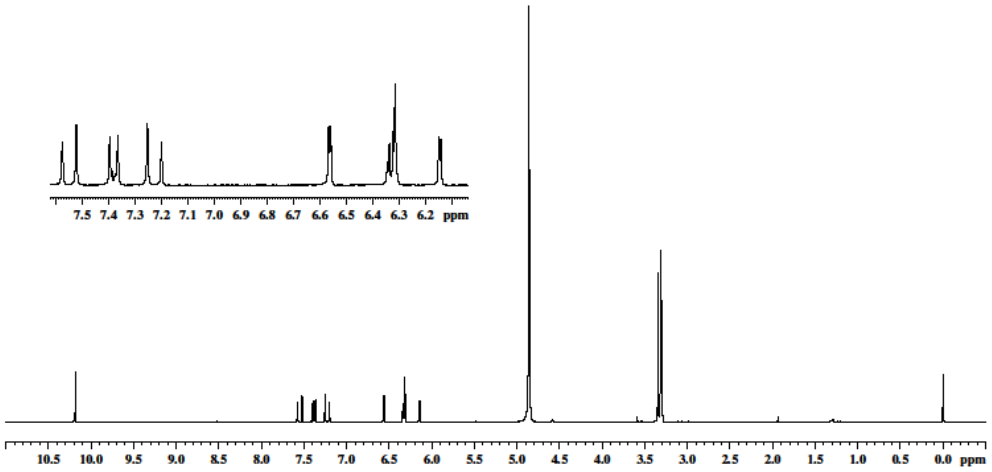

Figure 87 ^{1}H-NMR Spectrum of compound MC-17 (**55**)

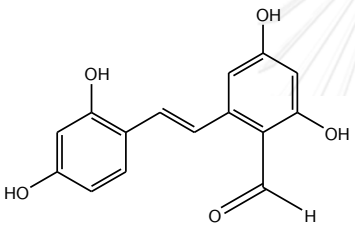

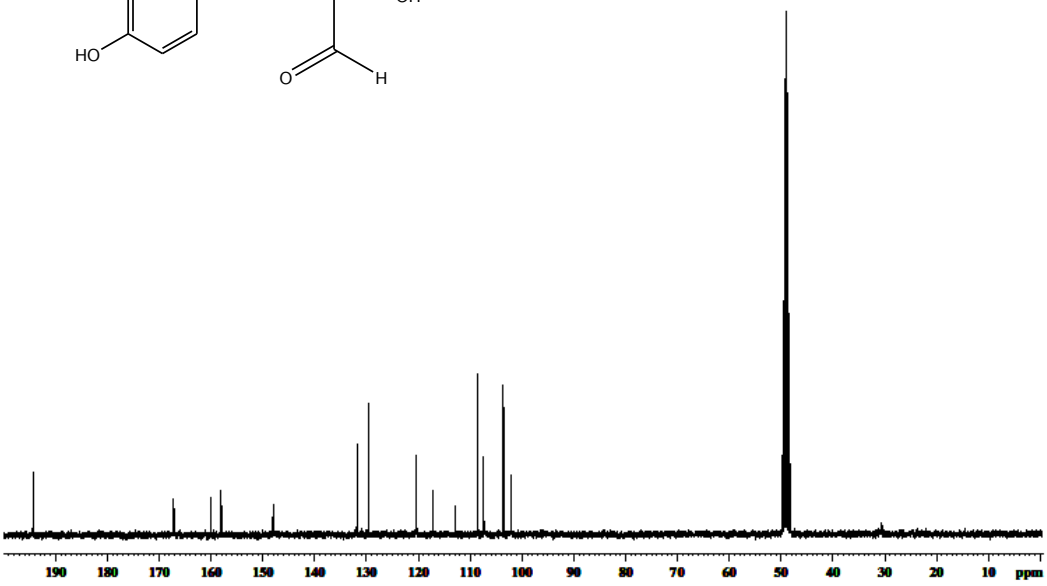

Figure 88 ^{13}C-NMR Spectrum of compound MC-17 (**55**)

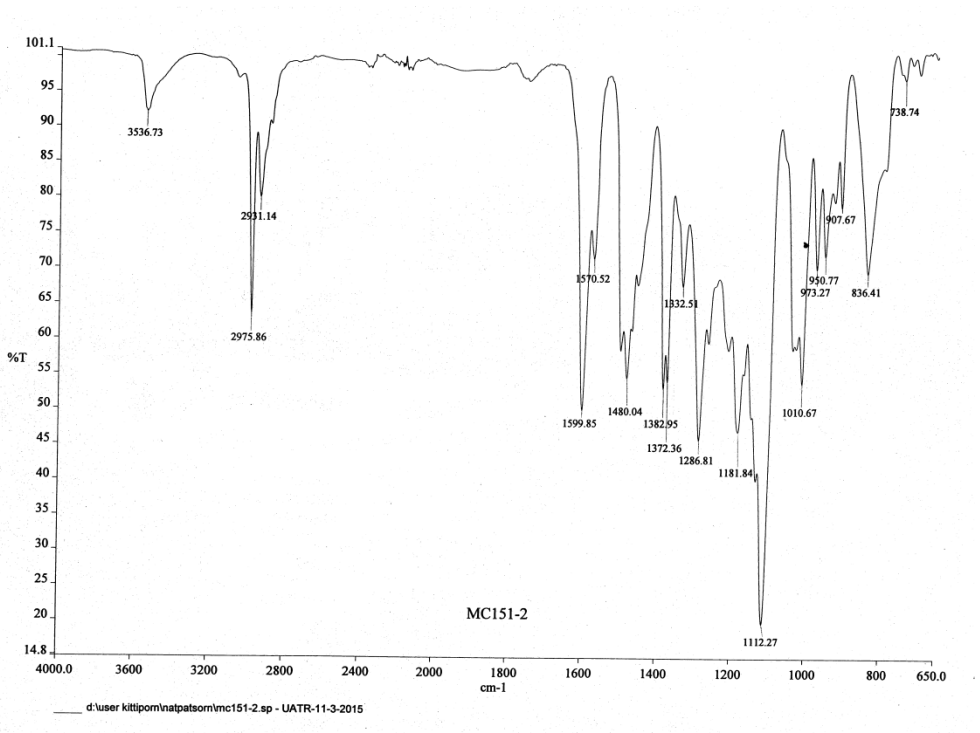

Figure 89 IR Spectrum of compound MC-18 (**56**)

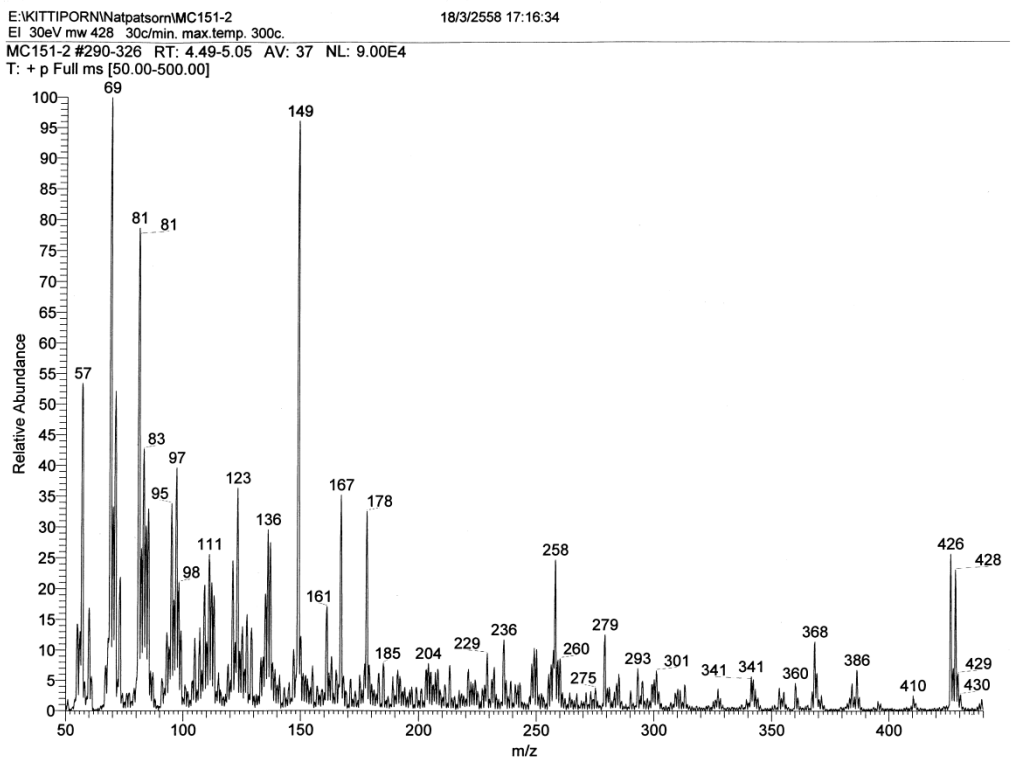

Figure 90 EI Mass spectrum of compound MC-18 (**56**)

Mass Spectrum List Report

Analysis Info

Analysis Name	TOFCRI019353 Nutpassorn MC15-1-2 E+.d	Acquisition Date	2/12/2015 2:37:31 PM
Method	Nitirat ESI pos 2014-1.m	Operator	Administrator
Sample Name	ESIpos	Instrument	micrOTOF 74

Acquisition Parameter

Source Type	ESI	Ion Polarity	Positive	Set Corrector Fill	64 V
Scan Range	n/a	Capillary Exit	90.0 V	Set Pulsar Pull	405 V
Scan Begin	120 m/z	Hexapole RF	120.0 V	Set Pulsar Push	405 V
Scan End	800 m/z	Skimmer 1	30.0 V	Set Reflector	1300 V
		Hexapole 1	22.9 V	Set Flight Tube	9000 V
				Set Detector TOF	1860 V

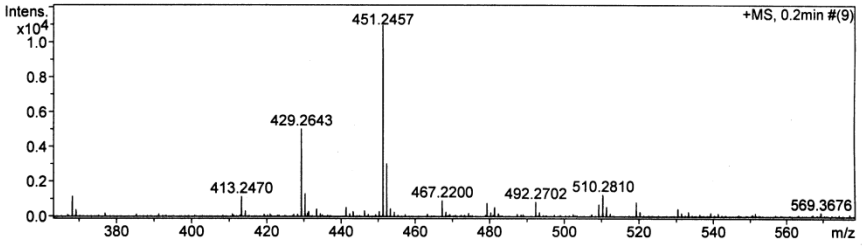

#	m/z	I	Res.
1	157.0892	1884	7328
2	158.9691	8029	7255
3	196.1710	614	8226
4	199.9917	1523	8782
5	210.1863	1180	8052
6	216.9233	1073	8360
7	218.0027	721	7956
8	226.9510	1582	8851
9	240.9685	649	9205
10	277.2121	584	9027
11	279.2280	1240	9600
12	294.9383	1063	10082
13	301.1384	761	10008
14	320.2553	898	10338
15	368.1557	1154	10177
16	413.2470	1138	8668
17	429.2643	5009	10356
18	430.2656	1307	10906
19	441.2957	518	10454
20	451.2457	10931	10480
21	452.2484	3019	10565
22	467.2200	908	10441
23	479.2399	761	11464
24	481.2561	535	10267
25	492.2702	831	10748
26	509.2049	701	10634
27	510.2810	1241	10027
28	511.2779	552	8763
29	519.2328	810	10976
30	587.2214	729	11351

Figure 91 HRTOF Mass spectrum of compound MC-18 (**56**)

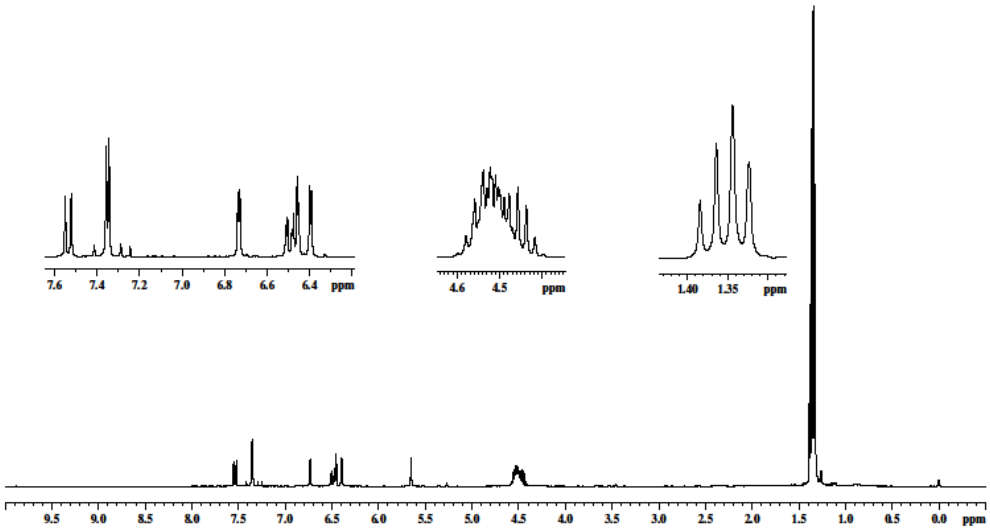

Figure 92 ^{1}H-NMR Spectrum of compound MC-18 (**56**)

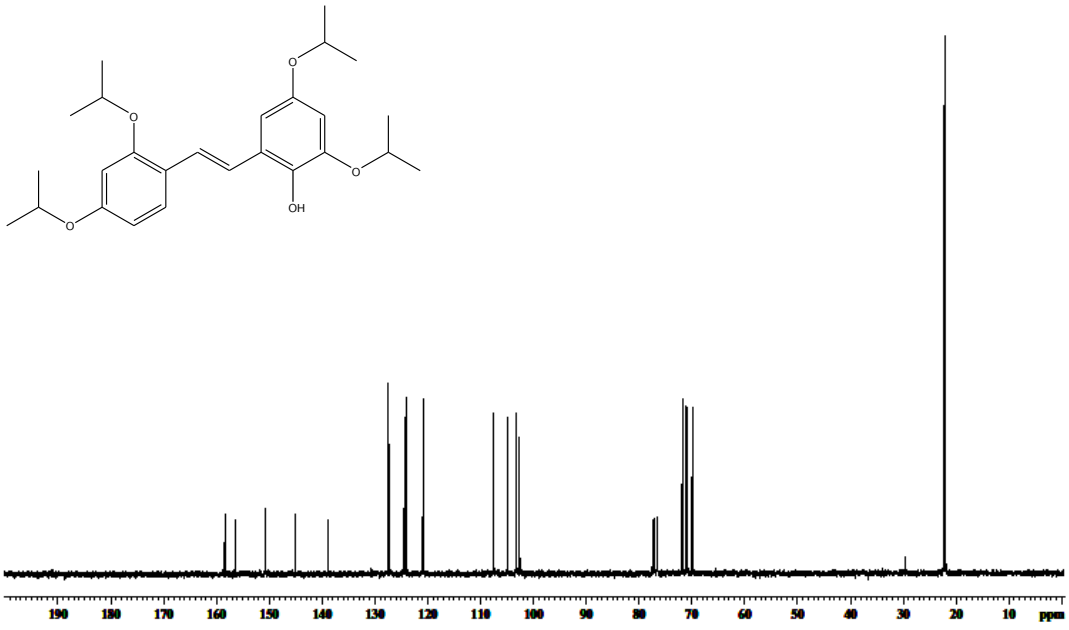

Figure 93 ^{13}C-NMR Spectrum of compound MC-18 (**56**)

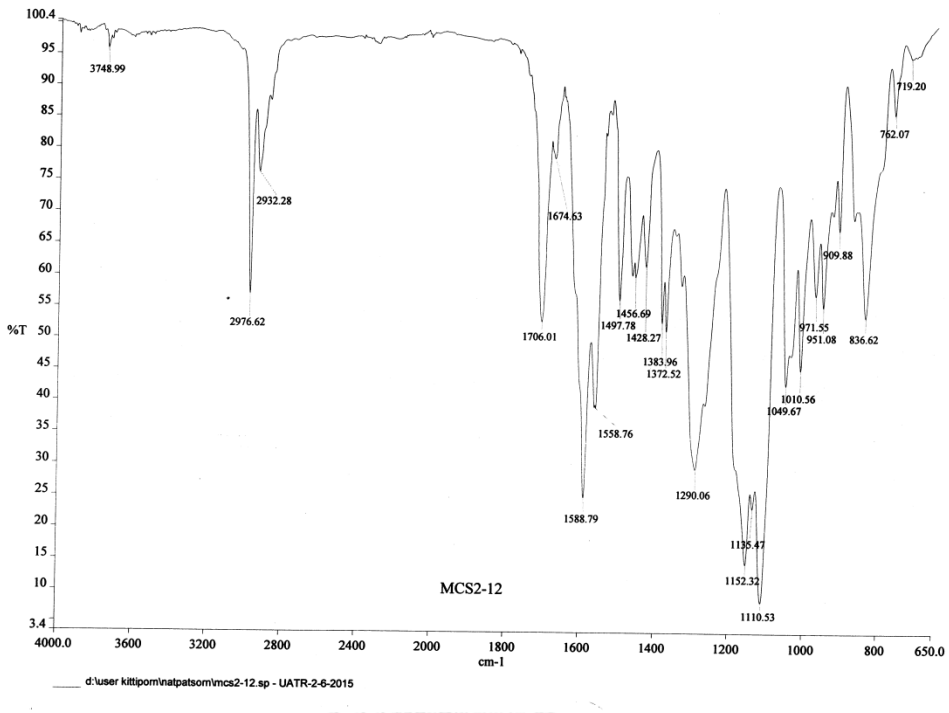

Figure 94 IR Spectrum of compound MC-19 (**57**)

Mass Spectrum List Report

Analysis Info

Analysis Name	TOFCRI018723 Natpassorn MC32A1 E+.d	Acquisition Date	10/31/2014 10:44:04 AM
Method	Nitirat ESI pos 2014-1.m	Operator	Administrator
Sample Name	ESIpos	Instrument	micrOTOF 74

Acquisition Parameter

Source Type	ESI	Ion Polarity	Positive	Set Corrector Fill	64 V
Scan Range	n/a	Capillary Exit	110.0 V	Set Pulsar Pull	405 V
Scan Begin	100 m/z	Hexapole RF	150.0 V	Set Pulsar Push	405 V
Scan End	1000 m/z	Skimmer 1	35.0 V	Set Reflector	1300 V
		Hexapole 1	22.9 V	Set Flight Tube	9000 V
				Set Detector TOF	1860 V

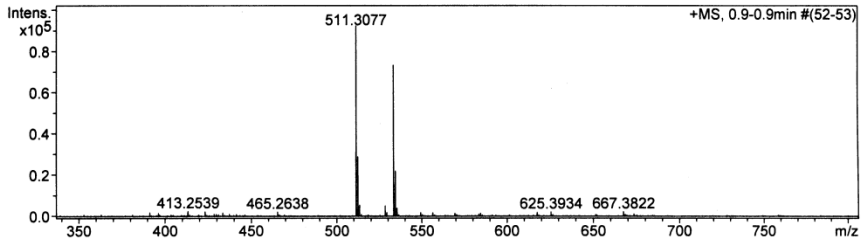

#	m/z	I	Res.
1	189.0869	1797	7426
2	273.1667	2135	8341
3	279.2273	2520	8971
4	284.4865	1144	9419
5	294.9370	1442	9129
6	303.1750	2117	8940
7	317.1730	10767	9214
8	318.1769	2089	8467
9	391.2839	1852	10315
10	396.1957	1443	9498
11	413.2539	2405	9667
12	423.2210	2239	8969
13	433.3795	1615	11126
14	465.2638	2046	10438
15	511.3077	92250	9406
16	512.3103	28788	10301
17	513.3114	5368	10838
18	528.3323	4982	11317
19	529.3349	1776	10997
20	533.2899	73305	9652
21	534.2910	21826	10623
22	535.2986	3983	9385
23	549.2623	1837	10263
24	556.3668	1743	9999
25	569.3586	1418	10890
26	584.3899	1408	10659
27	617.3397	1975	10514
28	625.3934	2121	12521
29	667.3822	2202	11768
30	673.4012	1142	10317

Figure 95 HRTOF Mass spectrum of compound MC-19 (**57**)

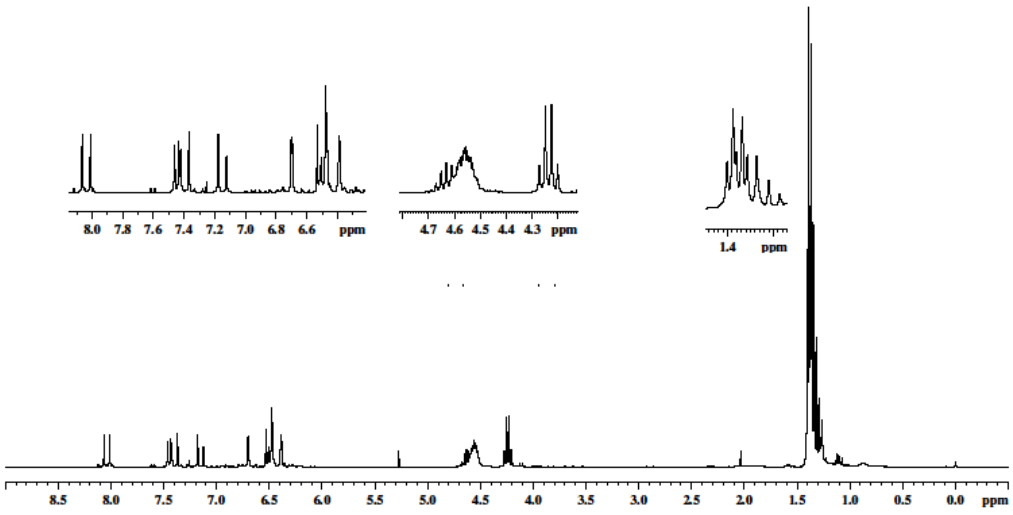

Figure 96 ^{1}H-NMR Spectrum of compound MC-19 (**57**)

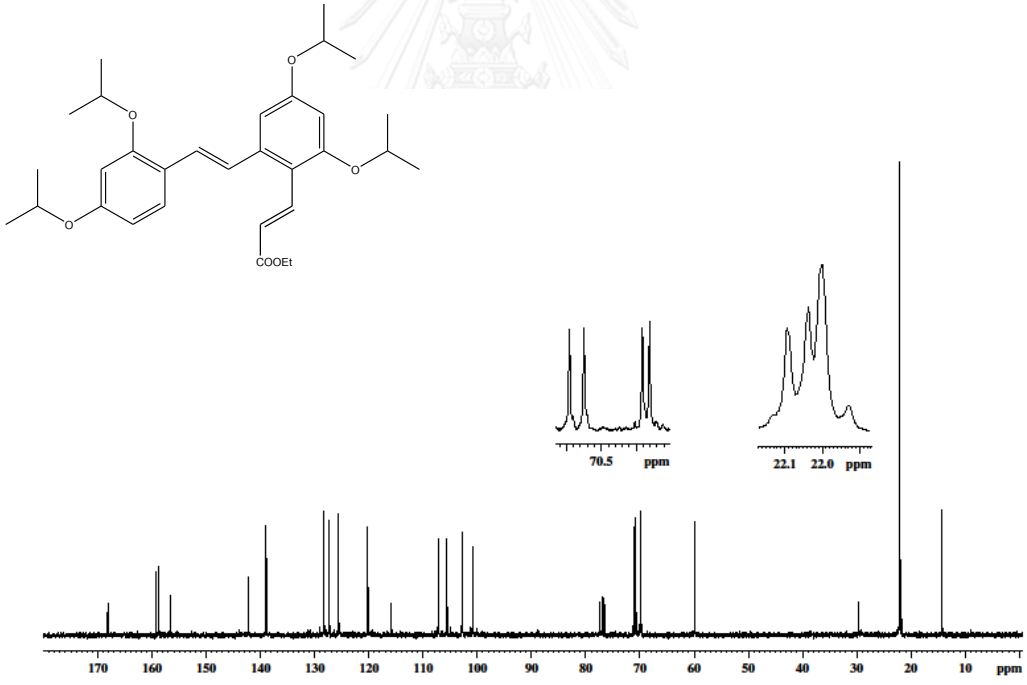

Figure 97 ^{13}C-NMR Spectrum of compound MC-19 (**57**)

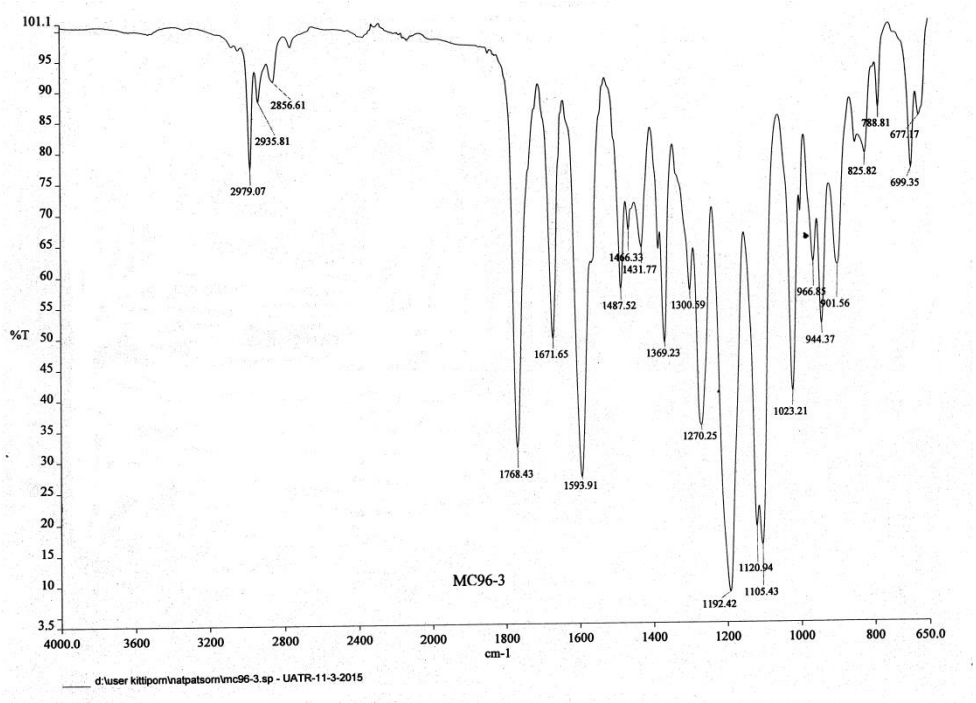

Figure 98 IR Spectrum of compound MC-20 (**58**)

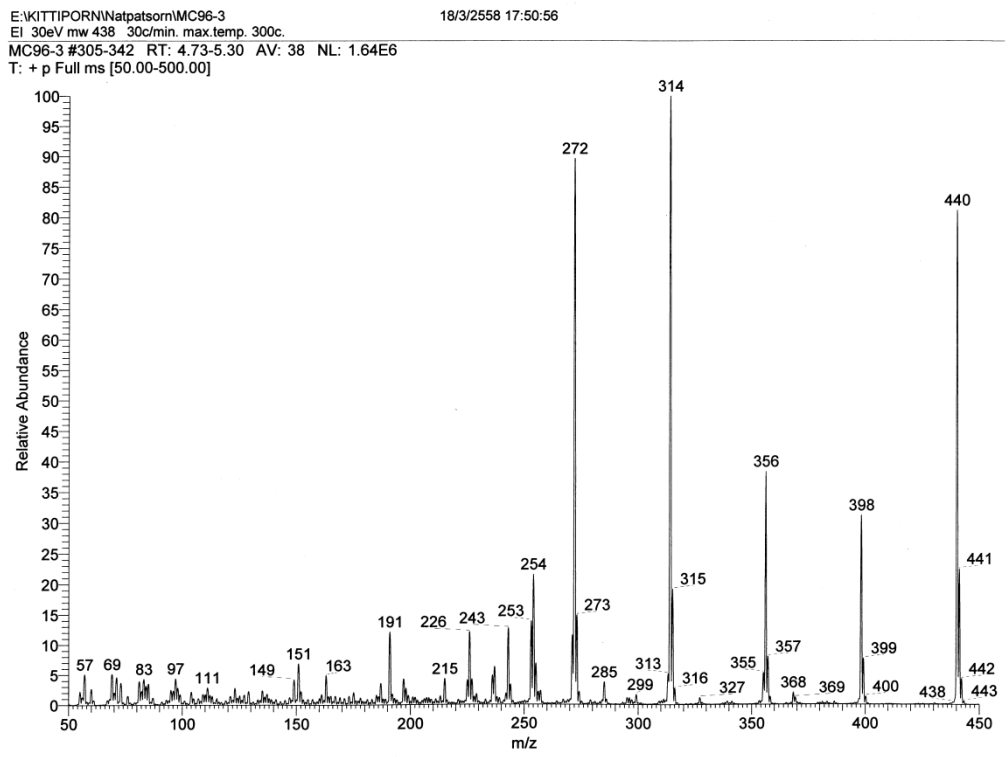

Figure 99 EI Mass spectrum of compound MC-20 (**58**)

Mass Spectrum List Report

Analysis Info

Analysis Name	TOFCRI017450 Natpassorn MC97-3 E+.d	Acquisition Date	2/20/2014 2:00:53 PM
Method	Nitirat ESI pos 2013-4.m	Operator	Administrator
Sample Name	ESIpos	Instrument	micrOTOF 74

Acquisition Parameter

Source Type	ESI	Ion Polarity	Positive	Set Corrector Fill	66 V
Scan Range	n/a	Capillary Exit	120.0 V	Set Pulsar Pull	406 V
Scan Begin	150 m/z	Hexapole RF	120.0 V	Set Pulsar Push	406 V
Scan End	700 m/z	Skimmer 1	40.0 V	Set Reflector	1300 V
		Hexapole 1	23.0 V	Set Flight Tube	9000 V
				Set Detector TOF	1840 V

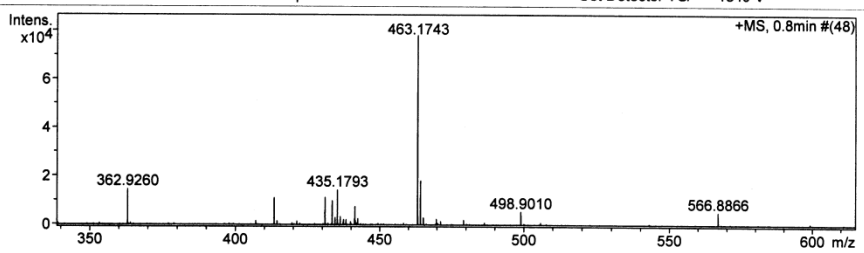

#	m/z	I	Res.
1	157.0894	10908	7669
2	158.9698	29671	7450
3	210.0930	3045	8696
4	223.1646	2369	8716
5	226.9517	4876	8977
6	251.1973	5158	8873
7	265.2120	4045	9131
8	273.1652	2702	7895
9	277.2100	2538	8746
10	279.2278	9553	9104
11	294.9390	14374	8325
12	303.1793	3579	8731
13	362.9260	14467	9369
14	413.2615	11043	10971
15	430.9142	11218	9748
16	433.3770	9845	11131
17	434.3799	2840	10945
18	435.1793	14178	9948
19	436.1833	3350	9066
20	441.1956	2752	8722
21	441.3000	7476	8472
22	442.3041	2549	9415
23	463.1743	78024	9022
24	464.1752	18008	10010
25	465.1778	2954	10621
26	469.7077	2311	33259
27	498.9010	5423	10075
28	566.8866	5274	10474
29	634.8807	4863	11991
30	702.8721	2345	9261

Figure 100 HRTOF Mass spectrum of compound MC-20 (**58**)

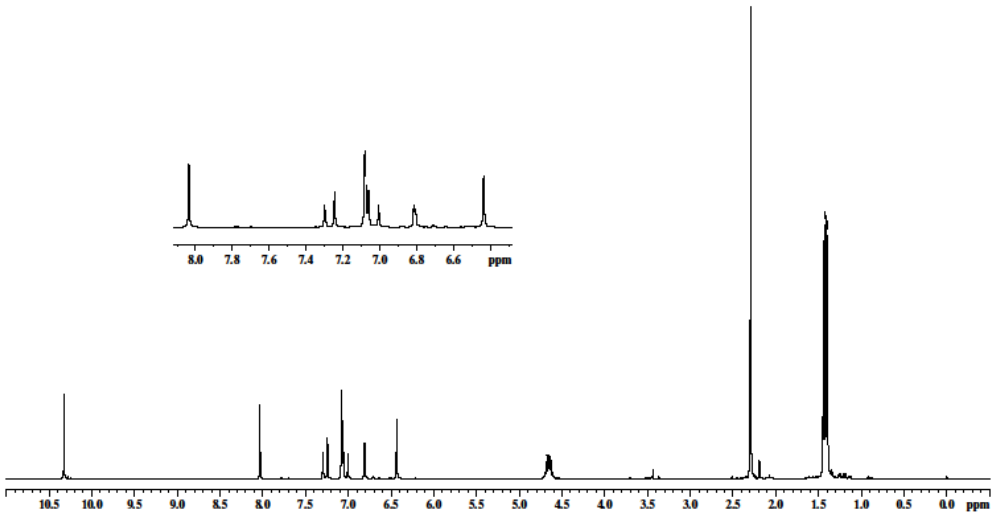

Figure 101 ^{1}H-NMR Spectrum of compound MC-20 (**58**)

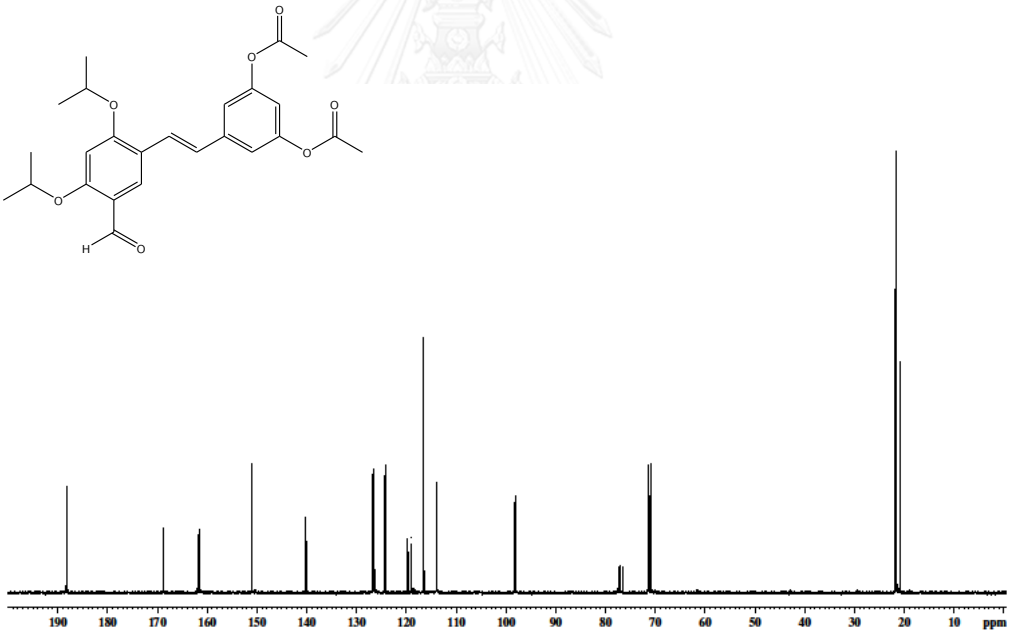

Figure 102 ^{13}C-NMR Spectrum of compound MC-20 (**58**)

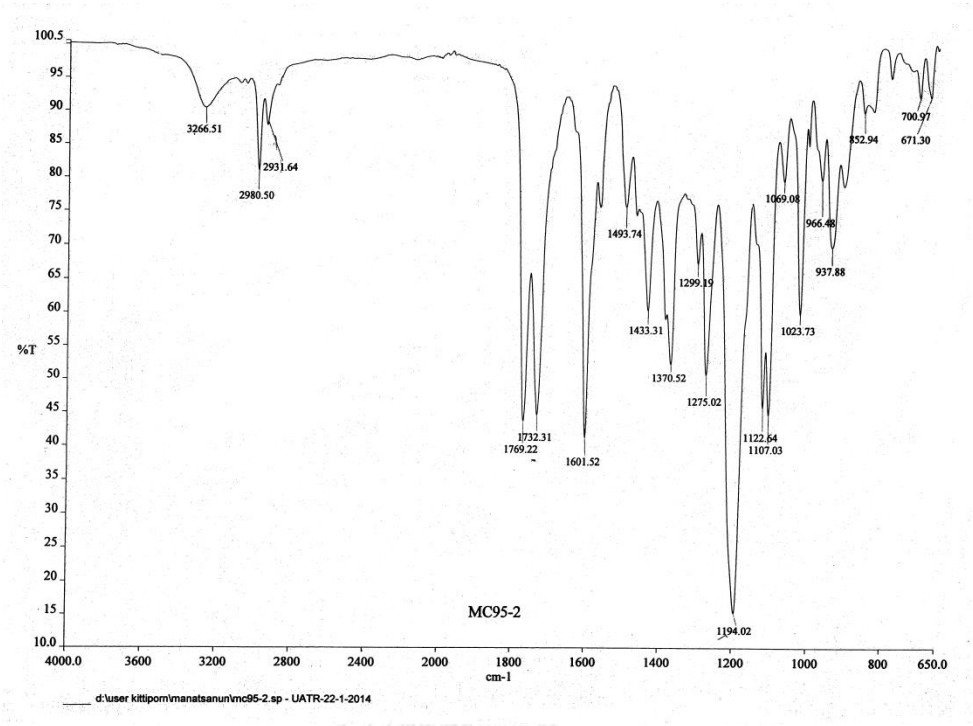

Figure 103 IR Spectrum of compound MC-21 (**59**)

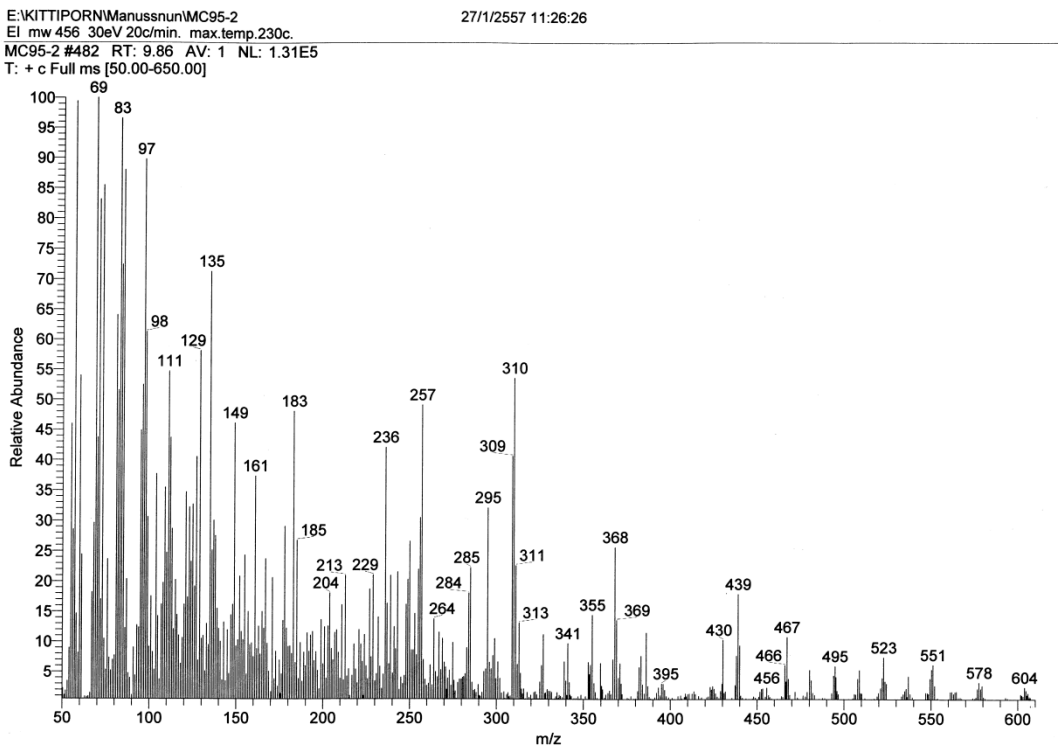

Figure 104 EI Mass spectrum of compound MC-21 (**59**)

Mass Spectrum List Report

Analysis Info

Analysis Name	TOFCRI017141 Manusnan MC95-2 E+.d	Acquisition Date	1/15/2014 12:31:28 PM
Method	Nitirat ESI pos 2013-4.m	Operator	Administrator
Sample Name	ESIpos	Instrument	micrOTOF 74

Acquisition Parameter

Source Type	ESI	Ion Polarity	Positive	Set Corrector Fill	66 V
Scan Range	n/a	Capillary Exit	120.0 V	Set Pulsar Pull	406 V
Scan Begin	100 m/z	Hexapole RF	180.0 V	Set Pulsar Push	406 V
Scan End	1000 m/z	Skimmer 1	40.0 V	Set Reflector	1300 V
		Hexapole 1	23.0 V	Set Flight Tube	9000 V
				Set Detector TOF	1850 V

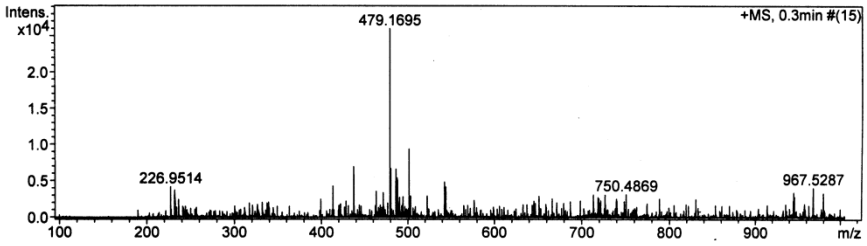

#	m/z	I	Res.
1	226.9514	4214	7584
2	231.5655	3275	17851
3	231.6705	3782	21623
4	231.7650	3002	6130
5	413.2714	4340	9574
6	437.2390	6964	28389
7	463.1712	3632	10251
8	471.3940	3421	32228
9	479.1695	25989	9650
10	480.1691	6713	10425
11	485.8232	4556	32228
12	485.9734	5016	23224
13	486.1055	5784	8235
14	487.3083	5440	28957
15	487.4574	4054	19132
16	487.6026	3337	8435
17	487.9036	4617	28588
18	488.0426	3180	31878
19	501.1528	9435	9714
20	503.0079	2959	29656
21	522.3846	2967	35298
22	542.3023	2976	23628
23	542.4455	4867	24063
24	543.8667	4201	34361
25	726.5133	3138	28315
26	750.4869	3196	37520
27	944.6831	3463	23128
28	967.3528	2994	46385
29	967.5287	4080	42108
30	979.4222	3357	40785

Bruker Daltonics DataAnalysis 3.3 printed: 1/15/2014 3:58:21 PM Page 1 of 1

Figure 105 HRTOF Mass spectrum of compound MC-21 (**59**)

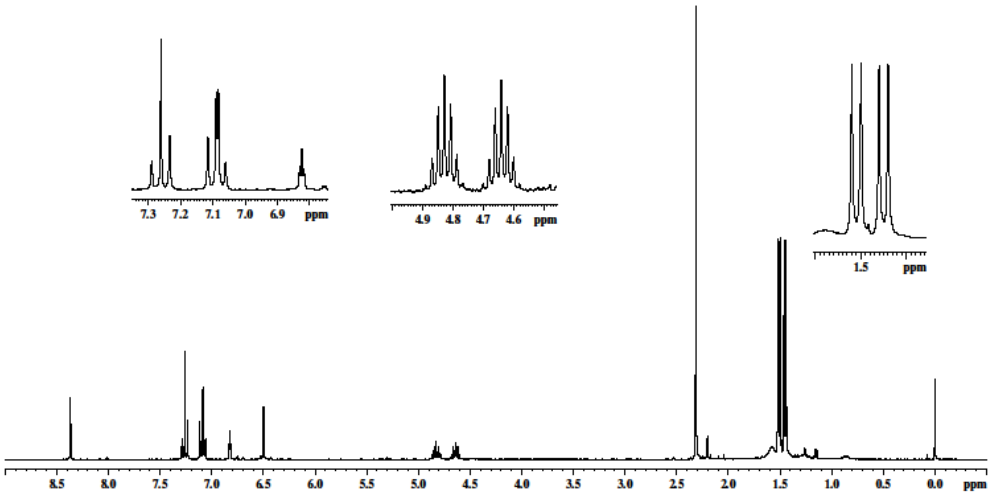

Figure 106 ^{1}H-NMR Spectrum of compound MC-21 (**59**)

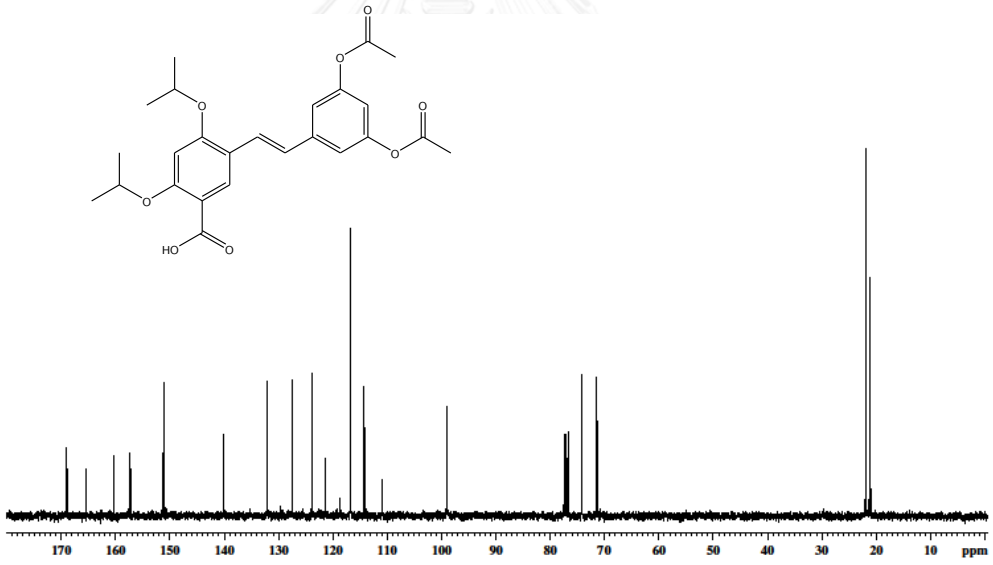

Figure 107 ^{13}C-NMR Spectrum of compound MC-21 (**59**)

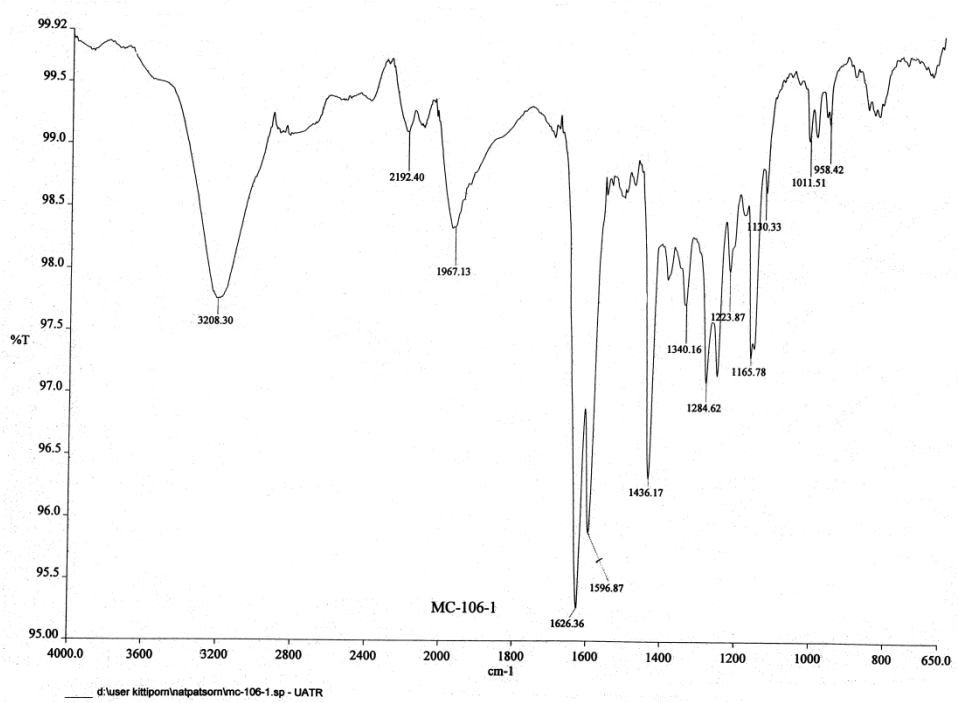

Figure 108 IR Spectrum of compound MC-22 (**60**)

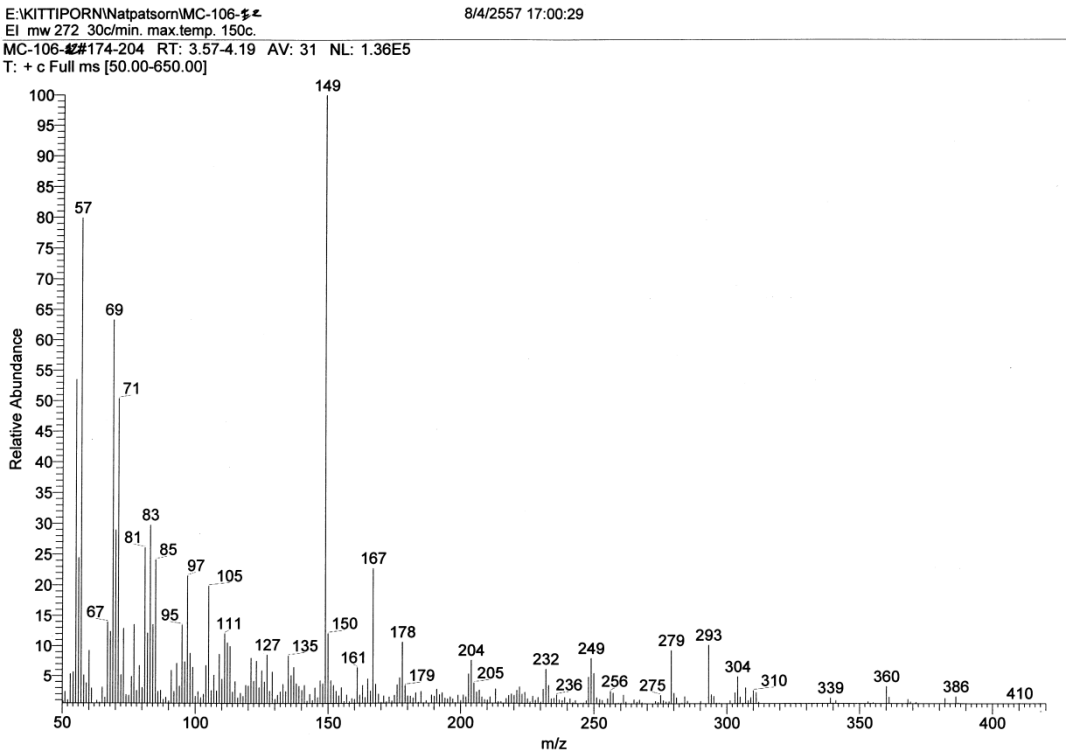

Figure 109 EI Mass spectrum of compound MC-22 (**60**)

Mass Spectrum List Report

Analysis Info

Analysis Name	TOFCRI017459 Nutpassorn MC-106-2 E-.d	Acquisition Date	2/20/2014 2:19:55 PM
Method	Nitirat_ESI neg 2013-2.m	Operator	Administrator
Sample Name	ESIneg	Instrument	micrOTOF 74

Acquisition Parameter

Source Type	ESI	Ion Polarity	Negative	Set Corrector Fill	56 V
Scan Range	n/a	Capillary Exit	-110.0 V	Set Pulsar Pull	409 V
Scan Begin	100 m/z	Hexapole RF	150.0 V	Set Pulsar Push	409 V
Scan End	1000 m/z	Skimmer 1	-35.0 V	Set Reflector	1300 V
		Hexapole 1	-24.0 V	Set Flight Tube	9000 V
				Set Detector TOF	1845 V

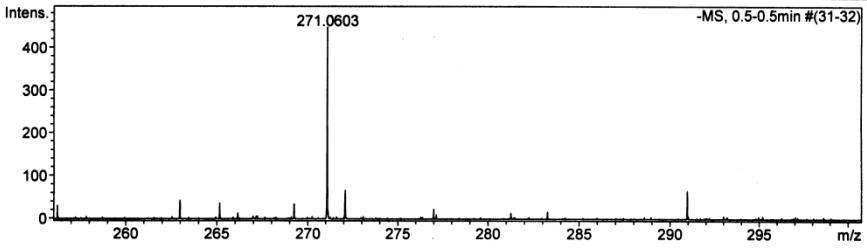

#	m/z	I	Res.
1	248.9594	1977	8997
2	249.9605	126	9563
3	255.2289	141	9987
4	271.0603	447	9647
5	316.9470	106	10729
6	384.9353	482	12094
7	452.9221	102	11435
8	520.9102	321	12823
9	656.9061	158	12943
10	792.8874	115	12861

Figure 110 HRTOF Mass spectrum of compound MC-22 (**60**)

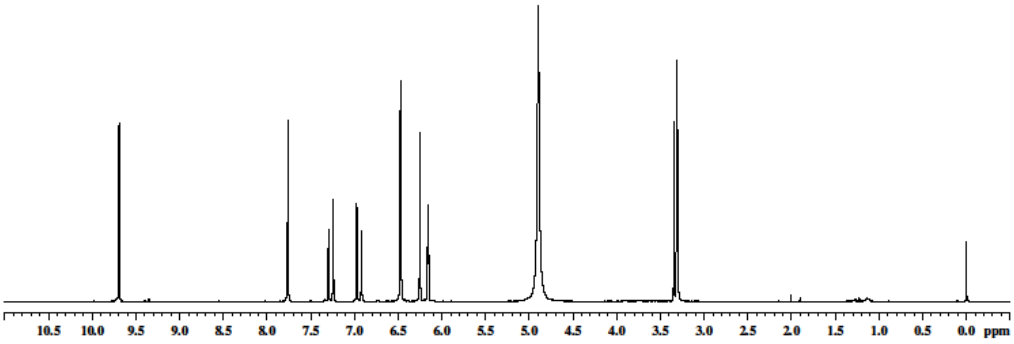

Figure 111 ^{1}H-NMR Spectrum of compound MC-22 (**60**)

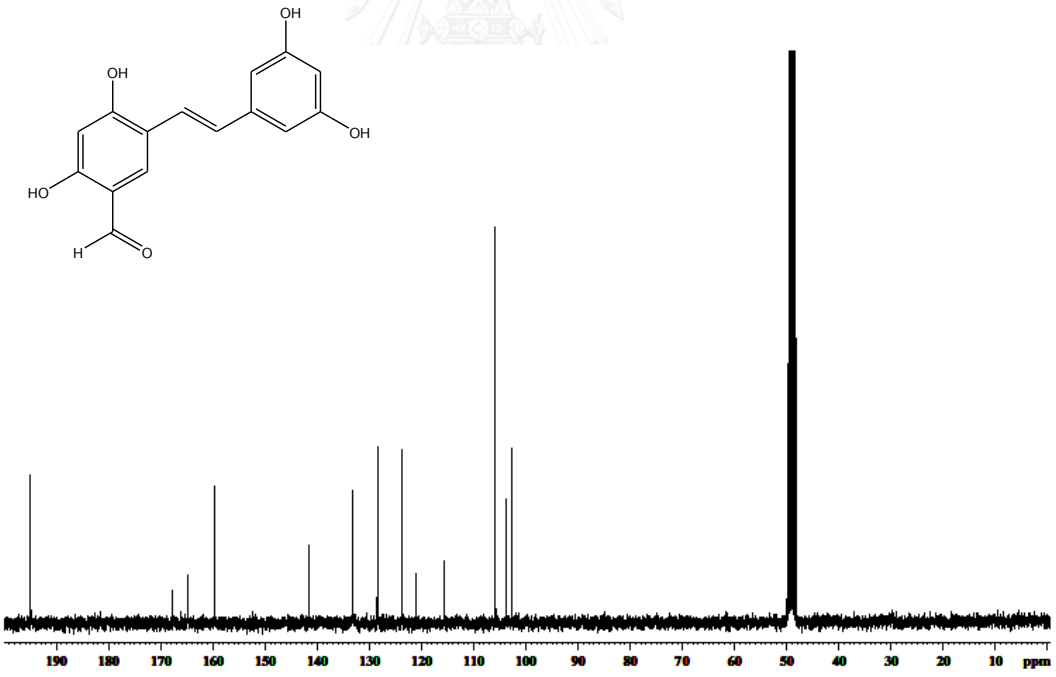

Figure 112 ^{13}C-NMR Spectrum of compound MC-22 (**60**)

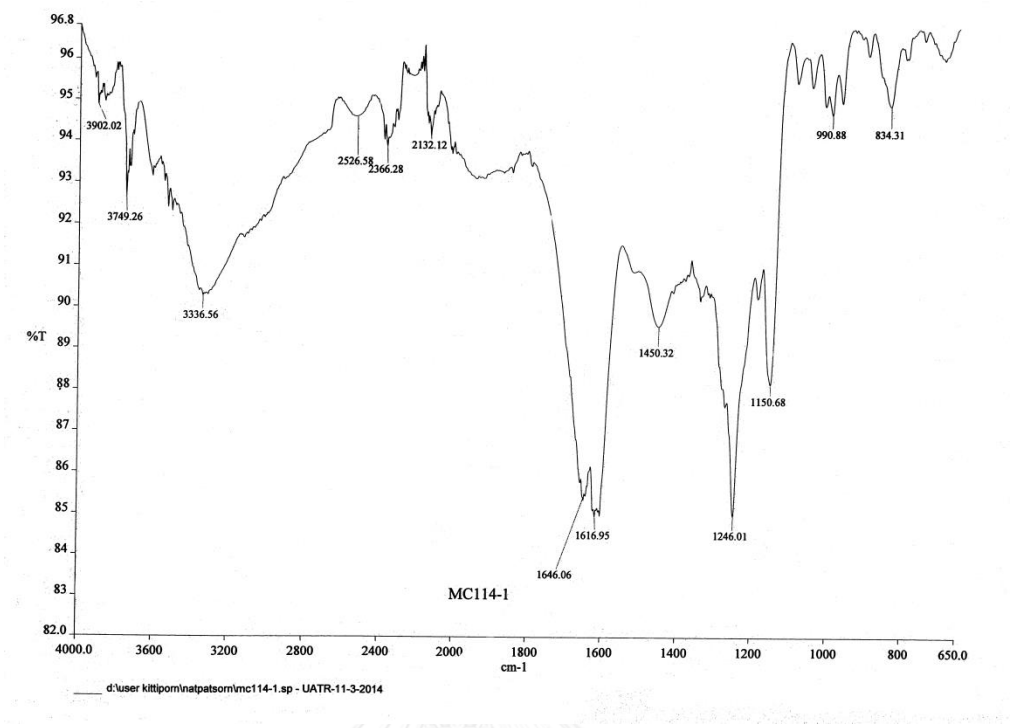

Figure 113 IR Spectrum of compound MC-23 (**61**)

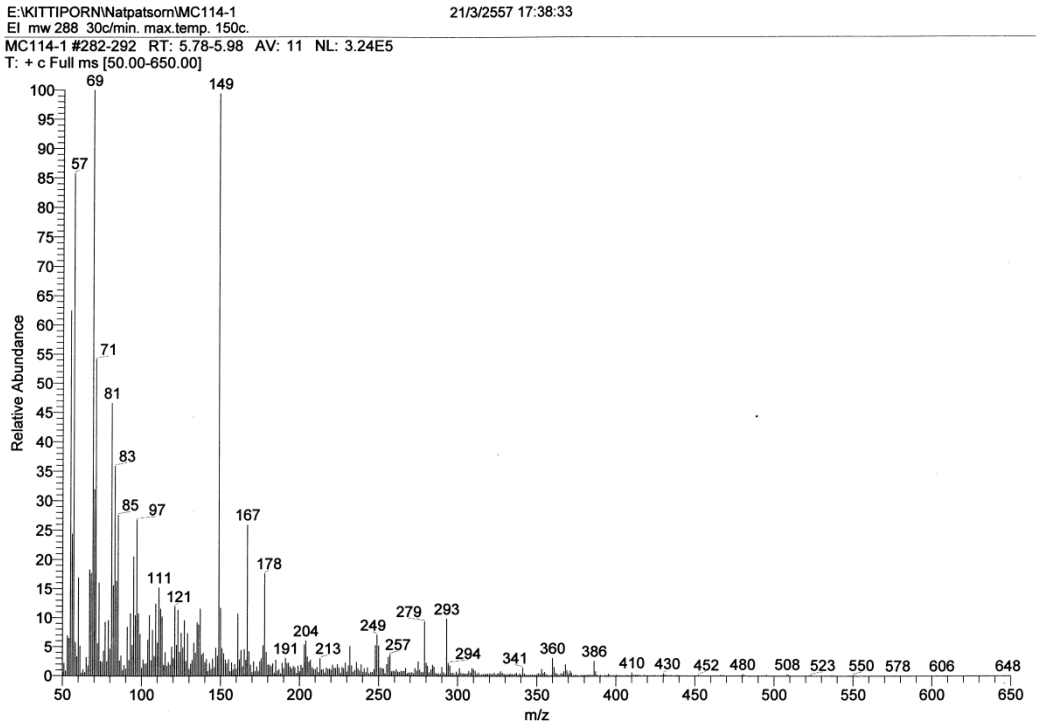

Figure 114 EI Mass spectrum of compound MC-23 (**61**)

Mass Spectrum List Report

Analysis Info

Analysis Name	TOFCRI017598 Natpassorn MC114-1 E-.d	Acquisition Date	3/13/2014 12:43:02 PM
Method	Nitirat_ESI neg 2013-2.m	Operator	Administrator
Sample Name	ESIneg	Instrument	micrOTOF 74

Acquisition Parameter

Source Type	ESI	Ion Polarity	Negative	Set Corrector Fill	56 V
Scan Range	n/a	Capillary Exit	-110.0 V	Set Pulsar Pull	409 V
Scan Begin	88 m/z	Hexapole RF	75.0 V	Set Pulsar Push	409 V
Scan End	700 m/z	Skimmer 1	-35.0 V	Set Reflector	1300 V
		Hexapole 1	-24.0 V	Set Flight Tube	9000 V
				Set Detector TOF	1845 V

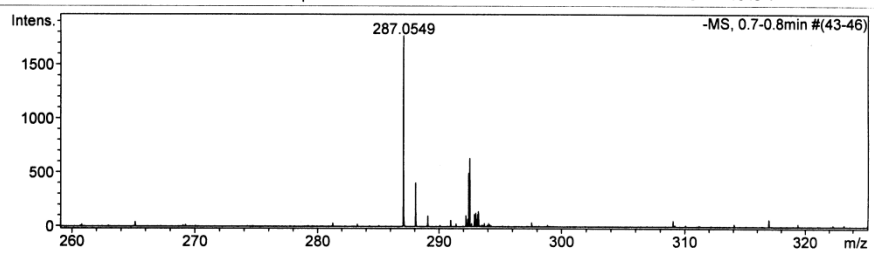

#	m/z	I	Res.
1	154.9698	306	8384
2	180.9709	127	8832
3	248.9594	2483	8722
4	249.9596	146	9871
5	255.2291	179	9745
6	287.0549	1766	10280
7	288.0586	404	8833
8	329.0628	137	10879
9	355.0428	264	11819
10	384.9353	799	11596
11	423.0293	539	12159
12	424.0349	159	10833
13	452.9263	233	11945
14	520.9122	829	12218

Figure 115 HRTOF Mass spectrum of compound MC-23 (**61**)

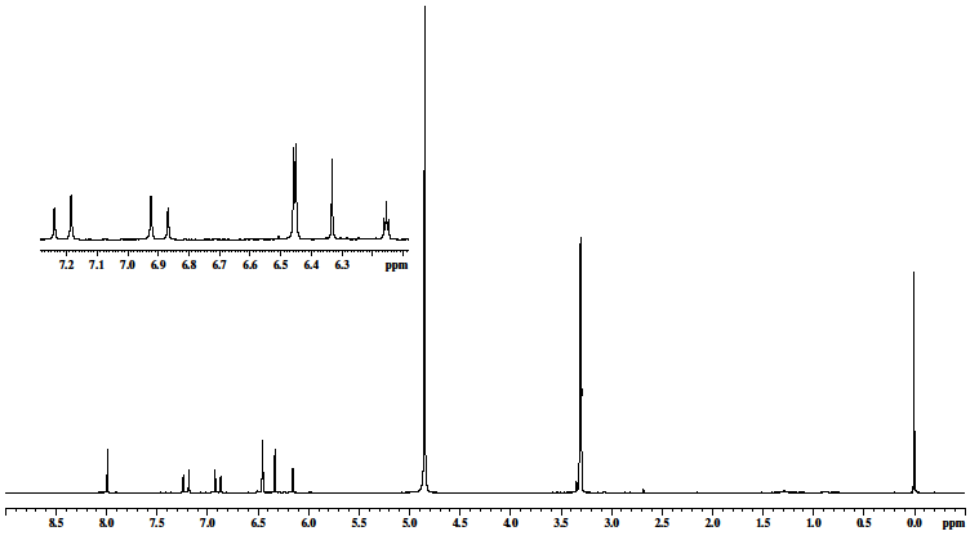

Figure 116 ^{1}H-NMR Spectrum of compound MC-23 (**61**)

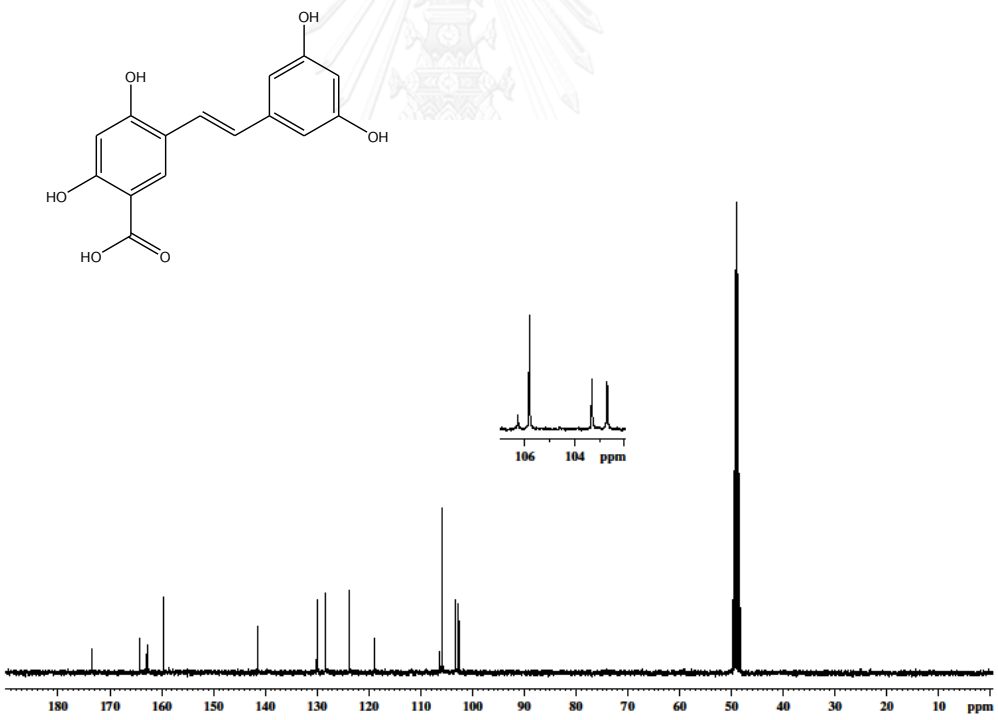

Figure 117 ^{13}C-NMR Spectrum of compound MC-23 (**61**)

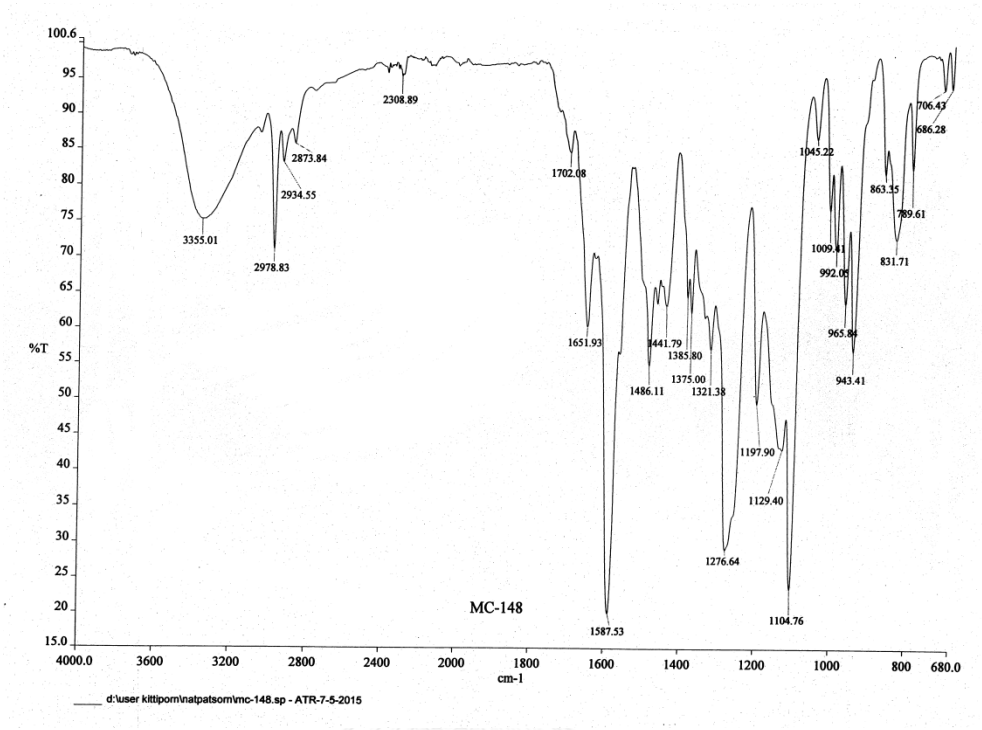

Figure 118 IR Spectrum of compound MC-24 (**62**)

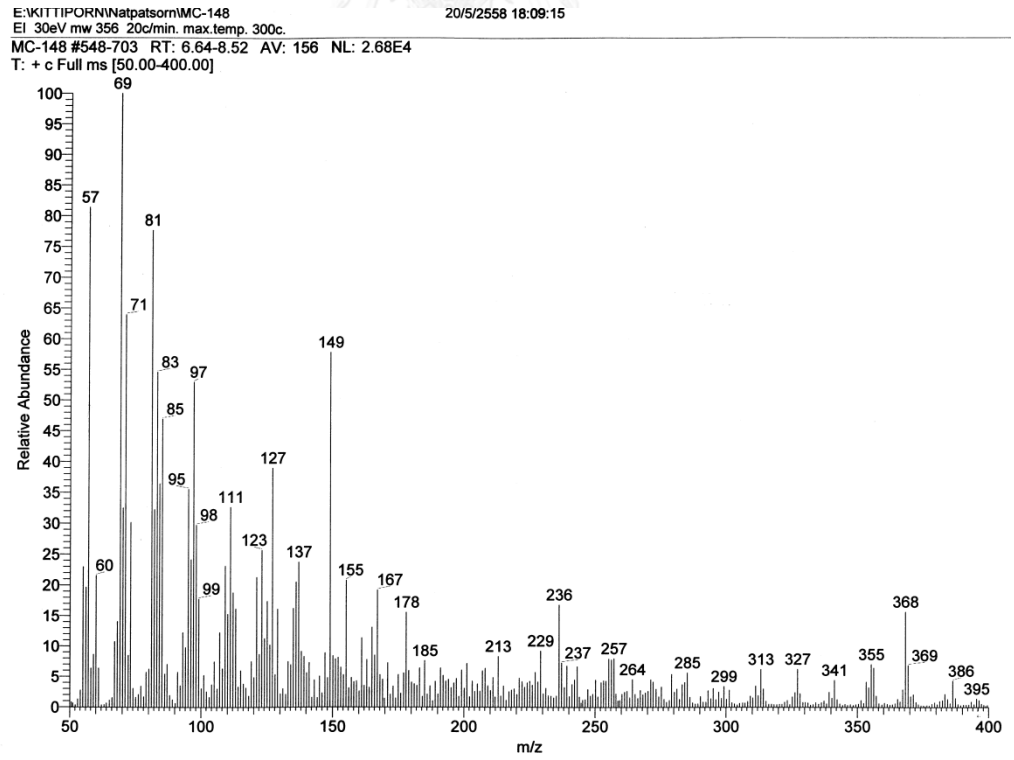

Figure 119 EI Mass spectrum of compound MC-24 (**62**)

Mass Spectrum List Report

Analysis Info

Analysis Name	TOFCRI018724 Natpassorn MC1481 E+.d	Acquisition Date	10/31/2014 10:45:33 AM
Method	Nitirat ESI pos 2014-1.m	Operator	Administrator
Sample Name	ESIpos	Instrument	micrOTOF 74

Acquisition Parameter

Source Type	ESI	Ion Polarity	Positive	Set Corrector Fill	64 V
Scan Range	n/a	Capillary Exit	110.0 V	Set Pulsar Pull	405 V
Scan Begin	100 m/z	Hexapole RF	150.0 V	Set Pulsar Push	405 V
Scan End	1000 m/z	Skimmer 1	35.0 V	Set Reflector	1300 V
		Hexapole 1	22.9 V	Set Flight Tube	9000 V
				Set Detector TOF	1860 V

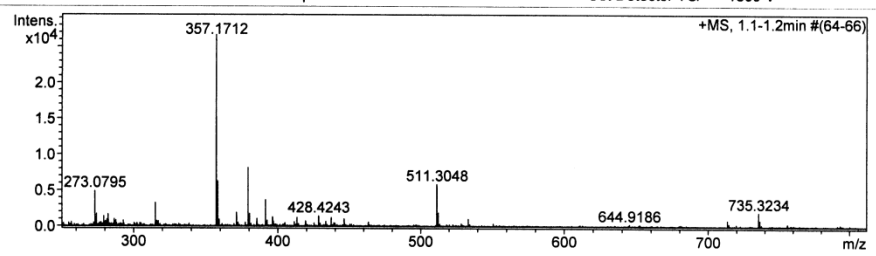

#	m/z	I	Res.
1	183.2500	915	19403
2	273.0795	4887	8720
3	274.2762	1746	9529
4	279.2342	1411	9100
5	281.3845	968	19123
6	282.2808	1686	8951
7	282.4227	965	13397
8	286.5546	1037	20742
9	287.5870	872	15623
10	315.1259	3310	8997
11	357.1712	26639	9266
12	358.1742	6278	10235
13	359.1768	972	9474
14	371.1855	1946	10089
15	379.1520	8167	10079
16	380.1558	1786	10192
17	385.1896	1099	19301
18	391.2849	3717	10819
19	392.2896	840	9221
20	396.1937	1317	9742
21	413.2637	1248	10494
22	428.4243	1486	9721
23	437.1081	1227	10869
24	446.1977	1068	30193
25	511.3048	5872	11429
26	512.3074	1943	10916
27	533.2877	1025	10726
28	713.3421	925	11112
29	735.3234	2015	11437
30	736.3308	928	11671

Figure 120 HRTOF Mass spectrum of compound MC-24 (**62**)

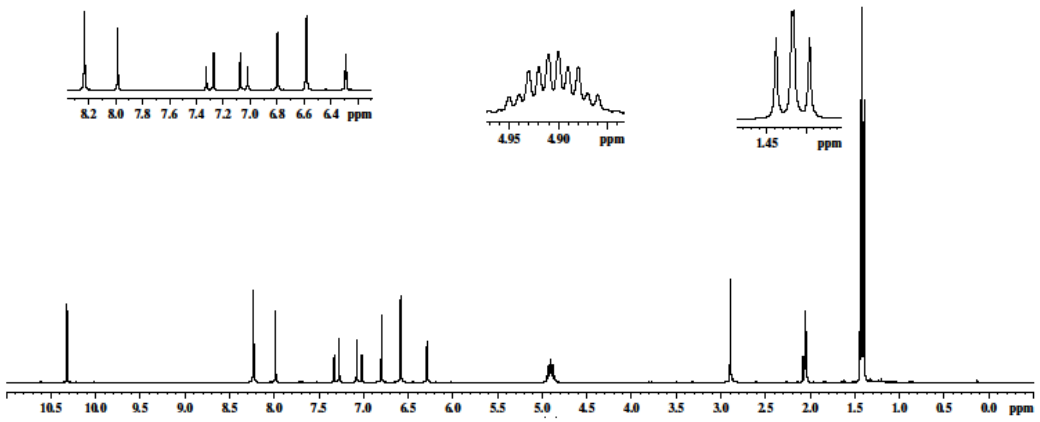

Figure 121 ^{1}H-NMR Spectrum of compound MC-24 (**62**)

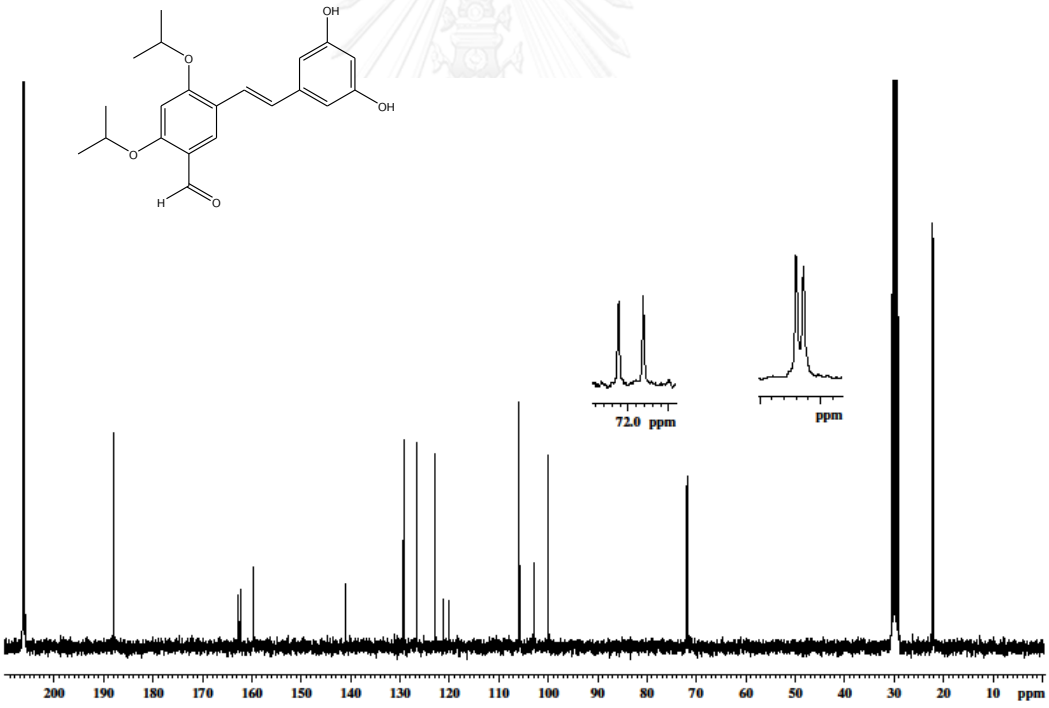

Figure 122 ^{13}C-NMR Spectrum of compound MC-24 (**62**)

Mass Spectrum List Report

Analysis Info

Analysis Name	TOFCRI019890 Nutpassorn MC149A E-.d	Acquisition Date	6/10/2015 2:54:38 PM
Method	Nitirat_ESI neg 2014-1.m	Operator	Administrator
Sample Name	ESIneg	Instrument	micrOTOF 74

Acquisition Parameter

Source Type	ESI	Ion Polarity	Negative	Set Corrector Fill	63 V
Scan Range	n/a	Capillary Exit	-110.0 V	Set Pulsar Pull	405 V
Scan Begin	100 m/z	Hexapole RF	90.0 V	Set Pulsar Push	405 V
Scan End	800 m/z	Skimmer 1	-35.0 V	Set Reflector	1300 V
		Hexapole 1	-24.0 V	Set Flight Tube	9000 V
				Set Detector TOF	1885 V

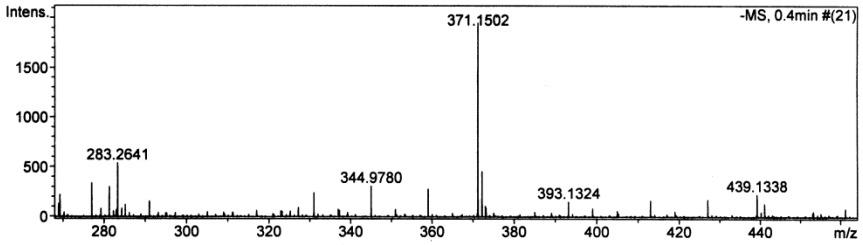

#	m/z	I	Res.
1	197.0465	177	6878
2	199.1681	218	6915
3	227.1997	594	8043
4	241.2150	381	7967
5	253.2117	214	9654
6	255.2315	1749	7992
7	256.2354	284	8218
8	262.9745	311	8720
9	269.2452	222	8828
10	276.9896	340	8917
11	281.2454	303	8480
12	283.2641	539	8703
13	291.0048	158	8936
14	330.9640	242	9378
15	344.9780	308	9753
16	358.9932	280	10074
17	371.1502	1949	10182
18	372.1541	453	10096
19	412.9632	167	10878
20	426.9822	175	10156
21	439.1338	228	11163
22	480.9595	160	8846
23	494.9702	203	9699
24	508.9881	182	12261
25	562.9613	236	11644
26	576.9781	195	10707
27	590.9914	169	12497
28	630.9545	235	12569
29	644.9649	227	12183
30	658.9855	182	12563

Figure 123 HRTOF Mass spectrum of compound MC-25 (**63**)

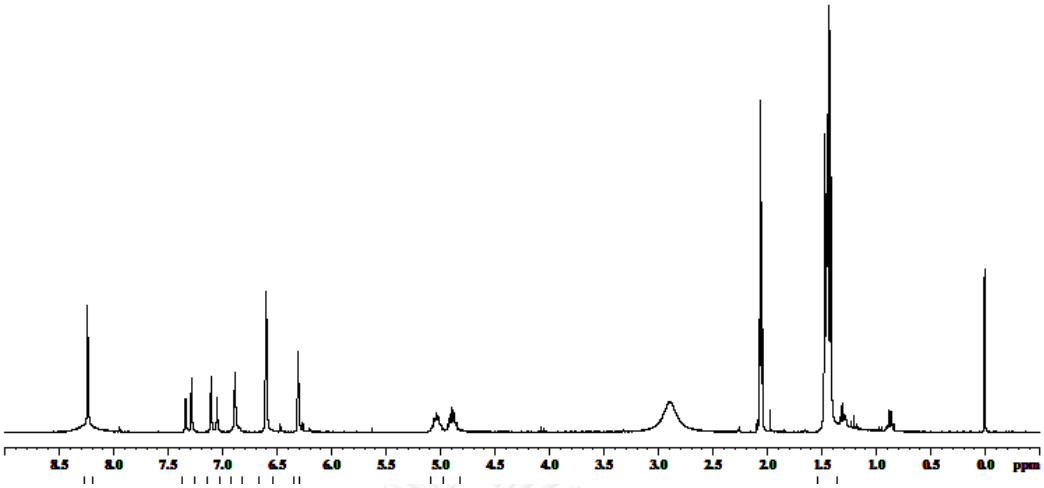

Figure 124 ^{1}H-NMR Spectrum of compound MC-25 (**63**)

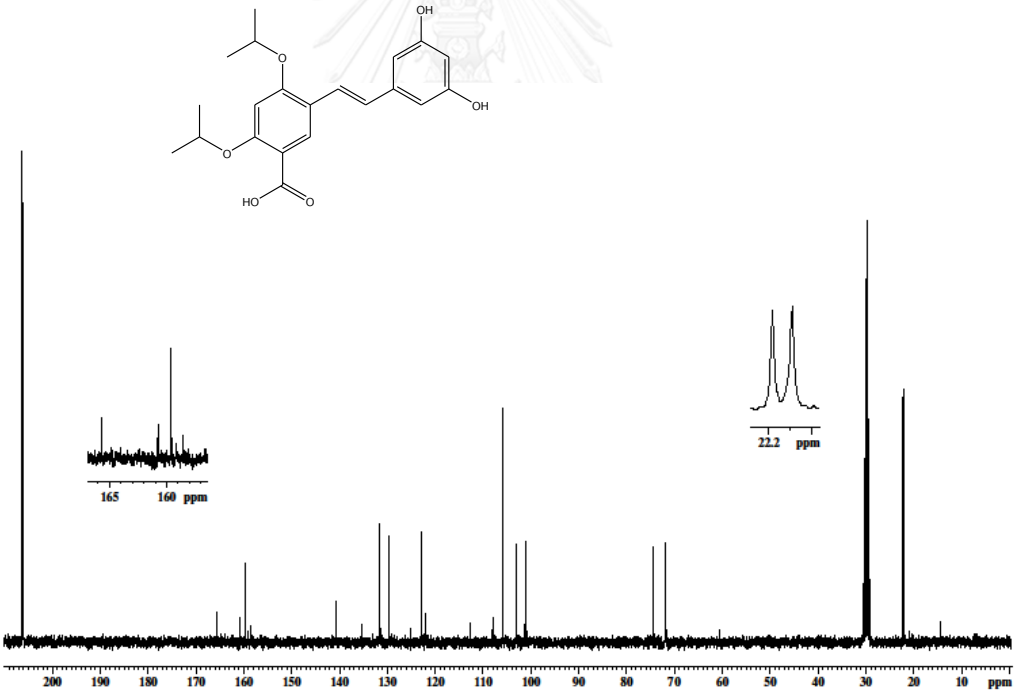

Figure 125 ^{13}C-NMR Spectrum of compound MC-25 (**63**)

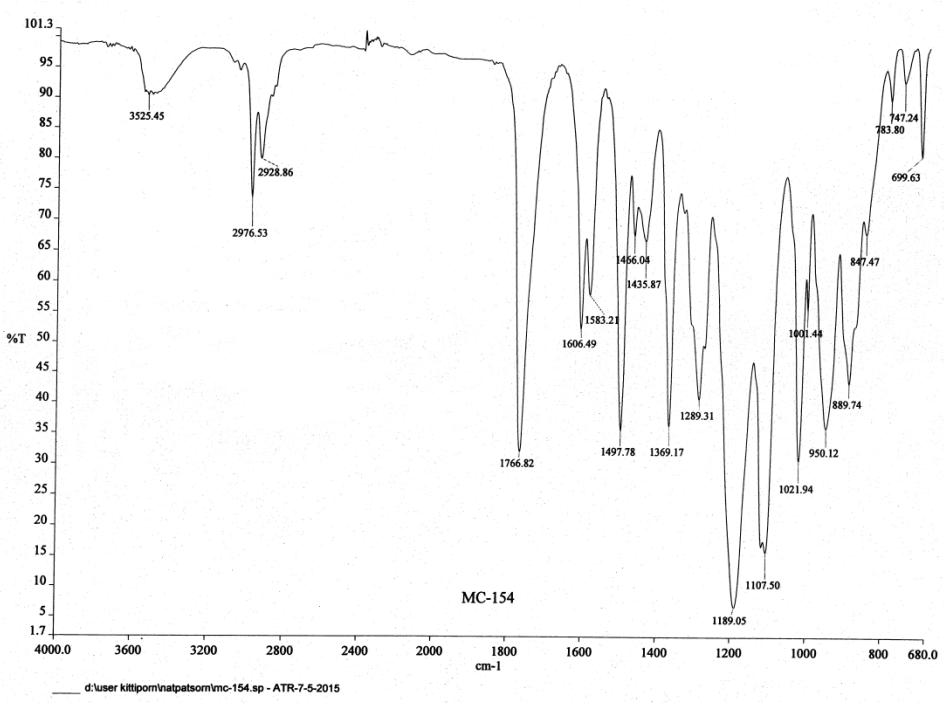

Figure 126 IR Spectrum of compound MC-26 (**64**)

Mass Spectrum List Report

Analysis Info

Analysis Name	TOFCRI019702 Natpassorn MC-154 E+.d	Acquisition Date	5/1/2008 5:32:10 PM
Method	Nitirat ESI pos 2014-1.m	Operator	Administrator
Sample Name	ESIpos	Instrument	micrOTOF 74

Acquisition Parameter

Source Type	ESI	Ion Polarity	Positive	Set Corrector Fill	64 V
Scan Range	n/a	Capillary Exit	90.0 V	Set Pulsar Pull	405 V
Scan Begin	120 m/z	Hexapole RF	90.0 V	Set Pulsar Push	405 V
Scan End	600 m/z	Skimmer 1	30.0 V	Set Reflector	1300 V
		Hexapole 1	22.9 V	Set Flight Tube	9000 V
				Set Detector TOF	1870 V

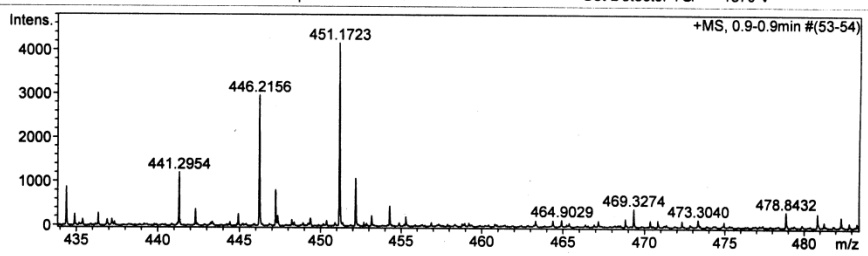

#	m/z	I	Res.
1	135.0098	2108	6706
2	148.9409	1546	7584
3	157.0886	4593	6820
4	158.9689	7049	7174
5	216.9232	3155	8294
6	218.9202	1058	8164
7	226.9515	5552	8281
8	233.1054	1319	8109
9	240.9664	1081	8454
10	251.1966	1546	8449
11	265.2135	1444	7786
12	274.2735	3624	8943
13	277.2132	2021	8670
14	279.2284	4823	8871
15	284.9109	1305	9112
16	293.2410	1197	8460
17	294.9388	2178	9209
18	305.2455	1978	9003
19	306.2447	1052	7965
20	320.2555	2972	9114
21	352.8973	1216	9424
22	362.9264	1309	9943
23	391.2837	1073	9783
24	413.2645	3218	10331
25	428.4252	1362	10387
26	433.3793	2729	10588
27	441.2954	1208	10375
28	446.2156	2969	10223
29	451.1723	4165	9768
30	452.1757	1082	9637

Figure 127 HRTOF Mass spectrum of compound MC-26 (**64**)

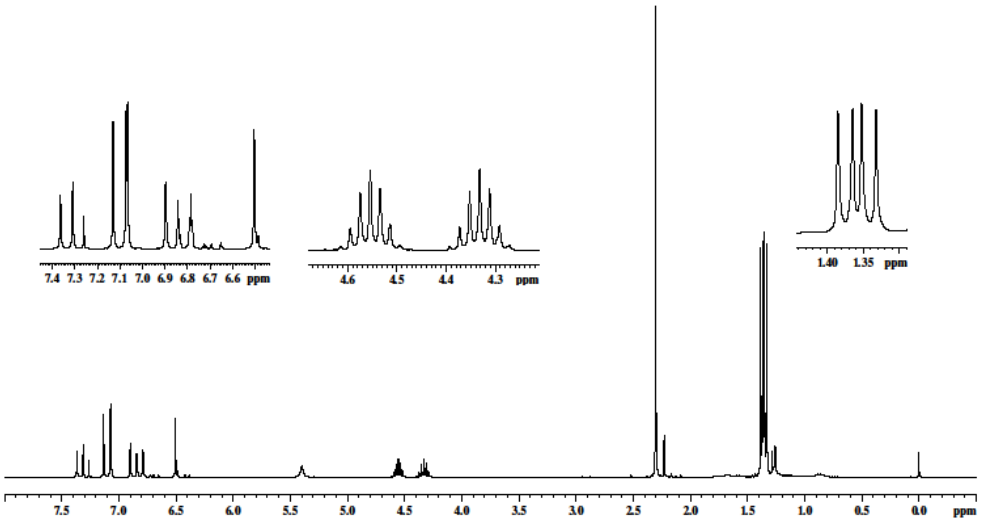

Figure 128 ^{1}H-NMR Spectrum of compound MC-26 (**64**)

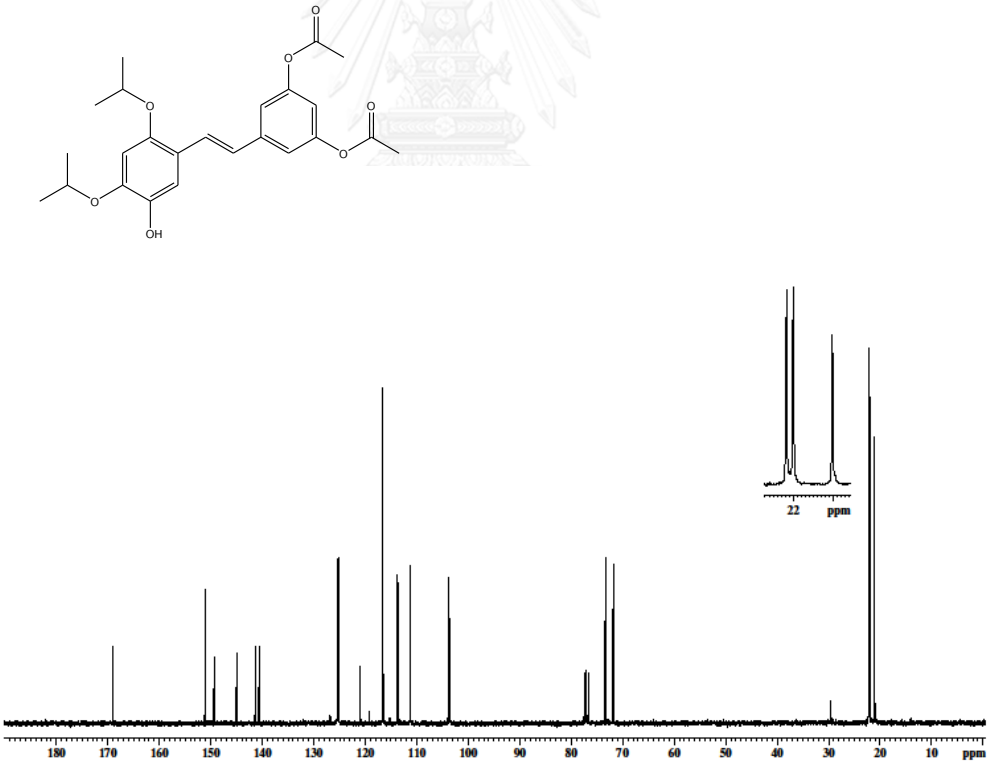

Figure 129 ^{13}C-NMR Spectrum of compound MC-26 (**64**)

VITA

Miss Nutputsorn Chatsumpun was born on December 29, 1980 in Bangkok, Thailand. She received her Bachelor's Degree in Pharmaceutical Sciences and Master's Degree of Science in Pharmacy in 2003 and 2008, respectively, from the Faculty of Pharmaceutical Sciences, Chulalongkorn University, Thailand.

Publications:

(1) Chatsumpun, M., Sritularak, B., and Likhitwitayawuid, K. (2010). Phenolic compounds from stem wood of Millettia leucantha. Chemistry of Natural Compounds, 46(4), 634-635.

(2) Chatsumpun, M., Chuanasa, T., Sritularak, B., and Likhitwitayawuid, K. (2011). Oxyresveratrol protects against DNA damage induced by photosensitized riboflavin. Natural Product Communications, 6(1), 41-44.